

**Bi-directional Evolutionary Structural Optimization  
(BESO) for Topology Optimization of Material's  
Microstructure**

A thesis submitted in fulfilment of the requirements for the degree of  
Doctor of Philosophy

**Arash Radman**  
B.Sc., M.Sc.

School of Civil, Environmental and Chemical Engineering  
College of Science, Engineering and Health  
RMIT University  
August 2013

## **Declaration**

I certify that except where due acknowledgement has been made, the work is that of the author alone; the work has not been submitted previously, in whole or in part, to qualify for any other academic award; the content of the thesis is the result of work which has been carried out since the official commencement date of the approved research program; any editorial work, paid or unpaid, carried out by a third party is acknowledged; and, ethics procedures and guidelines have been followed.

Arash Radman  
August 20, 2013

## **Acknowledgments**

I would like to express my deepest appreciation to all those who provided me with the possibility to complete this thesis. My special and sincere gratitude goes to my supervisor Dr. Xiaodong Huang for his valuable suggestions, comments and contribution throughout this entire research process. I would also like to express my warm appreciation to my second supervisor, Professor Mike Xie, for his encouragement, beneficial comments, contribution and helpful advice.

I also very much appreciate the help and guidance received throughout my candidature, from the SCECE School Manager Ms. Marlene Mannays and Research Coordinator Ms. Sharon Taylor. I would also like to warmly thank Ms. Katherine Noall for proofreading this thesis. Additionally, I am very grateful for the financial supports of Australian government and RMIT University.

This thesis is dedicated to my mother whom I would like to deeply thank, for her endless kindness, love and support.

## Table of Contents

Notations: .....	vi
Abstract: .....	1
Publications list .....	4
Chapter 1 .....	5
Introduction .....	5
Background .....	5
1.1. Problem statement and methodology .....	9
1.2. Significance .....	12
1.3. Organization of the thesis .....	14
Chapter 2 .....	16
Literature review .....	16
2.1. Structural Topology Optimization .....	18
2.1.1 Genetic Algorithm .....	21
2.1.2 Level-set method .....	24
2.1.3 Homogenization method .....	27
2.1.4 The SIMP method .....	31
2.1.5. Evolutionary Structural Optimization (ESO) .....	39
2.1.6 Bi-directional Evolutionary Structural Optimization (BESO) .....	42
2.1.7 Numerical issues in material distribution methods .....	48
2.2. Material modelling .....	54
2.2.1 Rules of mixtures .....	56
2.2.2 Bounds on materials properties .....	57
2.2.3. Self-consistent methods .....	60
2.2.4. Mechanics of materials approaches .....	63
2.2.5. Homogenization theory .....	67
2.3. Application of structural topology optimization techniques in material design .....	71
2.3.1. Design of materials with extreme or prescribed properties .....	71
2.3.2. Design of multi-phase composites .....	74
2.3.3. Design of materials with extra functionality .....	78
2.3.4. Design of functionally graded materials .....	80
2.4 Concluding remarks .....	83
Chapter 3 .....	85
Topology optimization of microstructures of cellular materials for maximum stiffness or thermal conductivity .....	85
3.1. Methodology .....	87
3.1.1 Optimization problem statement .....	87

---

3.1.2 Topology optimization through the soft-kill BESO.....	90
3.1.3. Homogenization and Sensitivity Analysis .....	92
3.1.4. Numerical instabilities .....	97
3.1.5. Procedure .....	98
3.2. Results and Discussion .....	101
3.2.1. 2D examples for maximizing the bulk modulus .....	101
3.2.2. 2D examples for maximizing shear modulus .....	106
3.2.3. 3D examples for maximizing bulk modulus .....	109
3.2.4 3D examples for maximizing shear modulus.....	112
3.2.5 2D examples for maximizing thermal conductivity .....	114
3.2.6. 3D examples for maximizing thermal conductivity .....	117
3.3. Concluding remarks .....	119
Chapter 4.....	121
Topology optimization of microstructures for isotropic cellular materials .....	121
Background.....	121
4.1. Methodology.....	124
4.1.1. Problem statement of isotropic material topology optimization .....	124
4.1.2. Solution Method.....	127
4.1.3. Determination of the Lagrangian multiplier .....	129
4.1.4. Procedure .....	130
4.2. Results and discussion.....	132
4.2.1. 2D cellular materials with maximum bulk modulus .....	134
4.2.2 2D cellular materials with maximum shear modulus.....	136
4.2.3. 3D cellular materials with maximum bulk modulus .....	138
4.2.4. 3D cellular materials with maximum shear modulus.....	143
4.2.5. 2D isotropic cellular materials with negative Poisson's ratio.....	145
4.3. Concluding remarks .....	148
Chapter 5.....	150
Topology optimization of multi-phase periodic composites with extreme properties .....	150
Background.....	150
5.1. Methodology.....	152
5.1.1. Optimization problem statement and sensitivity numbers.....	152
5.1.2. Numerical procedure.....	155
5.2. Results and discussion.....	158
5.2.1. 2D two- phase materials with maximum bulk modulus .....	158
5.2.2.2D three-phase materials with maximum bulk modulus.....	161

---

5.2.3. 3D three-phase material with maximum bulk modulus .....	163
5.2.4. 2D three-phase material with maximum shear modulus .....	165
5.2.5. 3D three-phase material with maximum shear modulus .....	167
5.2.6. 2D three-phase material with maximum thermal conductivity .....	169
5.2.7. 3D three-phase material with maximum thermal conductivity .....	170
5.3. Concluding remarks .....	173
Chapter 6.....	175
Topology optimization of functionally graded materials .....	175
Background.....	175
6.1. Methodology.....	178
6.1.1. Topology optimization problem and connectivity between base cells .....	178
6.1.2. Solution method.....	181
6.1.3. Numerical implementation.....	184
6.2. Results and discussion.....	185
6.2.1. 2D FGM with the variation in bulk modulus .....	185
6.2.2. 2D FGM with variation in shear modulus.....	189
6.2.3 3D FGM with variation in bulk modulus .....	191
6.2.4. 3D FGM's with variation in shear modulus .....	192
6.2.5 2D FGM with variation in thermal conductivity.....	194
6.2.6 3D FGM with variation in thermal conductivity.....	195
6.3. Concluding remarks .....	197
Chapter 7.....	198
Topology optimization of multi-objective graded composites.....	198
Background.....	198
7.1. Methodology.....	200
7.1.1. Problem statement and sensitivity numbers .....	200
7.1.2. Solution method and Lagrangian multipliers.....	203
7.1.3. Numerical implementation.....	206
7.2. Results and discussion.....	208
7.2.1. 2D Examples .....	208
7.2.2. 3D Examples .....	211
7.3. Conclusions.....	214
Chapter 8.....	216
Conclusion .....	216
References .....	221

## Notations:

$\hat{\alpha}_i$	Filtered sensitivity number of element $i$
$\tilde{\alpha}_i$	average sensitivity number with values of previous iteration $i$
$\alpha$	variable
$\alpha_i$	sensitivity number of elements $i$
$\alpha_{1i}$	sensitivity number of element $i$ with respect to bulk modulus
$\alpha_{2i}$	sensitivity number of element $i$ with respect to thermal conductivity
$\alpha_{i1}, \alpha_{i2}$	groups 1 and 2 sensitivity of element $i$ in 3-phase materials
$\beta_j$	move limit in MMA methods
$\gamma_i$	move limit in MMA methods
$\boldsymbol{\varepsilon}$	strain tensor
$\eta$	a very small number
$\boldsymbol{\mu}$	induced temperature vector
$\lambda$	Lagrangian multiplier
$\nu$	Poisson's ratio
$\boldsymbol{\sigma}$	stress tensor
$\sigma_{\max}^v$	maximum von Mises stress
$\sigma_e^v$	average von Mises stress
$\sigma_{ij}$	stress tensor
$\varphi$	Scalar function
$\Omega$	Design domain
$A$	Zener anisotropy ratio
$\mathbf{B}$	strain-displacement matrix
$C_{iso}$	isotropy condition
$c$	constant number
$d$	dimension of the model
$\mathbf{D}$	Stiffness matrix
$D_{ij}^1, D_{ij}^2$ and $D_{ij}^3$	Stiffness matrices of constituent phases 1,2,3

---

$D_{sq}$	deviation from square symmetry properties
$D_{iso}$	deviation from isotropic symmetry properties
$D_1, D_2$ and $D_3$	three main coefficients of cubic symmetric material
$E_{ijkl}$	elasticity tensor
$E_{ijkl}^s$	elasticity tensor of the base material
$E^s$	Young's modulus of the solid material in cellular composite
$\mathbf{E}^H$	materials homogenized elasticity tensor
$ER$	evolution rate
$E^1, E^2$ and $E^3$	Young's modulus of constituent phases 1,2,3
$f$	function
$\tilde{f}$	approximate of function $f$
$\bar{f}$	Constraint value of function $f$
$f^1, f^2, f^3$	Volume fractions of constituent phases 1,2,3
$G$	Material shear modulus defined as average shear modulus along principal axes
$G^i$	shear modulus of constituent phase $i$
$G^s$	shear modulus of solid phase
$G^*$	prescribed value of shear modulus
$\mathbf{I}$	unit matrix
$K^*$	prescribed value of bulk modulus
$\mathbf{K}_i$	element $i$ stiffness matrix
$K$	bulk modulus
$K^i$	bulk modulus of constituent phase $i$
$K^s$	bulk modulus of solid phase
$k_{ij}^H$	homogenized thermal conductivity matrix
$k_c$	material thermal conductivity defined as average of conductivities along principal axes
$k^s$	thermal conductivity of the solid phase in cellular materials
$k^1, k^2$ and $k^3$	thermal conductivity of constituent phases 1,2 and 3
$\mathbf{k}$	Thermal conductivity matrix
$k_c^*$	prescribed value of thermal conductivity
$L^2$	function space of the norm
$L_i$	moving asymptotes variable
$\ell$	Coefficient for determining the Lagrangian multiplier
$\ell_{low}, \ell_{up}$	axillary variables for determination $\ell$
$N$	number of finite elements in structural model
$p$	penalty exponent
$P_1, P_2$	material properties
$q$	force



---

$r_{ij}$	distance between element $i$ and element $j$
$r_{min}$	filter radius
$RR$	rejection ratio
$S$	Level-set function
$\mathbf{t}$	Traction vector
$t$	iteration number
$\mathbf{u}_i$	displacement vector
$U$	strain energy
$U_i$	moving asymptotes variable
$V$	volume
$V^*$	prescribed volume
$V_i$	volume of element $i$
$V_f$	volume fraction of solid phase in cellular materials
$w, w_1, w_2$ and $w_{ij}$	Weight factors
$\mathbf{x}^{(0)}$	vector of design variables at the starting point
$\mathbf{x}$	design variables
$x_i$	design variables of element $i$
$x_i^{(1)}, x_i^{(2)}$ and $x_i^{(3)}$	design variables in multiphase composites
$x_{min}$	lower bound of design variable
$x_{ij}$	design variable which indicates the density of the $i^{th}$ element for the $j^{th}$ material
$\mathbf{Y} = (Y_1, Y_2, Y_3)$	constant vector that represents the period of the medium
$\mathbf{z} = (z_1, z_2, z_3)$	position vector
$z$	level-set iso- value

Note: Specific notations are defined by various subscripts or superscripts; see definitions in the text.

## **Abstract:**

It is known that composite materials with improved properties can be achieved through modifications to the topology of their microstructures. Structural topology optimization approaches can be utilized as a systematic way for finding the best spatial distribution of constituent phases within the microstructures of materials/composites. This study presents a new approach to designing material's microstructures based on the bi-directional evolutionary structural optimization (BESO) methodology. It is assumed that the materials/composites are composed of repeating microstructures known as periodic base cells (PBC). The goal is to find the best spatial distribution of constituent phases within the PBC, in such a way that materials with desired or improved functional properties are achieved. To this end, the Homogenization theory is applied to establish a relationship between properties of materials microstructure and their macroscopic characteristics.

As the first step of this study, the optimization problem is formulated to find microstructures for materials with maximum stiffness, in the form of bulk or shear modulus, or thermal conductivity. Cellular materials, which are composed of one solid phase and one void phase, are considered at this stage. By conducting finite element analysis of the PBC, and applying the Homogenization theory, elemental sensitivity numbers are derived. By gradual removing and adding elements in an iterative process, the optimal topology of the solid phase within the PBC is found.

In the next stage of this study, the aim is to combine additional performance constraint to the above procedure. Maximization of bulk or shear modulus is selected as the objective of the material design, subject to the constraint on the isotropy of material and volume constraint. The proposed BESO procedure utilizes a gradient-based method to impose the isotropy constraint. The developed approach provides bases for the design of materials, with other objective functions and extra performance constraint or multi-functional properties.

Compared with cellular materials, composites of two or more different constituent phases are more advantageous, since they can provide a wider range of performance characteristics. The methodology

is extended into topology optimization of microstructures for composites of two or more non-zero constituent phases. For design of material with maximum stiffness or thermal conductivity, the constituent phases are divided into groups and sensitivity analysis is performed between different groups. The addition and removal of elements is conducted based on the relative ranking of elemental sensitivities and imposing volume constraints.

The developed methodology is extended into the design of functionally graded material (FGM), in which the mechanical property of material gradually changes. It is assumed that the microstructure of the FGM is composed of a series of base cells in the direction of gradation and self-repeated in other directions. The objective of optimization is to generate the lightest materials with prescribed variation in bulk modulus, shear modulus or thermal conductivity. In particular the study proposes a new computationally efficient approach for maintaining the connectivity between different base cells of an FGM.

Finally, an approach is proposed for the topological design of FGMs with two non-zero constituent phases and multi graded properties, which utilizes and encompasses the methodologies developed in the previous stages. The objective of optimization is defined to find the stiffest materials with prescribed gradation of thermal conductivity. The proposed approach applies a gradient-based sensitivity analysis to impose the constraint on thermal conductivity. This is similar to the aforementioned approach for imposing performance constraint on isotropy. Similar to the approach used for cellular FGMs, the connectivity of base cells is maintained by considering three base cells at each stage.

The effectiveness and computational efficiency of the proposed approaches are numerically tested, through designing a range of 2D and 3D microstructures for materials. A series of new and interesting microstructures of materials are presented. The results clearly indicate the advantages of BESO

utilization in terms of computational costs and convergence speed, quality of generated microstructures, and ease of implementation as a post processing algorithm.

## Publications list

*The contents of this thesis have been presented through the following publications.*

### Journal papers

- 1- Huang, X., Radman, A. & Xie, Y.M. 2011. Topological design of microstructures of cellular materials for maximum bulk or shear modulus. *Computational Materials Science*, 50, 1861-1870.(JIF (5 years) : 1.965)
- 2- Radman, A., Huang, X. & XIE, Y.M. 2012. Topological optimization for the design of microstructures of isotropic cellular materials. *Engineering Optimization*, 1-18. (JIF (2012) : 0.962)
- 3- Radman, A., Huang, X. & Xie, Y.M. 2013. Topology optimization of functionally graded cellular materials. *Journal of Materials Science*, 48, 1503-1510. (JIF (2012) : 2.163)
- 4- Radman, A., Huang, X., Xie, Y.M. 2014. Maximizing stiffness of functionally graded materials with prescribed variation of thermal conductivity. *Computational Materials Science*, 82, 457-463.(JIF (5 years) : 1.965)
- 5- Radman, A., Huang, X., Xie, Y.M. Topology Optimization of Multi-phase Materials' Microstructures for Maximum Stiffness or Thermal Conductivity. In press.

### Refereed conference papers

- 6- Radman, A., Huang, X., Xie, Y. M. 2012. "Material structural design with isotropy constraint". *22nd Australasian Conference on the Mechanics of Structures and Materials (ACMSM-2012)*. December 11<sup>th</sup> to 14<sup>th</sup> 2012, Sydney, Australia.
- 7- Huang, X., Radman, A. & Xie, Y. M. 2011. Design of microstructures for porous material with maximum bulk modulus. *The Third International Conference of Heterogeneous Material Mechanics (ICHMM-2011)*. May 22<sup>th</sup> to 26<sup>th</sup> 2011, Shanghai, China.
- 8- Radman, A., Huang, X., Xie, Y. M. 2013. Topology optimization of microstructures for multi-functional graded composites. *The 2013 World Congress on Global Optimization (WCGO III)*. July 8<sup>th</sup> to 12<sup>th</sup> 2013, Anhui, China.
- 9- Xie, Y.M., Zuo, Z.H., Huang, X., Tang, J., Yang, X. & Radman, A. 2013. Creating Innovative and Efficient Structures and Materials. *The 2nd International Conference on Civil Engineering, Architecture and Sustainable Infrastructure (ICCEASI-2013)*. July 13<sup>th</sup> to 15<sup>th</sup> 2013, Zhengzhou, China.

# **Chapter 1**

---

## **Introduction**

### **Background**

The main objective of structural engineering is to develop load carrying systems that can economically satisfy the design performance objectives and safety constraints. Economical consideration is the main driver for developing design processes that enables the minimization of the resource consumption. Many engineering disciplines are involved in optimization and apply mathematical language for this purpose. For the optimization of structures, this objective can be achieved by finding the best topology, layout of members or material distribution within the design domain of the structural system.

The history of the structural optimization can be traced back to Michell's (1904) theoretical studies in Melbourne, on optimality conditions of structural systems. However, the early studies were mainly restricted to the size and shape optimization of predetermined topologies. Wider access to computational machines in 1990s justified the development of numerical procedures for the topology optimization of structures, aimed at finding the best layout, configuration and spatial distribution of materials in the design domain of the continuum structure (Bendsøe and Kikuchi, 1988, Rao, 1995, Burns, 2002, Schramm and Zhou, 2006). It was not so long afterwards when the first topology optimization commercial software packages such as "Altair OptiStruct" emerged (Schramm and Zhou, 2006). Since then refining the theories and developing new methods are among the active fields in structural engineering.

In addition to topology optimization of structures at macro-scale, one common approach for saving resources is the application of porous or composite materials that have extreme or tailored properties. In fact, the responses of structural systems are highly dependent on the material they are built from. Although the application of composite materials in structures has had a rapid development in the past few decades, the idea of combining materials in order to achieve improved characteristics is not new. For example, the strengthening and stiffening of cheap materials with fibres can be traced back to 5000 years ago (Barbero, 1999). Some of the earliest records of strengthening mud bricks and pottery with straw are found in archaeological carvings in Egypt. The processional road in ancient Babylon was made up of a mixture of bitumen and straw, as the reinforcement fibres.

There are different reasons for the interests in materials with tailored or improved properties and a variety of performance demands in terms of functional properties are being placed on material systems. These include lightweight materials with improved or tailored mechanical, thermal, electromagnetic, optical, chemical, and flow properties (Evans et al., 2001, Torquato, 2002). For instance, applications of lightweight multifunctional products in vehicles save energy in terms of lower fuel costs and can significantly reduce the environmental impact of gas emissions. It is estimated that reducing one kilogram of the weight of an aircraft can save US \$80,000 over its lifetime; while decreasing one kilogram on a satellite weight can reduce the launching costs US\$8 million (Cree and Pugh, 2010).

Traditionally, the objectives of material design are achieved by the application of composites in the form of fibre, particulate or laminar (Figure 1.1), in which the properties of materials are controlled by modifying the location, orientation, material constituents, or volume fraction of fibre, particles or laminar inclusions (Staab, 1999). The traditional material design method follows a trial-and-error process through which design changes are made, and the material is re-analysed until its performance meets the objectives (Torquato, 2010). Although material design has achieved its objectives in certain cases through this approach, the desire for development of systematic means, has made material design an active field of research (Gibson, 2010, Cadman et al., 2013).

In newer types of composite materials, namely the functionally graded materials (FGM) which are characterized by gradual change in properties, the gradation of response is still a result of variation in composition and/or microstructural layout of material. To achieve materials with desired heat resistance properties, the primary FGMs were developed as



composition of ceramic and metallic constituent phases. Spherical or near spherical particles of metallic or ceramic phase are randomly dispersed within the matrix of the other material with varying proportion. As a result, inhomogeneity and gradual variation of thermo-physical characteristics are developed into the material, solely by varying the volume fractions of the constituent phases (Koizumi, 1997, Birman and Byrd, 2007).

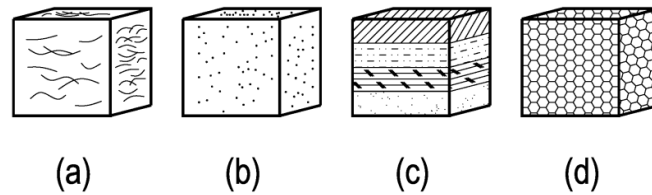


Figure 1.1: Composite classes: (a) Fibre Composite; (b) Particulate Composite; (c) Laminar Composite; (d) Cellular Composite

Technological advancement in manufacturing methods such as Selective Laser Melting (SLM) (Mutmta and Hopkinson, 2007, Yang et al., 2010), and Solid-Freeform Fabrication (SFF) or Layered Manufacturing (LM) for 3D printing (Zhao and Luc, 2000) in the last decades, has enabled the economically viable manufacturing of materials with large heterogeneity. The development of high precision fabrication technologies is paralleled by research on an emerging class of composite materials that are made by representative unit cells (RUC) or periodic base cells (PBC) (Zhou and Li, 2007). Materials with repeating or periodic microstructures usually consist of one constituent phase and a void phase (known as porous or cellular materials), or combinations of two or more different constituent phases with or without the void phase (also named as “periodic composites” (Huang et al., 2012). The overall properties of these types of materials are controlled by the spatial distribution of the

constituent phases within the PBC, as well as the properties of constituent phases. In comparison with traditional composites, periodic composites demonstrate greater flexibility in terms of their capability to be tailored for prescribed physical properties, by controlling the compositions and/or microstructural topology of the constituent phases (Cadman et al., 2013). They can also be easily tailored to have gradation in their functional properties, in the form of an FGM through gradual changes in the microstructural topologies.

### **1.1. Problem statement and methodology**

The periodic base cell (PBC) can be viewed as a heterogeneous continuum structure, which is composed of different constituent materials (or constituent phases) (Bendsøe and Sigmund, 2003). It has been shown that the properties of materials are influenced by the topology of the PBC (Hassani and Hinton, 1998a, b, c). Hence, a major challenge in the design of these materials would be the determination of the optimal spatial distribution of the constituent materials within the PBC. In the simplest form, the periodic composite materials consist of a 2D or 3D scaffold of matrix, in which the other phases are included. Therefore, it is reasonable to apply the structural topology optimization methodologies for determination of the spatial distribution of the phases.

Progress in the area of numerical methods is often ahead of mathematical approaches. The reason is largely attributable to the fact that the mathematical approaches usually require exhaustive formulation and rigorous solutions for rather simple optimization problems; while in numerical approaches complicated models could be dealt with using rather simple principles (Cherkaev, 2000). On the other hand, numerical topology optimization usually

involves with large numbers of design variables that make the use of conventional mathematical optimization algorithms inappropriate. They may not be efficient enough to solve the problems with large heterogeneity, mainly as the result of high time consumption (Cadman et al., 2013). In the past two decades, several numerical topology optimization algorithms have been examined, with the goal of developing a systematic approach for the design of periodic materials. One of the main concerns in these attempts has been the computational efficiency of the approach.

Basically, topology optimization techniques, such as homogenization method (Bendsøe and Kikuchi, 1988), solid isotropic material with penalization (SIMP) (Bendsøe, 1989, Zhou and Rozvany, 1991, Rozvany et al., 1992), Level-Set method (Wang et al., 2003, 2004), Evolutionary Structural Optimization (ESO) (Xie and Steven, 1993, 1997), and Bi-directional Evolutionary Structural Optimization (BESO) (Querin et al., 1998, Yang et al., 1999, Huang and Xie, 2007b, Huang and Xie, 2010b) were developed to find the stiffest structural layout under given constraints. Prior to the commencement of this research, the SIMP (Sigmund, 1994b, 1995), Level-set (Wilkins et al., 2007, Challis et al., 2008, Zhou et al., 2010) and ESO (Patil et al., 2008) have been extended into the design of periodic microstructures of materials and composites.

Different topology optimization techniques have advantages and disadvantages in terms of computational efficiency, quality of generated microstructures, robustness, and the level of effort for implementation as a computational post-processing procedure, to name few. Among various topology optimization algorithms, ESO (Xie and Steven, 1993, 1997) was originally developed based on the concept of gradually removing inefficient elements from the finite

element model of the structure so that the resulting topology evolves towards an optimum. A later version of the ESO method, namely the bi-directional evolutionary structural optimization (BESO) (Querin et al., 1998, Yang et al., 1999) allows removal of elements from the least efficient regions, and the adding of elements to the most efficient regions of the finite element model of the structure. Further developments of BESO have been made by theoretically introducing the hard-kill BESO (Huang and Xie, 2007b) and soft-kill BESO (Huang and Xie 2009a, 2010a) under particular circumstances. The new BESO (Huang and Xie, 2009a) alleviated most of the imperfections of previous versions (Rozvany, 2001a, 2009, Huang and Xie, 2010a,c). It offers several advantages in comparison with other topology optimization algorithms in terms of quality of the generated topology and convergence speed.

This study is the first attempt to extend the application of the BESO to the design of microstructures of materials. Since materials with high stiffness are more desirable from the structural application point of view, the first step of this study is the development of the new algorithms for designing lightweight cellular materials with extreme stiffness. Thereafter, the methodology will be extended into other scenarios of material design. While offering innovative methodologies in material design, in particular other steps are arranged in such a way to provide keystones for the systematic design of composite materials with gradation in properties. For this purpose, new procedures will be introduced for design of composites with multi-functional properties.

In particular the objectives of this study are:

- Development of a computational algorithm for topological design of cellular materials with extreme properties;

- Development of a computational algorithm for topological design of microstructures with additional constraint on material properties;
- Development of a computational algorithm for designing microstructures of composites with extreme properties;
- Development of a computational algorithm for designing microstructures of functional graded materials (FGM);

It should be mentioned that the properties of materials varies by their chemical and atomic configurations as well as by their particular microstructural topology (Mercier et al., 2002). However, this study deals with materials with a microstructural length scale much larger than the atomic dimensions, and also considerably smaller than the overall dimensions of the structure. Therefore, it is assumed that the interatomic forces are negligible. It is generally known that at the molecular level, the properties of materials are substantially different. For example (Duan et al., 2006) showed that at the Nano-level, materials can be much stiffer than its constitutional phases. However, these types of materials are out of scope of this research.

## **1.2. Significance**

As discussed earlier, the performance enhancement of materials will lead to significant saving of energy and resources. For instance, lightweight materials can save energy in terms of lower fuel costs and emissions, thus reducing their carbon footprint. The demand for new materials with improved functional properties is constantly increasing. As a consequence this growth necessitates the development of more advanced design tools. In the case of periodic materials, as the problem involves continuum microstructures with large heterogeneity, this objective

can be achieved by the application and development of appropriate structural topology optimization methods.

In spite of the fact that the new BESO procedure was only very recently developed, the method has acquired great successes in solving topology optimization problems in different areas of structural engineering. These include minimizing structural volume with a displacement or compliance constraint (Huang and Xie 2009b; 2010a), stiffness optimization of structures with multiple materials (Huang and Xie, 2009a), design of periodic structures (Huang and Xie, 2008a), structural frequency optimization (Huang et al., 2010), topology optimization for energy absorption structures (Huang et al., 2007) and geometrical and material non-linearity problems (Huang and Xie 2007; 2008).

This study will extend the application of BESO to the design of microstructures for materials, and introduces a new methodology for solving engineering problems related to the design of materials. The outcomes signify the theoretical importance of the research. On the practical side, the advantages of BESO in simplicity, versatility and ease of implementation will provide engineers with a new methodology and an advanced design tool for the exploration and creation of novel materials that possess the required functions.

More importantly, the previous studies on material design through structural topology optimization methodologies have indicated that the generated micro-structural topologies are highly dependent on the applied optimization algorithm and parameters (Sigmund, 1994a, 1994b, Neves et al., 2000). This relates to the fact that a number of topologically different microstructures could provide similar material property. In other words, there are many local

optima in the design of microstructures for materials. Therefore, it is important to attempt new and different optimization algorithms, such as BESO, in order to find a much wider range of possible solutions to the material design.

### **1.3. Organization of the thesis**

This study deals with the topology optimization of microstructures for materials and composites. In the next chapter a review on various structural topology optimization techniques will be presented. The process of material design involves the determination of material properties, through the modelling of its representative volume element (RVE). Chapter 2 also briefly introduces some of these methods. This is followed by a brief summary of previous research on the applications of structural topology optimization methodologies in the design of microstructures for materials.

Chapter 3, deals with the topology optimization of materials with extreme properties using the BESO technique. In this chapter, cellular materials whose microstructures consist of one material phase and one void phase are considered. The statement of the optimization problem will be presented and the details of design algorithms will be explained. Numerical examples will be presented and compared with literature.

Chapter 4 examines the possibility of combining additional constraint with the procedure explained in Chapter 3. This is done by defining the constraint on the isotropy to the material properties. The result of this study will provide bases for the further development of procedures for the design of materials, with constraint on other functional properties.

In Chapter 5 a method for designing composites of two or more constituent phases with extreme functional properties will be introduced. Compared with cellular materials whose microstructures are made of a solid phase and a void phase, composites of two or more different material phases, are more advantageous since they can provide a wider range of performance characteristics (Zhou and Li 2008a, d). After presenting the details of the proposed method, numerical examples will be presented to validate the effectiveness of the procedure.

Chapter 6 proposes a BESO method for the design of materials with graded properties. It is supposed that the FGMs consist of one material phase and a void phase, with gradation in stiffness or thermal conductivity. In particular the procedure introduced in this chapter addresses the connectivity issue for the design of a series of base cells for these types of materials. The high computational efficiency of the proposed algorithm will be demonstrated by numerical examples.

In Chapter 7 a combinations of the methods used in Chapters three, four, five and six will be applied to the design of FGMs, with two constituent phases and incorporating gradual changes in multiple functional properties. The functional properties that are considered in this chapter are the stiffness and the thermal conductivity of materials.

Chapter 8 summarizes the research outcomes and presents recommendations for future studies.



## **Chapter 2**

---

### **Literature review**

It is known that the physical properties of materials can be controlled by changing the compositions or microstructural topology of constituent phases. The analytical model for the prediction of optimal materials properties proposed by Bendsøe et al.(1993), has demonstrated that the topology of microstructures of materials can be designed in such a way that materials with extreme properties are achieved. Inspired by this work, Sigmund (1994a, 1994b, 1995) developed a computational algorithm based on a structural topology optimization technique, to solve the problem of finding the microstructures for materials with given homogenized (averaged) properties. The methodology is known as “inverse homogenization” (Sigmund 1994; Steven 2006; Cadman et al. 2012).

Since the introduction of the approach, different structural topology optimization techniques have been applied for the design of microstructures for materials. Topology optimization techniques differ in terms of their computational costs and efficiency, the quality of generated microstructures, their robustness, and the level of effort for implementation as a computational post-processing procedure, to name few. In addition to the solid isotropic material with penalization approach (SIMP) that has been used in the original work by Sigmund (1994a), some other structural topology optimizations techniques such as the *Level-set*, *Genetic Algorithm* and *Evolutionary Structural Optimization (ESO)*, were also used for topology optimizations of materials' microstructures.

This dissertation is dedicated to the extension of the Bi-directional Evolutionary Structural Optimization (BESO) approach, into topological design of materials' microstructures with specified functional properties. The first section of this chapter, deals with a critical review of the structural topology optimizations methodologies that have so far been applied to material design. The procedure of solving the inverse problem of finding microstructures of materials with desired functional properties, also involves with a modelling technique in which the homogenized or averaged properties of material is estimated. Among several proposed approaches for the estimation of average material properties, two of them, namely the "bounding of material properties" and the "Homogenization theory" are utilized in this dissertation for different purposes and to various extents. Section two of this chapter provides a brief survey about the development of these approaches. Section three briefly introduces some of the applications of structural topology optimization techniques in material design.

## 2.1. Structural Topology Optimization

The emergence of mathematical optimization can be traced back to the introduction of calculus of variations by Bernoulli, Euler and Lagrange between the 17<sup>th</sup> and 18<sup>th</sup> centuries (Kamat, 1993). Generally, the calculus of variations deals with finding the minima and maxima of functions that are represented by differential equations. The solution of these differential equations identifies the optimal points of the functions. Although the calculus of variations provides a robust solving method for the extremization problems, except in very simple cases, obtaining a closed-form solution for non-linear differential equations is very difficult. On the other hands the numerical approaches for solving the variational equations involves an approximation of derivatives, in which the time consumption, accuracy and convergence of applied approaches are serious problems in structural optimization (Kamat, 1993).

The theory of structural optimization has been introduced by Michell (1904) in Melbourne, for developing minimum weight truss-like structures (Eschenauer and Olhoff, 2001). However it was not until 1950's when with the advent of digital computers, the idea of structural optimization started to gain momentum, linear programming methods were proposed (Dantzig, 1963) and significant improvement was made into its theory and applications, by solving a range of structural optimization problems (Prager 1969; 1974; Save 1975).

The topology optimization, which is sometimes interchangeably referred to as layout optimization or generalized shape optimization (Olhoff and Taylor, 1979, Rozvany et al.,

1992, Haber et al., 1996, Eschenauer and Olhoff, 2001), aims to find the best topology, layout or configuration in the domain of continuum structure (Design Domain). The Greek word of “Topo” can be translated to “place”, “landscape” or “domain”. Mathematically, all subsets of the  $\mathbf{R}^3$  space (including lines, curves and so forth) are called topological domains. Topology in the structural engineering field basically describes the spatial distribution of materials or location of members and joints in a structure.

In the 1960s, topology optimization was improved by the introduction of the so-called ground structure (Dorn et al., 1964), in which mathematical programming (MP) algorithms are used. Other remarkable early works on topology optimization were the introduction of “optimal layout theory” by Prager (1969) (Prager and Rozvany, 1977) and stiffness maximization of solid plates with volumetric constraints by Cheng and Olhoff (1981). Later, the finite element based “homogenization method” was introduced as the first numerical structural topology optimization technique by Bendsøe and Kikuchi (1988). The development in the field followed another finite element based topology optimization method, namely the “Evolutionary Structural Optimization” (Xie and Steven, 1993), which will be discussed later in this chapter.

The structural topology optimization problems are often involved with the minimization or maximization of a defined performance function, subject to a set of constraint conditions (Kamat, 1993). The variables are generally defined as either the quantities that define the geometry of physical system and/or the sizes of the structural elements. For example supposing that each point in the domain of a continuum structure (design domain) can be either a material or void, the topology optimization of a continuum structure may consist the

determination for every point in space, existence or absence of material, so that the objective function is extremized and the constraints are satisfied simultaneously (Kamat, 1993).

In contrast to the classical mathematical optimization methods, which make use of the differential equations for solution, the structural optimization methods often use simplified algebraic equations which are solved in an iterative numerical procedure. In a simple maximization problem, the structural topology optimization techniques often involve the following general steps:

1. Selection of the initial design variables (material type, thickness of plate...)
2. Evaluation of the objective function for the current setting of design variables
3. Comparison between the current properties with the prescribed values
4. A procedure to update the design variables, so that the objective function is improved and repetition of steps 2 to 4 until no further improvement of the result is achievable

Various strategies that are taken in order to update the design variables include the methods that select the new design variables randomly, or the methods that use the gradient of the objective function to obtain the optimum. It should be mentioned that the selection of initial topology or the procedure of updating the design variables may result in a solution which is a local optimum. Even if the solution has one global optimum with no local optima, still the selection of the initial design and updating scheme will affect the number of repeats of the above mentioned procedure.

In the following sub-sections, some of these optimization techniques are briefly introduced and compared with the BESO. Because the BESO, which is the applied approach in this thesis, is based on materials distribution, here more emphasis will be given to materials distribution methods of SIMP, ESO and BESO.

### **2.1.1 Genetic Algorithm**

Genetic Algorithm is a global search stochastic approach, which is developed based on the rules of genetic evolution of biological systems and relies on the “survival of the fittest” strategy. Genetic Algorithm was originally developed by John Holland (1975) and coworkers in Michigan University, with applications in biological and artificial intelligence systems. It gained much of its success as an optimization tool for the works of Goldberg of the University of Illinois (Goldberg., 1989, Jenkins, 1991). The Genetic Algorithm was used for structural optimization by many researchers (Goldberg and Samtani, 1986, Jenkins, 1991, Coello et al., 1994, Pezeshk, 2000), including topology optimization of structural frames (Grierson and Pak, 1993), trusses (Ohsaki, 1995) and continuum structures (Sandgren et al., 1990, Jakiela et al., 2000). Zohdi (2002) applied this topology optimization technique for the design of materials, with prescribed bulk and shear moduli of elasticity.

The Genetic Algorithm operates on coded strings (usually binary numbers) that contain the discrete design variables information for a particular solution. The value (or *fitness*) of design variables in fulfillment of the objective function is assessed by analyses that are made on the system, which are saved by converting or ‘*mapping*’ of the values to binary strings (bits). The mathematical bit string is analogous to the chromosome in natural biological systems. The

initial generation (generation 0) is produced by the random selection of bits in each string. Usually, a population of  $2n$  to  $4n$  ( $n$  is the number of variables) of families of strings is created as the initial trial solutions.

After the first round of analysis, the pairs of “*parent*” strings are selected among the best potential solutions. The next step is to break the selected parent strings into segments and then exchange the segments with the corresponding parent segment, which is called the *crossover* procedure. To enable the exploration of the entire search space, usually a *mutation* procedure is devised whereby some bits are switched on or off (0 to 1 or 1 to 0) based on a probabilistic formulation. The mutation procedure is a measure to allow the development of new features that do not pre-exist in parents’ strings. It is controlled by the user through the prescription of mutation probability. The fitness of each family is again assessed and the procedure continues into the next generation until the convergence is attained, or the specified maximum number of generations is reached.

One of the characteristics of Genetic Algorithm is that the procedure searches among a population of points in design space, simultaneously. In comparison with the methods that shift the solution from a single point in design space to the next, parallelization of search among optima increases the “probability” of finding a global optimum point (Goldberg., 1989). This fact contributes to the robustness of the Genetic Algorithm. Another favorable feature of the method is that the solutions are developed based on the payoff or quality of the solution itself. Therefore calculation of auxiliary information, such as the derivatives with respect to the objective function (sensitivity analysis) is not necessary.

However, in contrast to gradient based approaches (see below) that improve one solution at a time, the Genetic Algorithm needs to operate on a population of solutions simultaneously. This means that a larger number of design variables need to be defined and every iteration (generation) needs several finite element analyses. Consequently the finite element model of the structure should contain only a few elements (Goldberg and Samtani, 1986, Jenkins, 1991). Otherwise, the procedure can become prohibitively expensive (with  $10^4$  to  $10^6$  ground elements) (Rajeev and Krishnamoorthy, 1992, Hajela and Lee, 1995, Rozvany, 2009). For instance, topology optimization of a cantilever plate with 2800 elements roughly requires about 150,000 finite element analyses of the structure (Kane and Schoenauer, 1996)!

Another major drawback of the Genetic Algorithm for topology optimization is that the integrity and continuity of the structure is not guaranteed. As the adding or removing of elements is based on a random search algorithm, it is more likely that during the design process the structure is divided into several unconnected regions (Fanjoy and Crossley, 2002b). As the load transfer does not happen between unconnected regions, the structural analysis may result in false information. Therefore, the optimization procedure fails. Different approaches have been introduced in the literature to tackle this problem, including the introduction of a chromosome mask to modify the chromosome information in unconnected locations (Fanjoy and Crossley 2002a; 2002b), switching the unconnected elements to void (Jakiela et al., 2000) and penalizing the unconnected elements (Wang et al., 2006). However these approaches either fail to completely alleviate the discontinuity problem or result in a poor fitness values with even more computational expenses (Zuo et al., 2009).



### 2.1.2 Level-set method

The mathematical concept of Level-set was introduced by Osher and Sethian (1988) for computation of moving interfaces (Burger and Osher, 2005). It was recently used as a numerical procedure for the structural topology optimization, as an alternative approach to material distribution methods (Sethian and Wiegmann, 2000, Osher and Santosa, 2001, Wang et al., 2003). Its applications have also been extended into a variety of topology optimization problems such as compliance minimization (de Gournay et al., 2008) and the design of microstructures for materials (Mei and Wang, 2004, Wilkins et al., 2007, Challis et al., 2008), including materials with negative Poisson's ratio (Wang and Wang, 2005b), with specific electromagnetic characteristics (Zhou et al., 2010) and negative permeability (Zhou et al., 2011).

The Level-set approach derives its name from the function that describes the boundary of the structure (Challis, 2010). The level-set of the scalar function  $\varphi: \mathbf{R}^3 \rightarrow \mathbf{R}$  is defined in some domain  $\Omega$  as:

$$S(t) = \{\mathbf{x}(t): \varphi(\mathbf{x}(t), t) = z\} \quad (2.1)$$

where  $z$  is a constant value, which is known as the iso-value and is usually taken as equal to zero in structural problems. The standard definition of the Level-set divides the design domain into 3 regions (Wang et al. 2003):

$$\varphi(\mathbf{x}) = \begin{cases} < 0 & \text{if } \mathbf{x} \in \Omega \\ = 0 & \text{if } \mathbf{x} \in \partial\Omega \\ > 0 & \text{if } \mathbf{x} \notin \Omega \end{cases} \quad (2.2)$$

where the area covered by  $\Omega$  is filled by material and the  $\partial\Omega$  represents the structural boundary. In finite element modeling of the structures usually the discrete level-set definition is used (Challis 2010). When the elements are either material or void, the level-set function can be defined based on the position of the center of elements simply as (Challis 2010):

$$\varphi(c_i) = \begin{cases} < 0 & \text{if } x_e = 1 \\ > 0 & \text{otherwise} \end{cases} \quad (2.3)$$

In the process of structural optimization, the level-set function  $\mathcal{S}(t)$  dynamically changes in time so the structural boundary  $\partial\Omega$  also changes. The evolution of the surface is determined by specifying the “speed vector” of the level-set surface at different points. By differentiating the equation (2.1), with respect to time and applying the chain rule, the so called “Hamilton-Jacobi” type equation is obtained:

$$\frac{\partial \varphi}{\partial t} = -|\nabla \varphi| \frac{dx}{dt} = -|\nabla \varphi| v \quad (2.4)$$

which correlates the speed vector of the point on the surface to the objective of optimization. The optimal structural boundary is expressed as a numerical solution of this partial differential equation on  $\varphi$  (Wang et al., 2003).

One of the advantages of the Level-set is that the approach can provide sharp interfaces between different constituent phases of the structure. This makes the interpretation of boundary and manufacturing easier, in comparison with other topology optimization methods that use continuous variables such as the SIMP (Burger and Osher, 2005). However one of the drawbacks of the above mentioned classical formulation is that it does not allow the systematic formation of new holes in the topology of structure (Allaire et al., 2004). The Level-set method is generally devised to describe the propagation of interfaces with a defined speed function; therefore, holes within existing shapes and away from the boundaries cannot be initiated (Burger et al., 2004).

Different solution methods have been proposed to solve the problems of nucleation of new holes in the structure. One way is by introducing large number of discrete holes in the initial design (Allaire et al., 2004). The above mentioned Level-set setting is capable of merging or cancelling these holes and creates a structure with fewer holes in later iterations. However, the nucleation of further necessary holes in later stages will remain an unsolved problem. It is known that the number and location of the initial holes have an important effect on the final solution (Allaire et al., 2004, Wang et al., 2003).

The other method that has been proposed for solving the problem of new holes nucleation is by the modifications of the Hamilton-Jacobi equation, through the introduction of a forcing term  $q$  (Burger et al., 2004). The modified Hamilton-Jacobi differential equation that needs to be solved is:

$$\frac{\partial \varphi}{\partial t} = -|\nabla \varphi|v - wq \quad (2.5)$$

in which  $w$  is a positive weighting factor which determines the influence of the term  $q$ . The determination of the forcing term  $q$  and the speed vector  $v$  are involved with the sensitivity analysis of the objective function. The selected  $q$  is dependent on the problem at hand and its weighting factor  $w$  should be determined by the user as an initial parameter (Challis, 2010). Therefore its successful application is highly dependent on the user's experience. Since introducing additional constraint in the Level-set approach also involves with further modification of the Hamilton-Jacobi differential equation (2.5) by adding extra weighted terms (Challis et al., 2008), the successful implementation of the method in conjunction with extra constraints is very cumbersome, especially in 2D problems.

In general the Level-set approach is mathematically more complicated and harder to be implemented as a computational procedure, in comparison to the materials distribution approaches. Therefore, the approach has not reached the stage of regular application so far (Rozvany, 2009). In the subsequent sections, three methods that are based on material distributions, namely the SIMP, ESO and BESO are briefly reviewed. Due to the mathematical simplicity of these approaches, the methods also received more attention.

### **2.1.3 Homogenization method**

Homogenization method is a mathematical approach for finding optimal topologies of structures. It was the first practical methodology for topology optimization of structures which was developed by (Bendsøe and Kikuchi, 1988). It is sometimes referred to as “generalized shape optimization”. So far, the approach has been used extensively for topology optimization of structures for example in (Allaire and Kohn, 1993, Suzuki and Kikuchi,

1991). This methodology has also been used in topology optimization of materials in a number of publications, for example in (Terada and Kikuchi, 1996, Fujii et al., 2001). The Homogenization method was the inspiration for development yet another important structural topology optimization approach namely the SIMP method (Bendsøe, 1989), which will be discussed in the next section.

In the Homogenization method, the boundary shape optimization problem is changed into the material optimization problem in an extended design domain (Fujii et al., 2001). In this method the structure is seen as a combination of microstructures. The physical properties of these microstructures are assigned to the elements of the discretized domain. The microstructures are introduced with different material models such as square unit cells with rectangular void or rank layered materials (Figure (2.1)). The physical properties of the microstructures are controlled by their geometrical parameters. The parameterization of the cells is made in such a way that they can yield the two limiting cases of completely solid element or void elements. This means that by changing the design variables such as void dimensions, the void region, defined inside a microstructure, can cover the whole area of the microstructure. It is also assumed that large numbers of these microstructures exist in the structural domain. In topology optimization through homogenization method, the geometrical parameters are defined as design variables and the objective of optimization is to find their optimal values (for example the sizes and orientation of the void regions in square unit cells).

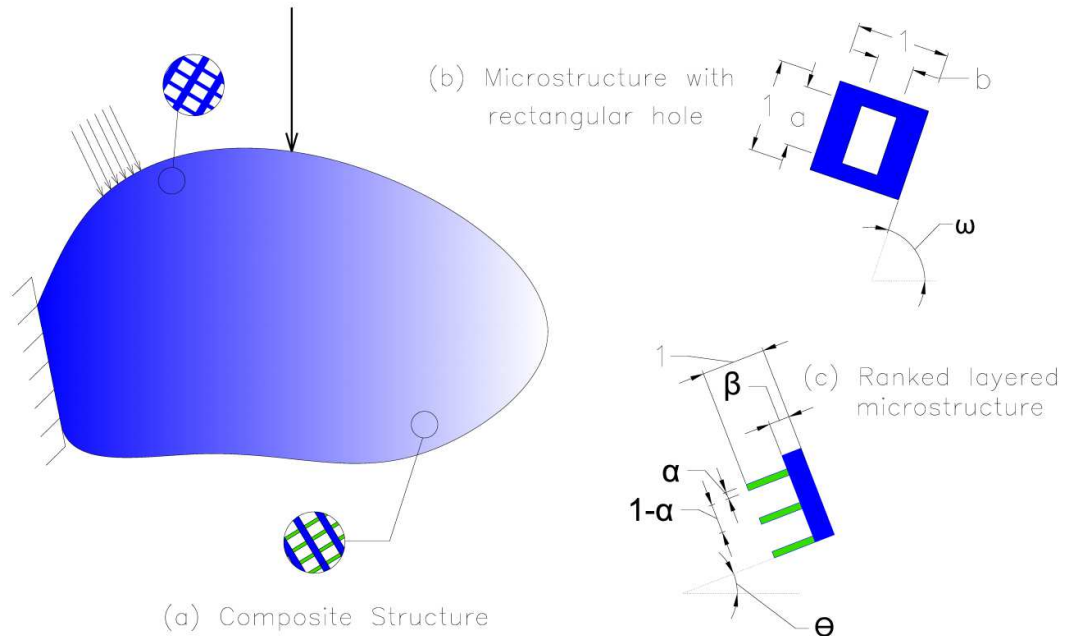


Figure 2.1: Examples of microstructural models used in Homogenization method

In homogenization method, it is assumed that there exist many microstructures of similar geometry next to each other which are referred to as periodic microstructures. The assumption of periodicity for microstructural boundary conditions enables the “Homogenization theory “ to be used for finding the effective properties of the equivalent homogenized structure made by the these microstructures. In the case of ranked layered microstructures the homogenization problem can be solved analytically but for other voided microstructures, numerical approaches such as finite element methods need to be applied. The “Homogenization theory” will be discussed in more details in section 2.25.

In the homogenization method the number of design variables is proportional to the numbers of elements in the design domain. Therefore, the application of mathematical programming approaches for solving topology optimization problems is very costly due to existence of large number of design variables in the model. To overcome this difficulty, the approach of “optimality criteria” is usually applied. As it will be described in (see section 2.1.4), the optimality criteria methods are indirect optimization approaches that arrive at optimal solution by satisfying a set of conditions related to the performance of the structure.

In the finite element based homogenization method for topology optimization, the Homogenization theory is applied and the effective properties of microstructures are assigned to the elements of finite element model of the structure. Then the finite element analysis is performed to evaluate the performance of the structure in satisfying the objective function. The next step is to use the Homogenization theory and optimality criteria principals to update the design variable in such a way that the structural performance get closer to the objective function. The iterative procedure continues until no further improvement in the objective function can be achieved.

It is noted that the problem is solved in a fixed domain, so the finite element model used in the analysis doesn't need to be altered during the optimization procedure. The final topology may contain three types of regions, namely, solid regions (filled with material), empty regions (without material) and porous regions (regions with infinitesimal cavity sizes). However, the optimal solutions usually have high manufacturing costs since there are many small cavities in the structure (Rozvany et. al. 1992). For the design of microstructures of materials this problem may cause more difficulties since the microstructures are generally of smaller sizes.

### 2.1.4 The SIMP method

The idea of the finite element based material distribution method can be traced back to the studies of Rossow and Taylor (1973) which used the continuous design variables without penalization of intermediate densities in topology optimization (Rozvany 2009). In another pioneering study, inspired by the “homogenization method” (Bendsøe and Kikuchi, 1988), the principals of the SIMP were first proposed by Bendsøe (1989) for the topology optimization of structures. The method was named “the direct approach” by Bendsøe (1989). ‘Solid Isotropic Microstructures with Penalization’ or SIMP was coined by Rozvany et al. (1992) , and later on, used by Bendsøe and Sigmund (1999) with ‘M’ standing for ‘Material’. The method is widely used for the design of microstructures for materials (Sigmund 1994a, 1994b, 1995).

In the topology optimization of continuum structures via material distribution, the aim is to assign each point of space a solid or void property (Bendsøe, 1989). Typically these topology optimization problems are treated by discretizing the continuum structures into a finite element model, which enables the alternation of the topology, without the need for re-meshing. In the simplest form where there is one objective function  $f(x)$  (for example the compliance) and no other performance constraint, a structural topology optimization problem can be mathematically formulated as:

Minimize:  $f(x)$

$$\text{Subject to: } V^* - \sum_{i=1}^N V_i x_i = 0 \quad (2.6)$$



$$x_i = 0 \quad \text{or} \quad 1$$

in which  $V^*$  is the prescribed volume of structure and  $V_i$  is the volume of element  $i$ ; the design variable  $x_i$  indicates the presence (1) or absence (0) of the element. Similar formulation for the point-wise material/no material (also known as black/white (Bendsøe and Sigmund, 1999)) optimization was suggested by Kohn and Strang(1986) and Strang and Kohn (1986). However, as practically examined by Bendsøe and Kikuchi (1988), these classes of problems are ill-posed and would be dependent on the selection of the elements' sizes and discretization mesh. For example it can be shown that by using finer and finer mesh in the finite element model of structure, the optimization procedure results in structures with more and more members of smaller sizes and no convergence is achievable by using even finer mesh sizes (Bendsøe and Sigmund, 1999, Huang and Xie, 2010b).

To tackle these problems the SIMP method uses a relaxation method, in which the design variables are freed to take any value between 0 and 1 (Bendsøe, 1989, Sigmund and Petersson, 1998). Then some form of penalization approach is used to steer the solution to a discrete 0/1 values. The new definition of the optimization problem has the following format:

Minimize:  $f(\mathbf{x})$

$$\text{Subject to: } V^* - \sum_{i=1}^N V_i x_i = 0 \tag{2.7}$$

$$0 < x_{min} \leq x_i \leq 1$$

in which lower bound  $x_{\min}$  is defined in order to avoid singularity of the problem. Supposing that  $f(\mathbf{x})$  defines some energy form of the structural properties (e.g. compliance), it can be seen that the new formulation of the problem makes the energy linearly dependent on the design variable (Sigmund and Petersson, 1998).

The key issue in “SIMP” topology optimization method is defining a relationship between materials properties and a continuous design variable. As mentioned before, the continuous design variable is often interpreted as the elemental density. This relationship is known as the “interpolation scheme”. In the original study of Bendsøe (1989) the so-called *power-law* approach was used as material interpolation scheme. For example the local material elasticity can be interpolated as:

$$E_{ijkl}(x_i) = x_i^p E_{ijkl}^s \quad (2.8)$$

in which  $E_{ijkl}^s$  is the elasticity tensor of the base material. If the penalization factor is selected as  $p=1$ , the intermediate densities are allowed to exist in the model. By increasing the penalization factor  $p > 1$  the intermediate values of the design variables (gray elements) are suppressed and the stiffness tends to be very close to either 1 or 0. By using most filtering techniques it is still not possible to have a pure 0/1 solution and some grey elements will always remain in the structure.

For the cases where the volume constraint is active, numerical experiences indicates that the solution gets very close to 0/1 designs, if the selected  $p$  is sufficiently large. The reason is attributable to the fact that for such a choice, the volume still remains linearly proportional to

$x_i$  , but the intermediate densities are suppressed in stiffness calculations and stiffness will become less than proportional (Bendsøe and Sigmund, 1999).

On the other hand, the interpolation scheme of equation (2.8) does not guarantee that the summation

$$V = \sum_{i=1}^N V_i x_i \quad (2.9)$$

in fact corresponds to the specific volume. However it is possible to establish conditions on  $p$ , so that the power law scheme has a meaningful physical interpretation. Bendsøe and Sigmund (1999) showed that the power-law model can achieve a real physical meaning provided that the following equations hold:

$$p \geq \max \left\{ \frac{2}{1-\nu}, \frac{4}{1+\nu} \right\} \quad \text{in 2D cases} \quad (2.10.a)$$

$$p \geq \max \left\{ 15 \frac{1-\nu}{7-5\nu}, \frac{3(1-\nu)}{2(1-2\nu)} \right\} \quad \text{in 3D cases} \quad (2.10.b)$$

where  $\nu$  is the Poisson's ratio. Instead of using the power-law scheme with a penalty exponent, some researchers applied the analytical bounds on materials properties (such as Hashin and Shtrikman (1963) bounds), as the interpolation scheme (Zhou and Li, 2008d). Hence the necessity for determination of penalty exponent is circumvented.

For finite elements' based structural optimization, there are several solution algorithms (Coville, 1968, Asaadi, 1973, Schittkowski et al., 1994, Chen et al., 2001). Two numerical approaches that are frequently used in conjunction with the SIMP method, namely the "Method of Moving Asymptotes", and "Optimality Criteria methods" are briefly introduced here.

#### **2.1.4.1 Method of Moving Asymptotes (MMA)**

The MMA was originally introduced by Svanberg (1987) as a further advancement to "Sequential Convex Programming" (Fleury, 1979). To illustrate the method, suppose the following optimization problem statement:

Minimize:  $f_0(\mathbf{x})$

Subject to:  $f_j(\mathbf{x}) \leq \bar{f}_j \quad j=1, \dots, m$  (2.11)

$$0 < x_{\min} \leq x_i \leq 1 \quad i=1, \dots, n$$

in which  $f_0(\mathbf{x})$  is the implicit objective function and  $f_j(\mathbf{x})$  ( $j=1, 2, \dots, m$ ) are the implicit behavioral constraints; the general sequential solution consists of the following steps:

Step 1: Select the starting point  $\mathbf{x}^{(0)}$

Step 2: Calculate  $f_j(\mathbf{x}^{(t)})$  and  $\nabla f_j(\mathbf{x}^{(t)})$  for  $j=0, 1, \dots, m$

Step 3: Calculate approximate explicit functions of  $\tilde{f}_j(\mathbf{x}^{(t)})$  ( $j=0, 1, 2, \dots, m$ ) (see below)

Step 4: Calculate better approximation of the design variables

Step 5: If the solution is not converged go to Step 2; otherwise end

Several methods have been suggested for the approximation of the original functions in the neighboring points of  $\mathbf{x}^{(t)}$  in step 3 (Schmit and Farshi, 1974, Fleury and Braibant, 1986). For example, in the well-known “Sequential Linear Programming” or SLP the approximation function has a rather simple form of (Haug and C ea, 1981):

$$\tilde{f}_j^{(t)}(\mathbf{x}) = f_j(\mathbf{x}^{(t)}) + \sum_i \frac{\partial f_j}{\partial x_i} (x_i^{(t+1)} - x_i^{(t)}) \quad (2.12)$$

In the MMA, another linearization scheme is suggested which uses variables of the type  $1/(x_i - L_i)$  and  $1/(U_i - x_i)$ . The variables  $L_i$  and  $U_i$  are experimentally adjusted through iterations and are known as “moving asymptotes” (Svanberg, 1987, Schittkowski et al., 1994). The transformed sub-problem has the following form:

Minimize:

$$\tilde{f}_0^{(t)}(\mathbf{x}) = f_0(x^{(t)}) + \sum_{i=1}^n \left( \frac{p_{0i}^{(t)}}{U_i^{(t)} - x_i} + \frac{q_{0j}^{(t)}}{x_i - L_i^{(t)}} \right) - \sum_{i=1}^n \left( \frac{p_{0i}^{(t)}}{U_i^{(t)} - x_i^{(t)}} + \frac{q_{0i}^{(t)}}{x_i^{(k)} - L_i^{(t)}} \right) \quad (2.13)$$

Subject to:

$$\tilde{f}_j^{(t)}(\mathbf{x}) = f_j(x^{(t)}) + \sum_{i=1}^n \left( \frac{p_{ji}^{(t)}}{U_i^{(t)} - x_i} + \frac{q_{ji}^{(t)}}{x_i - L_i^{(t)}} \right) - \sum_{i=1}^n \left( \frac{p_{ji}^{(t)}}{U_i^{(t)} - x_i^{(t)}} + \frac{q_{ji}^{(t)}}{x_i^{(k)} - L_i^{(t)}} \right) < \bar{f}_j \quad j=1, \dots, m$$

$$\gamma_i^{(t)} < x_i < \min(L, \beta_j^{(t)}) \quad i=1, \dots, n$$

where:

$$p_{ji}^{(t)} = \begin{cases} (U_i^{(t)} - x_i^{(t)})^2 \frac{\partial f_j}{\partial x_i} & \text{if } \frac{\partial f_j}{\partial x_i} > 0 \\ 0 & \text{otherwise} \end{cases} \quad (2.14)$$

$$q_{ji}^{(t)} = \begin{cases} -(L_i^{(t)} - x_i^{(t)})^2 \frac{\partial f_j}{\partial x_i} & \text{if } \frac{\partial f_j}{\partial x_i} < 0 \\ 0 & \text{otherwise} \end{cases}$$

in which  $\gamma_i^{(t)}$  and  $\beta_j^{(t)}$  are the move limits that are correlated to the moving asymptotes. The solution to the above mentioned sub-problem can be performed using a dual method as described in (Svanberg, 1987). Numerical experiences show that the method allows a better approximation, in comparison with other convex procedures (Schittkowski et al., 1994). However the successful convergence of the procedure is dependent on the selection of the initial  $\mathbf{x}^0$  and the moving asymptotes. It may happen that the procedure does not converge (Schittkowski et al., 1994).

#### **2.1.4.2. Optimality criteria method**

The basic idea of Optimality Criteria (OC) for structural optimization was proposed by Michell (1904). Later on, the OC method has been developed as an alternative to mathematical programming approach. A historical survey on the method has been presented in (Rozvany, 1989). As opposed to mathematical programming methods which directly

maximize or minimize the objective functions, the OC tackles the problem indirectly through satisfying a series of intuitive or mathematical criteria (Hassani and Hinton, 1998c). An example of intuitive optimality criteria is the so-called “fully stressed” design in which the structure is deemed to be an optimum when its components are fully stressed. Mathematical criteria for OC methods are usually based on the Karush-Kuhn-Tucker (KKT) optimality conditions (Karush, 1939, Kuhn and Tucker, 1951).

The KKT conditions present the necessary criteria for the optimality of a solution in a non-linear programming. Supposing an optimization statement in the form:

$$\text{Minimize } f_0(\mathbf{x})$$

$$\text{Subject to: } f_i(\mathbf{x}) \leq 0 \quad i = 1, \dots, m \quad (2.15a)$$

$$\text{and } f_i(\mathbf{x}) = 0 \quad i = m + 1, \dots, n$$

$$x_{\min} \leq x_i \leq 1$$

It is assumed that the functions  $f_j(\mathbf{x})$  ( $j=0, \dots, m$ ) are differentiable at  $\mathbf{x}$  and also the gradients of the active constraints are linearly independent (such a point is also known as the regular point). In the case that  $\mathbf{x}^*$  is a local minimum, the KKT conditions state that there exist constants of  $\eta_i$  and  $\theta_j$  (known as dual variables) such that:

$$\nabla f_0(\mathbf{x}^*) + \sum_{i=1}^m (\eta_i \nabla f_i(\mathbf{x}^*)) + \sum_{i=m+1}^n (\theta_{i-m} \nabla f_i(\mathbf{x}^*)) = 0$$

$$f_i(\mathbf{x}^*) = 0 \quad i = m + 1, \dots, n \quad (2.15b)$$

$$f_i(\mathbf{x}^*) \leq 0 \quad ; \quad \eta_i f_i(\mathbf{x}^*) = 0 \quad , \quad \eta_i \geq 0 \quad i = 1, \dots, m$$

It should be pointed out that the irregular points that violate the conditions of KKT can also be local minima and the criteria does not state the sufficiency conditions of an optimal solution (Kamat, 1993).

### 2.1.5. Evolutionary Structural Optimization (ESO)

In 1993, Xie and Steven (1993) introduced an approach called Evolutionary Structural Optimization (ESO). It is based on the concept of gradually removing inefficient materials from the finite element model of the structure so that the topology of the structure develops gradually toward an optimum. Due to the simplicity of the approach, it gained great popularity since its primary introduction and has been the subject of extensive studies (Burns, 2002). Solving stiffness and displacement problems (Chu et al., 1996), dynamic analysis of structures (Xie and G.P.Steven, 1996, Zhao et al., 1997), buckling analysis (Manickarajah et al., 1998) or multi-criteria optimization (Proos et al., 2001) are examples of its continuous development. The Bi-directional Evolutionary Structural Optimization (BESO) is also considered to be an important development, resulting from the studies on ESO (Querin et al., 1998). Recently use of the ESO method has been extended into the design of microstructures for materials, to attain the desired thermal conductivity (Patil et al., 2008).

The failure of the structure happens when stress or strain on some elements exceed the maximum values. Inversely, low-stress or strain elements can be accounted as inefficient



materials. These two arguments imply that in an ideal structure, identical level of stress should exist in every element (Burns 2002). This concept leads to rejection criteria based on the stress level in elements. In the original stress-based ESO method (Xie and Steven, 1993), the criteria for removing elements was based on the level of Von Mises stress in the elements of the structure, which is a measure of average stress in the structure. In the plane stress problems, the Von Mises stress is expressed as:

$$\sigma_e^v = \sqrt{\sigma_{11}^2 + \sigma_{22}^2 - \sigma_{11}\sigma_{22} + 3\sigma_{12}^2} \quad (2.16)$$

The stress level in elements is determined by a finite element analysis. In the stress-based ESO the Von Mises stress of each element is compared to the maximum Von Mises stress of the structure  $\sigma_{\max}^v$ . At the end of each finite element analysis, the elements which satisfy the following condition are completely removed from the finite element model of the structure:

$$\frac{\sigma_e^v}{\sigma_{\max}^v} < RR^t \quad (2.17)$$

in which  $RR^t$  is the rejection ratio at the iteration  $t$ . The iterative procedure continues until there are no more elements to be removed from the structure which is known as a “steady state”. At the steady state, all elements in the structure will have a stress level that is higher than  $\sigma_{\max}^v \times RR^t$ . If it is necessary, at this stage the rejection ratio is increased, by the evolutionary rate ( $ER$ ) that is defined as an initial parameter in the ESO:

$$RR^{t+1} = RR^t + ER \quad (2.18)$$

After this increment, the same process is repeated, until the new steady state is reached. The procedure comes to an end when the structure attains the desired stress level; for instance when there are no more elements with the stress level less than 20% of the maximum stress. However, this may not be the absolute best solution and only in a few special cases can the fully stressed structure be attained (Burns, 2002).

Other criteria for removing elements can be based on the sensitivity numbers. The sensitivity number is a measure for the determination of the effects of individual elements on the variation of the objective function. For the compliance optimization, Chu et al. (1996) changed the elements removal criteria in the original ESO by applying the sensitivity of elements  $\alpha_i$ :

$$\alpha_i = \mathbf{u}_i^T \mathbf{K}_i \mathbf{u}_i \quad (2.19)$$

in which  $\mathbf{K}_i$  is the elemental stiffness matrix and  $\mathbf{u}_i$  is the displacement vector of the  $i^{th}$  element resulting from the finite element analysis of the structure. The optimization algorithm used in the compliance-based procedure is basically the same as the stress-based ESO. The only necessary modifications is the replacement of  $a_{max}$  and  $\alpha_i$  with  $\sigma_{max}^v$  and  $\sigma^v$  respectively. It should be mentioned that there are no noticeable discrepancies between the topologies obtained by stress-based ESO and the compliance-based approach (Li et al., 1999).

The first impression of the ESO is that the approach is based on the Optimality Criteria with the aim of satisfying some intuitive conditions which extremize the objective function. Tanskanen (2002) studied the theoretical bases of the compliance-based ESO and tried to

mathematically explain the validity of the approach. The study concludes that the ESO in fact minimizes the product of mean compliance and volume. If the design domain is modeled using equally sized elements, the ESO was considered to be similar to the Sequential Linear Programming (SLP) optimization method (Tanskanen 2002).

The numerical instability such as checkerboard pattern and mesh dependency (see section (2.1.7)) in the ESO, can be circumvented by devising a smoothing algorithm by averaging the sensitivity or stress of elements, with weighted values of surrounding elements (Li et al., 2001). The main advantage of ESO is its simplicity both in theory and application as a topology optimization approach. It can be easily implemented as a post processing algorithm to most finite element packages. Moreover, by gradually removing elements, the size of the finite element model decreases which make the approach less expensive. In addition, the resulting topology consists of a clear distinctive region without any gray area, which makes the interpretation of the results easier. However, in the ESO approach, if some elements of the structure have prematurely or mistakenly been removed from the structure, the recovery is not feasible (Zhou and Rozvany, 2001). To avoid these situations, with the ESO it is usually necessary to use very small evolutionary rate which makes the optimization costly.

### **2.1.6 Bi-directional Evolutionary Structural Optimization (BESO)**

With the goal of improving the search capability of the original ESO, the Bi-directional Evolutionary Structural Optimization (BESO) aims at simultaneously adding or removing elements from the finite element model of the structure. In the ESO, because the inefficient elements are completely removed from the structure, there is no information about the effects

of these elements on the objective function, in later stages of optimization. The general idea of the BESO is to devise a scheme to restore the deleted elements, if necessary. The BESO approach can be seen as a significant development that has resulted from studies on the ESO.

All of the BESO schemes that have been introduced so far apply the idea of ground structure (Dorn et al., 1964), in which its elements covers the whole design domain including solid and void regions. The BESO turns these elements on and off, but keeps the record of their geometrical information through the whole optimization procedure. The primary schemes on the improved ESO algorithm were suggested by Querin et al. (1998, 2000a, 2000b) and Yang et al.(1999) and further improvement by introducing the enhanced hard-kill (Huang and Xie, 2007b) and soft-kill BESO methods (Huang and Xie, 2009a).

#### ***2.1.6.1. Hard-kill BESO***

In contrast to the ESO which gradually removes the inefficient elements from the finite element model of the structure, the “Additive Evolutionary Structural Optimization” (AESO) has been developed with the aim of generating optimum structures by starting from a minimum ground structure and gradually adding elements to it (Querin et al., 1998,2000a). In this method, the elements are added around the free edges surrounding the most efficient elements. The most efficient elements are selected among the elements with highest stress or sensitivity numbers (Querin et al., 2000a). ESO has been combined with AESO in order to develop a BESO (Querin et al., 2000a). In each iteration, the numbers of added or removed elements are controlled by two given parameters, namely, the inclusion ratio (IR) and rejection ratio (RR) respectively.

In another BESO that has been introduced by Yang et al. (1999), the criteria for adding or removing elements was based on their effects on the variation of the objective functions. As mentioned before such effects are expressed by sensitivity numbers. For solid elements, the sensitivity number is calculated based on the results of structural analysis. For void elements the nodal displacement is calculated by extrapolating the nodal displacements of their surrounding solid elements. The sensitivity number of the void elements can then be calculated using these extrapolated nodal displacements. The procedure follows by the ranking of elements based on the magnitude of their sensitivities and switching to solid for elements with higher sensitivities and to void for elements with lower sensitivity numbers. Similar to the previous method, the numbers of removed and added elements are treated with different criteria, through introducing the rejection ratio and an inclusion ratio.

As it was discussed earlier, the optimization with a solid-void material distribution is an ill-posed problem. Such an optimization is dependent on the selection of the elements' sizes and discretization mesh (Bendsøe and Kikuchi, 1988). One drawback of these early approaches is that the numerical instability is not addressed properly and computational efficiency is low, due to the convergence problem (Rozvany, 2009, Huang and Xie, 2010b, 2010c). It has also been noticed that the best solution needs to be selected among several topologies that can be generated by varying  $RR$  and  $IR$  (enumeration method) (Huang and Xie, 2010b, Rozvany, 2009).

In 2007, Huang and Xie (2007b) developed a new algorithm for the hard-kill BESO, in which many issues such as a proper statement of optimization problem and numerical instability (see section 2.1.7) of the procedure has been addressed (Huang and Xie, 2010b). Suppose that the

aim of optimization is to find the stiffest structure under volumetric constraint. In the hard-kill

BESO setting the optimization problem statement is defined as:

$$\text{Minimize: } f(\mathbf{x})=K \quad (2.20.a)$$

$$\text{Subject to: } V^* - \sum_{i=1}^N V_i x_i = 0 \quad (2.20.b)$$

$$x_i = 0 \quad \text{or} \quad 1 \quad (2.20.c)$$

in which the design variable  $x_i$  indicates the absence (0) or presence (1) of the element in the model. In contrast to the SIMP approach here, the elements itself is considered as the design variable. Huang and Xie (2007b) have used a filtering scheme to extrapolate the sensitivity number of voids. The filtering is performed by using the following weighting equation

$$\hat{\alpha}_i = \frac{\sum_{j=1}^N w_{ij} \alpha_j}{\sum_{j=1}^N w_{ij}} \quad (2.21)$$

in which  $N$  is the total number of finite elements in structural model and  $\alpha_j$  is the calculated sensitivity number. The weight factor of  $w_{ij}$  is defined as:

$$w_{ij} = \begin{cases} r_{\min} - r_{ij} & \text{if } r_{ij} < r_{\min} \\ 0 & \text{otherwise} \end{cases} \quad (2.22)$$

in which  $r_{ij}$  denotes the distance between element  $i$  and element  $j$  centres. The filter radius of  $r_{min}$  is to identify the neighbouring elements that affect the sensitivity of element  $i$ . The sensitivity numbers of void elements are set to be zero initially, and then modified through the filter scheme. The addition and removal of elements is based on the ranking of elements, followed by switching elements to void for elements with lower sensitivity numbers and solid for elements with higher sensitivity numbers.

The above mentioned filtering scheme, together with incorporating the historical information of elemental sensitivities, has shown to be able to overcome a great deal of the numerical instabilities, which had been a controversial problem of the original versions (Huang and Xie, 2010b, Zhou and Rozvany, 2001, Rozvany et al., 2006, Rozvany, 2009). On the other hand the unified criterion for adding and removing elements, offers an explicit control over the volumetric constraint. The new hard-kill BESO also have a very high computational efficiency, as the results of the mentioned improvements, as well as the fact that the eliminated elements are not involved in finite element analysis (Huang and Xie, 2010b).

#### ***2.1.6.2. Soft-kill BESO***

In the hard-kill BESO, solid elements can only grow in the proximity of the existing elements, which in some cases may failed in rectifying the incorrect elemental rejection (Rozvany, 2001b, Zhu et al., 2007, Zhou and Rozvany, 2001). The complete removal of elements also may cause some theoretical predicaments, especially in multi-physics problems (Sigmund, 2001, Zhu et al., 2007, Huang and Xie, 2010b). An alternative approach can be the assigning of very small density for the void elements (Hinton and Sienz, 1995). The strain values of

these elements can then be directly calculated; hence the solid elements can grow in the desired regions of the structure away from existing solid regions (Zhu et al., 2007, Rozvany, 2001b).

Hinton and Sienz (1995) devised a fully stressed Bi-directional approach based on ESO, in which, instead of completely removing elements, they are replaced by elements with lower elastic modulus of the order  $10^{-6}$ . Zhu et al. (2007) developed a sensitivity based BESO method, in which the void elements are replaced by a microstructural system known as Orthotropic Cellular Microstructure (OCM). The OCM has a low density and in this approach for adding or removing elements, they are assigned as OCM's or solid elements respectively. The numerical stability is addressed through a scheme, to limit the number of connected solid elements along each principal direction (Zhu et al., 2007). However the convergence of both approaches encounter difficulties (Huang and Xie, 2010b).

In the soft-kill BESO proposed by Huang and Xie (2009a), the design variable  $x_i$  is limited to a minimum value  $x_{min}$  (e.g. 0.001). That means the void elements are not completely removed from the structure. Therefore the equation (2.20.c) is replaced by:

$$x_i = x_{min} \quad \text{or} \quad 1 \tag{2.23}$$

The Optimality Criterion for stiffness optimization is applied based on the sensitivity of elements with respect to the objective function. To improve the convergence of the procedure the effective property (for example Young's modulus in stiffness optimization) is determined through a power-law material interpolation scheme (Bendsøe, 1989):



$$E(x_i) = E_{(s)} x_i^p \quad (2.24)$$

in which  $E_{(s)}$  is the Young's modulus of the solid material. It is shown that by selecting the penalty exponent  $p$  large enough the convergence of the procedure considerably improves. The results obtained from the soft-kill BESO shows similarities to those of the hard-kill BESO (Huang and Xie, 2007b) which can be considered as the justification of the validity of hard-kill methodology (Huang and Xie, 2010b).

Although the new soft-kill BESO has been introduced very recently (Huang and Xie 2009a; 2010b), it has shown its capability for solving a wide range of shape and topology optimization problems with high computational efficiency. In the following chapters this methodology will be extended into the design of microstructures for materials.

### **2.1.7 Numerical issues in material distribution methods**

As discussed earlier, in general, the structural topology optimization through material distribution involves with discretizing a predefined domain into finite elements and devising a numerical procedure to find the element-wise design parameters. Such a procedure frequently encounters numerical instabilities that are categorized into “mesh dependency”, “checkerboard pattern” and “local minima” (Sigmund and Petersson, 1998). In the following subsections, these problems will be briefly addressed.

### ***2.1.7.1 Checkerboard pattern***

*Checkerboard pattern* refers to the situation where regions of alternating solid-void (strong-weak) elements are formed in some areas of the structure (Díaz and Sigmund, 1995, Petersson and Sigmund, 1998). Díaz and Sigmund (1995) and Jog and Haber (1996) have shown that the main cause of the checkerboard patterns lies in poor numerical modeling of the structure specifically when the low-order finite elements are used. In fact arranging 4-node elements in a checkerboard fashion would maximize the calculated strain energy density in elasticity problems (Díaz and Sigmund 1995); therefore, the checkerboard areas have larger stiffness due to numerical errors which prevents the algorithm to converge to the optimum solution (Sigmund and Petersson, 1998). The topology optimization approaches such as SIMP, ESO and BESO, based on material distribution are prone to such numerical instability.

It has been shown in 2D continuum structures' elasticity problems that the checkerboard pattern can be prevented by using 8 or 9-node finite elements (Jog and Haber, 1996, Díaz and Sigmund, 1995). This is attributed to the fact that the higher order elements have many more degrees of freedoms per design variable. This makes the numerical calculations more accurate. However, increasing the degrees of freedom makes the topology optimization procedure costly. In addition, when a large value of penalty exponent is used with the SIMP method, applying elements of higher order often does not yield a checkerboard-free result (Sigmund and Petersson, 1998). In addition, the technique may not be helpful with the ESO and BESO methods.

Inspired by the filtering scheme from image processing, Sigmund (1994b) implied a technique in combination with the SIMP topology optimization to overcome the checkerboard pattern. The filtering scheme modifies the design sensitivity of each element based on the weighted average of the element itself, as well as its neighboring elements (Sigmund and Petersson, 1998). Although the filtering scheme is a computationally efficient method, it usually weakens the effects of the SIMP method to eliminate the intermediate densities and results in blur boundaries (Zhou and Li, 2008b). Several other techniques have been purposed for solving this issue in the SIMP topology optimization. Heaviside projections algorithm (see next section) (Guest et al., 2004), nonlinear diffusion techniques (Wang et al., 2004a) and the phase field approach based on Cahn-Hilliard model (Zhou and Wang, 2007) are some of the these methods.

Recently an adaptive refinement approach was applied which uses an “analysis-mesh separated density field” for tackling the numerical instabilities and achieving an improved boundary description with SIMP (Wang et al. 2013). In this method, the design variables are defined on some points in the finite element model which are known as density points. By defining an interpolation scheme the density of these points are evaluated and restricted to be either 0 or 1. The approach uses an additional refinement procedure to identify and rectify the densities on the boundary regions. It is shown that the method enables the reduction in the number of design variables in the model, hence reduces the computational time of optimization.

As mentioned before, in relation to the sensitivity based ESO, Li et al. (2001) introduced a checkerboard suppression algorithm, based on the smoothing the sensitivities through a

filtering scheme. In the modified soft-kill BESO a similar filtering scheme has been applied which has been shown that efficiently suppresses the numerical instability of checkerboard pattern and mesh dependency. The details of this scheme will be discussed in the next chapters.

### ***2.1.7.2 Mesh dependency***

By using finer mesh sizes in topology optimization, it is expected that the same structure with better description of boundaries is attained. However the “mesh dependency” using finer mesh results in qualitatively different topologies with more members of smaller sizes (Bendsøe and Sigmund, 1999, Huang and Xie, 2010b). One of the reasons for such numerical problems is the so called *non-uniqueness* of the solution which means that there might be several optimum solutions with the same performance and structural weight or volume (Sigmund and Petersson 1998). Another source of this instability is the *non-existence* of the solution. In a solid-void topology optimization, it is known that the introduction of more void spaces into the structure provides higher stiffness and no closeness in the possible sets of solution could be found (Sigmund and Petersson 1998; Jog and Haber, 1996).

The *non-uniqueness* of the solution can be controlled, to some extent, by introducing the manufacturing performance constraint (Ambrosio and Buttazzo, 1993). On the other hand one way for solving the problem of the *non-existence* of solution is by *relaxation* as used in the Homogenization and the SIMP topology optimization approaches. However, because of the existence of composite regions (grey areas) in the final solution, the result of a relaxed formulation cannot be interpreted easily for manufacturing purposes (Sigmund and Petersson

1998). In many studies, the imposing of restrictions on the variation of design variables has been demonstrated as an efficient method for alleviating the mesh-dependency problem.

Restriction on variation of design variables can be imposed through different techniques. Many of these restriction techniques can also address the problem of checkerboard patterns as were discussed previously. As other examples of the restriction methods, Haber et al. (1996) proposed a method based on imposing constraints on the circumferences of the void regions and outer boundaries of the structure. In the SIMP approach, Bourdin (2001) used a technique in which the densities are filtered and regulated using a convolution operator. Wang and Wang (2005a) applied the bilateral filtering technique to solve the numerical instabilities in topology optimization. The bilateral filtering is a type of non-linear filtering scheme and has already been used in the image processing. Also the nonlinear diffusion technique has been developed by Wang et al. (2004a) based on a similar method for the image processing (Aubert and Kornprobst, 2006).

Recently, Heaviside filtering method has widely applied for suppressing the intermediate densities together with the SIMP approach. It has been developed by Guest et al (2004) in order to obtain 0/1 solutions. The original formulation of the method modifies the densities by a filtering scheme in the form of:

$$\hat{x}_i = \frac{\sum_{j=1}^N w_{ij} x_j}{\sum_{j=1}^M w_{ij}} \quad (2.25a)$$

in which  $x_j$  is the density of element and  $w_{ij}$  is a weighting function. The next step is to apply a smoothing function for instance in the form of:

$$\bar{x}_i = 1 - e^{-\alpha_i} + \hat{x}_i e^{-\tau} \quad (2.25b)$$

When  $\tau = 0$  the formulations act as an isotropic filtering which diffuses the mass linearly among surrounding elements. When  $\tau$  approaches infinity the element's density becomes  $\bar{x}_i = 1$  if  $\hat{x}_i > 0$  and will be equal to 0 otherwise. Therefore if an element is surrounded by other elements with a density higher than zero, its density will switch to 1 too. It can be seen that the method suppresses the checkerboard pattern and mesh dependency concurrently. For practical application however,  $\tau$  needs to be properly determined by the user experimentally; otherwise a stable convergence may not be attainable (Sigmund 2007).

### 2.1.7.3 Local optima

The occurrence of local optima in structural topology optimization refers to the situation where different solutions are obtained by changing the design parameters, such as move limits or evolutionary rate, geometry of the initial design, number of finite elements or filtering parameters and so forth. Mathematically, the function  $f(\mathbf{x})$  has a local minimum (maximum) at the point  $\mathbf{x}^*$  if  $f(\mathbf{x}^*) \leq f(\mathbf{x})$  (or  $f(\mathbf{x}^*) \geq f(\mathbf{x})$ ) for all  $\mathbf{x}$  in a small neighbourhood of  $\mathbf{x}^*$  and has a global minimum (or maximum) if the statement holds for all feasible points of  $\mathbf{x}$ . Structural topology optimization problems usually have many local optima and essentially are not convex. The flatness of the objective function in most topology optimization problems causes the algorithms to be unable to avoid a nearby solution and trap in local optima.

To solve this problem in procedures that use intermediate densities, the idea of the *continuation method* was introduced. Different procedures for the *continuation methods* have been proposed. For instance Allaire and Kohn (1993) proposed an approach in which in the first step of the optimization procedure, the intermediate densities are allowed in the structure by applying a low penalization factor and after convergence of the procedure they are penalized to earn a 0-1 solution. In a different approach Sigmund (1997) and Sigmund and Torquato (1997) used a filtering scheme with a large filtering size at the initial steps and gradually reducing filtering size. It should be mentioned that the concept of the continuation method is not mathematically coherent. Although the experimental application of the procedure may lead to better solutions, it still does not guarantee the earning of a global optimum (Sigmund and Petersson 1998).

## **2.2. Material modelling**

The responses of a composite material are different from its individual constituents. In the design of materials, the prediction of the macroscopic behaviour of materials with a large heterogeneous nature is a challenging issue (Markworth et al., 1995), and has a long history that even attracted the attention of luminaries such as Maxwell (1873) and Einstein (1906). In general, experimental tests and numerical methods are possible ways to evaluate the characteristics of composite materials (Beran 1965; Christensen 1979; Willis 1981;1992). However, the experimental tests are often prohibitive from the standpoints of time and cost, and are not appropriate in the design stage. The application of numerical methods to a media with large heterogeneities is also very hard and expensive, even by applying today's high-speed computers. As an example, suppose that the objective is the modelling of a 3D material

that consists of 1000 repeating units along each principal direction. Suppose that the topology of each unit is modelled by 25 elements along principal directions. The finite element model of such a structure will contain more than  $1.5 \times 10^{13}$  elements which makes the analysis impossible with most computers at this time.

The process of calculating effective properties of materials is also termed as "homogenization" (Suquet, 1987, Hollister and Kikuchi, 1992). Although the analytical solutions of the overall properties of materials are available for some cases where the material is composed of simple periodic microstructure (Sabina et al., 2001, Adams and Crane, 1984, Torquato and Donev, 2004, Zhou and Li, 2007), development of such analytical solutions would be very cumbersome for a microstructure with complicated arbitrary topologies. Therefore, attempts have been made by many researchers to establish empirical or numerical relationships between the properties of constituent phases and overall material characteristics. The developed methods are often based on the analysis made on the "representative volume element" (RVE) or a "repeating unit cell" (RUC).

The primary definition of the phrase RVE was made by Hill (1963) for referring to a sample volume that has two characteristics: (a) it is structurally typical of the whole domain on average and (b) it contains a sufficient number of inclusions so that the overall response of material is effectively independent of the imposed loads and displacements. On the other hand, the RUC characterizes periodic heterogeneous materials without being necessarily homogenous on a microstructural scale (Drago and Pindera, 2007). RVE and RUC concepts have been interchangeably used in literature (Drago and Pindera, 2007) and in this text are referred to simply as RVE, unless otherwise is emphasized.



Simplified RVE approaches such as “rules of mixtures” basically neglect the spatial distribution of the constituent phases within the microstructures. More advanced methods such as “Homogenization theory” or the “mechanics of material” usually decouple the analysis into two scales. Local scale analysis is performed to determine the physical properties of the microstructure. These local level analysis results are further used for the calculation of homogeneous material properties on a global scale (Hollister and Kikuchi, 1992). The accuracy of these approaches is largely dependent on the applied boundary conditions in modeling, as well as the ratio of RVE sizes to the global dimensions of the material domain (Hollister and Kikuchi 1992).

In the following sub-sections, some of the methods that are used for estimation of mechanical properties of materials are briefly reviewed. It should be mentioned that the topic of determination of the physical characteristics of materials has received significant attention and is a rapidly developing area of literature (Birman and Byrd, 2007). The list of references made here is by no means complete. The goal here is to identify and describe a simplified outline of some frequently used methods.

### **2.2.1 Rules of mixtures**

The term “rule of mixture” refers to the expressions that enable the estimation of the material properties based on the mechanical properties and volume fractions of constituent phases. The earliest method for the prediction of mechanical properties of composite materials dates back to the end of 19<sup>th</sup> century and beginning of 20<sup>th</sup> century by well-known “mixture rules” by

Voigt (1889) and Reuss (1929). The Voigt's rule of mixture is an arithmetic mean, which is expressed as (Fan et al., 1994):

$$P = P_1 f_1 + P_2 f_2 \quad (2.26a)$$

where  $P$  is the mechanical property of material and  $P_1, f_1, P_2$  and  $f_2$  are the properties and volume fractions of materials 1 and 2 respectively. Reuss' (1929) estimate is a harmonic mean in the form of:

$$\frac{1}{P} = \frac{f_1}{P_1} + \frac{f_2}{P_2} \quad (2.26b)$$

It can be shown that these simple rules define loose upper and lower bounds on material properties (Peiponen and Gornov 2006). The modified rule of mixture of Tamura *et al.* (1973), Wakashima *et al.* (1990) and later Teraki, *et al.* (1993), and the "generalized law of mixtures" of Fan, *et al.* (1994) are recent developments in these kinds of approximations. However these simplified approaches have limited validity (Fan et al., 1994).

### 2.2.2 Bounds on materials properties

In contrast to the rule of mixtures, bounds provide a theoretical range of the possible material properties. In the simplest forms, the bounds linearly or non-linearly combine the individual properties of the constituent phases, in terms of their volume fractions, to provide a proper estimation over the admissible range of composite effective properties (Zhou and Li, 2008a, 2008d). These limits were derived mainly based on the variational method and have been

developed for various scenarios (Gibiansky, 1993). The bounds have been an important theoretical tool for the development of new composites over the last decades. They are frequently used for the verifications of the optimality of materials microstructures (Challis et al., 2008, Zhou and Li, 2008a, 2008d).

The earliest known bounds on composites effective permittivity was proposed by Wiener (Peiponen and Gornov, 2006), which had the simple form of Voigt's (1889) approximation for upper limit and Reuss' (1929) approximation for the lower limit of the composite properties (equations (2.26)). Later, with the help of the variational principals, tighter bounds on effective magnetic permeability of macroscopically isotropic and homogenous multiphase materials were proposed by Hashin and Shtrikman (1962) (Figure 2.2). Due to the mathematical analogy, these bounds are also applicable to the estimation of other characteristics of materials, such as electrical and thermal conductivity.

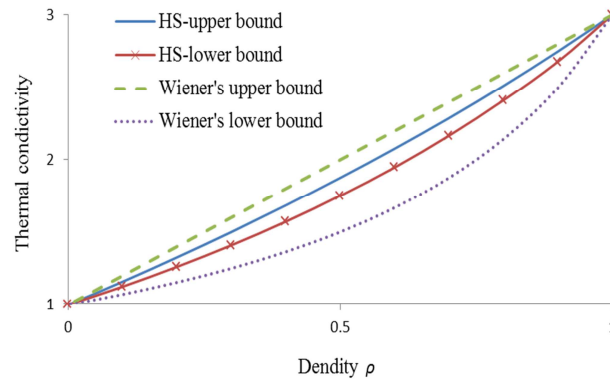


Figure 2.2: Comparison between Wiener's and Hashin-Shtrikman bounds on thermal conductivity of materials

The Hashin-Shtrikman bounds are known as the best possible bounds of an isotropic two-phase material, if no structural information apart from the volume fractions is available (Hale, 1976). Later on, Hashin-Shtrikman extended the methodology for the estimation of the possible range of elastic moduli for macroscopically quasi-homogenous quasi-isotropic multi-phase material with well-ordered constituent phases  $(K_{(1)} - K_{(2)})(G_{(1)} - G_{(2)}) \geq 0$ , where  $K$  and  $G$  are the bulk and shear modulus respectively and subscripts indicate the materials number (Hashin and Shtrikman, 1963). Walpole (1966) developed a similar variational method and derived bounds that did not require any phase ordering. For the composites with well-ordered constituent phases, the Walpole bounds are equivalent to the Hashin-Shtrikman bounds. As indicated by Gibiansky and Sigmund (2000) the Hashin-Shtrikman and Walpole bounds on the bulk modulus are not only valid for isotropic materials but also applicable for materials with square symmetry (in 2D cases) and cubic symmetry (in 3D cases). Milton and Kohn (1988) used variational principals for deriving the bounds of the effective elasticity moduli and the effective conductivity for anisotropic materials. These theoretical bounds have demonstrated their validity in many cases (Cherkaev and Gibiansky, 1993, Gibiansky, 1993).

Although further advancements made the bounds tighter, improved bounds are only provided with a G-closure rather than an exact value (Zhou and Li, 2008a, 2008d). The G-closure or GU-set is the set of the effective properties of all the composites that can be manufactured by combining the arbitrary amounts of the constituent phases (Gibiansky, 1993). On the other hand, the establishment of a relationship between different effective characteristics of composite materials is important, especially when one property of composite is known and the intension is to estimate the possible ranges for other characteristics (Gibiansky and Torquato, 1996a). Such cross-property bounds are also useful in the design of multi-

functional materials (Cadman et al., 2013), and frequently used for verifications of the optimality of the materials' microstructures (Challis et al., 2008).

Cross-property relationships have been the subject of extensive investigation (Milton, 1984, 1997, Berryam and Milton, 1988, Milton and Kohn, 1988, Torquato, 1991, Cherkaev and Gibiansky, 1993, Gibiansky and Torquato, 1996a, 1996b, 1995, Dominguez and Sevostianov, 2011) . For example, using the classical variational method, Milton (1984) derived cross-property bounds for two-phase isotropic materials that link the conductivity and bulk modulus. Later on, Gibiansky and Torquato (1996a) used the translation method to develop similar cross-property bounds for 3D two-phase isotropic or cubic-symmetric composites.

As mentioned before, in addition to the properties and volume fraction of the constituent phases, the effective properties of the composites depend strongly on their microstructural geometries (Gibiansky, 1993). However, except for especial cases, the bounding methods generally disregards the microstructural configurations and provides only a theoretical range for the physical properties of a composite which with given volumes could be achieved (Zhou and Li, 2008d).

### **2.2.3. Self-consistent methods**

The self-consistent methods estimate the effective material properties by analyzing the representative volume element (RVE) of materials. Therefore the microstructural geometry has a greater role in the overall estimation of material properties. These methods, which are also known as “effective-medium” methods (Torquato, 2000), include a number of approaches that analyze RVE as an initially homogeneous matrix into which, inclusions of

other materials are incorporated. The basic assumption is the equilibrium of stress in inclusion ( $\sigma^I$ ) with the stress within matrix ( $\sigma^M$ ) plus a deviation due to presence of inclusion, which is known as polarization stress ( $\sigma^P$ ) (Nemat-Nasser et al., 1982):

$$\sigma_{mn}^M + \sigma_{mn}^P = \sigma_{mn}^I \quad (2.27)$$

It is also assumed that the total strain in the composite material at any point, is a summation of the strain that exist in the homogenous matrix  $\epsilon^M$  plus a deviation  $\epsilon^D$  that is induced due to the embedment of the inclusion in the matrix. By assuming  $\mathbf{E}^M$  and  $\mathbf{E}^I$  as stiffness tensor of matrix and inclusion phases respectively, the equilibrium equation can be expressed as:

$$E_{mnkl}^M (\epsilon_{kl}^M + \epsilon_{kl}^D + \epsilon_{kl}^P) = E_{mnkl}^I (\epsilon_{kl}^M + \epsilon_{kl}^D) \quad (2.28)$$

The difference between various self-consistent methods is the relationship that is established between the transformation strain  $\epsilon^P$  and the deviation strain  $\epsilon^D$  to solve the above equilibrium equation. For instance, the simplest assumption is to neglect any interaction between nearby inclusions (particles), which is valid when the volume fraction of the particles approaches zero, while the volume fraction of matrix phase get close to unity. Such conditions are known as “dilute approximation” (Zuiker, 1995) and its formulation was proposed by Eshelby (1957). For the cases in which the particles have spherical shapes, the expressions for the estimation of bulk modulus and the shear modulus of elasticity are suggested as (Christensen, 1979):

$$K = K_1 + \frac{f_2(K_2 - K_1)(K_1 + (4/3)G_1)}{(4/3)G_1 + K_2} \quad (2.29)$$

$$G = G_1 - \frac{15f_2G_1(1-\nu_1)(G_1 - G_2)}{7G_1 - 5\nu_1G_1 + (8-10\nu_1)G_2} \quad (2.30)$$

In which  $K$ ,  $G$ ,  $\nu$  and  $f$  are the bulk modulus, shear modulus, Poisson's ratio and volume fraction respectively; subscripts 1 and 2 refer to the matrix and inclusion respectively.

The self-consistent method has been the subject of a significant amount of research (Budiansky, 1965, Hill, 1965, Christensen and Lo, 1979, Nemat-Nasser et al., 1982, Benveniste, 1987, Walpole, 1969, Reiter et al., 1997), and has been developed for the estimation of composite properties under different scenarios. For example, Walpole (1969) studied the case where the matrix was embedded by aligned or randomly distributed inclusions of a/the needle shape (e.g. short fibres). As another example, the disc shape inclusions (e.g. flakes) have been studied by Reiter *et al.* (1997). Hashin and Shtrikman (1962) had also used the concept of polarization stress in combination with the variational principles, to derive bounds on composites properties where spherical inclusions exist (Hashin, 1983). The studies on the self-consistent method have also paved the way toward the development of another semi-analytical modelling approach namely the Mori-Tanaka method which is suitable for composites with moderate inclusion volume fraction (Mori and Tanaka, 1973, Hollister and Kikuchi, 1992).

The self-consistent method offers some advantages in terms of the simplicity of the solution expressions. However, as mentioned before, the self-consistent method can only be applied

where an inclusion phase with specific shape is inserted into the matrix. Thus the final expressions for the estimation of effective properties are dependent on the constituent materials properties, as well as the topology of the embedded inclusion. It has been shown that when the constituent phases of the composite have large discrepancies in properties, the accuracy of the method decreases (Christensen, 1979, Torquato, 1998). On the other hand, different analytical solutions need to be developed for composites with different inclusion shapes. For a proper approximation of material characteristics through this method, it is necessary for the material's microstructure to have a certain type of '*topological symmetry*' (Torquato 1998; 2000). Analytical dependency of the approximation, on the properties and topology of the constituent phases, is a prohibitive factor for the implementation of the method into a numerical procedure.

#### **2.2.4. Mechanics of materials approaches**

In a number of studies either an analytical or finite element method has been used on RVE, to evaluate the material properties simply based on the mechanics of materials principals (Gibson and Ashby, 1982, Huber and Gibson, 1988, Gibson and Ashby, 1997, Beaupre and Hayes, 1985, Christensen, 1986, Steven, 2006). In these approaches, RVE is analyzed under the test loading fields and the overall properties of materials are estimated based on the response of the structure. For example, three independent traction fields in 2D elasticity problems and six independent traction fields in 3D problems are applied on the boundaries of RVE. Alternatively, RVE can be subjected to independent cases of boundary displacement fields. The tractions or displacements are usually imposed uniformly on the boundaries (Figure 2.3) (Hollister and Kikuchi, 1992):



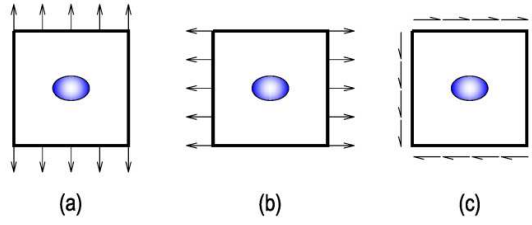


Figure 2.3: Uniform boundary conditions applied to the 2D RVE (a),(b) normal and (c) shear stresses tractions

The average stress ( $\bar{\sigma}_{ij}$ ) or average strain ( $\bar{\epsilon}_{ij}$ ) in RVE are defined by the average of the stress or strain tensors over the volume of RVE:

$$\bar{\sigma}_{ij} = \frac{1}{V} \int \sigma_{ij} dV \quad (2.31)$$

$$\bar{\epsilon}_{ij} = \frac{1}{V} \int \epsilon_{ij} dV \quad (2.32)$$

It can be easily shown that the above equations ensure the equivalence of strain energy between equivalent homogenous materials defined as:

$$U = \frac{1}{2} \bar{\sigma}_{ij} \bar{\epsilon}_{ij} V \quad (2.33)$$

and the original heterogeneous material represented by the RVE (Sun and Vaidya, 1996):

$$U' = \frac{1}{2} \int_V \sigma_{ij} \epsilon_{ij} dV \quad (2.34)$$

The average quantities of equations (2.31) and (2.32) can be calculated directly from the results of finite element analyses. However, a more computationally efficient way is to correlate the average stress or strain to the boundary tractions or displacements respectively. Using the Gauss theory by converting the volume integrals to surface integrals one can write:

$$\bar{\sigma}_{ij} = \frac{1}{V} \int_V \sigma_{ij} dV = \frac{1}{2V} \oint_S (t_i n_j + t_j n_i) dS \quad (2.35)$$

$$\bar{\varepsilon}_{ij} = \frac{1}{V} \int_V \varepsilon_{ij} dV = \frac{1}{2V} \oint_S (u_i n_j + u_j n_i) dS \quad (2.36)$$

in which  $\mathbf{t}$  or  $\mathbf{u}$  are the imposed boundary traction or displacement respectively;  $n$  denotes RVE local coordinates and  $V$  is the volume of RVE. Suppose that for producing the average stress  $\bar{\sigma}_{kl}$ , the RVE is under boundary traction fields  $t^{kl}$  that produce the microstructural strains of  $\varepsilon_{mn}^{kl}(\mathbf{u})$ . It can be shown that the following equilibrium equation needs to be solved (Hollister and Kikuchi 1992):

$$\frac{1}{2} \int_S t_i^{kl} v_i dS = \frac{1}{2} \int_V E_{ijmn} \varepsilon_{ij}(\mathbf{v}) \varepsilon_{mn}^{kl}(\mathbf{u}) dV \quad (2.37)$$

in which  $\mathbf{E}$  is the stiffness tensor of RVE constituent material;  $\mathbf{v}$  and  $\varepsilon_{ij}(\mathbf{v})$  are virtual displacement and virtual strain, respectively. The effective stiffness tensor  $\mathbf{E}^H$  is calculated as (Hollister and Kikuchi 1992):

$$E_{ijkl}^H = \frac{1}{V} \int_V E_{ijmn} R_{mnkl} dV \quad (2.38)$$

where the local tensor  $\mathbf{R}$  defines the relationship between average and microstructural total strain:

$$\boldsymbol{\varepsilon}_{ij}^{kl} = R_{ijmn} \bar{\boldsymbol{\varepsilon}}_{mn}^{kl} \quad (2.39)$$

As previously stated, in the mechanics of materials' approaches, it is necessary to analyze the response of RVE under either the displacement or traction test fields. It is known that, if the actual in-situ boundary conditions are different from the assumed ones, each of these test fields will yield different bound on the predicted stiffness. If RVE is analyzed under applied uniform displacement, through the principles of minimum strain energy it can be shown that the predicted stiffness is higher than in-situ case. Similarly, when the boundary conditions are applied in the form of uniform traction a lower stiffness is predicted, as it can be proved through the principals of minimum complementary energy (Hollister and Kikuchi 1992).

In the case of materials with periodic base cells it can be shown that increasing the modeled RVE size, in such a way that it encompasses larger numbers of periodic base cells, can increase the accuracy of predicted overall material properties. According to the St. Venant's principle (Fung, 1965), when the RVE size is increased the boundary layer effects diminish and hence it enables the approach to yield a better estimation. Nevertheless, for the periodic cellular material with the RVE size to the global size ratio of 0.2, Hollister and Kikuchi (1992) has shown that the predicted local strain energy by the mechanics of materials' approaches may differ from direct analyses by more than 70%. Moreover, modeling a larger RVE increases the computational cost of the finite element analysis.

### 2.2.5. Homogenization theory

If a heterogeneous composite possesses certain types of regularity, its properties can be estimated by an equivalent material model, with the help of the theory of Homogenization. Homogenization is a rigorous mathematical theory which emerged in the 70's from the studies on partial differential equations with rapid varying coefficients. Since then, the theory has been the subject of large amount of research (Benssusan et al., 1978, Lions, 1981, Hassani and Hinton, 1998a, 1998b, 1998c).

The theory assumes that the composite is made of the repetition of 'microscopic' cells known as the periodic base cell (PBC). It is also assumed that due to existence of periodic microstructures, the response fields vary on multi-scales. The physical properties of such a periodic medium should be able to be defined by the following type of functions,

$$F(z_1 + m_1 Y_1, z_2 + m_2 Y_2, z_3 + m_3 Y_3) = F(z_1, z_2, z_3) \quad (2.40)$$

where  $\mathbf{z} = (z_1, z_2, z_3)$  is the position vector,  $\mathbf{Y} = (Y_1, Y_2, Y_3)$  is the constant vector that represents the period of the medium, and  $m$  denotes the arbitrary integers;  $\mathbf{F}$  can be scalar, vectorial or tensorial function. As per assumptions of the theory, the period  $\mathbf{Y}$  should be much smaller than the overall dimensions of the medium domain. In such circumstances it can be assumed that all quantities have two explicit dependencies on the macroscopic  $\mathbf{x}$  and the microscopic level

$$\mathbf{y} = \mathbf{z}/\eta \quad (2.41)$$

where  $\eta$  is a very small number. Equation (2.41) suggests that quantities on a local level, like stress and strain vary  $1/\eta$  times more rapidly than global level. The theory uses the asymptotic expansion to derive the composite response. By assuming  $\varphi^\eta(x)$  as the exact value of the field function, its asymptotic expansion would have the following expression

$$\varphi^\eta(x) = \varphi^0(x, y) + \eta\varphi^1(x, y) + \eta^2\varphi^2(x, y) + \dots \quad (2.42)$$

where  $\varphi^0$  can be described as the average value of the function, while  $\varphi^1$  and  $\varphi^2$  as perturbations (Hollister and Kikuchi, 1992) which take equal values on the opposite sides of the parallel-piped base cells (Hassani and Hinton, 1998a). It can be shown that in general elasticity problems, the first term on the expansion  $\varphi^0$  is only dependent on the macroscopic scale  $\mathbf{x}$  (Hassani and Hinton, 1998a). This imposes self-equilibrating restrictions on possible applied tractions on the boundaries of the periodic base cell.

Using the double scale asymptotic expansion and by imposing the periodicity on the microstructure boundary conditions, it can be shown that the homogenized elasticity tensor of composite materials can be calculated as:

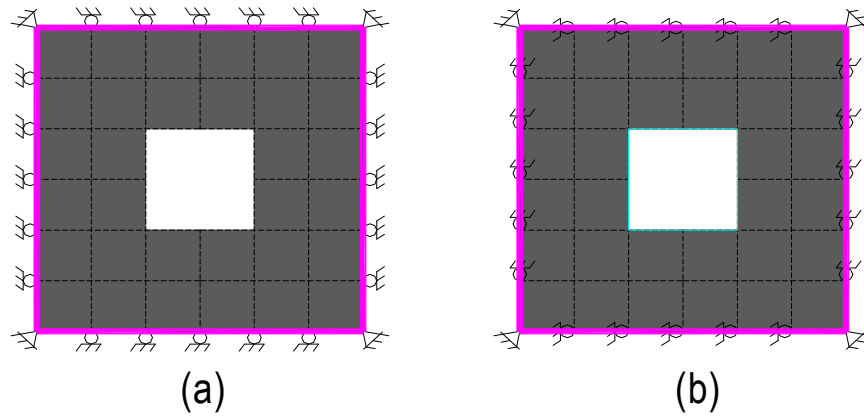


Figure 2.4: Boundary Conditions in 2D problems; (a) Under longitudinal strains fields (i.e.  $\epsilon_0^1 = [1, 0, 0]^T$ ,  $\epsilon_0^2 = [0, 1, 0]^T$ ); (b) Under shear strain field ( $\epsilon_0^3 = [0, 0, 1]^T$ )

$$E_{ijkl}^H = \frac{1}{V} \int_{\mathcal{V}} (E_{ijkl} - E_{ijpq} \frac{\partial \zeta_p^{kl}}{\partial y_q}) dV. \quad (2.43)$$

in which  $\zeta$  is the solution of:

$$\int_{\mathcal{V}} E_{ijpq} \frac{\partial \zeta_p^{kl}}{\partial y_q} \frac{\partial v_i(\mathbf{y})}{\partial y_i} dV = \int_{\mathcal{V}} E_{ijkl} \frac{\partial v_i(\mathbf{y})}{\partial y_i} dV \quad \forall \mathbf{v} \in \mathcal{V} \quad (2.44)$$

where  $V$  denotes a rectangular parallel-piped in  $\mathbf{R}^3$ , with its solid part indicated as  $\mathcal{V}$ .

In contrast to the mechanics of material approaches, in Homogenization theory the difference between average field behavioral responses under admissible and actual boundary conditions is smaller when  $\eta \rightarrow 0$  (Tyrus et al., 2007). Detailed error bounds are mathematically available for the Homogenization theory approach (Zhikov et al., 1979). It can be shown that

the average field behavioral response  $\phi^0$  converges to the corresponding macroscopic asymptotic expansion  $\phi^n$  as (Bakhvalov and Panasenko, 1989, Hollister and Kikuchi, 1992):

$$\|\phi^n - \phi^0\|_{L^2} \leq c\eta^j \quad (2.45)$$

where  $j$  and  $c$  are the order of retained terms of asymptotic expansion and a constant value respectively and  $L^2$  is the function space of the norm. The above equation indicates that the accuracy of results from the Homogenization theory increases when the microstructural length scale with respect to the global sizes of material body decreases.

In elasticity problems by applying periodical boundary conditions, the deformations in all PBCs are assumed to be identical. This is an accurate assumption for elements away from the external boundaries of the material body, but has less accuracy for elements near the boundaries. For cellular materials with periodic microstructure, Hollister and Kikuchi (1992) compared effective stiffness and local strain energy distributions obtained by applying the Homogenization theory and the mechanics of materials approaches. It was shown that with  $\eta = 0.2$ , the Homogenization theory predicted local strain energy may differ from the direct analysis within 30%. The study indicates that for periodic materials, the Homogenization theory gives a more accurate estimation of effective properties than mechanics of materials' approaches and also provides higher computational efficiency.

### **2.3. Application of structural topology optimization techniques in material design**

It is not more than two decades since the structural topology optimization has been primarily introduced for the systematic design of materials (Sigmund 1994a; 1994b). Since then, the methodology has been the subject of a considerable amount of research, in terms of either applying different topology optimization technique in the procedure or extending the methodology to various material design scenarios. In this part some of these advancements are introduced.

#### **2.3.1. Design of materials with extreme or prescribed properties**

Design of materials with extreme properties is considered as an important objective of material science (Sigmund, 2000). Materials with extreme stiffness, in the forms of bulk or shear modulus of elasticity, thermal conductivity, thermal expansion, permeability and permittivity, are examples of usual objectives of material design. On the other hand, the simplest form of structural topology optimization is to extremize some physical properties of structure.

As pointed out before, Sigmund applied the SIMP method for the design of materials with extreme or prescribed elasticity properties (Sigmund, 1994b, Sigmund and Torquato, 1997, Gibiansky and Sigmund, 2000). In this approach, it is assumed that the material is composed of repeating unit cells, also known as periodic base cells (PBC), with the dimensions that are much less than the characteristic length scales of the macroscopic structural body, but much larger than their atomic dimensions. In such circumstances the periodic microstructures of materials are modelled as 2D or 3D trusses or a continuum structure where the areas of the bar



elements in truss-like base cells or the thicknesses of elements in continuum-like materials, are defined as design variables (Torquato, 2000, Bendsøe and Sigmund, 2003). With the help of Homogenization theory, the physical characteristics of the base cells can be correlated to the overall properties of material. The topology optimization is used to determine the best material distribution in order to extremize the objective function. In the SIMP setting, the mathematical problem statement for the maximization of bulk modulus is defined as:

Maximize:  $f(\mathbf{x})$

$$\text{Subject to: } V^* - \sum_{i=1}^N V_i x_i = 0 \quad (2.46)$$

$$0 < x_{min} \leq x_i \leq 1$$

For instance, for designing 3D materials with maximum bulk modulus the objective function in terms of homogenized stiffness tensor  $E_{ijkl}^H$  is usually formulated as (Cadman et al., 2013):

$$f(\mathbf{x}) = \frac{1}{9} \left( \sum_{i,j=1}^3 E_{ijij}^H \right) \quad (2.47)$$

For the designing of materials with prescribed properties, the common approach is to define the objective function as the square of difference between the homogenized stiffness tensor  $E_{ijkl}^H$  and the prescribed tensor  $E_{ijkl}^*$  (Sigmund 1994a;1995; Cadman et al., 2013).

$$f(\mathbf{x}) = \sum_{i,j,k,l=1}^3 \delta_{ijkl} (E_{ijkl}^H - E_{ijkl}^*)^2 \quad (2.48)$$

where  $\delta_{ijkl}$  is the weighting factor.

Design of materials with extreme thermal expansion (Sigmund and Torquato, 1997), maximum bulk and shear modulus of elasticity (Gibiansky and Sigmund, 2000, Neves et al., 2000, Sigmund, 2000), negative Poisson's ratio (Sigmund 1994a; 1995) and extreme thermal conductivity (Zhou and Li, 2008a) are some other examples of the optimization of Microstructures for materials with the SIMP approach.

As stated before, the SIMP suffers from the disadvantage of the existence of grey elements in the final topology. Therefore, the final topology cannot be readily used for manufacturing. Seeking more computationally efficient approaches, many researchers applied other topology optimization techniques for design of materials, with the similar procedure described above. For example, Zohdi (2002) applied the Genetic Algorithm for the design of the microstructures' of materials with prescribed effective responses. In this approach the microstructural variables are defined in the form of genetic strings and the fittest microstructural design parameters are found. Wang et al. (2004b) used the Level-set topology optimization algorithm for the design of heterogeneous microstructures of materials to minimize the least squares differences between homogenized and prescribed elastic and/or thermo-elastic properties of materials. The Level-set represents the unit cells with interfacial boundaries, which is an advantage in comparison with the SIMP method. In another study, sensitivity-based ESO is applied for attaining microstructures of materials with prescribed thermal conductivity (Patil et al., 2008). The objective function is formulated for minimizing the least square of the difference between the prescribed and homogenized value of thermal conductivity subject to the volume constraint.

### 2.3.2. Design of multi-phase composites

In comparison with periodic cellular materials, with microstructures composing of one material phase and a void phase, composites with two or more material phases are more favourable and attractive for practical application. One of the reasons for such advantageous properties is that, by combining different materials, a wider range of properties could be achieved which are not attainable by individual phases. In fact, it is mathematically shown that increasing the number of constituent phases of the composite will widen the G-closure (Zhou and Li, 2008a). On the other hand, multi-functional materials are inevitably composites of two or more constituent phases (Gibson, 2010). Therefore the development of multi-phase composites provides the basis for development of materials with combined functional properties.

The SIMP method is used for the design of 2D periodic microstructures for composites with two material phases and a void phase (Gibiansky and Sigmund, 2000). The objective functions were the extremization of bulk modulus and thermal conductivity (Gibiansky and Sigmund 2000) or the thermal expansion (Sigmund and Torquato, 1997). The key point in these studies was the introduction of three design variables  $x_i^{(1)}$ ,  $x_i^{(2)}$  and  $x_i^{(3)}$ , for each element  $i$  that corresponds to three constituent phases. The design variables are defined in the interval of ]0, 1], with the following condition (superscript in parentheses denotes the phase numbers):

$$x_i^{(1)} + x_i^{(2)} + x_i^{(3)} = 1 \quad (2.49)$$

The above assumption makes it possible to define a simple artificial mixture function to correlate the local stiffness or thermal strain tensors of the element  $i$  with the design variables. For instance, in the case of designing microstructures with two material phases (phases 2 and 3) and one void phase (phase 1), the relationships between design variables  $x_i$ , and the elements of local stiffness tensor are defined as:

$$E_{ijkl}(x) = (x_i^{(23)})^p [(1 - (x_i^{(3)})^q) E_{ijkl}^{(2)} + (x_i^{(3)})^q E_{ijkl}^{(3)}] \quad (2.50)$$

where  $x_i^{(23)} = x_i^{(2)} + x_i^{(3)}$ ; the penalty exponents of  $p$  and  $q$  are introduced to prevent intermediate densities. The mixing rule for two materials and void mixture proposed by (Sigmund and Torquato 1997) is a combination of the classical Voigt's mixing rule for two solid materials and the power-law interpolation between the void phase and other (i.e.  $q=1$  and  $p>1$ ). However, as it is mentioned in Swan and Kosaka (1997), by using the Voigt's mixing rule, the phase separation does not happen appropriately in the final result. A formulation that uses hybrid combinations of the classical Reuss' and Voigt's mixing rules was proposed by Swan and Kosaka (1997), but it may not provide an accurate constitutive model of mixtures. Gibiansky and Torquato (1996b) used the power-law mixing rules for all phases in the multi-phase material design. The penalty exponents are taken equal to 3 ( $p=q=3$ ) (Gibiansky and Sigmund, 2000) at the beginning of the procedure to prevent the algorithm to trap in local optima. The penalty exponents are then gradually increased, to make intermediate densities uneconomical in a process known as "continuation method" (Bendsøe and Sigmund, 2003).

Nevertheless, as an inherent problem with the SIMP, such density-based method leads to intermediate (grey) densities in the final topology. In comparison with microstructures designed with one materials and a void phase, in multi-phase materials with closer physical properties, the SIMP usually causes more ambiguity in interpretation and identification of the boundaries and increasing the penalty values not only cannot solve the problem completely, but it may also result in numerical instability (Kohn and Strang, 1986, Swan and Kosaka, 1997, Zhou and Wang, 2007).

On the other hand, the application of optimality criteria (OC) causes numerical instability in multiphase topology optimization scenarios (Yin and Yang, 2001, Zhou and Li, 2008a). Zhou and Li (2008a) applied the Sequential Linear Programming (SLP) for the design of multiphase microstructures of materials. As mentioned before, the SLP solves the minimization problem sequentially, by approximating the objective and constraint functions using the first-order Taylor series. Although the application of SLP ensures a stable linearized procedure, numerical experience has shown that the move-limit for the design variables should be kept fairly small (Fujii et al., 2001) and that there may be some difficulties in convergence (Zhou and Li, 2008a). In the above studies, the procedure typically needed around 8000 iterations for a  $60 \times 60$  discretization elements model, including some interactions by the user (Sigmund and Torquato, 1997). Therefore the design process is not fully automatic and cost efficient.

In another study, Zhou and Wang (2007) applied a phase field model for compliance minimization of multi-phase structures based on Cahn-Hilliard theory (Cahn and Hillard, 1958). The introduced phase field is a model that enables interpretation of interface between

material constituent phases based on Cahn–Hilliard partial differential equations which deal with the dynamics of phase changes. By using a variational method, the topology optimization problem is transformed into a problem of solving a set of partial differential equations. In addition to mathematical complexity, the main disadvantage of the procedure is its time consumption. For example the topology design of a 2D cantilever beams may need 200,000 iterations (Zhou and Wang, 2007).

Zhou and Li (2008a) developed a method for the design of multi-phased periodic microstructures of materials for extremal conductivity. Although a similar density-approach has been applied, several modifications have been made to improve the abovementioned SIMP procedure. To make the design problem self-weighted, instead of using the SIMP interpolation scheme, the HS bound has been used for interpolation. Thereby the need for choosing the penalty factor is alleviated. In addition, due to the above mentioned numerical issues in applying the optimality criteria (OC) and SLP, an approach based on the Methods of Moving Asymptotes (MMA) has been applied. It has shown that it would result in faster convergence and more numerical stability. To reduce the blurring effects in the boundaries of constituent phases, a method based on non-linear diffusion (discussed in Chapter 6) has been adopted. However, the method is still unable to completely remove the grey areas that form the boundaries of the constituent phases.

A generalized new BESO has been developed which utilizes a material interpolation scheme, with penalization and which is capable of optimization of continuum structures with multiple material constituents (Huang and Xie, 2009b, Huang and Xie, 2010b). One of the advantages of the method is that the procedure is independent of the selection of the penalization factor.

Better convergence of the procedure together with high computational efficiency and more importantly the capability of the new BESO in separating the constituent phases, have made BESO a promising tool for topology optimization of structures with multiple materials (Cadman et al., 2013).

### **2.3.3. Design of materials with extra functionality**

Multi-functional performance objectives play a significant role in demand and development of composite materials in industry. The traditional design method for developing such structural systems is by combining components that provide the desired functional properties separately. The load-carrying framework is connected with different add-on components, to improve the non-structural performance characteristics such as electrical and thermal conductivities, resulting in sub-optimal systems. Hence, the development of multi-functional composite materials stems from the desire to develop integrated systems.

In the design of materials via inverse homogenization, Sigmund (1994a, 1995) used the concept of the Lagrangian multiplier to add the constraint function to the objective function. In these problems, the weight of the material is defined as the cost function to be minimized and six prescribed constitutive parameters are considered as constraints. The procedure enables a precise control over constraint values. However, the weight of material cannot be considered as a functional property. There is also no report, at the time of publishing, of the use of this concept in material optimization for two substantially different functional properties (i.e. optimization of elasticity properties with constraint on thermal conductivity).

In another instance, for the design of materials with maximum stiffness or thermal expansion, together with orthotropy, square symmetry or isotropy on functional property, (Sigmund and Torquato, 1997, Sigmund, 2000) devised the SIMP scheme in which the constraints are chosen to be implemented as a penalty function, added to the objective function with constant multipliers. The penalty functions are defined as the square of deviation from the fulfilment of square symmetry or isotropy constraint. Similar to the above mentioned study, the problem does not address a different functional property. Moreover, the selection of the penalization factors is highly dependent on the user's experience. In addition, the approach cannot be considered as a completely systematic procedure as there are frequent needs for manual modifications of the procedure by the user. As it has been indicated by Sigmund and Torquato (1997) in the above optimization problem, the convergency is very hard to attain using an SLP technique. The procedure needs several thousand iterations to be converged, due to the flatness of the modified objective function (Sigmund and Torquato, 1997).

Attempts have been made for the development of multi-functional materials such as materials with prescribed combinations of stiffness and thermal conductivity (Challis et al., 2008), heat and electricity transport (Torquato et al., 2003), stiffness and permeability (Guest and Prévost, 2006) and other multi-physical properties (Gibiansky and Sigmund, 2000, Cadman et al., 2013). The common approach in the design of materials with multi-functional characteristics is to minimize (or maximize) a linear combination of functional properties (Cadman et al., 2012). Assuming two functional properties of  $P_1$  and  $P_2$  for the composite, the optimization objective function is usually defined by applying some weighting factors to different terms of the objective functions:



$$\text{Minimize: } w_1 P_1 + w_2 P_2 \quad (2.51)$$

By changing the weighting factors  $w_1$  and  $w_2$ , materials with varying properties can be generated due to its effects on the two functional objectives (Torquato et al., 2003, Guest and Prévost, 2006, de Kruijf et al., 2007, Cadman et al., 2013). However, the disadvantage of such an approach is that the equidistant variations in weighting factors do not provide proportional changes in the final properties of the resulting materials (de Kruijf et al., 2007). The reason is partly due to the non-linear cross-property relationships between the objective functions. More importantly, it attributes to the existence of many local optima in material topology optimization which may cause the procedure to trap in a nearby solution. Therefore, the results of such an approach are usually expressed with a generated Pareto front (Torquato et al., 2003, de Kruijf et al., 2007) which enables a visual representation of the attainable functional properties, with respect to the changes in weighting factors for a particular setting of design parameters. Consequently, this optimization problem statement with fixed weighting factors is not appropriate for a situation where more precise control over the functional properties is necessary.

#### **2.3.4. Design of functionally graded materials**

Functionally graded materials (FGMs) are inhomogeneous composites which are characterized by gradual changes in their properties. Since the first published study on stress distribution in woody stem of trees (Metzger, 1893), it is known that biological materials demonstrate different properties through changes in their hierarchical structures occurring in order to adapt to environmental stimuli. However, it was not until 1972 when the industrial

advantages of materials with graded functional properties were first analytically addressed in published studies (Shen and Bever (1972), Bever and Duwez (1972)). The idea did not receive much attention because of the lack of appropriate manufacturing equipments at the time. It was not until the mid-1980s, when the emerging fabrication technologies allowed the concept to be applied for controlling the thermal response of materials for the aerospace industry in Japan (Yamanoushi et al., 1990, Hirai and Chen, 1999). As it is shown in Figure 2.5, the morphology of the invented FGM can be described as a ceramic phase, embedded in a metallic phase, with varying volume fractions along the thickness of material, thereby enabling the gradation in properties in the direction. The ceramic phase acts as a thermal barrier, protecting the metallic phase from oxidation and corrosion. The metallic phase, which possess low corrosion resistance in high temperatures, strengthens the composite; hence, demonstrating multi-functional characteristics within the thickness of the composite (Watanabe and Kawasaki, 1990).

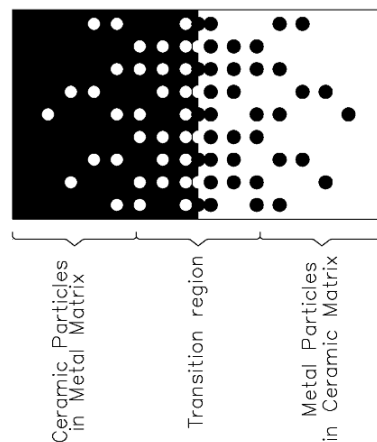


Figure 2.5: Example of FGM composition and functional properties

Apart from material selection, one of the challenging issues in design of an FGM lies in predicting its performance characteristics (Markworth et al., 1995). Depending on the rate of gradation with respect to the dimensions of RVE (or RUC), analytically there are two general approaches for estimation of the FGM characteristics. If a steep gradient in material response is expected, then by analysing the material in both the microscopic and macroscopic scales, the heterogeneity nature of the RVE should be taken into account. However, in the case of small variations being expected in the material properties, adequate accuracy can be attained by applying the RVE based approach to different regions of FGM (Birman and Byrd, 2007, Zhou and Li, 2008b, 2008c).

For designing an FGM, another challenging issue is the determination of the optimal distribution of constituent phases within the composite (Markworth et al., 1995). Based on the “inverse homogenization” technique, some researchers tried to apply the concept in design of the microstructures of materials with variations in properties. For example Lin et al. (2004,2005) used integrated global layout and local microstructure topology optimization, for the design of artificial spinal bone tissues. The optimization objective in the microstructural scale is the volume fraction and the desired elasticity tensor that has been dictated by the global scale analysis. As a result, an inhomogeneous tissue scaffold was obtained which demonstrated the gradation in physical properties. Chen and Feng (2004), Zhu et al. (2006) and Seepersad et al. (2004) also designed cellular materials, by designing a series of topologically different base cells for their individual objective function or volume fractions. However, these studies deal with designing separate base cells for graded cellular materials and do not provide a systematic approach for the design of FGMs. In particular, these

methods do not guarantee the proper interconnection between periodic base cells (PBCs) along the gradient direction.

Another challenging issue that should be accounted for in the design of an FGM is the minimization of stress discontinuity, especially between constituent materials with dissimilar thermal expansion coefficients (Lannutti, 1994). In studying FGMs' fracture mechanics, it has been shown that the stress concentration and delamination cracking is a significant problem (Erdogan, 1995). This is caused by the thermal stresses during cooling from the sintering temperature at the manufacturing stage and/or the stresses produced under operational conditions (Watanabe and Kawasaki, 1990). Zhou and Li (2008a, 2008c) made the first attempt to systematically address the connectivity issues between different PBCs. Three methods namely "connective constraint", "pseudo load" and "unified formulation" were presented (Zhou and Li, 2008b). In these methods the 'solid isotropic material with penalization' (SIMP) technique is used as the structural optimization tool in an inverse homogenization procedure. These methods will be discussed in more details in chapter 6 while a computationally more efficient method will be presented for solving the connectivity issue, between cells via the BESO method in this thesis.

## **2.4 Concluding remarks**

In this chapter topology optimization approaches that have already been used for the design of microstructures for materials were reviewed. Each of these approaches has its benefits and disadvantages. Recent studies on the new BESO in a range of engineering problems indicate its capability in generating structures with high computational efficiency. The approach is also

capable to generate structural topologies with clearly solid or void elements without grey areas which make the manufacturing of the generated topologies easier. Moreover, BESO can be easily implemented and linked to most FEA packages.

The process of material design involves the determination of material properties, through the modelling of its representative volume element (RVE). A brief review of the methods that are usually used for material modelling was presented. It has been indicated that the Homogenization theory has superiorities in terms of accuracy, simplicity of implementation and capability to be used for materials with arbitrary microstructural topologies.

Previous research on material design has indicated that the obtained micro-structural topologies are highly dependent on the applied optimization algorithm. Therefore, it is important to attempt new and different optimization algorithms, in order to find a much wider range of possible solutions to material design. The chapter briefly introduced some of the applications of structural topology optimization techniques in design of microstructures for materials. In later chapters the BESO methodology will be extended in addressing these design scenarios.

## **Chapter 3**

---

### **Topology optimization of microstructures of cellular materials for maximum stiffness or thermal conductivity**

Light-weight cellular materials might possess advanced physical, mechanical and thermal properties that extend far beyond those of solid materials. As discussed in previous chapters, the physical characteristics of materials can vary by changing the materials distribution within their microstructure. To make the best use of resources, the spatial distribution of constituent phases within the microstructures can be determined by taking advantages of the topology optimization techniques. In this chapter, the Bi-directional Evolutionary Structural Optimization (BESO) will be applied for the design of periodic microstructures for cellular materials consisting of one solid phase and one void phase. The objective function is defined to maximize a single physical property such as bulk modulus, shear modulus or thermal conductivity. Although the structural weight is not generally a functional property, it is one of

the important design considerations and is considered by imposing volume constraint in this study.

It is assumed that the material is composed of periodic base cell (PBC), which is the smallest repeating unit of material. The dimensions of the base cells are assumed to be much less than the overall length scales of the material body, and at the same time much larger than the atomic length scale. As discussed in Chapter 2, under such circumstances a relationship can be established between the properties of material in microstructural level and average properties of material in the macro-scale using the “Homogenization theory”. The PBC is discretized into a finite elements model under periodic boundary conditions. The finite element analysis is performed to extract necessary information for calculation of the effects of individual elements within the PBC, on the variation of homogenized (average) properties of material.

The effects of individual elements on the variation of the objective function are known as sensitivity numbers. The procedure which results in such numbers is known as sensitivity analysis (Haug et al., 1986, Huang and Xie, 2010b). As discussed in the previous chapter, the BESO uses an iterative process in which elements’ properties are changed from solid (with a design variable ( $x_i = 1$ )) to void (e.g.  $x_{\min} = 0.001$ ) or from void to solid, based on the ranking of their sensitivity numbers. As a result, the PBC’s topology is gradually modified until both volume constraint and the convergent criterion are met (Huang and Xie, 2010b).

The details of the procedure will be unfolded in this chapter, and will include numerical examples. The results of the numerical procedure are verified with the known analytical bounds on material properties.

### 3.1. Methodology

#### 3.1.1 Optimization problem statement

The stiffness of an elastic material can be described by the bulk modulus  $K$  or shear modulus  $G$ . In the design setting one may aim for designing cellular materials with the maximum effective bulk modulus or shear modulus subject to a prescribed weight. Therefore the topology optimization problem is to find the appropriate distribution of the solid phase within the PBC, subject to a prescribed volume fraction of the solid phase. Mathematically such an optimization problem can be defined as:

Maximize:  $f(\mathbf{x}) = K$  or  $G$

$$\text{Subject to: } V^* - \sum_{i=1}^N V_i x_i = 0 \quad (3.1)$$

$$x_i = x_{\min} \text{ or } 1$$

where  $V_i$  and  $V^*$  are the volume of an individual element and the prescribed total structural volume respectively. The total number of elements within the PBC is denoted by  $N$ . The binary design variable  $x_i$  denotes the density  $i$ th element.



Similarly, the topology optimization problem statement for finding a cellular material with maximum thermal conductivity  $k_c$  subject to volume constraint on the solid phase can be defined as:

Maximize:  $f(\mathbf{x}) = k_c$

$$\text{Subject to: } V^* - \sum_{i=1}^N V_i x_i = 0 \quad (3.2)$$

$$x_i = x_{\min} \text{ or } 1$$

The bulk and shear moduli of materials can be expressed in terms of the components of the effective elasticity matrix ( $D_{ij}^H$ ). The bulk modulus, which is an indication of materials stiffness to uniform pressure, is expressed in 2D problems as:

$$K = \frac{1}{4} (D_{11}^H + D_{12}^H + D_{21}^H + D_{22}^H) \quad (3.3a)$$

and in 3D problems as

$$K = \frac{1}{9} (D_{11}^H + D_{12}^H + D_{11}^H + D_{21}^H + D_{22}^H + D_{23}^H + D_{31}^H + D_{32}^H + D_{33}^H) \quad (3.3b)$$

Similarly the shear modulus defines the material stiffness with respect to shear deformation, and can be expressed in 2D problems as

$$G = D_{33}^H \quad (3.4a)$$

and in 3D cases as

$$G = \frac{1}{3}(D_{44}^H + D_{55}^H + D_{66}^H) \quad (3.4b)$$

The effective thermal conductivity of material can be correlated with the elements of conductivity tensor as:

$$k_c = \frac{1}{2}(k_{11}^H + k_{22}^H) \quad \text{in 2D problems} \quad (3.5)$$

$$k_c = \frac{1}{2}(k_{11}^H + k_{22}^H + k_{33}^H) \quad \text{in 3D problems}$$

where  $k_{ij}^H$  denotes the homogenized thermal conductivity matrix.

As only orthotropic cellular material with square symmetry in 2D problems or cubic symmetry in 3D cases are considered in this chapter, the following relationships hold:

in 2D cases:

$$D_{11} = D_{22} \quad (3.6)$$

$$D_{12} = D_{21}$$

$$D_{13} = D_{31} = D_{32} = D_{23} = 0$$

In 3D cases:

$$D_{11} = D_{22} = D_{33}, \quad (3.7)$$

$$D_{12} = D_{21} = D_{23} = D_{32} = D_{31} = D_{13}$$

$$D_{44} = D_{55} = D_{66}$$

$$D_{ij} = 0 \quad \forall i \neq j \text{ and } i, j \in \{4,5,6\}$$

For isotropic and orthotropic materials the following relationship exists:

$$k_{11}^H = k_{22}^H \quad (= k_{33}^H \quad \text{in 3D cases}) \quad (\text{all other elements are zero}) \quad (3.8)$$

### 3.1.2 Topology optimization through the soft-kill BESO

As mentioned before, the general idea in computer-based topology optimization through material distribution is to assign the solid or void properties to different points of the finite element model of the structure, with the goal of the objective function to evolve toward an optimum. In the soft-kill BESO, developed by Huang and Xie (2010b) this is done by evaluation of the effects of the individual elements on the variation of the objective function, which is known as sensitivity analysis. The result of such analysis is expressed by assigning each element a sensitivity number. The sensitivity numbers  $\alpha_i$  are the derivatives of the objective function with respect to the design variables  $x_i$  of the  $i$ th element:

$$\alpha_i = \frac{\partial f(\mathbf{x})}{\partial x_i} \quad (3.9)$$

The optimization process consists of defining optimality criteria and ranking the elements based on their sensitivity numbers (Huang and Xie, 2009a, 2010b). As the design variables are restricted to be either  $x_{\min}$  or 1, the optimality criterion can be formulated in such a way that that sensitivity numbers of solid elements ( $x_i = 1$ ) are higher than those of void elements ( $x_i = x_{\min}$ ) (Huang and Xie 2010b). Therefore a scheme can be devised so that the design variables ( $x_i$ ) of elements with higher sensitivity numbers are increased. In contrast, the design variable for elements with lower sensitivity numbers is decreased. The design variable ( $x_i$ ) can be interpreted as the density of elements. Considering a lower bound ( $x_{\min} = 0.001$ ) for the design variable reduces the effect of elements in the analysis, while the sensitivity of such elements could be calculated directly. This enables the solid elements to grow in the desired regions of the structure, away from existing solid regions and avoid the numerical problems associated with the complete removal of elements (Huang and Xie 2009a; 2010b).

With the help of introducing design variables, the Young's modulus of an element can be treated as isotropic and interpolated as the function of the element density with a power-law scheme as:

$$E(x_i) = E^s x_i^p \quad (3.10)$$

where  $E^s$  denotes the Young's modulus for solid element,  $p$  is the penalty exponent and  $x_i$  denotes the relative density of the  $i^{\text{th}}$  element. In the simplest form a linear interpolation scheme with the penalty exponent of  $p = 1$  may be used. However, there might be convergence problems in these cases (Huang and Xie, 2010a). On the other hand, the filtering

scheme reduces the difference between the sensitivity numbers of solid and void elements. Therefore when the penalty exponent is small, no recognizable solid or void regions may exist in some parts of the structure. When the filtering scheme is used for alleviating the numerical instabilities, experiences shows that selecting the  $p > 1$  (usually  $p = 3$ ) will result in a better differentiation between solid and void regions in the structure, hence improves the convergence of the procedure (Huang and Xie 2009a; 2010b).

Before tailoring the BESO for the design of materials microstructures, the key remaining issue is the evaluation of material effective properties and the derivation of the sensitivity numbers for the elements within the PBC.

### **3.1.3. Homogenization and Sensitivity Analysis**

As discussed before, the spatial distribution of the constituent phases within the microstructure of the composite affects the overall effective properties of the material. For the design of materials' microstructures, there is a need for the calculation of overall properties of composite materials, based on the distribution of constituent phases within RVE or RUC. For the cases in which the material is composed of periodic base cells, with dimensions that are much smaller than materials' macroscopic length scale but larger than the atomic length scale, the effective properties of the macro-material can be found with the help of "Homogenization theory" (Bendsøe and Kikuchi 1988; Hassani and Hinton 1998a; 1998b; 1998c). For instance, in terms of the material distribution in the domain of the base cell  $\Omega$ , the elasticity tensor of the composite can be calculated as:

$$E_{ijkl}^H = \frac{1}{|Y|} \int_{\Omega} E_{ijpq} (\bar{\epsilon}_{pq}^{kl} - \tilde{\epsilon}_{pq}^{kl}) d\Omega \quad (3.11)$$

where  $|Y|$  denotes the area (or volume in 3D cases) of the periodic base cell domain  $\Omega$ ;  $\bar{\epsilon}_{pq}^{kl}$  defines the linearly independent unit test strain fields which in 2D and 3D problems consists of 4 and 6 fields respectively. The strain fields  $\tilde{\epsilon}_{mn}^{kl}$  induced by the test strains can be found from the following equation

$$\int_{\Omega} E_{ijpq} \epsilon_{ij}(v) \tilde{\epsilon}_{pq}^{kl} d\Omega = \int_{\Omega} E_{ijpq} \epsilon_{ij}(v) \bar{\epsilon}_{pq}^{kl} d\Omega \quad (3.12)$$

where  $v \in H_{per}^1(\Omega)$  is the Y-periodic admissible displacement field. Equation (3.12) is the weak form of the standard elasticity equation applied to the PBC with periodic boundary conditions. This equation is usually solved by finite element analysis of the PBC, subject to the independent cases of pre-strain fields  $\bar{\epsilon}_{pq}^{kl}$ . With the help of the material interpolation scheme introduced in equation (3.10), the derivative of the homogenized elasticity tensor with respect to the design variable  $x_i$ , can be calculated from the adjoint variable method as (Haug et al., 1986):

$$\frac{\partial E_{ijkl}^H}{\partial x_i} = \frac{1}{|Y|} \int_{\Omega} \frac{\partial E_{pqrs}}{\partial x_i} (\bar{\epsilon}_{pq}^{kl} - \tilde{\epsilon}_{pq}^{kl}) (\bar{\epsilon}_{rs}^{ij} - \tilde{\epsilon}_{rs}^{ij}) d\Omega \quad (3.13)$$

The test strain fields are usually taken as unit strains along principal directions. For instance in 2D problems they are usually selected as:

$$\bar{\boldsymbol{\varepsilon}}_{pq}^{11} = (1 \ 0 \ 0 \ 0)^T$$

$$\bar{\boldsymbol{\varepsilon}}_{pq}^{22} = (0 \ 1 \ 0 \ 0)^T$$

$$\bar{\boldsymbol{\varepsilon}}_{pq}^{12} = (0 \ 0 \ 1 \ 0)^T$$

$$\bar{\boldsymbol{\varepsilon}}_{mn}^{21} = (0 \ 0 \ 0 \ 1)^T$$

By applying the unit strain fields on the PBC, the homogenized elasticity matrix  $\mathbf{D}^H$  of such materials, is simplified as:

$$\mathbf{D}^H(\mathbf{x}, \mathbf{u}) = \frac{1}{|Y|} \int_Y \mathbf{D}(\mathbf{x})(\mathbf{I} - \mathbf{B}\mathbf{u}) dY \quad (3.14)$$

in which  $\mathbf{u}$  denotes the displacement field, resulting from the finite element analysis of the base cell, under periodic boundary conditions and equivalent forces that causes uniform unit strains;  $\mathbf{I}$  is the unit matrix; and  $\mathbf{B}$  is the strain-displacement matrix. The derivation of  $\mathbf{D}^H$  with respect to the design variables  $x_i$ , can be expressed as:

$$\frac{\partial \mathbf{D}^H}{\partial x_i} = \frac{1}{|Y|} \int_Y (\mathbf{I} - \mathbf{B}\mathbf{u})^T \frac{\partial \mathbf{D}}{\partial x_i} (\mathbf{I} - \mathbf{B}\mathbf{u}) dY \quad (3.15)$$

Similarly, the matrix of homogenized thermal conductivity ( $\mathbf{k}^H$ ) can be calculated as:

$$\mathbf{k}^H(\mathbf{x}, \boldsymbol{\mu}) = \frac{1}{|Y|} \int_Y \mathbf{k}(\mathbf{x})(\mathbf{I} - \boldsymbol{\mu}) dY \quad (3.16)$$

in which  $\boldsymbol{\mu}$  is the induced temperature field resulting from finite element analysis of the base cell under the periodical boundary conditions and uniform heat flux (e.g.  $\{1, 0\}^T$  and  $\{0, 1\}^T$  in 2D cases). The sensitivity of the homogenized thermal conductivity, with respect to the design variables can be expressed as (Hassani and Hinton, 1998a, 1998b, 1998c, Zhou and Li, 2008a):

$$\frac{\partial \mathbf{k}^H}{\partial x_i} = \frac{1}{|Y|} \int_Y (\mathbf{I} - \boldsymbol{\mu})^T \frac{\partial \mathbf{k}}{\partial x_i} (\mathbf{I} - \boldsymbol{\mu}) dY \quad (3.17)$$

With the help of equations (3.15) and (3.17) in combination with equations (3.3), (3.4) and (3.5), the sensitivities with respect of different objective functions can be calculated.

**Example:**

For future applications, a series of tests were made, in order to verify the results obtained by the finite element solution of the homogenization theory (equation (3.15)) with existing literature. In the following tables two examples were presented. The square base cells of materials have a rectangular void hole with different sizes in each example. The material of the solid phase is assumed to be isotropic with the Young's modulus  $E=0.91$  and Poisson's ratio  $\nu=0.3$ . The models were meshed with different densities in order to compare the effects of mesh size on the results. The examples were compared with the benchmark results presented in (Hassani and Hinton, 1998d). It is noticed that, when a course mesh is used the predicted stiffness of material is slightly higher (also see (Zhou and Li, 2008d)). In most numerical examples presented in literature, the mesh density used for topology optimization



of the materials' microstructures doesn't exceed  $50 \times 50$  elements (for example (Sigmund, 1994a, 1995)).

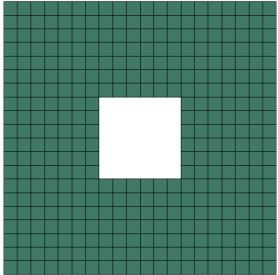
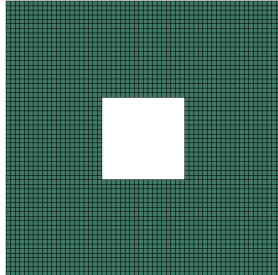
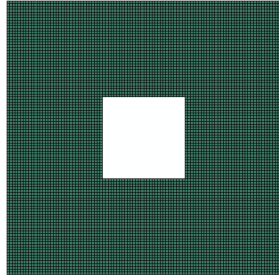
Base cell dimensions: $100 \times 100$ Void dimensions: $30 \times 30$ Base material properties: $E=0.91$ and $\nu=0.3$			
FE model of microstructures			
Mesh size	20x20	60x60	100x100
Material stiffness matrix $\mathbf{D} =$	$\begin{bmatrix} 0.7805 & 0.2111 & 0 \\ 0.2111 & 0.7805 & 0 \\ 0 & 0 & 0.2378 \end{bmatrix}$	$\begin{bmatrix} 0.7650 & 0.2043 & 0 \\ 0.2043 & 0.7650 & 0 \\ 0 & 0 & 0.2320 \end{bmatrix}$	$\begin{bmatrix} 0.7648 & 0.2040 & 0 \\ 0.2040 & 0.7648 & 0 \\ 0 & 0 & 0.2317 \end{bmatrix}$
Benchmark solution in (Hassani and Hinton, 1998d)	$\mathbf{D} =$		$\begin{bmatrix} 0.7644 & 0.2039 & 0 \\ 0.2039 & 0.7644 & 0 \\ 0 & 0 & 0.2313 \end{bmatrix}$

Table 3.1: Comparison between finite element application of equation (3.15) with the benchmark result in (Hassani and Hinton, 1998d). The  $100 \times 100$  rectangular base cells have  $30 \times 30$  rectangular hole inside.

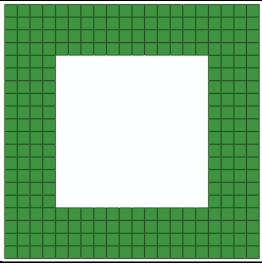
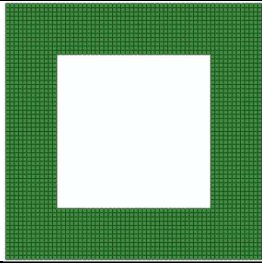
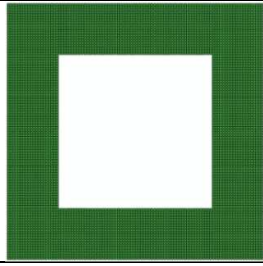
Base cell dimensions: $100 \times 100$ Void dimensions: $60 \times 60$ Base material properties: $E=0.91$ and $\nu=0.3$			
FE model of microstructures			
Mesh size	20x20	60x60	100x100
Material stiffness matrix $\mathbf{D} =$	$\begin{bmatrix} 0.3996 & 0.0629 & 0 \\ 0.0629 & 0.3996 & 0 \\ 0 & 0 & 0.0469 \end{bmatrix}$	$\begin{bmatrix} 0.3960 & 0.0609 & 0 \\ 0.0609 & 0.3960 & 0 \\ 0 & 0 & 0.0446 \end{bmatrix}$	$\begin{bmatrix} 0.3957 & 0.0607 & 0 \\ 0.0607 & 0.3957 & 0 \\ 0 & 0 & 0.0443 \end{bmatrix}$
Benchmark solution in (Hassani and Hinton, 1998d)	$\mathbf{D} =$		$\begin{bmatrix} 0.3955 & 0.0606 & 0 \\ 0.0606 & 0.3955 & 0 \\ 0 & 0 & 0.0441 \end{bmatrix}$

Table 3.2: Comparison between finite element application of equation (3.15) with the benchmark result in (Hassani and Hinton, 1998d). The  $100 \times 100$  rectangular base cells have  $60 \times 60$  rectangular hole inside.

### 3.1.4. Numerical instabilities

Topology optimization usually encounters numerical instability in the form of checkerboard patterns and mesh-dependency. As discussed in Chapter 2, the checkerboard problem is referred to as the situation where patterns of alternating solid and void elements appear in some regions of the structure. The problem has its roots mainly in numerical errors that can occur when the low-order finite elements are used for the structural modeling. On the other hand, the mesh dependency is referred to as the problem of obtaining a qualitatively different structure by using different mesh sizes in the modeling of the structure. It has been shown that both problems can be avoided, to a large extent, by imposing restriction on variation of design variables (Sigmund and Petersson, 1998).

In the soft-kill BESO it has been shown that by devising a filtering scheme, both above mentioned numerical problems can be avoided simultaneously (Huang and Xie, 2007b, 2010b). Inspired by a similar procedure that has been applied in image processing; the filtering scheme replaces the sensitivity number of each element with a weighted average of the sensitivities of the element itself and its neighboring elements (Huang and Xie 2007b, 2010b). The scheme works as a low-pass filter that eliminates features below a certain length-scale in the generated topologies. In the filtering scheme the elemental sensitivity number will be modified by the following equation:

$$\hat{\alpha}_i = \frac{\sum_{j=1}^N w_{ij} \alpha_j}{\sum_{j=1}^M w_{ij}} \quad (3.18)$$

where  $\hat{\alpha}_i$  is the modified sensitivity number and  $r_{ij}$  denotes the distance between the center of the element  $i$  and element  $j$ .  $w_{ij}$  is the weight factor that is defined as:

$$w_{ij} = \begin{cases} r_{\min} - r_{ij} & \text{for } r_{ij} < r_{\min} \\ 0 & \text{for } r_{ij} \geq r_{\min} \end{cases} \quad (3.19)$$

where  $r_{\min}$  is the filter radius that is specified as a given parameter.

To earn a convergent solution (Huang and Xie 2007b) proposed the elemental sensitivity number to be modified by averaging it with its value from the previous iteration:

$$\tilde{\alpha}_i = \begin{cases} \hat{\alpha}_i^k & \text{if } k = 1 \\ \frac{1}{2}(\hat{\alpha}_i^t + \hat{\alpha}_i^{t-1}) & \text{otherwise} \end{cases} \quad (3.20)$$

where superscript  $t$  denotes current iteration number. The average sensitivity number  $\tilde{\alpha}_i$ , is then replaced with the  $\hat{\alpha}_i$ . The latter is used for adding and removing elements and is recorded to be used in the next iteration. In fact, the procedure of averaging the sensitivities with historical information moderates the irregular oscillations of the design variable. A large number of numerical examples indicate the capability of procedure, for stabilizing the evolution process (Huang and Xie, 2010b).

### 3.1.5. Procedure

The whole BESO procedure for obtaining materials with maximum bulk or shear modulus consists of the following steps:

- Step 1: Define the BESO parameters, such as prescribed volume fraction  $V^*$  ; evolutionary ratio  $ER$  ; penalty  $p$  (normally  $p = 3$ ) and filter radius  $r_{\min}$  ;
- Step 2: Construct a solid-void finite element model for the PBC;
- Step 3: Define the periodic boundaries on PBC; define the loads that are equivalent to unit strain fields,  $\bar{\epsilon}_{pq}^{kl}$ . In 2D problems 3 cases of loading and boundary conditions and in 3D problems 6 cases are necessary to be defined. Perform the finite element analysis (FEA) and extract the induced displacement fields  $\mathbf{u}$  ;
- Step 4: Calculate the elemental sensitivity numbers  $\alpha_i$  for the objective function by applying equation (3.15) with the help of equation (3.3) or (3.4);
- Step 5: Filter sensitivity numbers in the PBC domain using equations (3.18) and (3.19); using equation (3.20), average sensitivities with their historical information;
- Step 6: Determine the target volume fraction of solid elements for the next iteration. If the current volume of solid elements  $V^t$  is larger than the prescribed volume  $V^*$ , the target volume for the next design is set as  $V^{t+1} = \max(V^t(1-ER), V^*)$  ; determine the number of void elements for the next iteration;
- Step 7: Rank all elemental sensitivity numbers; determine the threshold sensitivity  $\alpha_{th}$ ; the threshold sensitivity is determined in such a way that the number of elements with sensitivities lower than  $\alpha_{th}$ , are to be equal to the number of void elements.

Step 8: Reset the design variables of all elements. If the sensitivity of an element is less than the threshold  $\alpha_i \leq \alpha_{th}$ , then  $x_{\min}$  is assigned to its density. Otherwise 1 is assigned to its  $x_i$ .

Step 9: Repeat 2-8 until both the prescribed volume is achieved and the convergent criterion are satisfied.

The convergence criterion is defined in terms of the change in the objective function ( $K$ ,  $G$  or  $k_c$ ) as

$$\frac{\left| \sum_{i=1}^{\theta} (f^{t-i+1} - f^{t-N-i+1}) \right|}{\sum_{i=1}^{\eta} f^{t-i+1}} \leq \tau \quad (3.21)$$

where  $f$  is the effective value of the objective function;  $\tau$  is the prescribed allowable convergence error and  $\theta$  is the summation upper bound.  $\tau$  and  $\theta$  are usually set equal to 0.1% and 5 respectively which means that the convergence is deemed to be attained when the variations in the effective properties over the last 10 iterations is equal to or less than (0.1%).

The procedure for designing cellular materials with maximum thermal conductivity and prescribed volume fraction is very similar to the above mentioned algorithm. The only difference is the replacement of steps 3 and 4 with the following statements:

Step 3R: Define the periodic boundaries on PBC; apply uniform heat fluxes (e.g.  $\{1, 0\}^T$  and  $\{0, 1\}^T$  in 2D cases). In 2D problems 2 cases of boundary and thermal loading and in 3D problems 3 cases are necessary. Perform the finite element analysis for thermal conductivity and extract the induced temperature fields  $\mu$ .

Step 4R: Calculate the elemental sensitivity numbers  $\alpha_i$  for the objective function by applying equation (3.17) with the help of equation (3.5);

## 3.2. Results and Discussion

### 3.2.1. 2D examples for maximizing the bulk modulus

In this example, the square design domain with dimensions of  $100 \times 100$  is divided into  $100 \times 100$ , 4-node square elements. The Young's modulus and Poisson's ratio of solid material are selected as  $E^s = 1$  and  $\nu = 0.3$  respectively. The evolution rate is set  $ER = 0.02$ , filter radius  $r_{\min} = 5$  and penalty  $p = 3$ . The BESO procedure starts from an initial material distribution shown in Figure 3.1, which consists of four void elements at the centre of the model while solid properties are assigned to other elements.

When the prescribed volume (area) of the solid material is selected to be 50%, 40%, 30% and 20% of the total design domain volume (area), the corresponding resulting microstructures and their effective elasticity matrices are given in Figure 3.2. The total iterations for the corresponding cases are 49, 56, 64 and 80. The bulk moduli of these microstructures are 0.179, 0.132, 0.091 and 0.056 respectively.

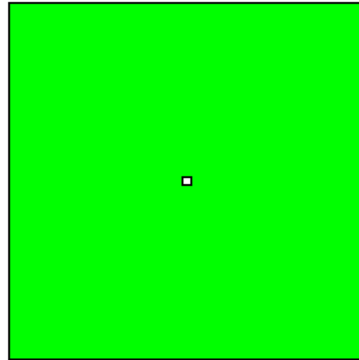
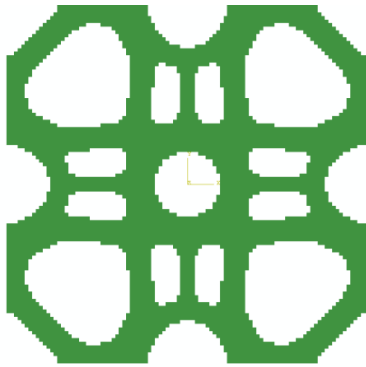


Figure 3.1: Initial material distribution in 2D problems (green area is solid)



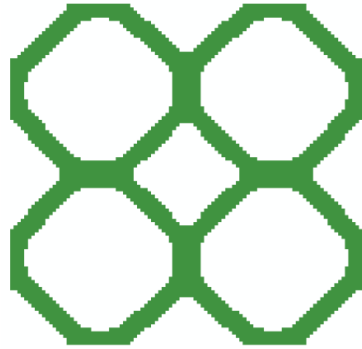
$$\begin{bmatrix} 0.256 & 0.102 & 0 \\ 0.102 & 0.256 & 0 \\ 0 & 0 & 0.045 \end{bmatrix}$$

(a)

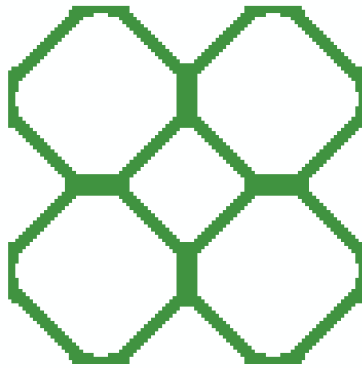


$$\begin{bmatrix} 0.149 & 0.114 & 0 \\ 0.114 & 0.149 & 0 \\ 0 & 0 & 0.037 \end{bmatrix}$$

(b)



$$\begin{bmatrix} 0.096 & 0.085 & 0 \\ 0.085 & 0.096 & 0 \\ 0 & 0 & 0.018 \end{bmatrix} \quad (c)$$



$$\begin{bmatrix} 0.057 & 0.054 & 0 \\ 0.054 & 0.057 & 0 \\ 0 & 0 & 0.005 \end{bmatrix} \quad (d)$$

Figure 3.2: Microstructures and effective elasticity matrices of 2D cellular materials with maximum bulk modulus for various prescribed volume (area) fractions (a) 50%; (b) 40%; (c) 30% and (d) 20%.

Figure 3.3 demonstrates the evolution histories of the bulk modulus, volume and microstructural topology, when the prescribed volume (area) of the solid phase is 30% of the total area of the design domain. As it can be seen, by decrement of the area of the solid phase, the bulk modulus also decreases. Once the volume constraint is satisfied, the bulk modulus and micro-structural topology converge to the final solutions with a good stability. The final microstructure of cellular material can be interpreted as four octagonal honeycomb cells, with



the bulk modulus that is equals to one octagonal honeycomb cell in Sigmund (1995) using a truss modelled base cell.

For well-ordered, quasi-homogenous and quasi-isotropic composites, the upper and lower bounds for bulk modulus have been derived by Hashin and Shtrikman (1963). As discussed in Chapter 2, these bounds are used for predicting the range of properties that a composite can achieve with a given material composition and volume fractions. They are also extensively used for verification of optimality of designed microstructures through topology optimization (Challis et al., 2008, Cadman et al., 2013). As indicated in (Gibiansky and Sigmund 2000) the Hashin-Shtrikman bounds on the bulk modulus are not only valid for isotropic materials but also applicable for materials with square symmetry (in 2D cases) and cubic symmetry (in 3D cases). For cellular materials that are made with a void phase and a solid phase of volume fraction  $V_f$ , bulk modulus  $K^s$  and shear modulus of  $G^s$ , the Hashin-Shtrikman upper bound on bulk modulus is given as:

$$K_{HS}^{up} = \frac{V_f K^s G^s}{(1 - V_f) K^s + G^s} \quad (3.22)$$

In figure 3.4 the bulk moduli of the materials made with the above microstructures is compared with the Hashin-Shtrikman upper bound. As it can be seen, the bulk moduli of results are very close to the Hashin-Shtrikman upper bound in equation (3.22). This closeness also verifies the effectiveness of the presented BESO procedure.

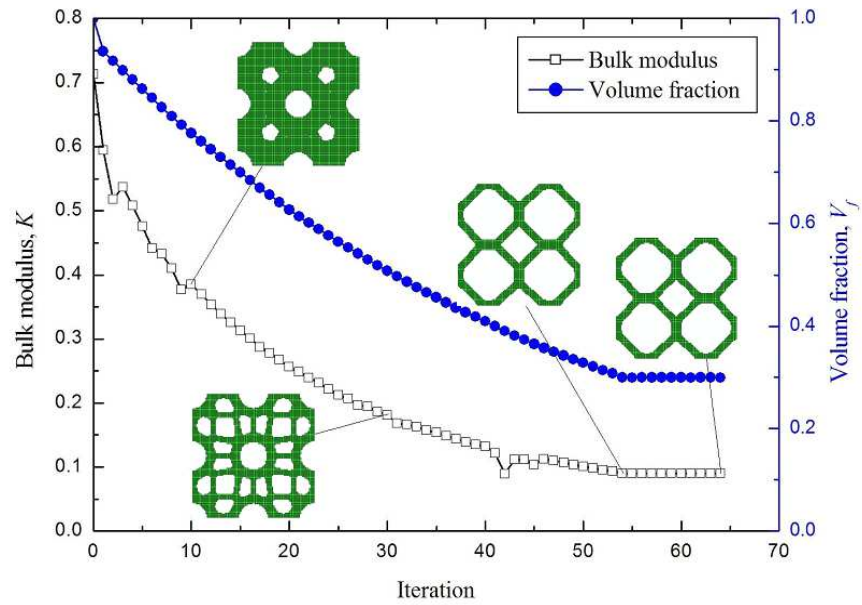


Figure 3.3: History of evolutions of bulk modulus, volume fraction and microstructural topology for maximizing bulk modulus

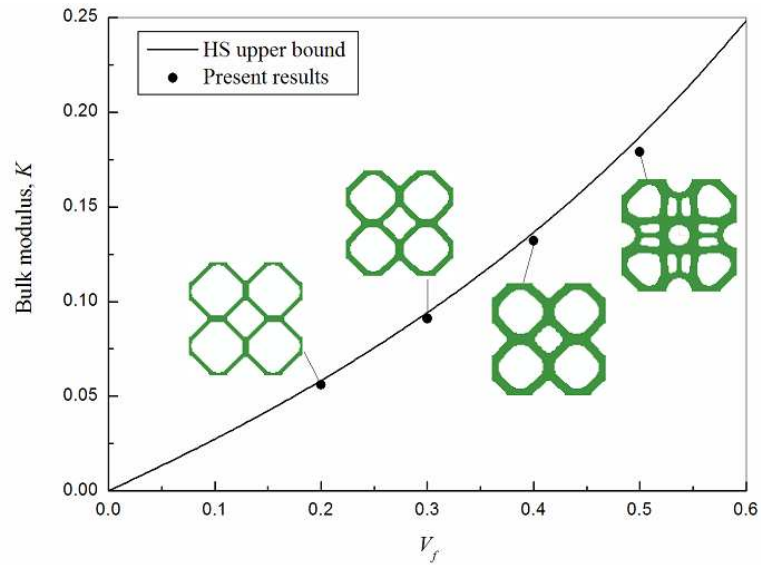


Figure 3.4: Comparison between materials' bulk modulus of resulted microstructures and the Hashin-Shtrikman upper bound

The cellular material can be constructed by repeating the presented microstructures. Figure 3.5 shows  $2 \times 2$  array of the generated base cells. These configurations of the cells can be generated directly, as a single PBC, providing one starts the procedure with different initial design or optimization parameters. In general, it can be seen that there are a number of microstructures having the same bulk modulus, near to analytical upper bounds and that the attained topologies are highly dependent on initial design, optimization parameters and applied algorithm.

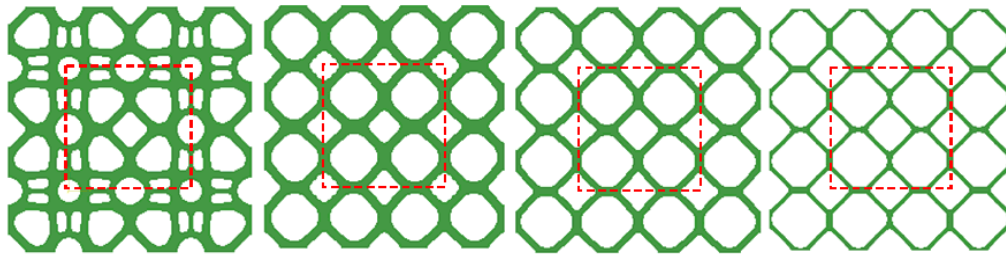


Figure 3.5:  $2 \times 2$  array of designed base cells with maximum bulk modulus and various volume fractions of solids (a) 50%; (b) 40%; (c) 30% and (d) 20%.

### 3.2.2. 2D examples for maximizing shear modulus

In the algorithm of the above example the objective function is changed to find microstructures for materials, with maximum shear modulus of elasticity for various prescribed volumes of the solid phase. Similar to the above example, the design domain is discretized into  $100 \times 100$ , 4-node square elements. The Young's modulus and Poisson's ratio of solid phase are selected as  $E^s = 1$  and  $\nu = 0.3$  respectively. The BESO parameters are

$ER = 0.02$ ,  $r_{\min} = 5$  and  $p = 3$ . BESO starts from the same initial topology that is shown in Figure 3.1.

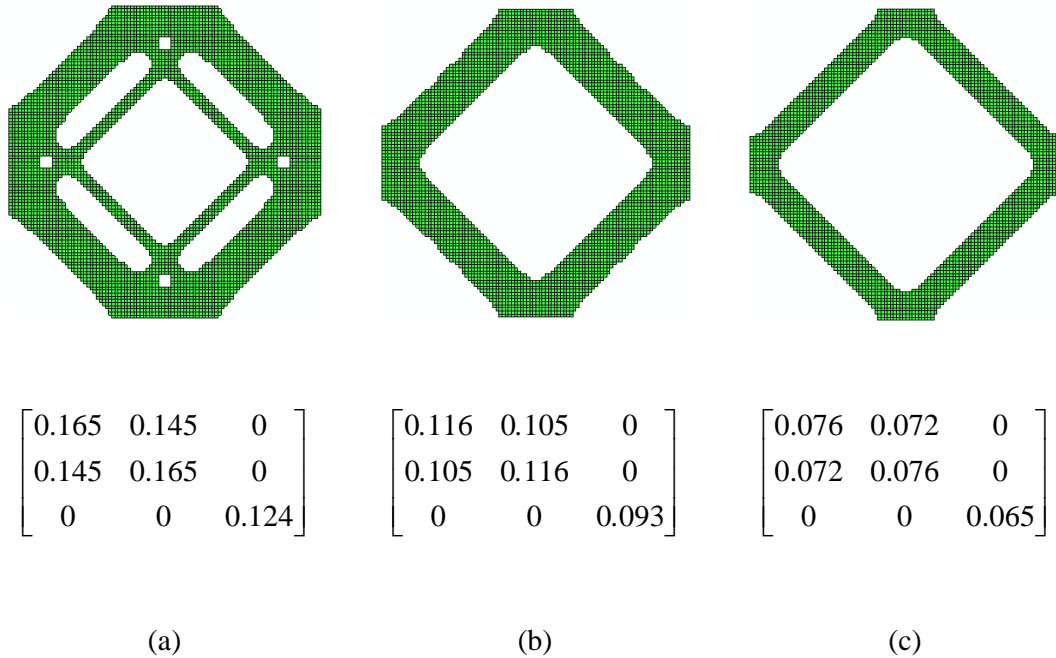


Figure 3.6: Microstructures and effective elasticity matrices of 2D cellular materials, with maximum shear modulus for various volume constraints (a) 45%; (b) 35%; and (c) 25%.

For the prescribed solid volume fractions of 45%, 35% and 25%, the convergence is attained with 48, 59 and 73 iterations. The resulting microstructures and their corresponding materially effective elasticity matrices are shown in Figure 3.6. Figure 3.7 demonstrates the evolution history of shear modulus, volume fraction of the solid phase and the microstructural topology, when the prescribed final volume fraction of the solid phase is set to  $V_f = 0.25$ . It demonstrates that shear modulus converges with a good stability after the volume constraint is

satisfied. The generated diamond shape microstructures are the same as those microstructures presented in (Neves et al., 2000). The material can be constructed by repeating the base cells. Figure 3.8 shows  $2 \times 2$  array of the generated microstructures.

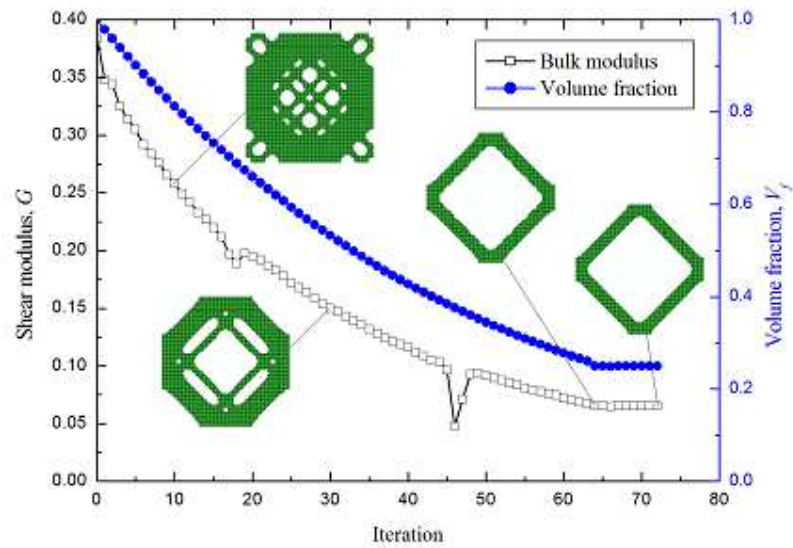


Figure 3.7: History of evolutions of shear modulus, volume fraction and microstructural topology for maximizing shear modulus.

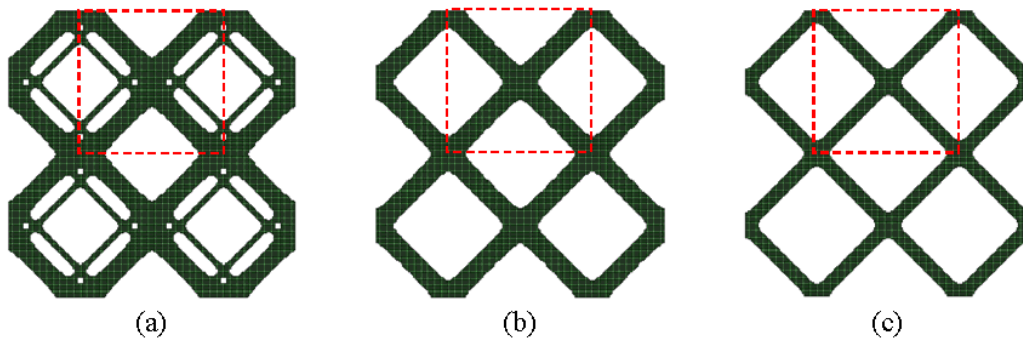


Figure 3.8:  $2 \times 2$  array of the base cells with maximum shear modulus with various prescribed volume of solid phase (a) 45%; (b) 35% and (c) 25%.

### 3.2.3. 3D examples for maximizing bulk modulus

The cubic domain with  $30 \times 30 \times 30$  is discretized into  $30 \times 30 \times 30$ , 8-node cubic elements. The mechanical properties of solids are selected as Young's  $E^s = 1$  and Poisson's ratio  $\nu = 0.3$ . The BESO parameters are set  $ER = 0.04$ ,  $r_{\min} = 3$  and  $p = 3$ . Figure 3.9 shows the initial topology, in which solid property is assigned to all elements except for 8 elements at the centre of the model.

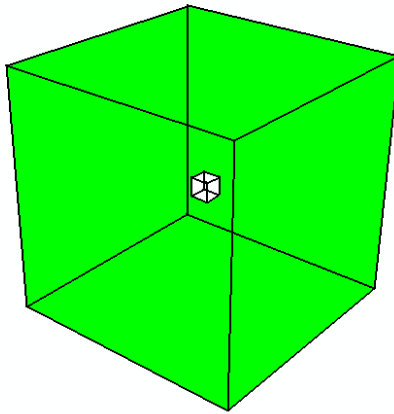


Figure 3.9: The initial design in 3D example

The objective is to optimize the topology of the materials' microstructures with various prescribed volume fractions of solid so that the materials' bulk moduli  $K$  are maximized. Figure 3.10 demonstrates the evolution histories of bulk modulus, volume fraction of solid phase and micro-structural topology when the prescribed volume fraction of the solid phase is set as  $V_f = 0.25$ . When the prescribed volume fraction of solid phase is 45%, 35% and 25%,

the resulting topologies for the PBC's, the  $2 \times 2 \times 2$  arrays of bases cells and the corresponding elasticity matrices are shown in Figure 3.11.

The Hashin-Shtrikman analytical upper bound on bulk modulus of 3D cellular materials can be expressed as (Hashin and Shtrikman, 1963):

$$K_{HS}^{up} = \frac{4K^s G^s V_f}{3K^s(1-V_f) + 4G^s} \quad (3.23)$$

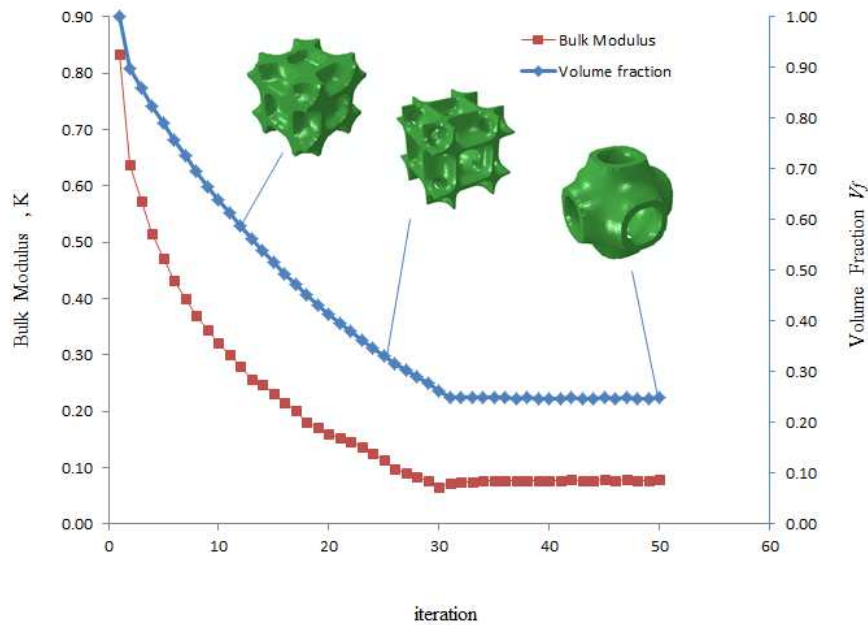


Figure 3.10: The evolution histories of bulk modulus, volume fraction and microstructures of 3D materials with maximum bulk modulus

When the volume fraction of the solid phase is 45%, 35% and 25%, the Hashin-Shtrikman upper bound is calculated as 0.19, 0.14, and 0.09 respectively from the equation (3.23). The attained effective bulk moduli of materials can be calculated as 0.18, 0.12 and 0.08, from the

elasticity matrices presented in Figure 3.11. it can be seen that the attained bulk moduli have very good agreement with the analytical upper bounds.

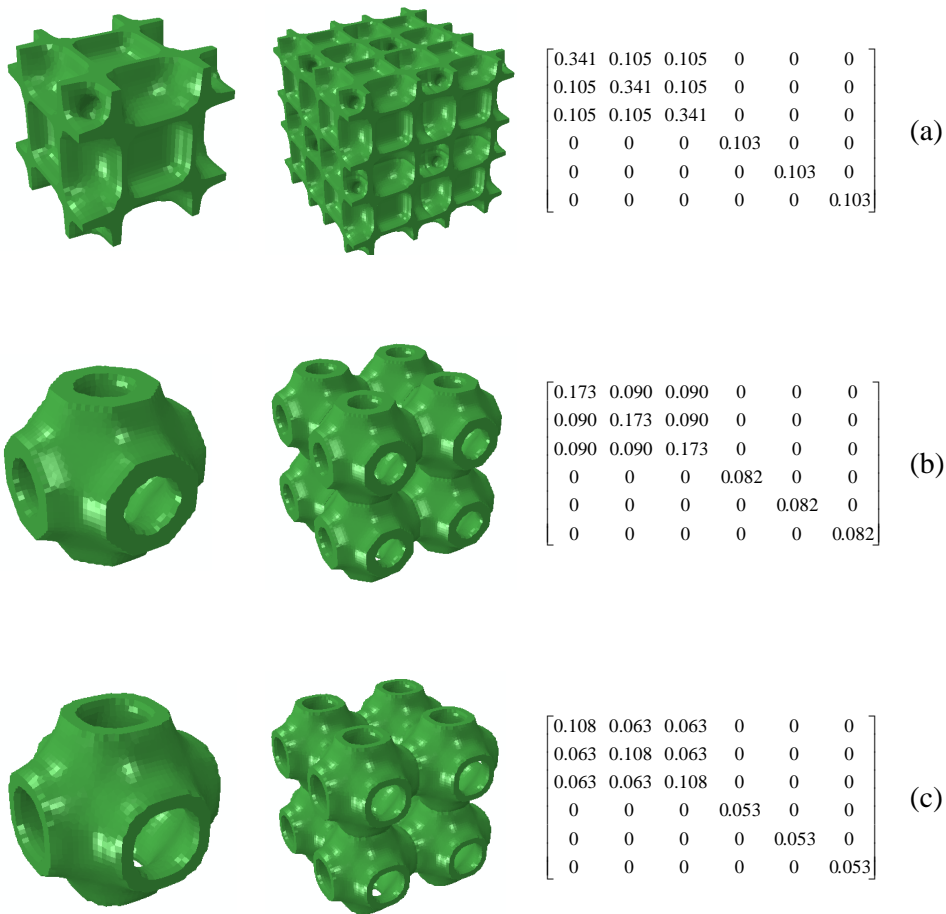


Figure 3.11: 3D base cells, 2x2x2 cells and effective elasticity matrices of 3D cellular materials with maximum bulk modulus (a) volume fraction is 45%; (b) volume fraction is 35%; and (c) volume fraction is 25%.



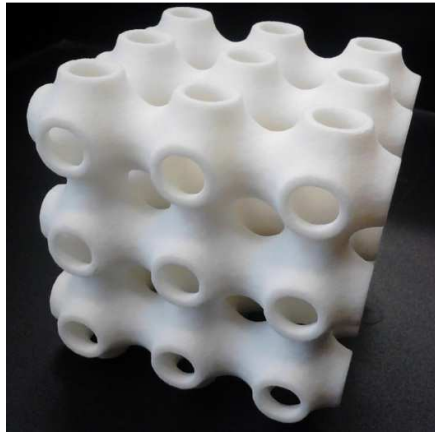


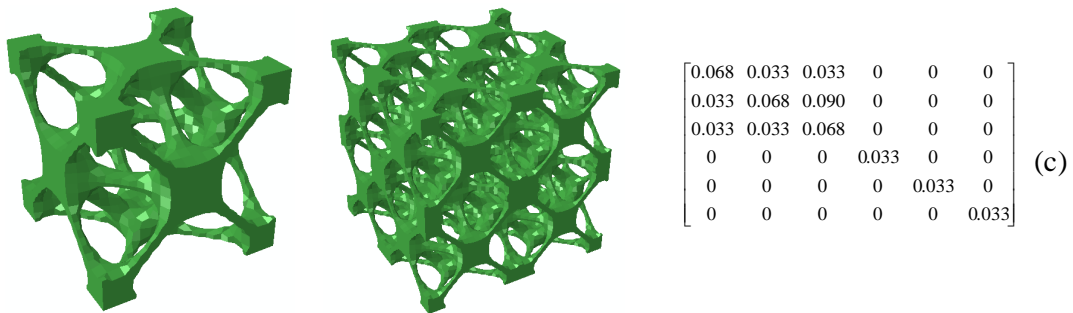
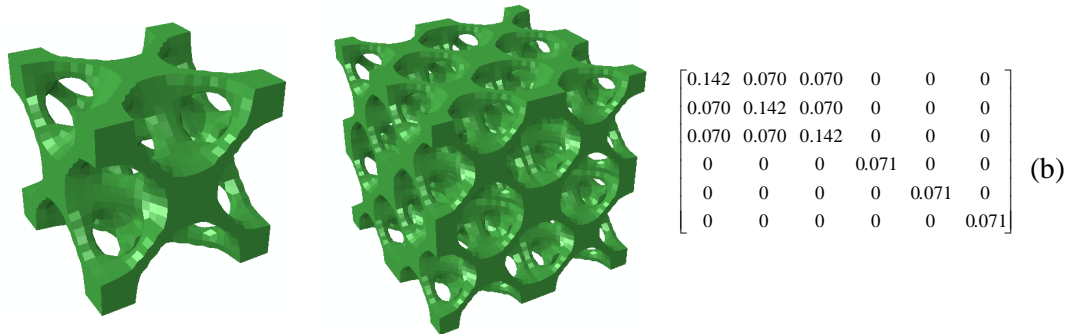
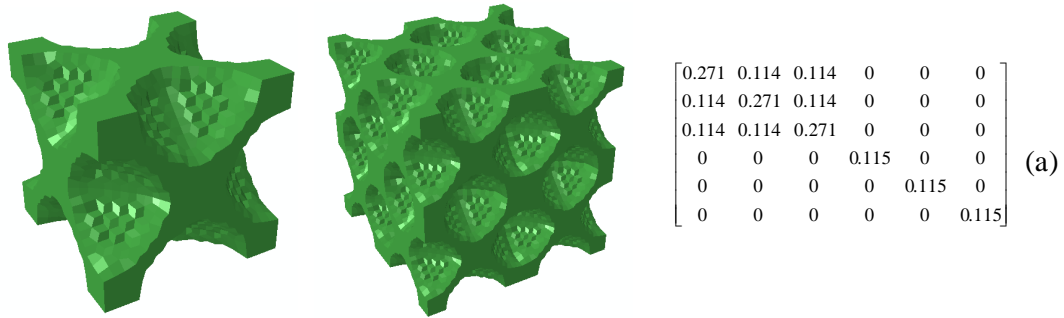
Figure 3.12: 3D microstructures with maximum bulk modulus generated by 3D printing.

### 3.2.4 3D examples for maximizing shear modulus

The cubic domain with dimensions  $20 \times 20 \times 20$  is discretized with  $20 \times 20 \times 20$ , 8-node cubic elements. The mechanical properties of the solid phase are the Young's modulus,  $E^s = 1$  and the Poisson's ratio  $\nu = 0.3$ . The BESO parameters are selected as the evolutionary rate  $ER = 0.04$ , the filter radius  $r_{\min} = 1.5$ . As before, the penalty exponent is selected  $p = 3$ . Here a small filter radius is used in order to have some thin members in the final micro-structural topology. The BESO starts from the same initial topology shown in Figure 3.9. The prescribed volume fractions of solid phase are set to be 45%, 35%, 25% and 15% of the whole design domain, respectively.

Figure 3.13 demonstrates the topology of the resulting microstructures for the base cell, as well as the  $2 \times 2 \times 2$  array of bases cells and effective elasticity matrices for the various prescribed volumes of the solid phase. The total iterations for these examples are 38, 39, 49

and 64, when the prescribed volume fraction of solid phase are 45%, 35%, 25% and 15% respectively.



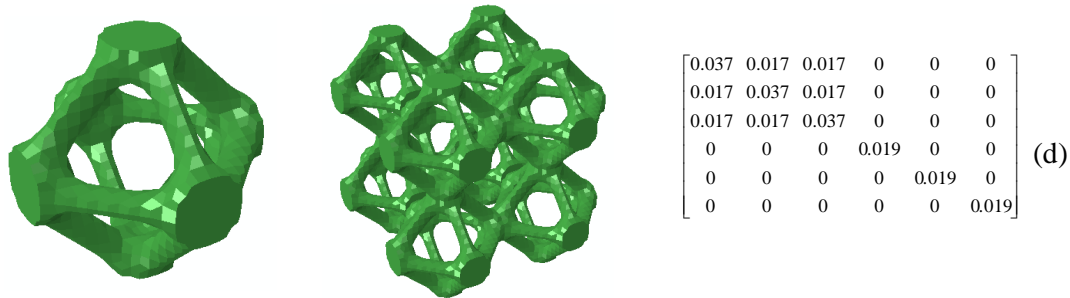


Figure 3.13: 3D base cells,  $2 \times 2 \times 2$  cells and effective elasticity matrices of 3D cellular materials with maximum shear modulus (a) volume fraction is 45%; (b) volume fraction is 35%; ; (c) volume fraction is 25% and (d) volume fraction is 15%.

### 3.2.5 2D examples for maximizing thermal conductivity

The objective of this example is to generate microstructures of cellular materials with maximum thermal conductivity. The square domain with dimensions  $100 \times 100$  is discretized into  $100 \times 100$ , 4-node square elements. It is assumed that the eigenvalue of thermal conductivity of the solid phase is  $k^s = 1$ . The evolutionary rate  $ER = 0.04$ , the filter radius  $r_{\min} = 12$  and the penalty exponent equal to 3 are selected. The topology at the iteration 0 is shown in Figure 3.1, which consists of 4 void elements at the centre of the model while solid property is assigned to the rest of elements.

Figure 3.14 demonstrates the topology of microstructures, as well as the  $2 \times 2$  array of generated base cells and the effective thermal conductivity matrices when the prescribed volume fraction of the solid phase is equal to 50% and 30% of the total volume (area) of the PBC. The total iterations for these examples are 25 and 36 respectively.

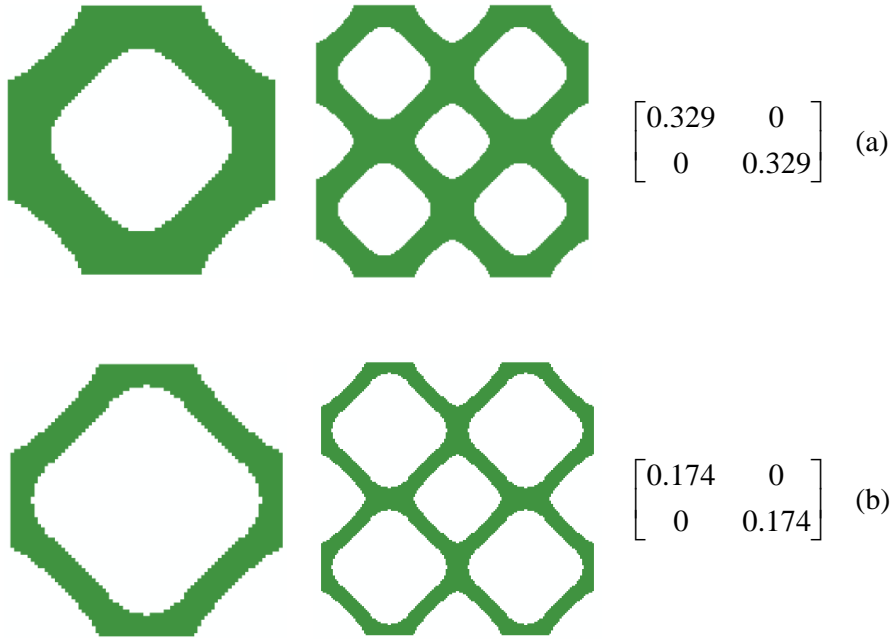


Figure 3.14: 2D base cells, 2×2 cells and effective thermal conductivity matrices of cellular materials, with maximum thermal conductivity (a) volume fraction of solid phase is 50%; (b) volume fraction is 30%

Hashin and Shtrikman (Hashin and Shtrikman, 1962) derived analytical bounds on the effective magnetic permeability of macroscopically homogeneous and isotropic materials based on the variational principals. The mathematical analogy enables the bounds to be also used for predicting the dielectric, electric conductivity, thermal conductivity, and diffusivity of such materials. The HS upper bound for cellular isotropic materials is expressed as:

$$k_{\max}^{HS} = \frac{k^s V_f}{2 - V_f} \quad (3.24)$$

When the volume fraction of the solid phase is equal to 50% and 30% of the total volume of the PBC, the Hashin-Shtrikman upper bound on thermal conductivity can be calculated as

0.333 and 0.176 respectively from the equation (3.24). As it can be seen from the thermal conductivity matrices presented in Figure 3.14, good consistency exists between the thermal conductivity of generated materials and the Hashin-Shtrikman upper bounds. Figure 3.15 demonstrates the evolution history of the microstructure when the prescribed volume (area) fraction of the solid phase is 30% of the total volume (area) of the PBC.

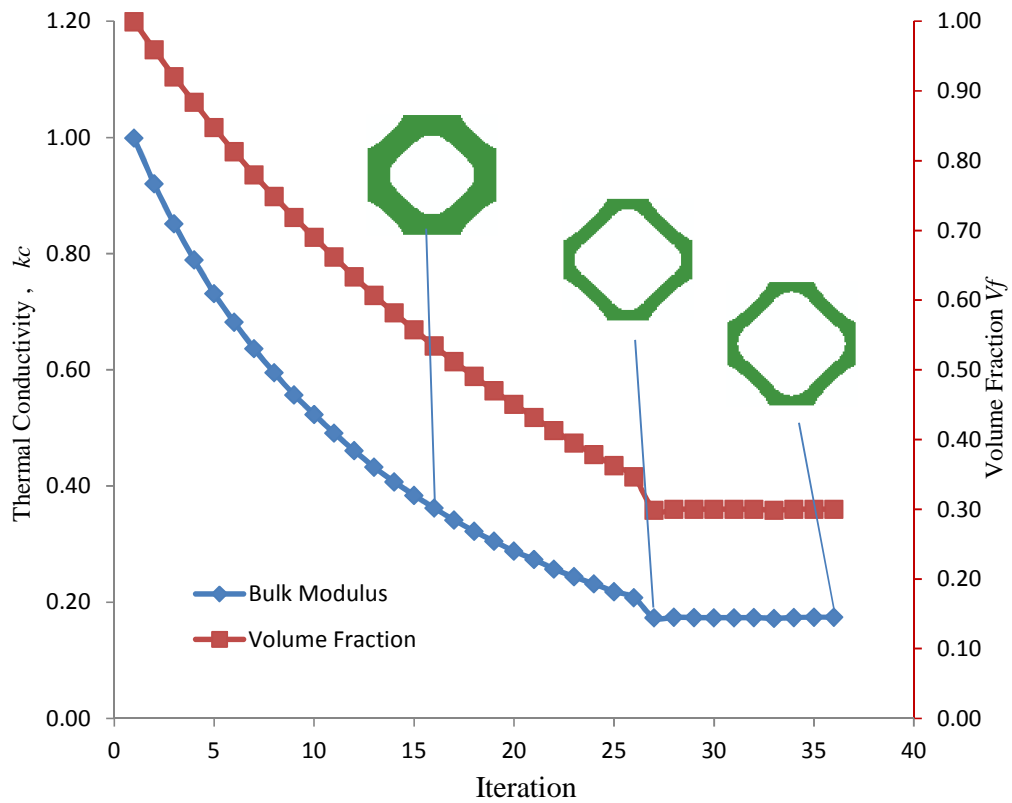


Figure 3.15: The evolution histories of thermal conductivity, volume fraction and microstructures of 2D material's microstructure with maximum thermal conductivity

### 3.2.6. 3D examples for maximizing thermal conductivity

For the topology optimization of 3D microstructures for material with maximum thermal conductivity, a cubic domain with dimensions  $30 \times 30 \times 30$  is discretized into  $30 \times 30 \times 30$ , 8-node cubic elements. It is assumed that the eigenvalue of thermal conductivity of the solid phase is  $k^s = 1$ . The BESO parameters are set as the evolutionary rate  $ER = 0.04$ , the filter radius  $r_{min} = 3$  and the penalty exponent as before is  $p = 3$ . The starting topology consists of 8 void elements at the centre of the domain while other elements are assigned with solid properties.

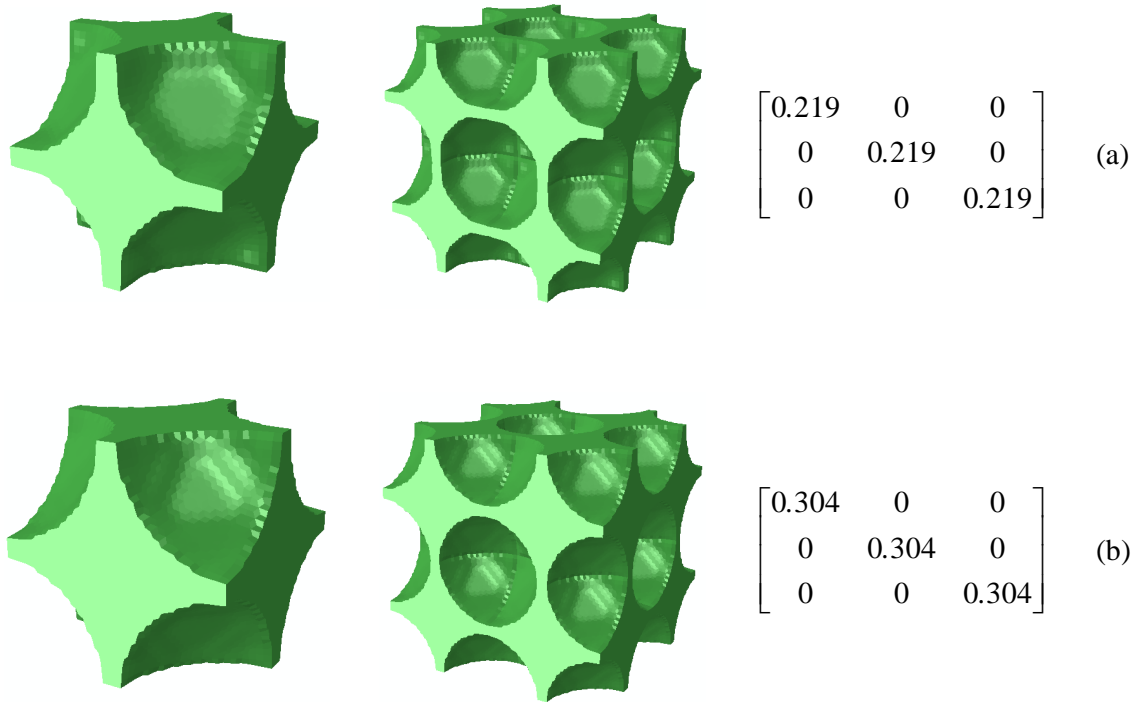


Figure 3.16: 3D base cells  $2 \times 2 \times 2$  array of cells and effective thermal conductivity matrices of cellular materials with maximum thermal conductivity (a) volume fraction of solid phase is 30%; (b) volume fraction is 40%

Figure 3.16 demonstrates the topology of microstructures, as well as the  $2 \times 2 \times 2$  array of generated base cells and effective thermal conductivity matrices when the prescribed volume fraction of the solid phase is equal to 30% and 40% of the total volume of the PBC. The total iterations for these examples are 38 and 31 respectively.

The Hashin and Shtrikman (1962) analytical bounds on the effective thermal conductivity of 3D cellular materials can be expressed as:

$$k_{\max}^{HS} = k^s + \frac{\alpha}{1 - \frac{\alpha}{3k^s}} \quad (3.25)$$

in which

$$\alpha = \frac{3(V_f - 1)k^s}{2} \quad (3.26)$$

The Hashin-Shtrikman upper bound is calculated 0.222 and 0.307 when the volume fraction of solid phase is 30% and 40% respectively which shows good agreement with the values shown in Figure 3.16.

Figure 3.17 demonstrates the evolution history of the microstructure when the prescribed volume (area) fraction of the solid phase is 30% of the total volume (area) of the PBC.

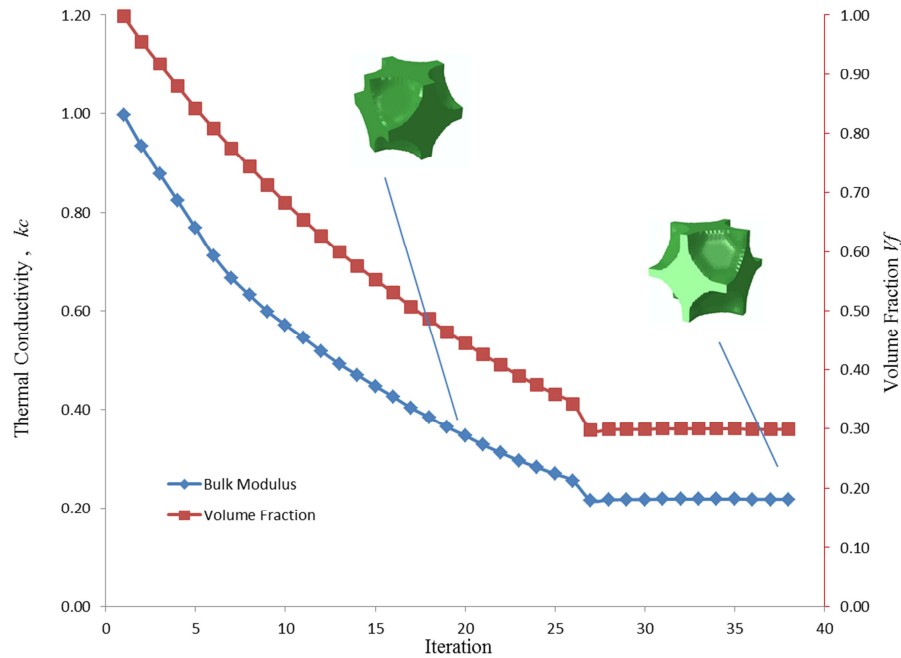


Figure 3.17: The evolution histories of thermal conductivity, volume fraction and microstructures of 3D material's microstructure with maximum thermal conductivity

### 3.3. Concluding remarks

In this chapter the BESO has been developed for the designing of microstructures for cellular materials with maximum bulk modulus, shear modulus or thermal conductivity. The developed BESO algorithm seeks optimal material distribution within the PBC by performing topology optimization subject to volume constraints. By applying the Homogenization theory the overall properties of material were calculated based on the analysis performed on the PBC. The Homogenization theory was also applied for calculation of elemental sensitivity numbers, which are a measure of estimation of the changes in homogenized material effective properties, as a result of alternation of elemental density within the PBC. Based on the



ranking of elemental sensitivity numbers, the BESO changes the density of elements from 1 to  $x_{\min}$  or from  $x_{\min}$  to 1 by imposing volume constraint iteratively, until the solution converges. Several 2D and 3D examples were presented to demonstrate the effectiveness of the proposed BESO method. The known analytical bounds were used for verification of the results. Some interesting topological patterns have been found for guiding cellular material design.

As it has been shown, the BESO can be easily implemented as a “post-processor” to commercial FEA software packages. In this study ABAQUS was used as the FEA analysis tool. The proposed method has other advantages in terms of the convergence speed and quality of the generated microstructures. The resulted topologies are represented by either solid or void elements without intermediate densities, which make the interpretation of results and manufacturing easier. The methodology developed in this chapter will be further extended to various other material design scenarios in the next chapters.

## **Chapter 4**

---

### **Topology optimization of microstructures for isotropic cellular materials**

#### **Background**

The objective of this chapter is to introduce a computational procedure to equip the methodology proposed in previous chapter with additional performance constraint. To this end, the design of materials with maximum stiffness in the form of bulk or shear modulus of elasticity with additional constraint on the isotropy of material is sought. In an isotropic material, the physical properties such as bulk or shear moduli are independent of material orientation and are identical in all directions. The elements of material constituent tensor of these types of materials remain unchanged under any transformation, from one coordinate system to another. Isotropic materials are the most common materials used in industry and are attractive for engineering applications (Barbero, 1999).

For the purpose of designing the microstructures of materials with symmetrical properties, a number of methods have been proposed in the literature. For instance a method based on the SIMP topology optimization has been introduced by Sigmund and Torquato (1997) and Sigmund (2000) in which the constraint on square symmetry of materials (in 2D problems in the form of  $D_{11} - D_{22} = 0$ ) and isotropy ( in 2D problems:  $D_{11} + D_{22} - (D_{12} + D_{21}) - 4D_{33} = 0$  ) are chosen to be implemented as a penalty function added to the objective function ( $f_0(x)$ ). The penalty functions are defined as the square of the deviation from fulfilment of square symmetry or isotropy constraint as:

$$D_{sq} = \left( \frac{D_{11} - D_{12}}{D_{11} + D_{12}} \right)^2 \quad (4.1.a)$$

$$D_{iso} = \left( \frac{D_{11} + D_{12} - 2(D_{12} + 2D_{33})}{D_{11} + D_{12}} \right)^2 \quad (4.1.b)$$

the modified objective function is then stated as:

$$f(x) = f_0(x) + w_1 D_{sq} + w_2 D_{iso} \quad (4.1.c)$$

where  $f_0(x)$ , is the optimization objective function. However, the selection of the penalization factors of  $w_1$  and  $w_2$  are highly dependent on the user's experience. In addition, the need for some interactions by the user during the optimization procedure makes the approach not fully systematic. Moreover, by using the Sequential Linear Programming (SLP) technique, this procedure needs several thousand iterations to be converged, due to the flatness of the modified objective function (Sigmund and Torquato, 1997).

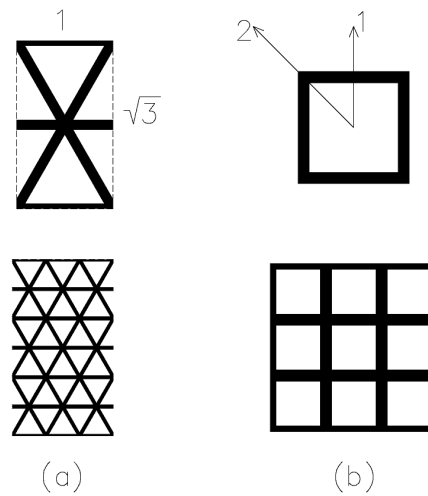


Figure 4.1: Examples of isotropic and anisotropic (square symmetric) microstructures of materials; (a) microstructures of an isotropic material; (b) microstructures of a square symmetric material

Imposing symmetrical constraints on microstructural geometry is another approach for the design of isotropic materials through inverse homogenization (Neves et al., 2000, Torquato, 2002). Based on the Neumann principle (Love, 1934, Sadd, 2005), it is known that certain type of geometrical symmetry of the material microstructures leads to the symmetry in the response of the material. Figure 4.1 demonstrates a microstructure of isotropic and an anisotropic material. In the Figure 4.1a the microstructure possesses  $60^\circ$  symmetry and the resulting material is isotropic (Bendsøe and Sigmund, 2003, Neves et al., 2000, Sadd, 2005). In the microstructure shown in Figure 4.1b such a  $60^\circ$  symmetry does not exist and dissimilar elasticity properties are expected, for example along directions 1 and 2. However, the  $45^\circ$  symmetry of the microstructure produces square symmetry characteristics on the material response. This feature could be used in the material design by imposing a geometrical constraint on the periodic base cell. However, it should be noted that the symmetry of the microstructure is sufficient but not a necessary condition for the symmetry of material

properties (Sigmund and Torquato, 1997) and imposing geometrical constraint may inhibit the realization of many potential solutions in an inverse homogenization based optimization.

Recently, a Level-set method was applied for the design of two-phase isotropic composites with maximum stiffness and thermal conductivity (Wilkins et al., 2007, Challis et al., 2008). In this proposed approach, a “nearest” feasible isotropic thermal conductivity and elasticity tensors are formulated at each iteration. The objective function is defined to minimize the difference between the thermal conductivity and elasticity tensors of material and their corresponding feasible and nearest isotropic tensor. The extra constraint is imposed by modifying the evolution rate in the Hamilton-Jacobi equation. The proposed method is capable of generating microstructures for 3D isotropic materials (Challis et al., 2008). However as mentioned in Chapter 2, the Level-set implementation is usually difficult and, so far, has not reached to the level of regular application (Rozvany, 2009).

In this chapter an alternative approach for topology optimization of cellular isotropic materials will be presented.

## **4.1. Methodology**

### **4.1.1. Problem statement of isotropic material topology optimization**

In this study, for the purpose of designing isotropic materials, the necessary and sufficient conditions of isotropy are defined as an additional constraint in the optimization procedure. As mentioned before, in an isotropic material the constituent tensor remains unchanged under

any transformation from one coordinate system to another. Considering the elasticity matrix of an orthotropic material in 3D form as:

$$D = \begin{bmatrix} D_{11} & D_{12} & D_{13} & 0 & 0 & 0 \\ D_{21} & D_{22} & D_{23} & 0 & 0 & 0 \\ D_{31} & D_{32} & D_{33} & 0 & 0 & 0 \\ 0 & 0 & 0 & D_{44} & 0 & 0 \\ 0 & 0 & 0 & 0 & D_{55} & 0 \\ 0 & 0 & 0 & 0 & 0 & D_{66} \end{bmatrix} \quad (4.2)$$

it can be shown that that relations (4.3) to (4.6) are necessary and sufficient conditions for isotropy of material.

$$D_1 = D_{11} = D_{22} = D_{33} \quad , \quad (4.3)$$

$$D_2 = D_{12} = D_{23} = D_{31} = D_{21} = D_{32} = D_{13} \quad , \quad (4.4)$$

$$D_3 = D_{44} = D_{55} = D_{66} \quad , \quad (4.5)$$

$$D_1 - D_2 = 2D_3 \quad (4.6)$$

In the cases where the equations (4.3), (4.4) and (4.5) hold, the material is known as cubic symmetric, in which, each of the three principal axes has fourfold symmetry. By engaging all elements of the cubic symmetric elasticity matrix, the condition (4.6) can be rewritten as equation (4.7a) for 3D cases:

$$C_{iso} = 2(D_{11} + D_{22} + D_{33}) - (D_{12} + D_{31} + D_{23} + D_{21} + D_{13} + D_{32}) - 4(D_{44} + D_{55} + D_{66}) = 0$$

$$(4.7a)$$

Similar relationships exist in 2D plane stress problems. By treating elements of square symmetric elasticity tensor equally, the condition (4.6) can be rewritten as:

$$C_{iso} = D_{11} + D_{22} - (D_{12} + D_{21}) - 4D_{33} = 0 \quad (4.7b)$$

As it was seen from numerical results of Chapter 3, the cubic symmetry conditions of relations (4.3) to (4.5) are always satisfied when the BESO procedure starts from an initial square or cubic symmetric topology and treats all corresponding elements in perpendicular directions equally. Therefore, in order to obtain an isotropic material, condition of equation (4.7) needs to be introduced, as an additional constraint in the BESO method.

In the BESO setting, the topology optimization problem of cellular material with a maximum stiffness and with constraints on the isotropy and volume fraction can be expressed mathematically as:

$$\text{Maximize } f_1(x) = K \text{ or } G \quad (4.8.a)$$

$$\text{Subject to: } C_{iso} = 0 \quad (4.8.b)$$

$$V^* = \sum_i^n x_i V_i \quad (4.8.c)$$

$$x_i = x_{\min} \text{ or } 1 \quad (4.8.d)$$

in which material's stiffness is expressed by bulk ( $K$ ) or shear ( $G$ ) moduli defined in equation (3.3) or (3.4); the equation  $C_{iso} = 0$  defines the constraint on materials isotropy with the expansion shown in equation (4.7);  $V_i$  is the volume of the  $i^{th}$  element and  $V^*$  denotes the prescribed volume of the solid phase. As before the design variable  $x_i$  represents the density of the  $i^{th}$  element, which is restricted to a binary value of either 1 for a solid element or a small value,  $x_{min}$  (e.g. 0.001) for a void element.

#### 4.1.2. Solution Method

For solving the problem (4.2), the optimality criterion can be described as that sensitivity numbers of solid elements ( $x_i = 1$ ) to be higher than void elements ( $x_i = x_{min}$ ). Therefore, an update scheme is devised to change the design variable  $x_i$  from 1 to  $x_{min}$  for elements with lower sensitivity numbers and from  $x_{min}$  to 1 for elements with higher sensitivity numbers (Huang and Xie, 2010b). As discussed in Chapter 3, in the BESO method, the volume constraint can be easily satisfied by gradually removing and adding elements through the introduction of evolutionary rate.

One of the explored features of the new soft-kill BESO method is its capability to be integrated with an extra performance constraint, in addition to the volume constraint. In the stiffness optimization of structures in macro-scale, the new soft-kill BESO procedure has been successfully combined with an additional constraint on allowable displacement (Huang and Xie, 2009b, Huang and Xie, 2010a). In the approach, the variation of the displacement for the next iteration is approximated through a gradient based estimation. The topology of the



structure is evolved toward the desired functional property, through introducing a Lagrangian multiplier. This methodology can be extended to impose the isotropy constraint by modifying the original objective function of equation (4.2) as:

$$f(x) = f_j(x) + \lambda \times C_{iso} \quad (4.9a)$$

in which the Lagrangian multiplier  $\lambda \in ]-\infty, +\infty[$ . This equation is equivalent to:

$$f(x) = f_j(x) + \frac{\ell}{(1-|\ell|)} \times C_{iso} \quad (4.9b)$$

where the new variable  $\ell \in [-1, 1]$  corresponds to the changes of the Lagrangian multiplier in the range of  $\lambda \in ]-\infty, +\infty[$ . It can be seen that the modified objective function is equivalent to the original one, when the isotropy constraint is satisfied. With the help of Homogenization theory the derivatives which reflect the variation of objective function with respect to the density change within the element can be expressed as:

$$\frac{df(x)}{dx_i} = \frac{df_j(x)}{dx_i} + \frac{\ell}{(1-|\ell|)} \times \frac{dC_{iso}}{dx_i} \quad (4.10a)$$

Since in BESO only the ranking of elements based on sensitivity numbers is important, by multiplying the above equation in the positive value of  $1-|\ell|$  the sensitivity number of elements can be expressed as:

$$\alpha_i = (1-|\ell|) \times \frac{df_j(x)}{dx_i} + \ell \times \frac{dC_{iso}}{dx_i} \quad (4.10b)$$

The derivatives of the first term in equation (4.10) can be calculated numerically using the equation (3.15). Likewise, the term  $C_{iso}$  can be readily expanded through equation (4.7) and the derivatives with respect to the design variable  $x_i$  can be calculated using the same equation (3.15). But before the calculation of  $\alpha_i$  the Lagrangian multiplier needs to be calculated.

#### 4.1.3. Determination of the Lagrangian multiplier

In an iterative process, the Lagrangian multiplier  $\lambda$  is determined in such a way that, the value of constraint  $C_{iso}$ , to be zero in the subsequent iteration. For this purpose, the following gradient-based expression is used to estimate the next iteration value of the constraint:

$$C_{iso}^{t+1} \approx C_{iso}^t + \sum_i \frac{dC_{iso}^t}{dx_i} \Delta x_i \quad (4.11)$$

where the superscript  $t$  and  $t+1$  denotes the current and the next iteration numbers respectively. The above equation yields a linearized estimation of the constraint function around the design point  $\mathbf{x}$  by using the expansion of the first term of Taylor series. Equation (4.11) is very similar to the expressions used in sequential linear programming (SLP) (see Chapter 3). The derivatives in equation (4.11) are determined numerically.

At the beginning of each iteration, initial elemental sensitivity numbers are calculated by assuming  $\ell = 0$ . Then, by ranking elements and imposing volume constraint, a set of possible updated design variables are evaluated. The constraint value for the next iteration  $C_{iso}^{t+1}$  is estimated by using the equation (4.11). If the constraint value  $C_{iso}^{t+1}$  is negative, then  $\ell$  has to

be gradually increased from 0 to 1. Thus the modified objective function maximizes the bulk or shear modulus and increases the  $C_{iso}^{t+1}$  simultaneously. Contrarily, if the calculated value of  $C_{iso}^{t+1}$  is positive, the summation term in equation (4.11) has to be decreased. This could be done by gradually decreasing  $\ell$  from 0 to -1; thereby, the modified objective functions maximize the bulk or shear modulus and minimize the positive  $C_{iso}^{t+1}$  simultaneously.

The precise value of  $\ell$  could be determined using the bisection algorithm in an internal loop, by exploiting two auxiliary variables  $\ell_{low}$  and  $\ell_{up}$ . For instance at the beginning of each internal loop with  $\ell=0$ , if the calculated value  $C_{iso}^{t+1}$  is positive, then the boundary values of the auxiliary variables are selected  $\ell_{low} = -1$ ,  $\ell_{up} = 0$  and the new value of  $\ell$  is calculated by setting  $\ell = (\ell_{up} + \ell_{low})/2$ . Then the sensitivity numbers are updated according to equation (4.9) and new set of design variables as well as  $C_{iso}^{t+1}$  are calculated by the ranking of elemental new sensitivity numbers. If the updated  $C_{iso}^{t+1} > 0$ , then the upper auxiliary variable ( $\ell_{up}$ ) should be replaced by the current  $\ell$  and the new coefficient is calculated as  $\ell = (\ell_{up} + \ell_{low})/2$ . If  $C_{iso}^{t+1} < 0$  then the lower auxiliary variable ( $\ell_{low}$ ) is replaced with current  $\ell$  and the updated value is calculated by setting  $\ell = (\ell_{up} + \ell_{low})/2$ . The procedure of the internal loop comes to an end when the discrepancy between boundary variables ( $\ell_{low}$ ,  $\ell_{up}$ ) is sufficiently small (e.g.  $10^{-5}$ ).

#### 4.1.4. Procedure

The whole BESO procedure can be described by the following steps:

Step 1: Define the BESO parameters such as prescribed volume fraction ( $V^*$ ); evolutionary ratio ( $ER$ ); penalty exponent  $p$  (normally  $p = 3$ ) and filter radius  $r_{\min}$ ;

Step 2: Construct a solid-void finite element model for the PBC;

Step 3: Define the periodic boundaries on PBC; define the loads that are equivalent to unit strain fields,  $\bar{\epsilon}_{pq}^{kl}$ . In 2D problems, 3 cases of loading and boundary conditions and in 3D problems 6 cases are necessary. Perform the finite element analysis (FEA) and extract the induced displacement fields  $\mathbf{u}$ ;

Step 4: Calculate  $\frac{df_1(x)}{dx_i}$  and  $\frac{dC_{iso}}{dx_i}$  numerically, filter the term  $\frac{df_1(x)}{dx_i}$ ;

Step 5: Let  $\ell = 0$ ;

Step 6: Calculate  $\alpha_i$  using equation (4.10b). Rank all elemental sensitivity numbers and obtain new set of design variables  $x_i$  by applying volumetric constraint as

$$V^{t+1} = \max(V^t(1-ER), V^*);$$

Step 7: Calculate  $C_{iso}^{t+1}$  using equation (4.11);

Step 8: If  $C_{iso}^{t+1} > 0$  then decrease  $\ell$  within the range  $[-1, 0]$  using the above mentioned bisection algorithm; otherwise, increase  $\ell$  within the range  $[0, 1]$ ;

Step 9: Repeat steps 6 to 8 until the difference between auxiliary variables  $\ell_{low}$  and  $\ell_{up}$  becomes sufficiently small (e.g.  $10^{-5}$ );

Step 10: Average the sensitivity numbers with their values of previous iteration and then update design variables  $x_i$  ;

Step 11: Repeat steps 2 through to 8, until both volume constraint and convergence criterion are met. The convergence criterion is regarded to be satisfied when the changes in the objective function are less than a specific tolerance, for example

$$error = \frac{\sum_{i=1}^5 (f^{t-i+1} - f^{t-i-9})}{\sum_{i=1}^5 f^{t-i+1}} < 0.001 \quad (4.12)$$

in which  $f$  is the objective function and superscript is the iteration number.

## 4.2. Results and discussion

This section presents some examples of the microstructures that are designed by the proposed method. Because the loadings and boundary conditions in a square base cell are symmetrical with respect to main perpendicular axes, in all 2D cases, only one-fourth of square PBC is modelled; this assumption reduces the computational costs. Similarly, only one-eighth of the PBC is modelled in all 3D problems.

The presented results are verified with known analytical bounds of bulk and shear moduli. As mentioned in previous chapters, in quasi-homogenous and quasi-isotropic composite materials the analytical upper bounds on materials attainable bulk and shear moduli were derived by Hashin and Shtrikman (Hashin and Shtrikman, 1963). For cellular materials that are made with a void phase and a solid phase of volume fraction  $V_f$ , bulk modulus  $K^s$  and shear modulus of  $G^s$ , the Hashin and Shtrikman (HS) upper bounds are given as:

$$K_{HS}^{up} = \frac{V_f K^s G^s}{(1-V_f)K^s + G^s} \quad \text{2D plane stress bulk modulus upper bound} \quad (4.13a)$$

$$K_{HS}^{up} = \frac{4K^s G^s V_f}{3K^s(1-V_f) + 4G^s} \quad \text{3D bulk modulus upper bound} \quad (4.13b)$$

$$G_{HS}^{up} = \frac{G^s K^s V_f}{2(K^s + G^s) - V_f(K^s + 2G^s)} \quad \text{2D plane stress shear modulus upper bound} \quad (4.13c)$$

$$G_{HS}^{up} = \frac{V_f G^s (9K^s + 8G^s)}{K^s(15 - 6V_f) + G^s(20 - 12V_f)} \quad \text{3D shear modulus upper bound} \quad (4.13d)$$

For cubic symmetric materials, Zener (1948) has proposed an index for measurement of the anisotropy of materials. This index is frequently used in literature (Ledbetter and Migliori, 2006, Wang et al., 2011) and is known as the Zener anisotropy ratio. In terms of the three main coefficients of the cubic symmetric material elasticity matrix defined in equations (4.3) to (4.5), the Zener anisotropy ratio is expressed as:

$$A = \frac{2D_3}{D_1 - D_2} \quad (4.14)$$

The above ratio defines a measure for resistance to elastic deformation along the direction [010], under a shear stress acting across plane (100) with respect to the resistance to deformation along the direction [110] under a shear stress acting across the (110) plane (Zener 1948). A comparison with equation (4.6) indicates that this ratio should be equal to 1.0 for an isotropic material. The Zener anisotropy ratio is also applicable for square symmetric material with  $D_3$  standing for  $D_{33}$  in equation (4.14).

#### 4.2.1. 2D cellular materials with maximum bulk modulus

To obtain microstructures for materials with maximum bulk modulus, the square design domain of PBC with dimensions of  $120 \times 120$  is discretized into  $120 \times 120$ , 4-node square elements. The Young's modulus and Poisson's ratio of the solid phase are selected as  $E^s = 1$  and  $\nu = 0.3$  respectively. The BESO parameters are set at the evolutionary rate  $ER = 0.006$  the filter radius  $r = 6$  and the penalty exponent as  $p = 3$ . The prescribed volume (area) fraction of the solid phase is selected to be equal to 20% of the total area of the base cell. At the beginning of the procedure, solid properties are assigned to all elements of the PBC, except for four elements at the centre of the base cell which are defined as void (Figure 3.1).

In order to compare the microstructures generated with and without imposing the isotropy constraint, two microstructures are presented in Figure 4.2. Figure 4.2a shows the microstructure of the isotropic cellular material, while Figure 4.2b demonstrates the microstructural topology of the cellular material which is generated without imposing the constraint on isotropy. Figure 4.2c and 4.2d illustrates the corresponding  $3 \times 3$  array of base cells. The effective elasticity matrices of these cellular materials are also given in the figure.

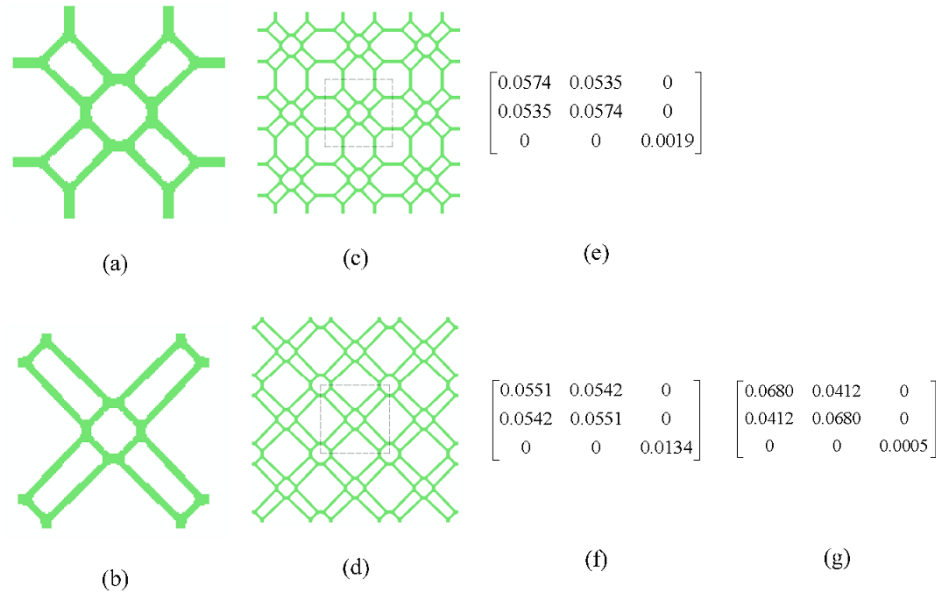


Figure 4.2: Microstructures of 2D cellular materials with maximum bulk modulus; (a) PBC generated by imposing the isotropy constraint; (b) PBC generated without imposing the isotropy constraint; (c)  $3 \times 3$  base cells of (a); (d)  $3 \times 3$  base cells of (b); (e) elasticity matrix of isotropic material; (f) elasticity matrix of square symmetric material; (g) elasticity matrix of square symmetric material with  $45^\circ$  transformation.

The bulk modulus of the isotropic cellular material is 0.0555, which demonstrates a good agreement with HS upper bound, calculated 0.0575 from equation (4.13.a). It can be shown that the elasticity matrix of the isotropic solution is invariant under any transformation (rotation) from one coordinates system to another. However, as it can be examined, for instance by  $45^\circ$  transformation of the elasticity matrix, the microstructure that is generated without isotropy constraint demonstrates different properties along different directions (Figure 4.2g).

To demonstrate the effects of imposing isotropy constraint, the variations of the Zener anisotropy ratio for the two generated cellular materials are compared in Figure 4.3. It can be



seen that the proposed algorithm effectively sustains the Zener anisotropy ratio close to 1, through the entire process for designing the microstructure of the cellular material with the isotropy constraint. When the isotropic constraint is not imposed, the Zener anisotropy ratio is about 27.5 at the final design stage of generating square symmetric material.

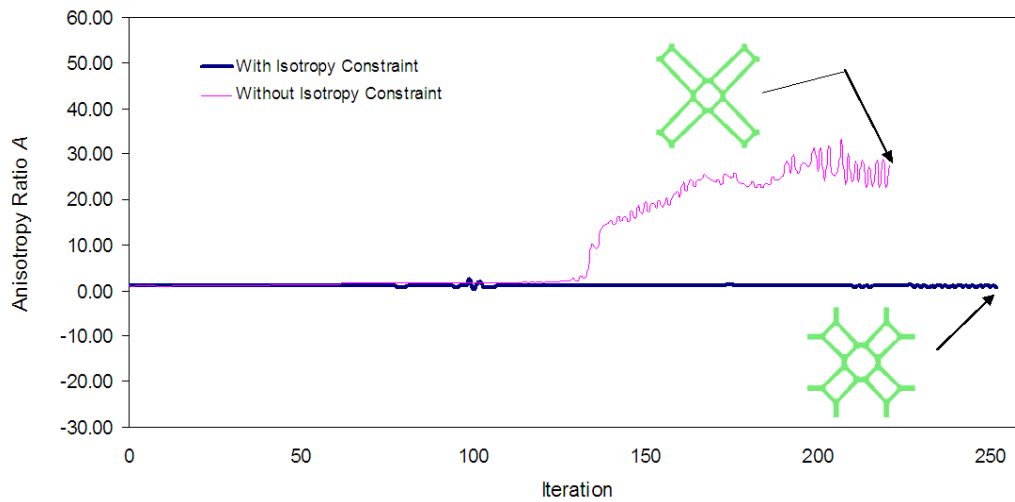


Figure 4.3: Evolution histories of the Zener anisotropy ratio for designing isotropic cellular material and square symmetric cellular material with maximum bulk modulus.

#### 4.2.2 2D cellular materials with maximum shear modulus

In this example, the objective is to design microstructures for cellular materials with maximum shear modulus and the solid phase volume (area) fraction of 25%. The PBCs with dimensions  $120 \times 120$  are divided into  $120 \times 120$  four-node square elements. The evolutionary rate  $ER = 0.005$  and filter radius  $r_{\min} = 5$  are set as BESO parameters. As before, the Young's modulus  $E^s = 1$  and Poisson's ratio  $\nu = 0.3$  are selected as the mechanical properties

of the solid constituent phase. The initial topology consists of a domain in which all elements are assigned solid properties except for four void elements at the centre (Figure 3.1).

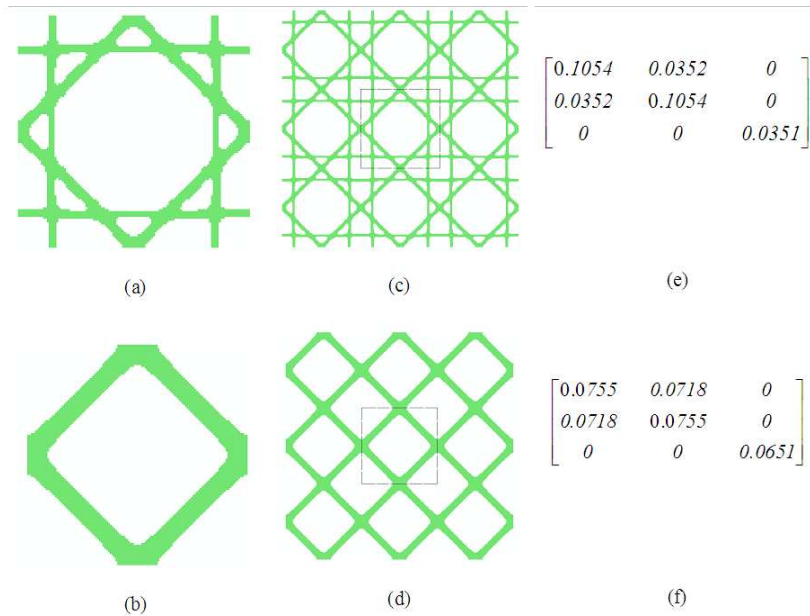
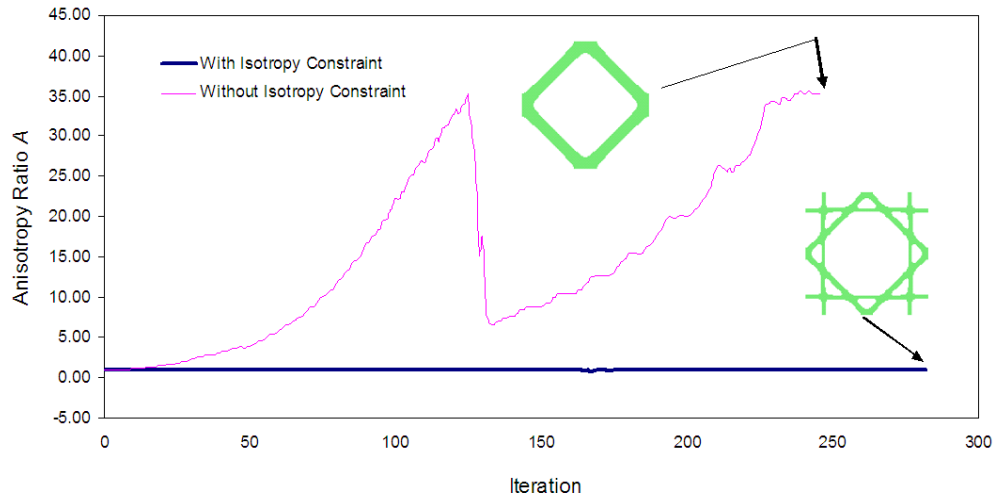


Figure 4.4: Microstructures of cellular materials with maximum shear modulus; (a) the PBC with the isotropy constraint; (b) the PBC without the isotropy constraint; (c) base cells of (a); (d) base cells of (b); (e) elasticity matrix of isotropic material; (f) elasticity matrix of square symmetric material.

The two microstructures that are generated with and without imposing the isotropy constraint are shown in Figure 4.4. The corresponding  $3 \times 3$  array of unit cells and material elasticity matrix are also presented. As is shown in Figure 4.4, the attained shear modulus for the resulting isotropic material is 0.0351, which is very close to the HS upper bound on shear modulus calculated at 0.0376 from equation 4.13b. It is also noted that although the objective of this example is to maximize the shear modulus of material, the attained bulk modulus of

the isotropic design is 0.0703, which is very close to the HS bulk modulus upper bound 0.0746 (calculated from equation (4.13.a)).



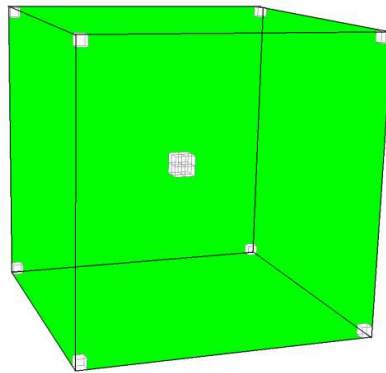
*Figure 4.5: Evolution histories of Zener anisotropy ratio for designing isotropic and square symmetric cellular materials with maximum shear modulus*

Figure 4.5 demonstrates the evolution history of the Zener anisotropy ratio throughout the whole optimization process. As can be seen from the figure, when the constraint on isotropy is imposed, the Zener anisotropy ratio is kept very close to 1 throughout the whole process. However, when such a constraint is not imposed, a square symmetrical material with a Zener anisotropy ratio of  $A = 35.3$  is generated (Figure 4.5).

#### **4.2.3. 3D cellular materials with maximum bulk modulus**

The proposed algorithm can be readily extended for topology optimization of microstructures in 3D cases, without any theoretical difference. The cubic PBC with dimensions  $46 \times 46 \times 46$  is

discretized into  $46 \times 46 \times 46$  eight-node cubic elements and the prescribed volume fraction of solid constituent phase is selected equal to 20% of the total volume of the PBC. The BESO parameters are chosen as the evolutionary rate of  $ER = 0.006$  and the filter radius  $r_{\min} = 2.5$ . The Young's modulus and Poisson's ratio of the solid phase are  $E^s = 1$  and  $\nu = 0.3$  respectively. As it is shown in Figure 4.6, the initial topology of the PBC entirely consists of solid elements except for eight void elements at the centre and one void element at the eight corners.



*Figure 4.6: Initial material distribution in 2D problems (solid elements are shown in green)*

With the abovementioned design parameters and initial topologies, Figures 4.7a and 4.7b show the two microstructures that are designed for the maximum bulk modulus, with and without isotropy constraints. The interior views of these microstructures and the corresponding  $2 \times 2$  arrays of unit cells and elasticity matrices of the materials are also shown in the Figure 4.7. The bulk modulus of cellular material with the isotropy constraint is 0.0599. Figure 4.8 demonstrates the evolution history of the Zener anisotropy ratio throughout the

design procedure for both base cells. As indicated, the Zener anisotropy ratio is very close to 1 for the design with the isotropy constraint.

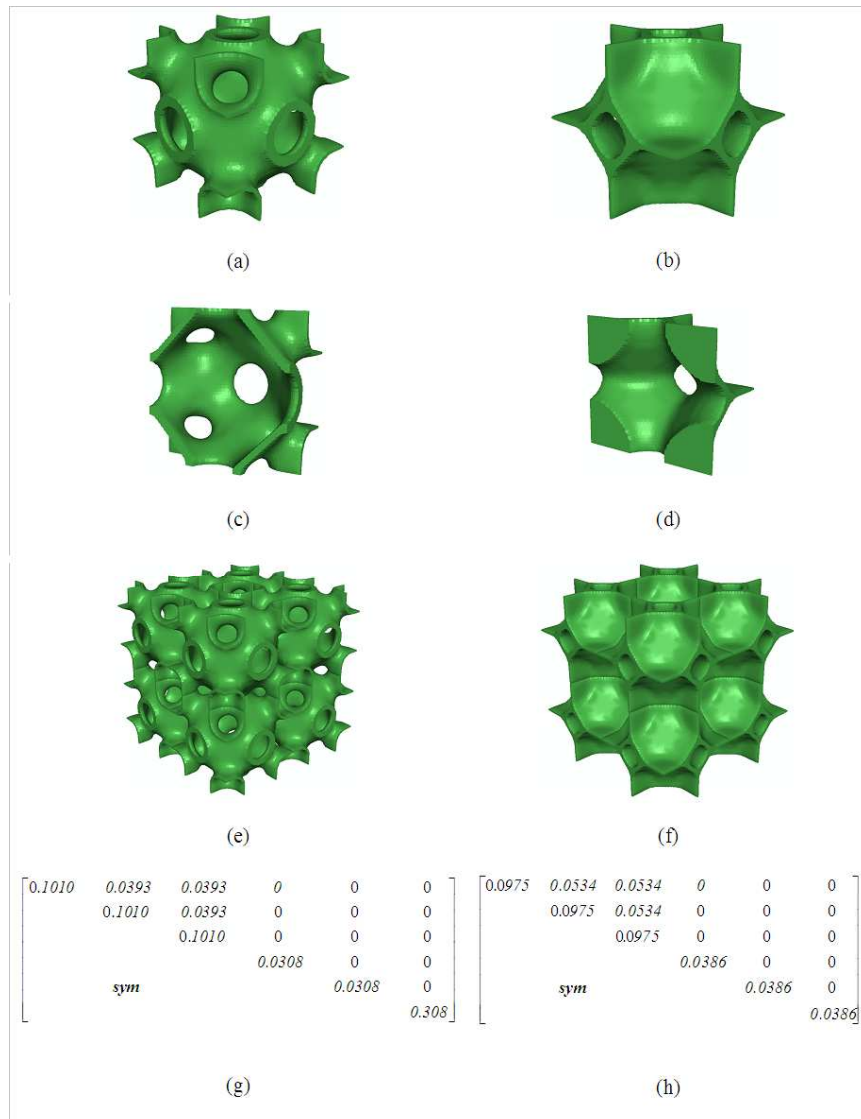


Figure 4.7: 3D microstructures of materials with maximum bulk modulus; (a) PBC with isotropy constraint; (b) PBC without isotropy constraint; (c) half of the PBC shown in (a); (d) half of the PBC shown in (b); (e)  $2 \times 2$  base cells of (a); (f)  $2 \times 2$  base cells of (b); (g) isotropic material elasticity matrix; (h) cubic symmetric material elasticity matrix

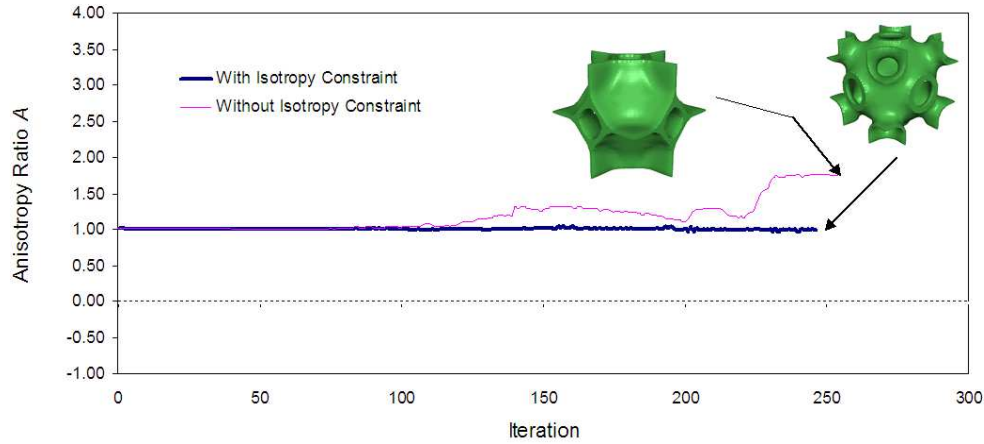


Figure 4.8: Evolution histories of Zener anisotropy ratio for designing isotropic cellular material and cubic symmetric cellular material with maximum bulk modulus.

Figure 4.9 shows another example of isotropic and cubic symmetric microstructures in which the BESO parameters are set as  $ER = 0.007$  and  $r_{\min} = 3$ . The PBC and elements dimensions are similar to the previous example. For both isotropic and cubic symmetric microstructures of this example, similar to the Figure 3.9, the initial topologies include eight void elements at the centre of the PBC while solid properties are assigned to other elements. The generated topologies are shown in Figure 4.9. The bulk moduli of the resulting isotropic and anisotropic cellular materials are 0.0585 and 0.0619 respectively. As it is shown in Figure 4.10, the Zener anisotropy ratio for the isotropic and anisotropic materials are  $A = 1.0$  and 2.52 respectively.

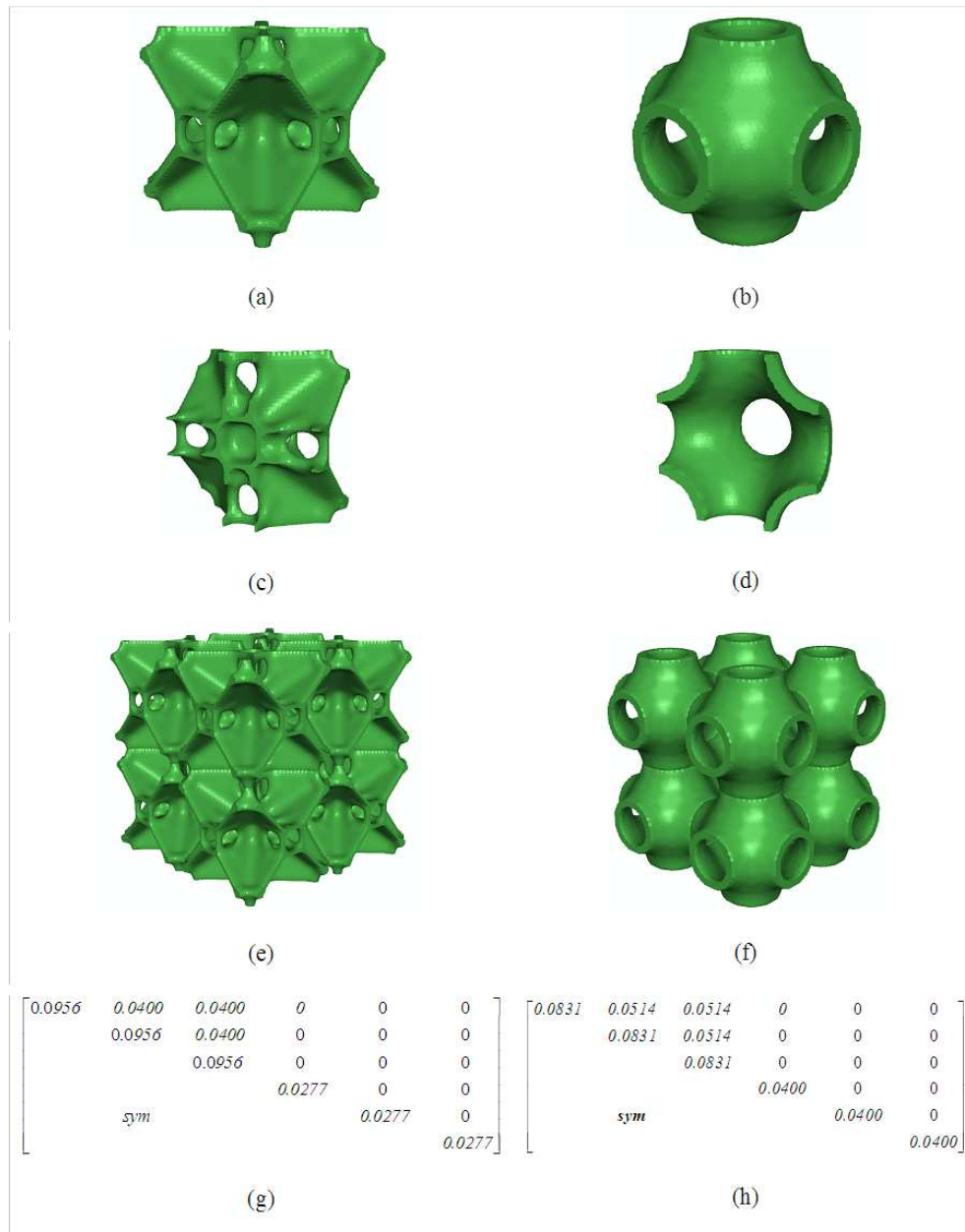


Figure 4.9: 3D microstructures of materials with maximum bulk modulus; (a) the PBC with the isotropy constraint; (b) PBC without the isotropy constraint; (c) half of the PBC shown in (a); (d) half of the PBC shown in (b); (e)  $2 \times 2 \times 2$  base cells of (a); (f)  $2 \times 2 \times 2$  base cells of (b); (g) isotropic material elasticity matrix;

(h) cubic symmetric material elasticity matrix

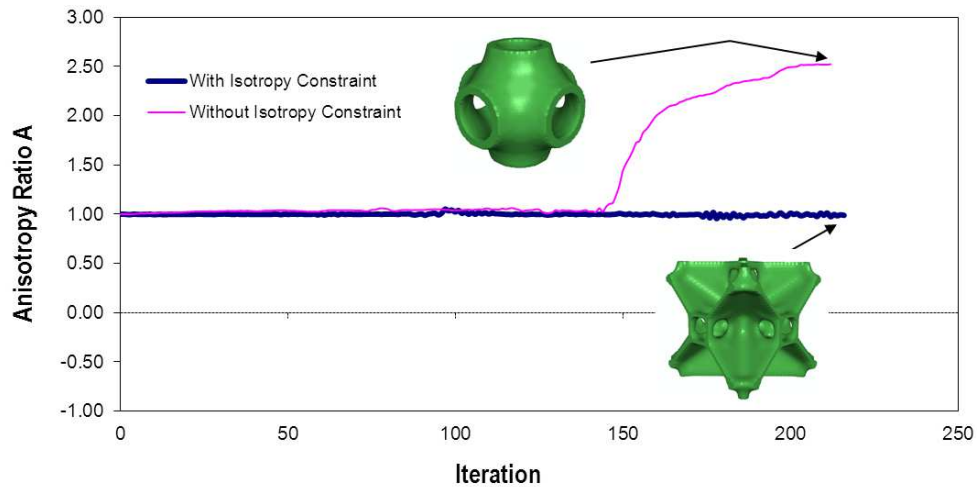


Figure 4.10: Evolution histories of Zener anisotropy ratio for designing isotropic cellular material and cubic symmetric cellular material with maximum bulk modulus.

#### 4.2.4. 3D cellular materials with maximum shear modulus

The objective of this example is to design 3D microstructures of cellular materials with maximum shear modulus. The finite element model of the base cell with dimensions  $60 \times 60 \times 60$  is discretized into  $60 \times 60 \times 60$ , eight-node cubic elements. The mechanical properties of the solid phase are selected as the Young's modulus of  $E^s = 1$  and the Poisson's ratio of  $\nu = 0.3$ . The evolution rate  $ER = 0.007$ , filter radius  $r_{\min} = 3$  and the penalty exponent  $p = 3$  are selected as the BESO parameters. The procedure starts from the initial topology, which consists of elements with solid properties except for eight void elements at the centre and four void elements at the centre of each 6 sides of the finite element model of the PBC. The prescribed volume fraction of the solid phase is selected as 40% of the total volume of the PBC.



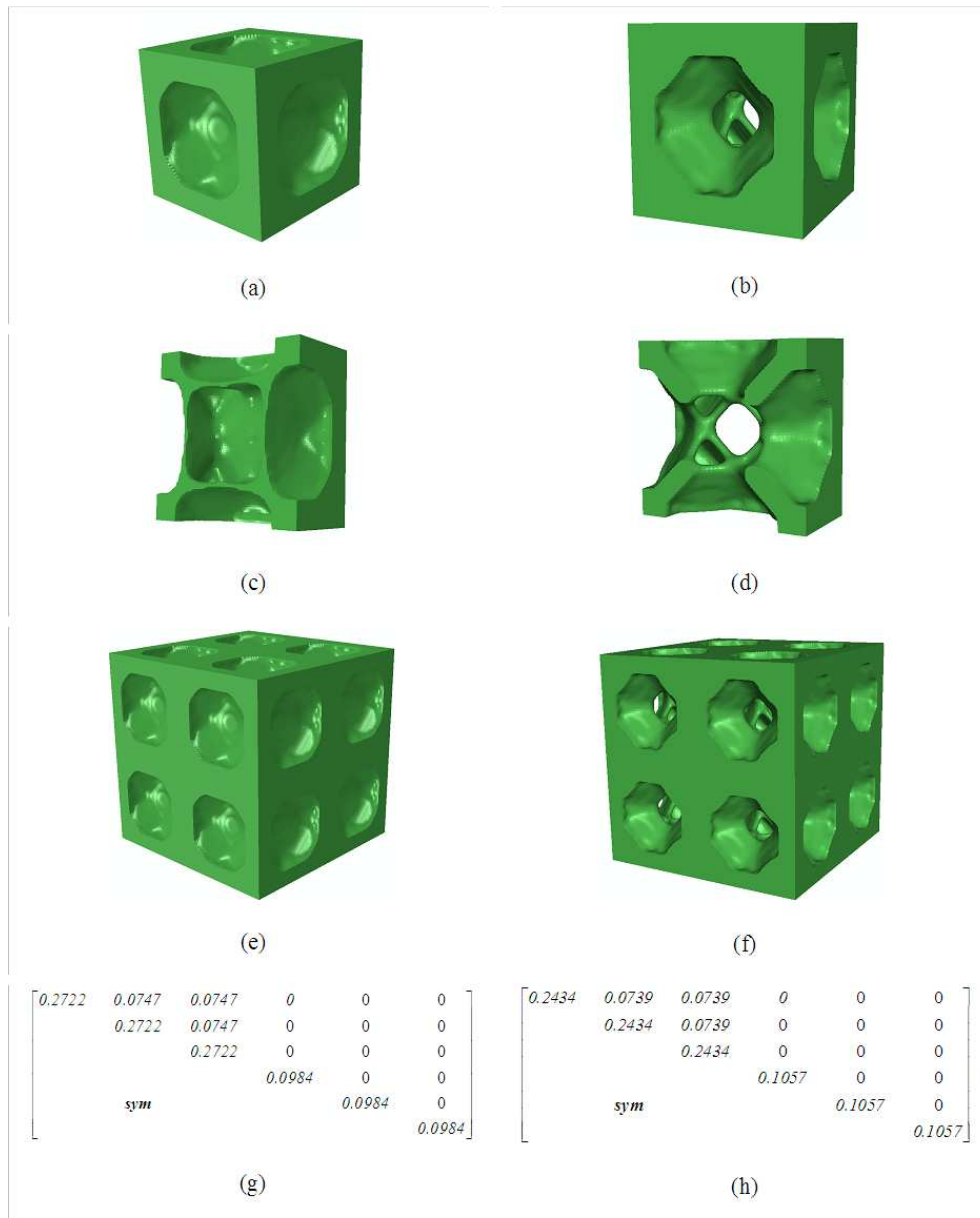


Figure 4.11: 3D microstructures of materials with maximum shear modulus; (a) the PBC with the isotropy constraint; (b) the PBC without the isotropy constraint; (c) half of the PBC shown in (a); (d) half of the PBC shown in (b); (e) base cells of (a); (f) base cells of (b); (g) isotropic material elasticity matrix; (h) cubic symmetric material elasticity matrix

Figure 4.11 demonstrates the generated microstructures and elasticity matrices of isotropic and cubic symmetric cellular materials. As indicated in the figure, the shear modulus of the isotropic cellular material is equal to 0.0984, which is very close to HS shear modulus upper bound that is calculated equal to 0.0995 from the equation (4.13d). The Zener anisotropy ratio for the isotropic cellular material is  $A = 1.0$ . However, the topology optimization without the isotropy constraint results in the microstructure with the Zener anisotropy ratio of 1.25. It is noticed that the bulk modulus of isotropic material (0.1405) is also very close to the HS upper bound (0.1688), although the objective of this example is to maximize the shear modulus.

#### **4.2.5. 2D isotropic cellular materials with negative Poisson's ratio**

To demonstrate the capability of the proposed procedure in imposing the isotropy constraint in combination with other objective function, in the following example 2D microstructures for isotropic cellular materials with negative Poisson's ratio are sought. Negative Poisson's ratios in foams were observed by Lakes (1993). It was further qualitatively demonstrated by (Phan-Thien and Karihaloo, 1994), that composite materials with randomly distributed microstructures can have isotropic behaviour with negative Poisson's ratio. The key feature of their microstructures is the existence of re-entrant corners, which was already noticed by Lakes (1993).

Through inverse homogenization, Sigmund (1994a, 1994b) found that by modelling the materials microstructure as a continuum environment, it is very difficult to attain topologies with negative Poisson's. The Poisson's ratio can attain the negative value of -1, if the shear

modulus of material is much larger than its bulk modulus. On the other hand, the numerical experiences in 2D problems demonstrates that the attainable values of  $D_{12}$  and  $D_{33}$  are correlated (Sigmund, 1994a, 1994b). In this study the following statement has been used as the objective function to find a material with negative Poisson's ratio,

$$\text{Minimize: } f_1(x) = D_{21} + D_{12} - 2D_{33} \quad (4.15)$$

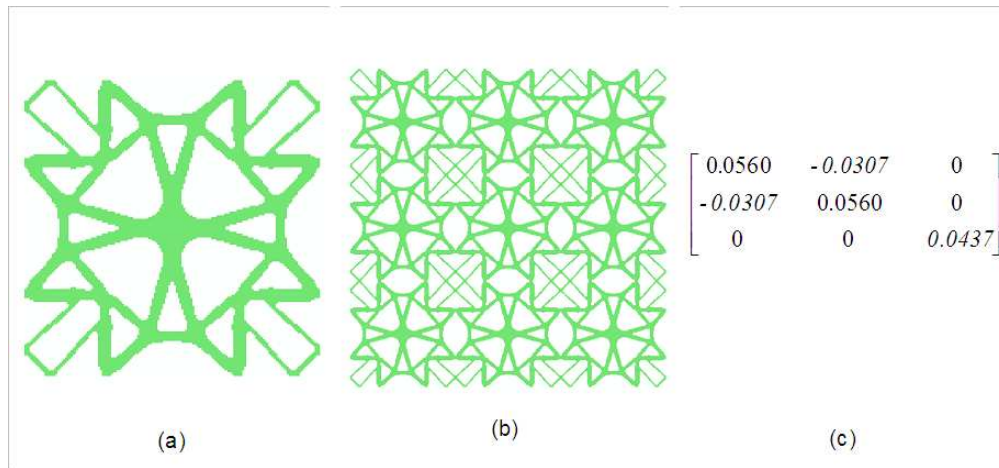


Figure 4.12: Microstructure of isotropic material with negative Poisson's ratio ( $r_{\min} = 4$ ); (a) periodic base cell; (b) unit cells; (c) isotropic material elasticity matrix

The PBC with dimensions  $160 \times 160$  is discretised into  $160 \times 160$  four-node square elements. The prescribed volume (area) fraction of the solid phase is selected equal to 35% of the total volume (area) of the base cell, with Young's modulus  $E^s = 1$  and Poisson's ratio  $\nu = 0.2$ . The BESO parameters are the evolution rate of  $ER = 0.004$  and the filter radius  $r_{\min} = 4$ ; the penalty exponent is selected equal to 3. Similar to the topology that is shown in Figure 3.1,

the BESO procedure starts from a domain of solid elements, except for four void elements at the centre.

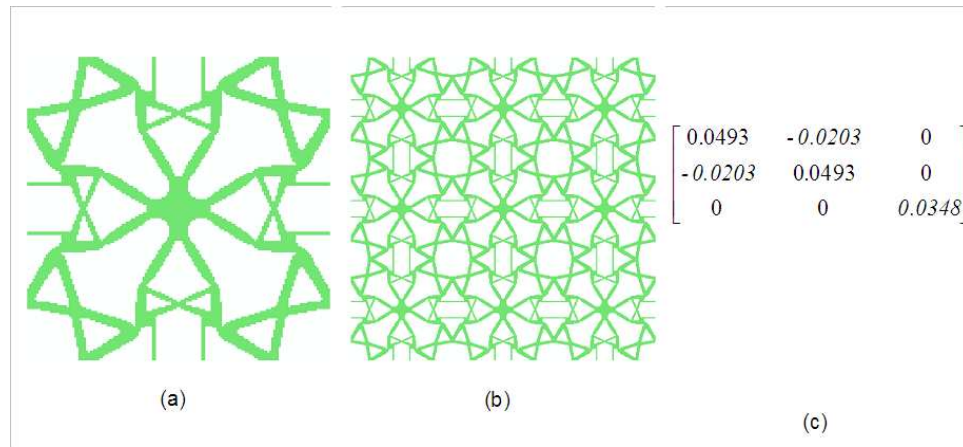


Figure 4.13: Microstructure of isotropic material with negative Poisson's ratio ( $r_{\min} = 1.5$ ); (a) periodic base cell; (b)  $3 \times 3$  unit cells; (c) isotropic material elasticity matrix

Figure 4.12 illustrates the generated microstructure of the isotropic cellular material which its Poisson's ratio is calculated equal to  $-0.5482$ . When a smaller filter radius  $r_{\min} = 1.5$  is defined as the BESO parameter and the prescribed volume fraction is set to 30% of the total volume of the PBC, the microstructure of Figure 4.13 is obtained. From the elasticity matrix of the Figure 4.13, the Poisson's ratio is calculated equal to  $-0.4118$ . The Zener anisotropy ratios of both materials are also very close to 1. One can easily perceive the lateral expansion of the microstructures in Figures 4.12 and 4.13 as the result of imposing tensile force, due to existence of the re-entrant corners. It is interesting to note that these microstructures are qualitatively similar to models of Phan-Thien and Karihaloo (1994). As it is stated before, changing the design parameters such as filter radius can cause obtaining qualitatively different

solutions in an optimization procedure. This is mainly because of existence of many local optima in topology optimization of material's microstructures. In the two examples presented in this section, it can be seen that reducing the filter radius produces a material's microstructure that has more regions of smaller width. In a continuum structure, these regions may act as hinges during the deformation. The formation of these hinge-typed regions is essential especially in materials with negative Poisson's ratio (Phan-Thien and Karihaloo, 1994, Lakes, 1993).

### **4.3. Concluding remarks**

Using the BESO method, a new approach for designing microstructures for isotropic cellular materials with maximum bulk or shear moduli was proposed in this chapter. The isotropy of the materials was defined as an additional constraint to the optimization problem. The modified objective function was constructed by introducing a Lagrange multiplier to implement the isotropy constraint. The proposed procedure utilizes a gradient-based method to impose the isotropy constraint and gradually evolves the microstructures of cellular materials to the optimum. Effectiveness of the proposed method has been demonstrated by the topology optimization of microstructures of isotropic cellular materials, with maximum bulk modulus or maximum shear modulus. Numerical examples clearly indicate the difference between the generated square (cubic) symmetric materials, without imposing the isotropy constraint and isotropic cellular materials in which the isotropy constraint is imposed. The histories of Zener anisotropy ratios through the evolution of microstructures indicate that the isotropy constraint has been properly incorporated into the optimization algorithm for designing all isotropic material cases. The presented examples also indicate that the proposed

method can be extended to the designing of isotropic cellular materials, with other desired functional properties such as materials with the negative Poisson's ratio.

## **Chapter 5**

---

### **Topology optimization of multi-phase periodic composites with extreme properties**

#### **Background**

In comparison to cellular material that is composed of one material phase and a void phase, composites of two or more materials are more advantageous and attractive for practical applications. As discussed in Chapter 2, one of the advantages of such materials is that by combining different constituent phases, a wider range of properties can be achieved, which are not attainable by the individual constituent phases (Zhou and Li, 2008a). On the other hand, multi-functional materials are inevitably composites of two or more constituent phases (Gibson, 2010). Such materials play a significant role in the development of composites in industry.

As mentioned in Chapter 2, the SIMP method has been applied in the form of inverse homogenization for the design of periodic microstructures for composites with two material phases and a void phase (Sigmund and Torquato, 1997, Gibiansky and Sigmund, 2000). The key point in these studies is the introduction of three design variables  $x_i^{(1)}$ ,  $x_i^{(2)}$  and  $x_i^{(3)}$ , for each element  $i$  that corresponds to the three constituent phases. By defining an artificial mixing function, the local material properties are correlated with the design variables. However an inherent problem with the SIMP method is that such an approach leads to intermediate densities in the final topology. In comparison with microstructures designed with one material phase and one void phase, in multi-phase materials design, the SIMP method usually causes more ambiguity in the interpretation and identification of the boundaries between constituent phases. Increasing of the penalty exponent not only cannot solve the problem completely, but may also result in numerical instability (Kohn and Strang, 1986, Swan and Kosaka, 1997, Yin and Yang, 2001, Zhou and Wang, 2007). For instance, the application of Optimality Criteria (OC) or Sequential Linear Programming (SLP) causes difficulties in the convergence of the solution (Yin and Yang, 2001, Zhou and Li, 2008a).

The BESO approach has been developed for stiffness optimization of macro-structures with multiple materials (Huang and Xie, 2009a, 2010b). Although the generated structures are topologically similar to the results of the SIMP approach, it has been shown that the procedure is independent of the selection of penalization factor. Better convergence of the procedure, together with high computational efficiency and more importantly, the capability of the BESO in separating the constituent phases, has made it a promising tool for topology optimization of multi-material structures.



In this chapter, the methodology for obtaining materials with extreme physical properties will be extended to multi-phase composite materials. The objective functions are maximum bulk modulus, shear modulus or thermal conductivity. It is assumed that the composite consists of  $N$  constituent phases. After ranking the constituent phases based on their contribution in the objective function, they are divided into  $N-1$  groups and the sensitivity analysis is performed between groups. Elements' material properties are changed based on the ranking of these sensitivity numbers and imposing volume constraint on the constituent phases. To tackle the numerical issues of the checkerboard pattern and mesh dependency, the filtering is conducted separately within the elements of each group.

## 5.1. Methodology

### 5.1.1. Optimization problem statement and sensitivity numbers

It is assumed that the composite material consists of  $N$  constituent phases with equal Poisson's ratios and the Young's moduli or the thermal conductivities that have been ordered descending (that is:  $E^1 > E^2 > \dots > E^N$  or  $k^1 > k^2 > \dots > k^N$ ). The optimization problem statement for attaining periodic materials with maximum bulk modulus, shear modulus or the thermal conductivity with constraints on the volume fraction of each constituent phase can be expressed as:

$$\text{Maximize} \quad f(x_i) = K, G \text{ or } k_c$$

$$\text{Subject to: } V^{j*} - \sum_{k=1}^{j-1} V^{k*} = \sum_{i=1}^M x_{ij} V_i \quad (5.1)$$

$$x_{ij} = x_{\min} \quad \text{or} \quad 1 \quad (j=1, 2, \dots, n-1)$$

in which  $V_i$  denotes the volume of element  $i$ ;  $V^{j*}$  is the prescribed volume of  $j^{\text{th}}$  material phase and  $K$ ,  $G$  or  $k_c$  are the bulk modulus, shear modulus or the thermal conductivity of materials;  $x_{ij}$  is the design variable which indicates the density of the  $i^{\text{th}}$  element for the  $j^{\text{th}}$  material. The  $x_{ij}$  can take a binary value of either 1 when the element is filled with material phase  $j$  or constituent phases with larger stiffness/thermal conductivity, or a very small value (i.e. 0.001) otherwise.

$$x_{ij} = \begin{cases} 1 & \text{if } E \geq E^j \text{ or } (k > k^j) \\ x_{\min} & \text{otherwise} \end{cases} \quad (5.2)$$

The local material of an element within the PBC can be assumed to be isotropic, with the physical property that varies between the properties of the two phases. The material properties are interpolated between two neighbouring phases using a power-law scheme. For instance, the elements of elasticity matrix  $\mathbf{D}$  are interpolated as (Huang and Xie, 2009a):

$$\mathbf{D}(x_{ij}) = x_{ij}^p \mathbf{D}^j + (1 - x_{ij}^p) \mathbf{D}^{j+1} \quad (5.3a)$$

$$j = 1, 2, \dots, n-1$$

in which the subscript of  $j$  and  $j+1$  indicates the phase numbers. Similarly the material thermal conductivity can be interpolated between two neighbouring phases as:

$$\mathbf{k} = x_{ij}^p \mathbf{k}^j + (1 - x_{ij}^p) \mathbf{k}^{j+1} \quad (5.4)$$

$$j = 1, 2, \dots, n-1$$

in which  $\mathbf{k}$  denotes the thermal conductivity matrix. Since the design variables are either  $x_{\min}$  or 1, the optimality criterion can be described as that the constituent phase  $j$  and those phases that have larger Young's modulus than  $j$  ( $x_{ij} = 1$ ) always have higher sensitivity than the rest of constituent phases ( $x_{ij} = x_{\min}$ ). With this assumption a scheme could be devised to update the design variable  $x_{ij}$  by changing from 1 to  $x_{\min}$  for elements with the lower sensitivity numbers and from  $x_{\min}$  to 1 for elements with the higher sensitivity numbers.

Similar to the relationships introduced in Chapter 3, the sensitivity of the elements of the homogenized elasticity matrix can easily be calculated with the introduced interpolation scheme (Haug et al., 1986) as:

$$\frac{\partial \mathbf{D}^H}{\partial x_{ij}} = \frac{1}{|Y|} \int_Y (\mathbf{I} - \mathbf{B}\mathbf{u})^T \frac{\partial \mathbf{D}}{\partial x_{ij}} (\mathbf{I} - \mathbf{B}\mathbf{u}) dY \quad (5.5)$$

where  $\mathbf{u}$  denotes the displacement fields of the unit cell caused by these uniform strain fields; and  $\mathbf{B}$  is the strain-displacement matrix. It should be noticed that the sensitivity of each group is calculated for all elements of the base cell, although it is only used for assigning the design

variables between the two neighbouring phases of  $j$  and  $j+1$  (Huang and Xie, 2010b). The appropriate equations for calculations of the sensitivities are similar to the equation (3.17).

### 5.1.2. Numerical procedure

To solve the above mentioned optimization problem using the BESO, the phases are divided into  $N-1$  ordered groups and the sensitivity calculation must be carried out between these  $N-1$  groups of phases (Huang and Xie, 2009a). Here the procedure is explained for the case where the material's microstructure is composed of 3 constituent phases. The procedure for the cases that the material is composed of more constituent phases follows the same procedure.

The BESO can start from a finite element model with nearly all elements from material 1 except for some limited number of elements from material 2. Through successive iterations, some more elements are turned into material 2, with the specified evolution rate ( $ER$ ) so that the volume of material 2 is restricted as:

$$V_{(2)}^{t+1} = \max(V_{(2)}^t (1 + ER), V_{(2)}^*) \quad (5.6)$$

where subscript in the parenthesis indicated the material number. The transition between materials 1 and 2 is performed based on the sensitivity number  $\alpha_{i1}$ .  $\alpha_{i1}$  is calculated assuming that elements from material 1 have higher sensitivity ( $x_{i1} = 1$ ) and the rest of elements have lower sensitivity ( $x_{i1} = x_{\min}$ ). The gradual addition of material 2 through iterations continuous until its volume reaches to the prescribed value. In later iterations, the volume of material 2 is kept constant although its distribution is allowed to change. At this stage the

volume of material 3 is allowed to gradually increase. The transition between combination of materials 1 and 2 with material 3 is performed by satisfying the volume constraint of material 3 and ranking the  $\alpha_{i2}$  sensitivities.  $\alpha_{i2}$  is calculated assuming that elements from material 1 and 2 have higher sensitivity ( $x_{i2} = 1$ ) and the rest of elements have lower sensitivity ( $x_{i2} = x_{\min}$ ). The procedure of increasing the number of elements with material 3 properties continuous until the volume of material 3 reaches to its prescribed value. If there are more than 3 constituent phases, the other materials can be included with a similar procedure. The numerical procedure comes to an end when the volumes of all materials satisfy the prescribed values and the variation of the objective function diminishes.

The design algorithm for 3-phase materials contains following steps:

Step 1: Define the BESO parameters with objective volume,  $V_{(1)}^*$ ,  $V_{(2)}^*$  and  $V_{(3)}^*$ , evolutionary

rate  $ER$ , filter radius  $r_{\min}$  and penalty factor  $p$  (normally  $p = 3$ );

Step 2: Build a finite element model for the PBC in which all elements are assigned with material 1 properties, except for some limited number of elements from material 2 as the initial topology;

Step 3: Apply periodic boundary conditions to the PBC. Impose nodal test load fields. The nodal loads are calculated to produce a uniform strain in that particular element. Carry out the finite element analysis (FEA) to obtain nodal displacements. In case of maximization of thermal conductivity the uniform heat fluxes are imposed and the induced temperatures are extracted;

Step 4: Calculate the elemental sensitivity numbers  $\alpha_{i1}$ . Calculate  $\alpha_{i2}$  if volumetric constraint on material 2 has already been satisfied;

Step 5: Filter sensitivity numbers  $\alpha_{i1}$ ; average  $\alpha_{i1}$  with its corresponding value from previous iteration;

Step 6: If the prescribed volume of material 2 has already been satisfied, filter the sensitivities  $\alpha_{i2}$  and perform similar averaging with historical information;

Step 7: Determine the target volume for the next iteration. When the current volume  $V_{(2)}^t$  is larger than the prescribed value  $V_{(2)}^*$ , the target volume for the next iteration can be calculated by

$$V_{(2)}^{t+1} = \min(V_{(2)}^*, V_{(2)}^t + V_{(2)}^t * ER) \quad (5.7)$$

Step 8: If  $V_{(2)} = V_{(2)}^*$  then the volume of material 3 is set as:

$$V_{(3)}^{t+1} = \min(V_{(3)}^*, V_{(3)}^t + V_{(3)}^t * ER) \quad (5.8)$$

Step 9: Rank elements based on  $\alpha_{i1}$ . Reset elemental densities  $x_{i1}$  by changing from 1 (material 1) to  $x_{\min}$  (material 2) for elements with lower sensitivities and from  $x_{\min}$  to 1 for materials with higher sensitivities, while satisfying the volume constraint of material 2.

Step 10: If  $V_{(2)} = V_{(2)}^*$  then rank elements based on  $\alpha_{i2}$ . Reset elemental densities  $x_{i2}$  by changing from 1 (material 2 or stiffer) to  $x_{\min}$  (material 3) for elements with lower sensitivities and from  $x_{\min}$  to 1 (material 2) for materials with higher sensitivities while satisfying the volumetric constraint of material 3.

Step 11: Repeat Steps 3 to 10, until both the volume constraints and convergent criterion are satisfied. The convergence criterion is defined in equation (3.21).

## 5.2. Results and discussion

### 5.2.1. 2D two- phase materials with maximum bulk modulus

For designing microstructures for composites with two constituent phases and maximum bulk modulus, the square design domain with dimensions  $80 \times 80$  is discretized into  $80 \times 80$ , 4-node square elements. The Young's modulus of materials 1 and 2 are selected  $E^1 = 3.0$  and  $E^2 = 1.0$  respectively; the Poisson's ratio of both materials is  $\nu = 0.3$ . The BESO parameters are the evolution rate  $ER = 0.04$ , filter radius  $r_{\min} = 6.0$  and penalty exponent  $p = 3$ . The initial finite element model of the PBC consists of all elements with material 1 properties, except for four elements of material 2 at the centre of the design domain (similar to Figure 3.1). The prescribed volume (area) fraction of material 1 is 30% of the total volume (area) of the PBC.

The designed microstructures and corresponding materials elasticity matrix are shown in Figure 5.1.

The HS upper bound for composites of two materials can be expressed as (Hashin and Shtrikman, 1963):

$$K_{\max}^{HS} = \frac{1}{\frac{f^1}{K^1 + G_{\max}} + \frac{f^2}{K^2 + G_{\max}}} - G_{\max} \quad (5.9)$$

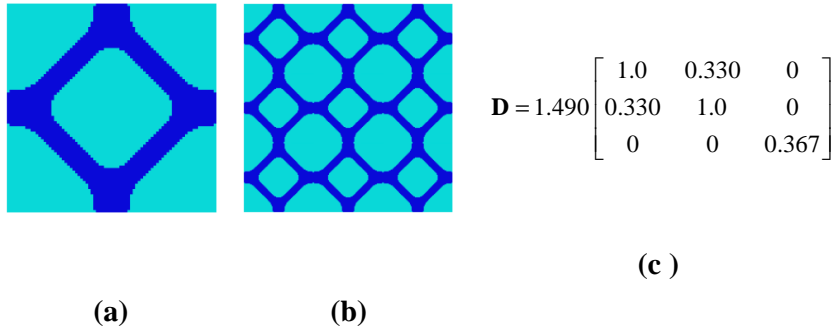


Figure 5.1: Microstructures and effective elasticity matrixes of a 2D composite material with 2 constituent phases and maximum bulk modulus (a) single base cell (b) 3x3 cells (c) elasticity matrix

in which  $f^1$  and  $f^2$  are the volume fractions of materials 1 and 2 respectively;  $K^1$  and  $K^2$  are the bulk moduli of the constituent phases and  $G_{\max}$  is the shear modulus of the stronger material defined as:

$$G_{\max} = E^1 / 2(1 + \nu) \quad (5.10)$$



The HS upper bound for the above material composition is calculated 0.9934 from the equation (5.9). As shown in Figure 5.1c, the bulk modulus of the designed material is 0.99108, which demonstrates a good consistency with the HS upper bound.

Figure 5.2 demonstrates the evolution histories of bulk modulus, volume fraction and the topology of the resulting microstructure. The total iterations for this design are 35. As can be seen from Figure 5.2, once the volume constraint is satisfied, the bulk modulus and the microstructural topology converge to their final solutions with a good stability.

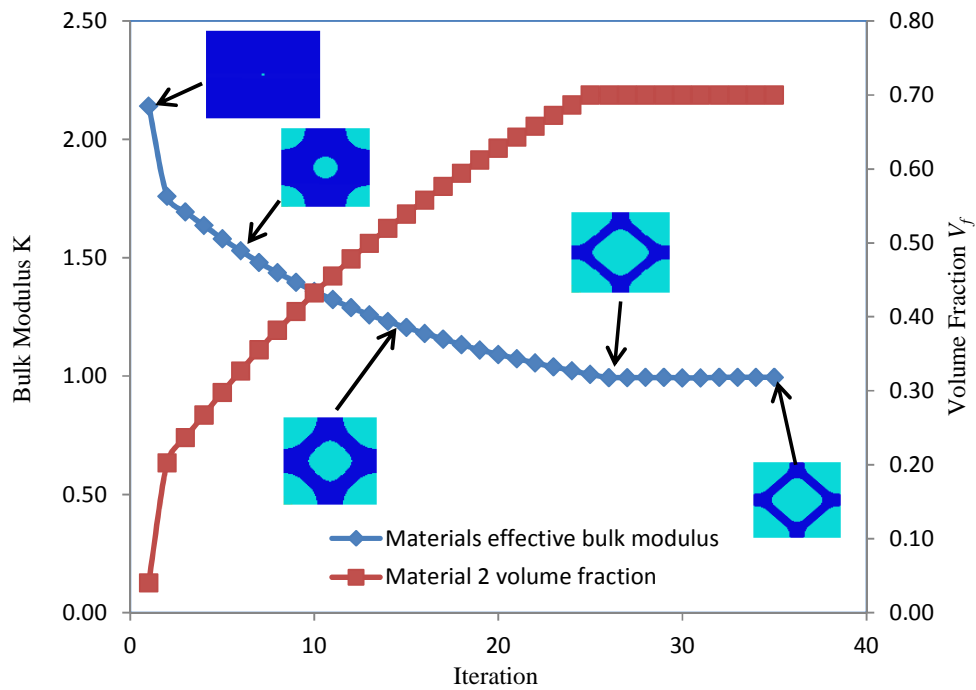


Figure 5.2: Evolution history of bulk modulus, volume fraction and microstructures for maximizing bulk modulus.

### 5.2.2.2D three-phase materials with maximum bulk modulus

The square design domain with dimensions  $80 \times 80$  is discretized into  $80 \times 80$ , 4-node square elements. The Young's modulus of materials, 1, 2 and 3 are selected  $E^1 = 4.0$ ,  $E^2 = 2.0$  and  $E^3 = 1.0$  respectively. The Poisson's ratio of all materials is assumed to be assumed  $\nu = 0.3$ . The evolution rate of  $ER = 0.02$ , filter radius  $r_{\min} = 8$  and the penalty exponent  $p = 3$  are selected as the BESO design parameters. The initial material distribution of the finite element model consists of all elements from material 1, except for four elements of materials 2 located at the centre of the model. The prescribed volume fractions of material 1, 2 and 3 are 30%, 40% and 30% respectively.

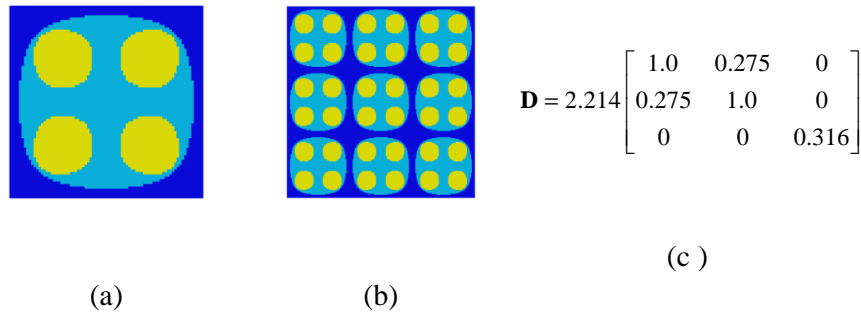


Figure 5.3: 3-phase material's microstructure with maximum bulk modulus; Material 1 is shown in dark blue ( $E^1=4$ ); material 2 in light blue ( $E^2=2$ ); and material 3 in yellow ( $E^3=1$ ); (a) single base cell; (b)  $3 \times 3$  cells; (c) elasticity matrix

The final microstructures and the material's effective elasticity matrix are shown in Figure 5.3. As calculated from the elasticity matrix, the bulk modulus of the material is 1.411. For

2D materials which consist of three constituent phases, the HS upper bound is given with the following expression (Hashin and Shtrikman, 1963):

$$K_{\max}^{HS} = \frac{1}{\frac{f^1}{K^1 + G_{\max}} + \frac{f^2}{K^2 + G_{\max}} + \frac{f^3}{K^3 + G_{\max}}} - G_{\max} \quad (5.11)$$

in which  $f^3$  and  $K^3$  are the volume fraction and the bulk modulus of material 3. The rest of variables have defined before. For the setting of this example, The Hashin-Shtrikman upper bound is calculated 1.435, which shows a good agreement with the attained result.

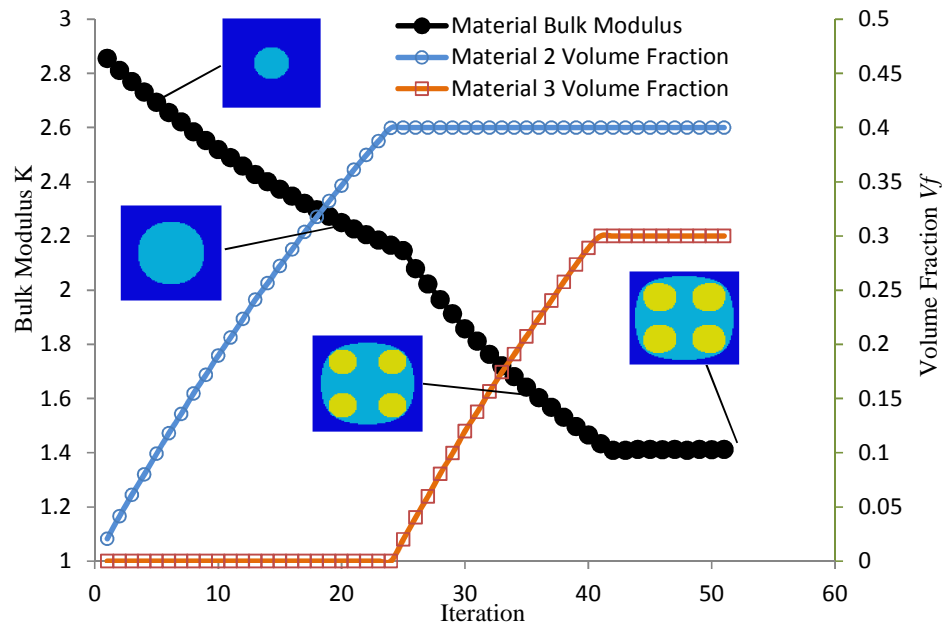


Figure 5.4: Evolution history of bulk modulus, volume fraction and microstructures for maximizing bulk modulus.

The whole procedure takes 51 iterations for this instance. Figure 5.4 shows the evolution histories of bulk modulus, volume fraction and microstructural topology of this example.

### 5.2.3. 3D three-phase material with maximum bulk modulus

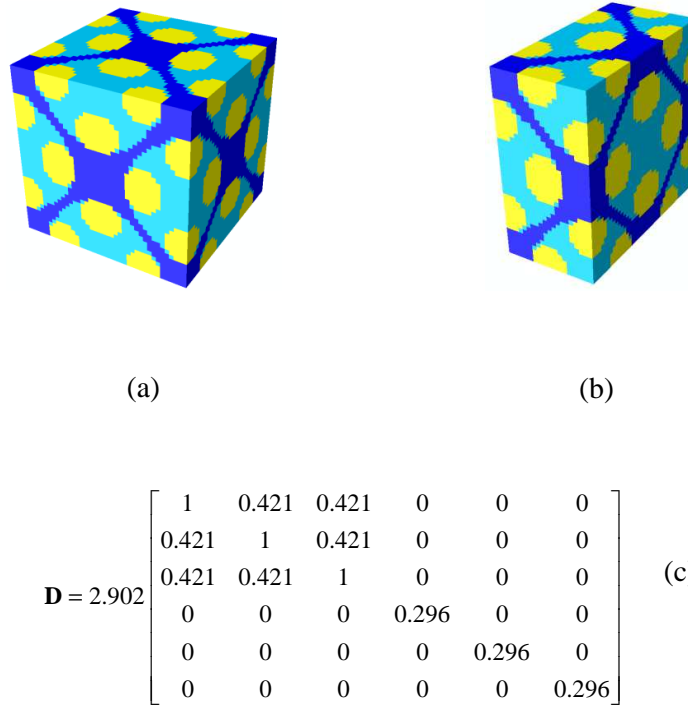


Figure 5.5: 3-phase material's microstructure with maximum bulk modulus. Material 1 is shown in dark blue ( $E^1=4$ ); material 2 in light blue ( $E^2=2$ ); and material 3 in yellow ( $E^3=1$ ); (a) single base cell; (b) middle-cut of the cell; (c) elasticity matrix of corresponding material

The cubic finite element model with dimensions  $40 \times 40 \times 40$  is discretized into  $40 \times 40 \times 40$ , 8-node cubic elements. As before, mechanical properties of constituent phases are selected as the Young's modulus  $E^1 = 4.0$ ,  $E^2 = 2.0$  and  $E^3 = 1.0$  for materials 1, 2 and 3 respectively, and the Poisson's ratio of all materials  $\nu = 0.3$ . The evolution rate of  $ER = 0.02$ , filter radius

$r_{min} = 2$  and penalty exponent  $p = 3$  are selected as the BESO design parameters. The initial material distribution in the finite element model consists of all elements from material 1, except for eight elements at the centre and eight elements at the eight corners from material 2. The prescribed volume fraction of material 1, 2 and 3 are 30%, 50% and 20% respectively.

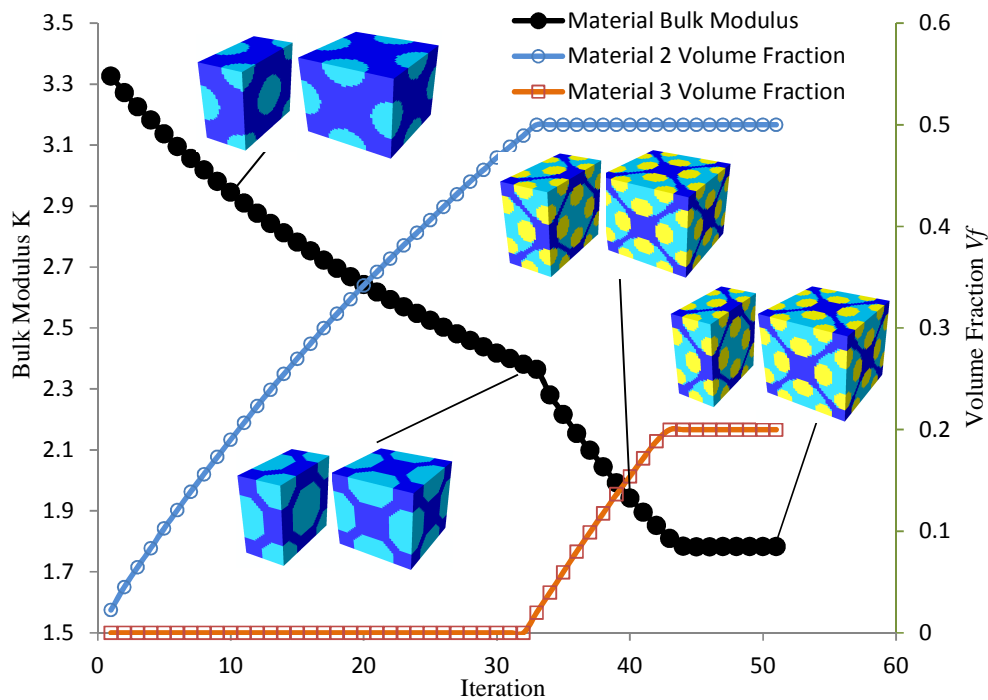


Figure 5.6: Evolution history of bulk modulus, volume fraction and microstructures.

The final microstructures and the material's effective elasticity matrix are presented in Figure 5.5. The HS upper bound for 3D materials which are composed of three constituent phases can be expressed as (Hashin and Shtrikman, 1963):

$$K_{\max}^{HS} = \frac{1}{\frac{f^1}{K^1 + 4/3G_{\max}} + \frac{f^2}{K^2 + 4/3G_{\max}} + \frac{f^3}{K^3 + 4/3G_{\max}}} - 4/3G_{\max} \quad (5.12)$$

The equation parameters were previously defined. The HS upper bound for the setting of this example is calculated 1.801. As it can be calculated from the elasticity matrix (Figure 5.5c), the bulk modulus of the designed material is 1.782.

The whole procedure converges in 53 iterations. Figure 5.6 demonstrates the evolution histories of bulk modulus, volume fraction and microstructural topology of this example.

#### 5.2.4. 2D three-phase material with maximum shear modulus

The objective of this example is the topology optimization of three-phase microstructures with maximum shear modulus, under prescribed volume fractions of the phases. The 2D square design domain with dimensions  $80 \times 80$  is discretized into  $80 \times 80$ , 4-node square elements. The Young's modulus of constituent phases are selected as  $E^1 = 4.0$ ,  $E^2 = 2.0$  and  $E^3 = 1.0$ . The Poisson's ratio of all materials is assumed equal to  $\nu = 0.3$ . The evolution rate of  $ER = 0.02$ , filter radius  $r_{\min} = 8$  and penalty exponent  $p = 3$  are selected as the BESO initial parameters. In the initial finite element model of the PBC, material 1 physical properties are assigned to all elements, except for four elements of materials 2 at the centre of the design domain. The prescribed volume fraction of materials 1, 2 and 3 are 30%, 40% and 30% respectively.

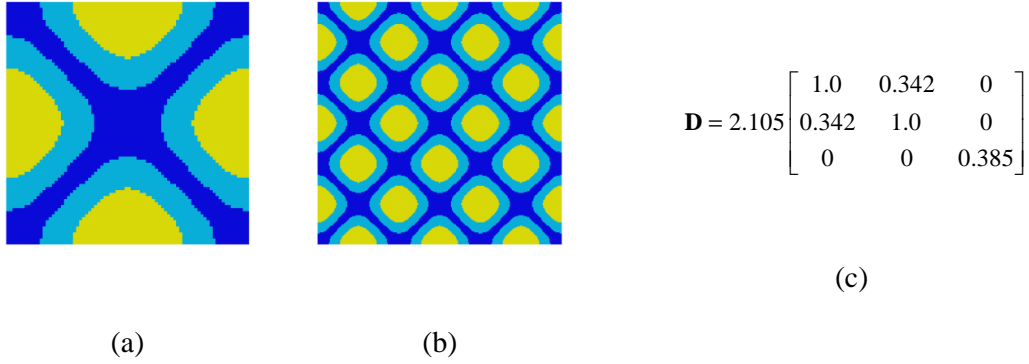


Figure 5.7: 2D 3-phase microstructure with maximum shear modulus. Material 1 is shown in dark blue ( $E^1=4$ ); material 2 in light blue ( $E^2=2$ ); and material 3 in yellow ( $E^3=1$ ); (a) single base cell; (b)  $3 \times 3$  cells; (c) elasticity matrix

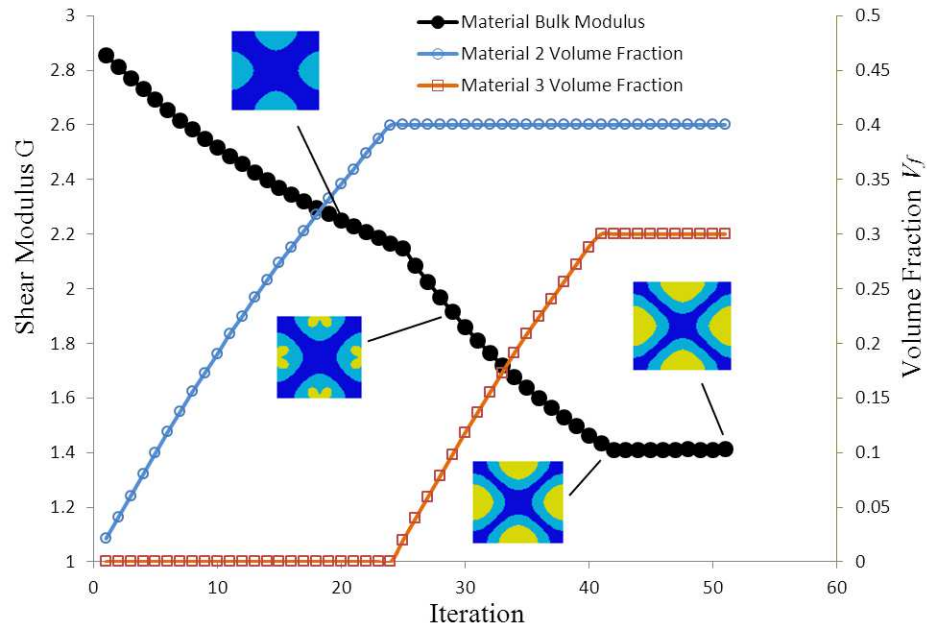


Figure 5.8: Evolution history of shear modulus, volume fraction and microstructures for the design of a 2D material's microstructure with maximum shear modulus

The generated microstructures, as well as the material effective elasticity matrix are shown in Figure 5.7. As it can be seen, there are similarities between the generated microstructure of this example with the microstructure of cellular material shown in Figure 3.8. Figure 5.8 demonstrates the evolution history of shear modulus and volume fraction of the generated microstructure throughout the process. The procedure converges to the final topology after 51 iterations.

### 5.2.5. 3D three-phase material with maximum shear modulus

For the design of three-phase microstructures of material with maximum shear modulus, a cubic design domain with dimensions  $24 \times 24 \times 24$  is discretized into  $24 \times 24 \times 24$ , 8-node cubic elements. As before, the Young's moduli of constituent phases are selected as  $E^1 = 4.0$ ,  $E^2 = 2.0$  and  $E^3 = 1.0$ ; the Poisson's ratio is assumed  $\nu = 0.3$ . The BESO parameters are the evolution rate  $ER = 0.02$ , filter radius  $r_{\min} = 2$  and penalty exponent  $p = 3$ . The prescribed volume fraction of materials 1, 2 and 3 are 25%, 45% and 30% respectively. The initial material distribution of the finite element model consists of all elements from material 1, except for four elements of materials 2 at the centre of the design domain.

The resulted microstructural topology is shown in Figure 5.9; the figure also demonstrates the spatial distribution of each of the constituent phases, as well as the homogenized effective elasticity matrix of material. Figure 5.10 demonstrates the evolution history of shear modulus and volume fraction of the designed microstructure throughout the iterative process. As can be seen from the figure, the procedure converges to the final topology after 56 iterations.



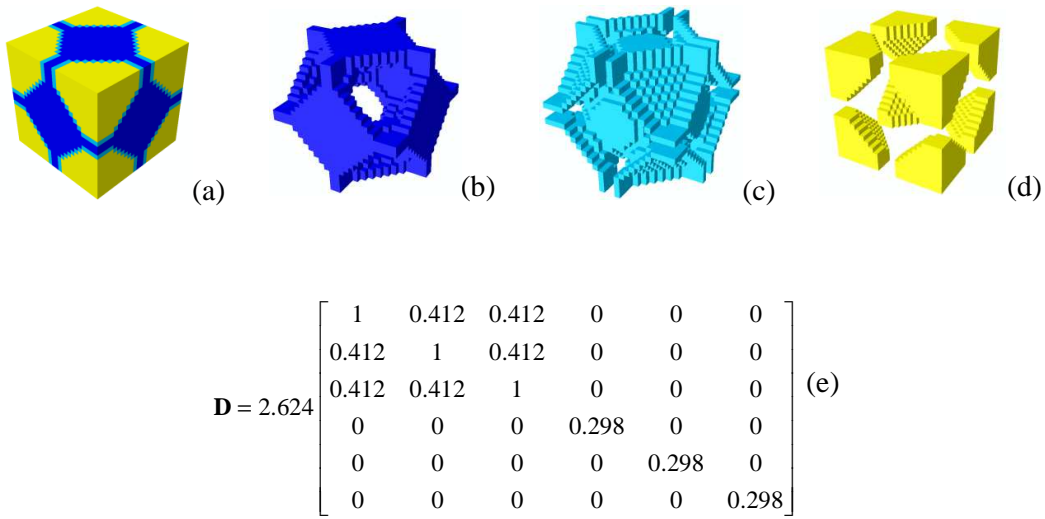


Figure 5.9: 3D 3-phase material's microstructure with maximum shear modulus; (a) single base cell; (b) distribution of constituent phase 1 ( $E^1=4$ ); (c) distribution of constituent phase 2 ( $E^2=2$ ); (d) distribution of constituent phase 3 ( $E^3=1$ ); (e) elasticity matrix of material

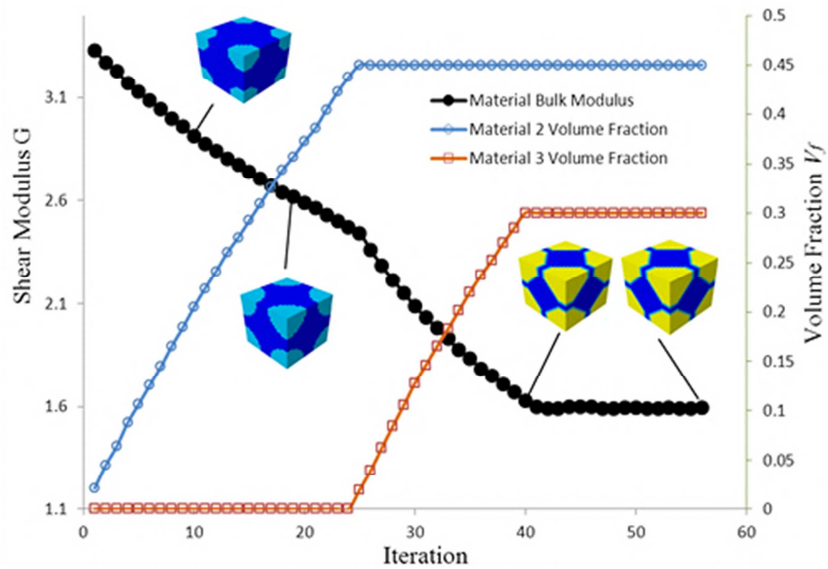


Figure 5.10: Evolution history of shear modulus, volume fraction and microstructures

### 5.2.6. 2D three-phase material with maximum thermal conductivity

To verify the procedure for the topology optimization of materials with maximum thermal conductivity, the square design domain of the PBC with dimensions  $80 \times 80$  is discretized into  $80 \times 80$ , 4-node quadrilateral elements. The thermal conductivities of materials 1, 2 and 3 are selected as  $k^1 = 4.0$ ,  $k^2 = 2.0$  and  $k^3 = 1.0$  respectively. The BESO parameters are set as the evolution rate  $ER = 0.02$ , filter radius  $r_{\min} = 8$  and penalty exponent  $p = 3$ . The initial finite element model of the PBC consists of elements with material 1 properties, except for four elements of materials 2 at the centre of the design domain. The prescribed volume fraction of materials 1, 2 and 3 are 25%, 25% and 50% respectively.

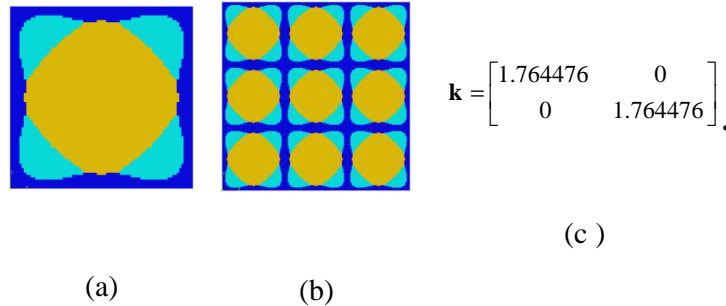


Figure 5.11: 3-phase material's microstructure with maximum thermal conductivity. Material 1 is shown in dark blue ( $k^1=4$ ); material 2 in light blue ( $k^2=2$ ); and material 3 in yellow ( $k^3=1$ ); (a) single base cell; (b)  $3 \times 3$  cells; (c) thermal conductivity matrix

The final microstructure and the material homogenized thermal conductivity matrix are given in Figure 5.11. As mentioned in Chapter 2, Hashin and Shtrikman (1962) used the variational theorem to derive the bounds on the effective magnetic permeability of macroscopically

homogeneous and isotropic multiphase materials. The mathematical analogy enables the results to be also used for dielectric, electric conductivity, heat conductivity, and diffusivity of composite materials. The Hashin-Shtrikman upper bound for three-phase isotropic materials is expressed as:

$$k_{\max}^{HS} = -k_{\max} + \frac{1}{\frac{f^1}{k^1 + k_{\max}} + \frac{f^2}{k^2 + k_{\max}} + \frac{f^3}{k^3 + k_{\max}}} \quad (5.13)$$

in which  $k_{\max}$  is the largest eigenvalue of the thermal conductivity of constituent phases. With the help of the above equation, the upper bound  $k_{\max}^{HS}$  is calculated equal to 1.783, which is very close to the thermal conductivity of generated materials (1.764476 from the material matrix in Figure 5.11c).

The whole procedure completes in 29 iterations in this instance. Figure 5.12 demonstrates the evolution histories of thermal conductivity, volume fraction and microstructural topology of this example.

### 5.2.7. 3D three-phase material with maximum thermal conductivity

The objective of this example is to design 3D microstructures for materials with maximum thermal conductivity. The PBC with dimensions  $42 \times 42 \times 42$  is discretized into  $42 \times 42 \times 42$ , eight-node cubic finite elements. As before the eigenvalues of thermal conductivity of materials 1, 2 and 3 are selected as 4, 2 and 1 respectively. The BESO parameters are evolution rate  $ER = 0.02$  and the filter radius  $r_{\min} = 3$  and penalty exponent  $p = 3$ . The

procedure starts from the initial design, in which all elements are assigned with material 1 property, except for 4 elements of material 2 at the centre of the finite element model. The prescribed volume fraction of the materials 1, 2 and 3 are 25%, 25% and 50% respectively.

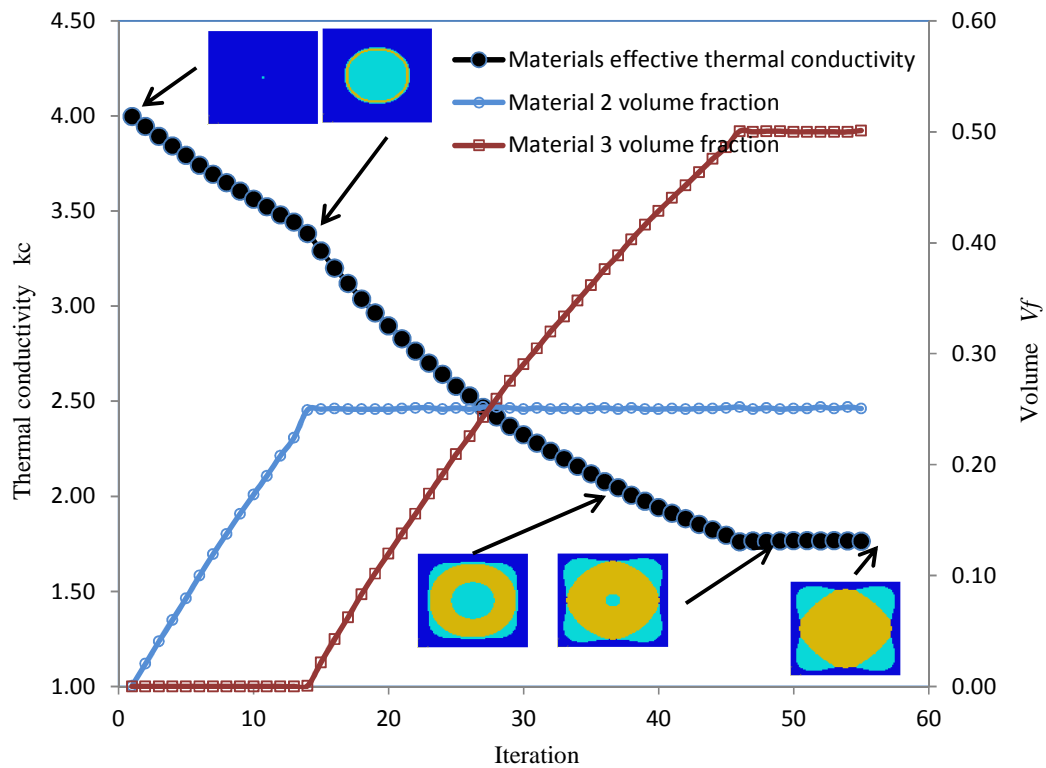


Figure 5.12: Evolution history of thermal conductivity, volume fraction and microstructures.

Figure 5.13 shows the resulting microstructures and the thermal conductivity matrix of material. The HS upper bound on thermal conductivity of 3-phase materials with the eigenvalues sorted as  $(k^1 > k^2 > k^3)$  can be expressed as (Hashin and Shtrikman, 1962):

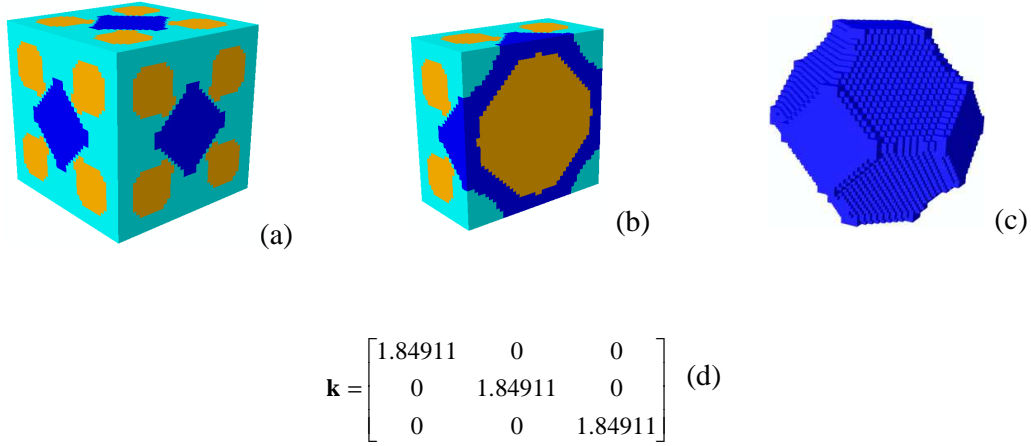


Figure 5.13: 3-phase material's microstructure with maximum thermal conductivity. Material 1 is shown in dark blue ( $k^1=4$ ); material 2 in light blue ( $k^2=2$ ); and material 3 in yellow ( $k^3=1$ ); (a) single base cell; (b) middle-cut of the cell; (c) spatial distribution of material 1; (d) thermal conductivity matrix

$$k_{\max}^{HS} = k^1 + \frac{\alpha}{1 - \frac{\alpha}{3k^1}} \quad (5.14)$$

in which:

$$\alpha = \frac{f^2}{\frac{1}{(k^2 - k^1)} + \frac{1}{3k^1}} + \frac{f^3}{\frac{1}{(k^3 - k^1)} + \frac{1}{3k^1}} \quad (5.15)$$

The HS upper bound from the above mentioned formula is calculated 1.863, which is 0.7% higher than the designed microstructure (1.84911) from the Figure 5.13d).

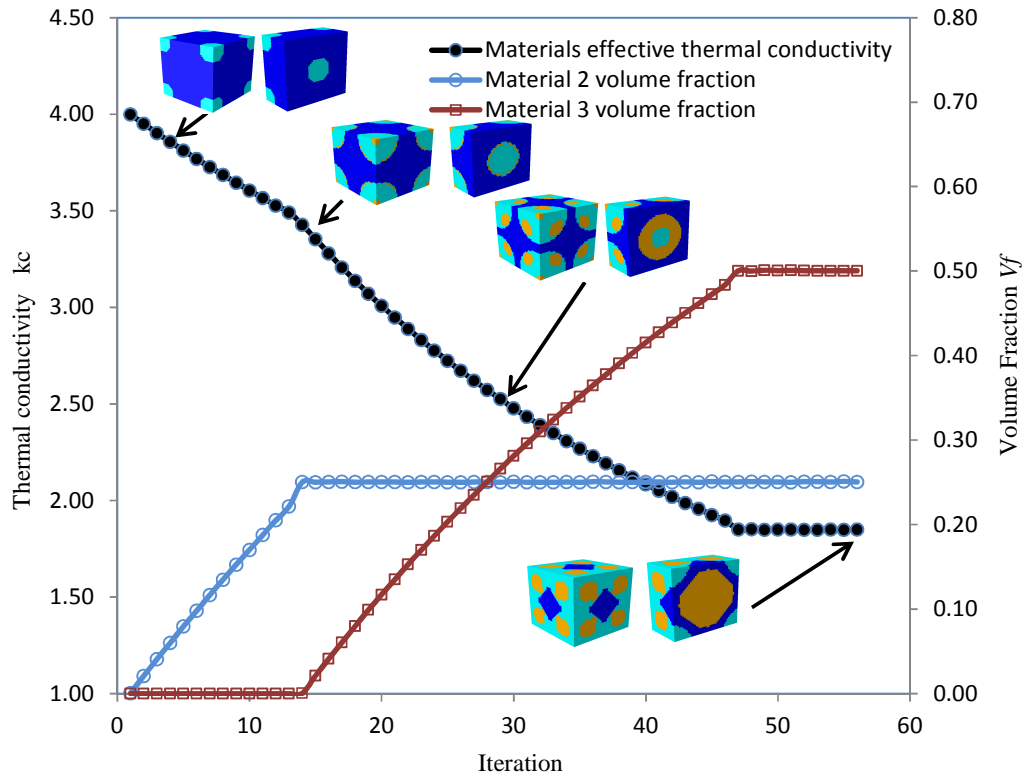


Figure 5.14: Evolution history of thermal conductivity, volume fraction and microstructures.

### 5.3. Concluding remarks

In this chapter, the BESO method was extended into the design of multi-phase microstructures for materials, with maximum bulk modulus, shear modulus or thermal conductivity. Following the ranking of the constituent phases based on their contribution to the objective function, they were divided into groups and the sensitivity analysis is performed between these groups. Changing the properties of elements was conducted based on the

ranking of these sensitivity numbers and imposing volume constraint. The numerical examples demonstrate that the proposed approach is capable of finding microstructures, with properties very close to the known analytical bounds. The procedure demonstrates very good convergence with high computational efficiency, which is independent of the selection of the penalization factor. Moreover, as an inherent property of the BESO, there are distinctive interfaces between the constituent phases in the generated microstructures. This makes the manufacturing of the generated materials easy.

The methodology of this chapter provides the basis for the development of a technique for the design of multi-phase multi-objective functionally graded materials which is the subject of Chapter 7.

## **Chapter 6**

---

### **Topology optimization of functionally graded materials**

#### **Background**

As discussed in Chapter 2, the functionally graded materials (FGMs) are characterized by a gradual variation in properties as a result of the inhomogeneity in materials' microstructural/compositional characteristics. One of the challenges in designing such materials is the prediction of the material characteristics. Depending on the rate of gradation with respect to the dimensions of the representative volume element (RVE) or representative unit cell (RUC), theoretically two general methods are applied. If a steep gradient in material property is expected, then the heterogeneity nature of the RVE should be taken into account by analysing the material at both the microscopic and macroscopic levels. However, in the case of a small gradient in the material properties, adequate accuracy can be achieved by



applying the homogenization theory with periodic boundary conditions (Birman and Byrd, 2007, Zhou and Li, 2008b).

Another challenging issue in the design of an FGM is the determination of the optimal spatial distribution of constituent phases (Markworth et al., 1995). Based on the “inverse homogenization” (Sigmund, 1994a, 1994b, 1995), some researchers have proposed techniques for designing microstructures for materials with graded properties. For instance Chen and Feng (2004) and Lin et al (2004) used similar techniques for the design of cellular microstructures, in which the gradient of properties was realized by gradually varying the volume fractions of solid phase. These studies however, are mostly focused on the topology optimization of a series of separate base cells for graded properties. They do not ensure proper connection between adjacent cells along the gradient direction.

As pointed out in Chapter 2, Zhou and Li (2008b; 2008c) have proposed systematic approaches for the designing of two-phase (solid/void) FGMs, with gradual change in the prescribed elasticity properties in one direction. In these approaches the gradation in properties is achieved by designing a series of base cells for different regions of the FGM. To preserve the connectivity between adjacent cells, three methods, namely *connective constraint*, *pseudo load* and *unified formulation with non-linear diffusion*, were proposed by the authors.

In the *connective constraint* method, some non-designable solid elements are defined on the boundaries of each base cell. Through the filtering of densities, these fixed solid regions guarantee the existence of materials in their vicinity. They hence serve as connectors between

adjacent periodic base cells. Localizing these solid elements is a critical step and may lead to different final solutions. In the *pseudo load* technique, the idea is to produce a load path along the gradient direction by defining a pseudo load and kinematic boundary conditions along the gradient direction. This treatment allows the growth of material around the pseudo boundaries and loading areas, and produces pseudo stiffness along all base cells. However, the weighting factor of the pseudo load should be selected carefully in the procedure. If not its effects can play an excessively dominant role and may lead to a non-optimal solution (Zhou and Li, 2008b).

In the *unified formulation*, the non-linear diffusion technique has been used for obtaining an edge preserving solution. The non-linear diffusion is a mathematical technique that was originally developed as an image processing technique and has been applied to tackle numerical instabilities in topology optimization (Wang et al., 2004a, Zhou and Li, 2007, 2008d, Aubert and Kornprobst, 2006). In topology optimization through the SIMP method, which uses continuous design variables, the non-linear diffusion can circumvent the existence of intermediate densities on the boundaries of the structure. The technique achieves this by diffusing the densities along the tangential direction on the boundaries of the structure, while in other regions the non-linear diffusion equation acts as an isotropic filtering equation and diffuses the density uniformly (Wang et al., 2004a). In the *unified formulation*, the topology of a series of connected microstructures (known as the graded base cell or GBC) are simultaneously optimized for different functional properties and their connectivity is preserved by non-linear diffusion of densities (Zhou and Li, 2008b).

Apart from the connectivity of the base cells, the prohibitive issue in designing a series of base cells for an FGM is the computational costs, especially in 3D cases. In this chapter an alternative and computationally more efficient solution method is introduced, for designing a series of base cells for FGMs with gradation in stiffness or thermal conductivity. It is assumed that the base cells are composed of one solid phase and one void phase and that the gradual variation in the FGM properties is controlled by changing the material distributions within these base cells. The elasticity and conductivity characteristics within each base cell are estimated using the Homogenization theory. In particular, the connectivity issue between adjacent base cells are addressed in the optimization algorithm.

## **6.1. Methodology**

### **6.1.1. Topology optimization problem and connectivity between base cells**

The FGM can be tailored to make material more efficient, under non-uniform distribution of stresses or thermal gradient. For the design of cellular materials, the volume or weight is another important factor which should be considered. For designing an FGM with the gradient in stiffness, in the form of bulk or shear modulus, or thermal conductivity, it is divided into a series of base cells along the gradation direction. As shown in Figure 6.1, it is assumed that there are totally  $N$  base cells along the gradation direction and that each base cell has a different prescribed bulk modulus, shear modulus or thermal conductivity. To achieve the optimal spatial distribution of materials within the base cells, the topology optimization problem can be mathematically defined for the  $j$ th base cell as:

$$\text{Minimize} \quad V^j = \sum_{i=1}^M x_i^j V_i^j \quad (6.1a)$$

$$\text{Subject to:} \quad K^j = K^{j*} \text{ (, } G^j = G^{j*} \text{ or } k_c^j = k_c^{j*}) \quad (6.1b)$$

$$x_i^j = x_{\min} \text{ or } 1; \quad (i = 1, 2, \dots, M) \text{ and } (j = 1, 2, \dots, N) \quad (6.1c)$$

where  $V$  denotes the volume (or weight);  $K^*$ ,  $G^*$  or  $k_c^*$  are the prescribed bulk modulus, shear modulus or the thermal conductivity respectively which are determined by the prescribed gradation of FGM for the  $j^{\text{th}}$  base cell;  $M$  denotes the total number of finite elements within each base cell. As described before, the design variable  $x_i^j$  is the density of the  $i^{\text{th}}$  element within the  $j^{\text{th}}$  base cell, which can take a binary value of either 1 for a solid element or a small value,  $x_{\min}$  (e.g. 0.001) for a void element.

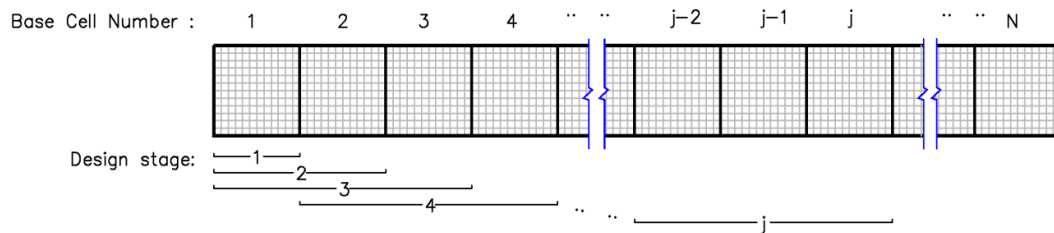


Figure 6.1: FGM base cells numbering along gradation direction and design stages.

The optimization problem (6.1) can be solved by designing base cells, one by one, for the prescribed elasticity modulus or thermal conductivity. It can be expected that both the topologies and volume fractions of base cells vary from one to another. However, this

procedure does not ensure a proper connection between neighbouring cells (Zhou and Li, 2008b). As mentioned before, Zhou and Li (2008b, 2008c) proposed three methods namely *connective constraint*, *pseudo load* and *unified formulation with non-linear diffusion* to overcome this problem.

In the proposed method of this study, it is assumed that the prescribed bulk modulus, shear modulus or the thermal conductivity of the FGM gradually decreases from the first cell to the last one. Therefore, the solid volume fraction should also be decreased from the first base cell to the last cell. Starting from a base cell that is almost entirely occupied by solid elements, the BESO procedure gradually reduces the number of solid elements. After obtaining the optimal topology for each base cell, the initial topology of the next base cell is constructed based on the resulting topology of the previous cell. The optimization procedure continues until the optimized topologies of all base cells are obtained. Comparing with designing a series of independent base cells, the proposed procedure significantly reduces the computational cost.

The connectivity of the adjacent base cells can be maintained by considering 3 base cells at each stage of design. Referring to the Figure 6.1, during the topology optimization of the  $j^{\text{th}}$  base cell, the connectivity between cells  $j$  and  $j-1$ , and between  $j-1$  and  $j-2$  are maintained by applying the filtering technique (Huang and Xie, 2007b) on the design domain of these three base cells together. However, the base cells  $j$ ,  $j-1$  and  $j-2$  are treated differently during the optimization process; whereas, base cells  $j$  and  $j-1$  are optimized based on the optimization statement (6.1) for their individual prescribed functional properties,

the topology of base cell  $j-2$  is kept unchanged. Due to the effect of the filtering, the material within base cell  $j-1$  is gradually redistributed to provide proper connections with base cells  $j-2$  and  $j$ .

The remaining key issue is how to optimize the topology of a base cell according to equation (6.1). Therefore, the superscript  $j$  is dropped in the next section.

### 6.1.2. Solution method

In order to solve the topology optimization problem in equation (6.1) for each base cell using the BESO method, similar to the procedure used in Chapter 4, the objective function is modified by introducing a Lagrangian multiplier  $\lambda$ . For instance, when the constraint function is the bulk modulus, the objective function is re-written as:

$$\text{Minimize } f(x_i) = \sum_{i=1}^M x_i V_i + \lambda (K^* - K) \quad (6.2)$$

It is seen when the constraint on bulk modulus is satisfied, the modified objective function is equivalent to the original one and the Lagrangian multiplier can take any value. The derivative of the modified objective function is expressed as:

$$\frac{df}{dx_i} = V_i - \lambda \frac{\partial K}{\partial x_i} \quad (6.3)$$

In the BESO only the ranking of sensitivity numbers is important. By discretising the base cells into uniform mesh size (in which all elements have equal volume or area), the sensitivity of each element can be re-written as:

$$\alpha_i = -\frac{1}{\lambda} \left( \frac{df}{dx_i} - V_i \right) = \frac{\partial K}{\partial x_i} \quad (6.4)$$

where  $\partial K/\partial x_i$  can be calculated using the homogenization theory from equations (3.15) and (3.3) :

$$\frac{\partial \mathbf{D}^H}{\partial x_i} = \frac{1}{|Y|} \int_Y (\mathbf{I} - \mathbf{bu})^T \frac{\partial \mathbf{D}}{\partial x_i} (\mathbf{I} - \mathbf{bu}) dY \quad (3.15) \text{ repeat}$$

$$K = \frac{1}{d^2} \sum_{i,j=1}^d D_{ij}^H \quad d = \begin{cases} 2 & 2D \text{ problems} \\ 3 & 3D \text{ problems} \end{cases} \quad (3.3) \text{ repeat}$$

Similarly, when the constraint function is defined on the shear modulus or the thermal conductivity, the sensitivity numbers are obtained from the equations (3.15), (3.4) or (3.17) and (3.5) respectively.

As was discussed in Chapter 3, to circumvent the numerical instabilities of mesh-dependency and checkerboard patterns, the filtering scheme is applied by averaging the elemental sensitivity numbers, with their neighbouring elements (Huang and Xie, 2007b, 2010b). Here the filtering scheme is applied across all elements of the 3 base cells, at each stage of procedure. As it will be shown by numerical examples, this technique can provide a good

interconnection between different base cells of the FGM. The following weighting equation is used for filtering the sensitivity numbers:

$$\hat{\alpha}_m = \frac{\sum_{n=1}^P w_{mn} \alpha_m}{\sum_{m=1}^P w_{mn}} \quad (6.5)$$

in which  $P = 3M$  denotes the total number of elements in the design domain of 3 adjacent base cells (see Figure 6.1). The weighting factor  $w_{mn}$  is defined as:

$$w_{mn} = \begin{cases} r_{\min} - r_{mn} & \text{if } r_{mn} < r_{\min} \\ 0 & \text{otherwise} \end{cases} \quad (6.6)$$

in which  $r_{mn}$  is the distance between element  $m$  and element  $n$  centres. The filter radius  $r_{\min}$  is defined to specify the neighbouring elements that affect the sensitivity of element  $m$ . To improve the convergence of the procedure, as described in Chapter 3, the elemental sensitivity numbers can be further modified by averaging with their values from the previous iteration.

The gradual change in the volume of the solid phase is ensured by imposing the constraint in the form of:

$$V^{t+1} = \begin{cases} V^t (1 - \min(ER, \frac{K^t - K^*}{K^k})) & \text{if } K^t \geq K^* \\ V^t (1 + \min(ER, \frac{K^t - K^*}{K^k})) & \text{otherwise} \end{cases} \quad (6.7)$$



where superscripts of  $t$  and  $t+1$  denote the current and the next iteration numbers respectively.  $ER$  is the evolution rate that is positive and defined as the BESO initial parameter.

### 6.1.3. Numerical implementation

The whole optimization procedure can be summarized with the following steps:

- Step 1: Define the prescribe modulus of elasticity (when the objective function is bulk or shear modulus) or thermal conductivity  $k_c^{j*}$  for the different base cells of the FGM; define the BESO parameters such as evolution rate ( $ER$ ), filter radius ( $r_{min}$ ) and penalty exponent;
- Step 2: Initiate a finite element model for the base cells  $j$  and  $j-1$  (if  $j>1$ ) ; apply periodic boundary conditions and loads which are equivalent to unit strain fields in elasticity analyses. Alternatively, apply uniform heat fluxes in thermal analyses; Carry out the finite element analyses to obtain output displacement fields  $\mathbf{u}$  in elasticity analyses or induced temperature fields  $\boldsymbol{\mu}$  in thermal analyses;
- Step 3: Calculate the elemental sensitivity numbers  $\alpha_i$  described above. Use the saved sensitivity numbers of base cell  $j-2$  (if  $j>2$ );
- Step 4: Filter sensitivity numbers of base cells  $j, j-1$  (if  $j>1$ ) and  $j-2$  (if  $j>2$ ) together using equation (6.5). Average sensitivity numbers of base cells  $j-1$  and  $j$  with their corresponding values from the previous iteration;

Step 5: Rank all elemental sensitivity numbers within the base cells  $j$  and  $j-1$  separately.

Reassign design variables  $x_i$  to 1 or  $x_{\min}$  so as to satisfying the volume constraint for the next iteration defined in equation (6.7) for base cells  $j$  and  $j-1$ ;

Step 6: Repeat steps 2 through to 5, until the objective function converges;

Step 7: Use the topology of base cell  $j$  as the starting topology for the next base cell. Repeat steps 2 to 6 for other base cells until optimized topologies of all base cells are achieved.

## 6.2. Results and discussion

### 6.2.1. 2D FGM with the variation in bulk modulus

The objective of the first example is to design a least weight cellular FGM, with a variation in bulk modulus from 40% to 15% of that of the solid constituent phase. It is assumed that the design domain of the FGM is simply divided into 10 base cells. Each base cell has the dimensions of  $80 \times 80$  and is discretized into  $80 \times 80$ , 4-node square elements. The Young's modulus and Poisson's ratio of the solid constituent phase are selected as  $E^s = 1$ , and  $\nu = 0.3$ . The BESO parameters are the evolution rate,  $ER = 0.03$  and filter radius  $r_{\min} = 6$ . The initial topology of the first base cell consists of four elements at the centre with void properties, while solid properties are assigned to other elements.

The designed microstructures are shown in Figure 6.2 in which the bulk modulus decreases linearly from the left to the right. The total number of iterations for this example is 176. As it

is demonstrated in the figure, the established BESO procedure provides appropriate connections between the adjacent cells. Comparing to the designing of all base cells simultaneously, the proposed procedure needs to conduct finite element analyses for only two base cells in each iteration. Consequently a significant saving in computational time and memory is achievable. Using an ordinary computer with a 2.7GHz, core i7 CPU and 8GB of RAM, the total computational time for this example is about 96min.



*Figure 6.2: Optimized FGM with linear gradation in bulk modulus of elasticity.*

Figure 6.3 demonstrates the variation of the bulk modulus of the generated FGM; the resulting bulk modulus conforms well to the prescribed values, with a deviation of less than 0.2%.

In order to compare the elapsed time with the conventional approach of simultaneous designing of all base cells (Zhou and Li 2008b; 2008c), an example with the same parameters of the above example is considered. The total number of iterations required for the convergence of simultaneous design of base cells is 75 but the elapsed time is 409 minutes which is more than 4 times greater than the approach proposed in this paper. The generated microstructures are shown in Figure 6.4.

In some cases FGMs with non-linear variation in functional properties are desirable. As another example, the above mentioned method is applied for the topology optimization of an FGM, with the same initial parameters but with the prescribed bulk modulus that varies non-

linearly along the gradation direction. Here the prescribed bulk modulus in the  $j^{\text{th}}$  base is defined as:

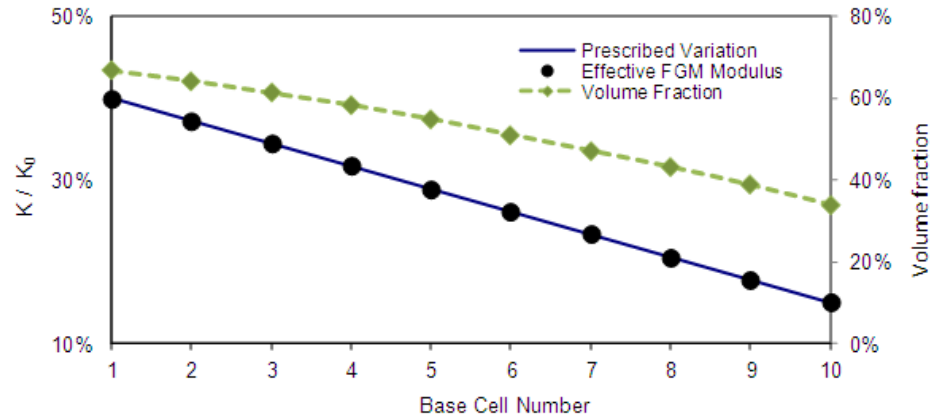


Figure 6.3: Linear variation of bulk modulus and volume fractions for the optimized FGM where  $K_0$  is bulk modulus of the solid.



Figure 6.4: Simultaneous Optimized cells for an FGM with linear gradation in bulk modulus of elasticity.

$$K_j^* = K_n^* + (K_1^* - K_n^*) \left( \frac{j-n}{n-1} \right)^2 \quad (6.8)$$

where  $n = 10$  is the total number of base cells in the design domain of the FGM.  $K_1^*$  and  $K_n^*$  are the prescribed bulk moduli of the first and last base cells, which in conformity to the above example, are selected equal to 40% and 15% of bulk modulus of the solid phase, respectively. The generated microstructures are shown in Figure 6.5. It demonstrates that the

proposed optimization procedure can successfully obtain a proper connected, optimized cellular FGM. Figure 6.6 shows the variation of volume fraction through the cells. The variation of the bulk modulus of the generated FGM is also compared with the prescribed values in the same figure. The total number of iterations in this instance was 166.



Figure 6.5: Optimized FGM with non-linear gradation in bulk modulus of elasticity.

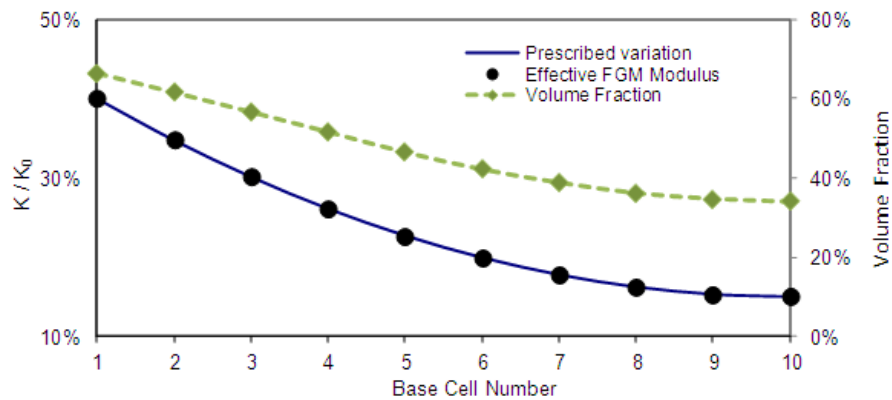
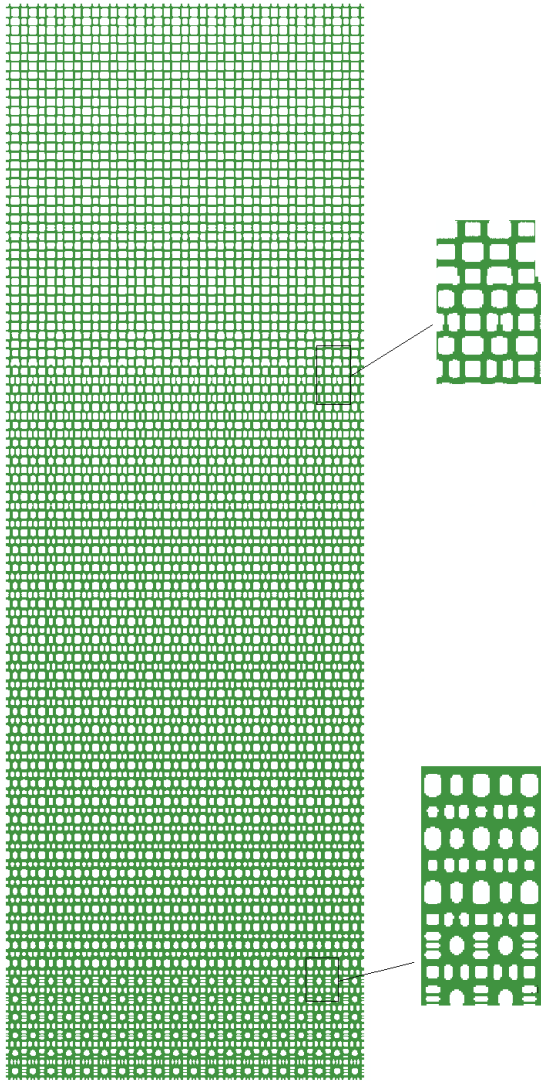


Figure 6.6: Non-linear variation of bulk modulus and volume fractions for the optimized FGM.

As discussed before, in Homogenization theory, the difference between average field behavioural responses under assumed and actual boundary conditions are smaller when the number of base cells is increased in the design domain. Figure 6.7 demonstrate another 2D example in which the FGM domain is divided into 60 base cells and the bulk modulus varies linearly from 40% to 15% of that of the solid constituent phase. Each base cell is divided into

a coarse mesh of  $40 \times 40$  elements and the filter radius  $r_{\min} = 4$ . Other parameters are similar to above examples.



*Figure 6.7: 2D FGM divided into 60 cells along the gradation direction with linear variation of bulk modulus. The designed microstructure has been repeated 20 times perpendicular to the gradation direction*

### 6.2.2. 2D FGM with variation in shear modulus

The objective of this example is to design a 2D plane stress FGM, in which the shear modulus varies linearly between 50% and 20% of that of the solid material. The design domain is

divided into 12 base cells, and each base cell with dimensions  $80 \times 80$ , is further discretized into  $80 \times 80$ , 4-node square elements. As before, the model of the first base cell is entirely composed of elements with solid properties, except for four void elements at the centre. The BESO parameters are the evolution rate  $ER = 0.04$  and the filtering radius  $r_{\min} = 5$ . The mechanical properties of the solid phase are selected as the Young's modulus and Poisson's ratio of  $E^s = 1$  and  $\nu = 0.3$  respectively.



Figure 6.8: Optimized FGM with linear gradation in shear modulus of elasticity.

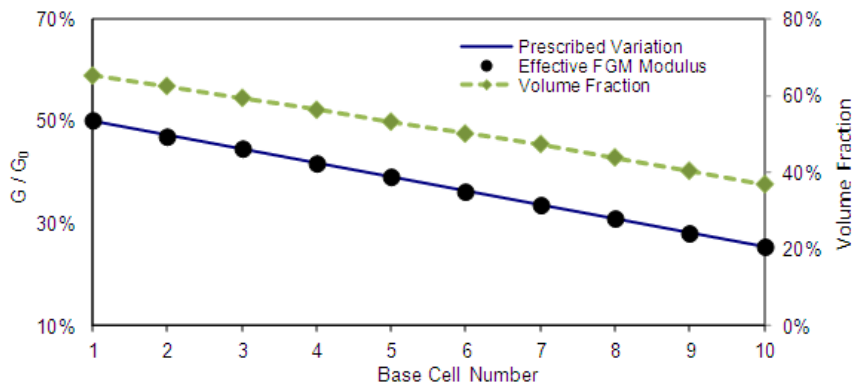


Figure 6.9: Variation of shear modulus and volume fractions for the optimized FGM where  $G_0$  is the shear modulus of the solid.

The optimized microstructure of the FGM is shown in Figure 6.8, which demonstrates the proper connections between base cells. Figure 6.9 presents the effective shear modulus of the

generated FGM in comparison with the prescribed values. It clearly indicates that the resulting FGM has the prescribed variation in shear modulus with high accuracy.

### 6.2.3 3D FGM with variation in bulk modulus

To test the algorithm in 3D problems, this example aims to generate a series of base cells for an FGM, with the gradation in bulk modulus from 50% to 5% of the solid constituent phase. The design domain is divided into 10 base cells, each of which discretized into  $31 \times 31 \times 31$ , 8-node cubic elements; the dimensions of each element are  $1 \times 1 \times 1$ . As before the dimensionless Young's modulus  $E^s = 1$  and the Poisson's ratio  $\nu = 0.3$  are selected for the solid constituent phase. The evolution rate  $ER = 0.03$  and filter radius  $r_{\min} = 3$  and the penalty exponent  $p = 3$  are the BESO design parameters. The initial finite element model of the first base cell is entirely occupied by solid elements, except for one void element at the centre.

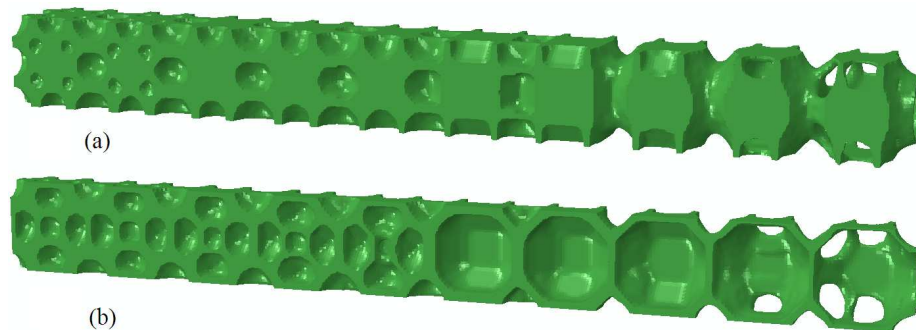


Figure 6.10: 3D FGM with gradation in bulk modulus of elasticity (a) optimized microstructure (b) cross section of FGM showing internal structure

The generated microstructures are shown in Figure 6.10 which demonstrates appropriate connections between the base cells. The total iteration number for this example is 205. Figure



6.11 represents the resulting bulk modulus of the FGM in comparison with the prescribed values and corresponding volume fractions. The deviation of FGM effective bulk modulus from the prescribed values is less than 0.15%.

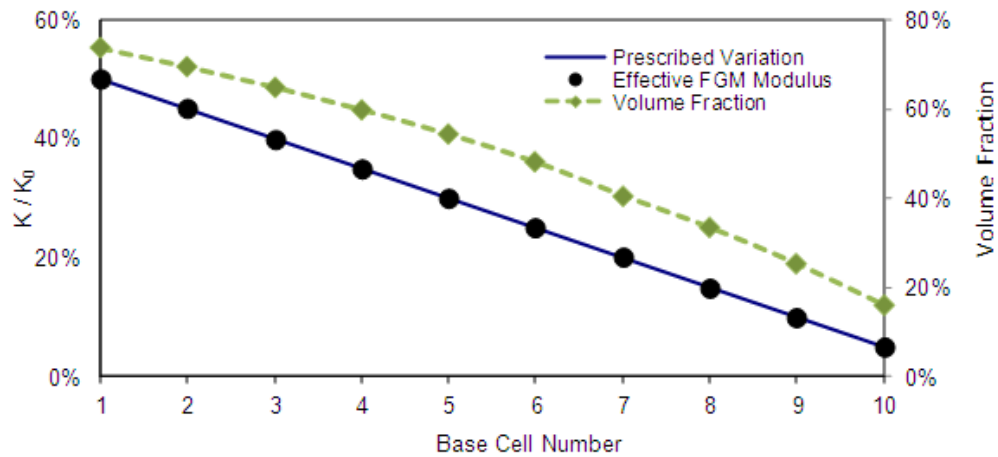


Figure 6.11: Variation of bulk modulus and volume fractions for the 3D FGM.

#### 6.2.4. 3D FGM's with variation in shear modulus

An FGM is designed with 8 base cells, with variation in the average shear modulus from 40% to 5% of that of the solid constituent phase. Each base cell with dimensions of  $30 \times 30 \times 30$  is discretized into  $30 \times 30 \times 30$ , 8-node cubic elements. The initial finite element model of the first base cell is entirely occupied by solid elements, except for 8 void elements at the centre of the model. As before, the Young's modulus and Poisson's ratio of the solid phase are selected as  $E^s = 1$  and  $\nu = 0.3$  respectively; the design parameters are selected as  $ER = 0.03$ ,  $r_{\min} = 3$  and  $p = 3$ .

The resulting topology, with appropriate connection between the base cells is shown in Figure 6.12. The total number of iterations is 169. The resulting shear modulus and volume fractions are also presented in the Figure 6.13, which demonstrates a very good agreement with the prescribed shear modulus (the deviation from prescribed values is less than 0.2%).

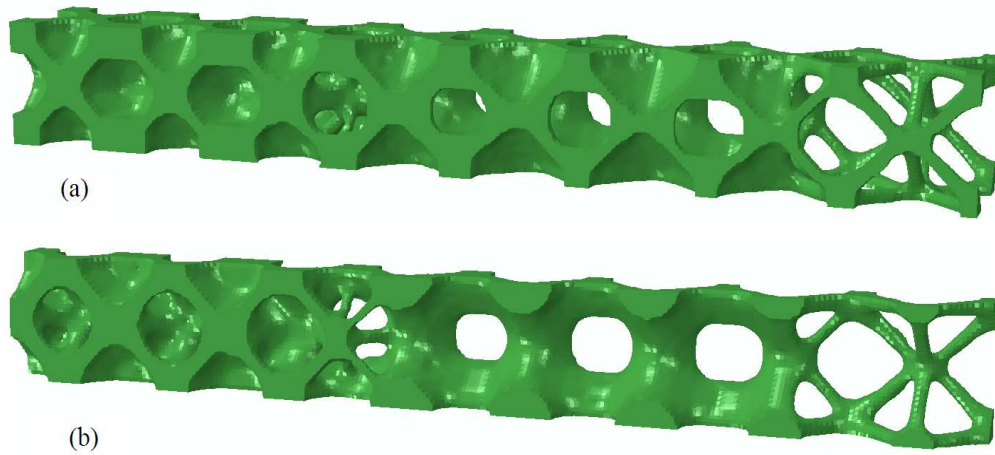


Figure 6.12: 3D FGM with variation in shear modulus of elasticity (a) optimized microstructure (b) cross section of FGM showing internal structure.

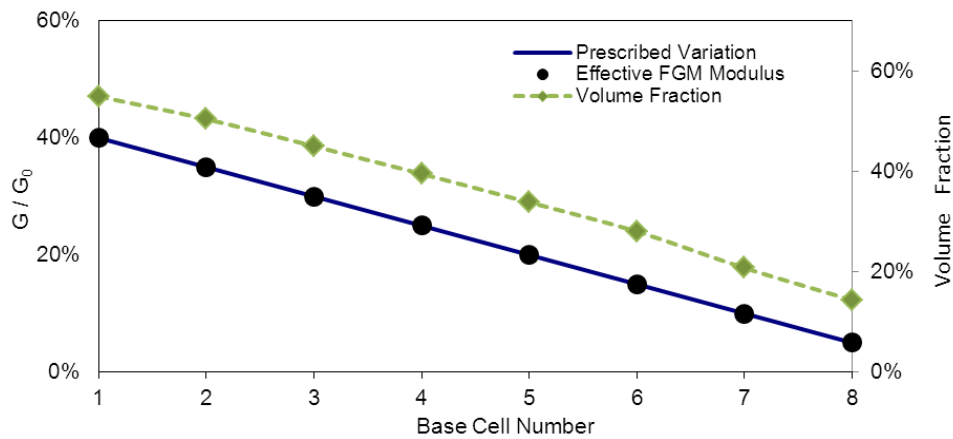


Figure 6.13: Variation of shear modulus and volume fractions for the 3D FGM

### 6.2.5 2D FGM with variation in thermal conductivity

The objective of this example is to generate a series of base cells for an FGM, with prescribed variation in the thermal conductivity. Each base cell is discretized into  $80 \times 80$  square elements with the dimensions  $1 \times 1$ . The BESO design parameters are selected as  $ER = 0.02$ ,  $r_{\min} = 8$  and  $p = 3$ . It is assumed that the FGM is divided into 10 cells and the prescribed average thermal conductivity of FGM varies between 50% and 20% of the nonporous solid phase. The thermal conductivity of the solid material is assumed to be  $k^s = 1$ .



Figure 6.14: 2D FGM with variation in thermal conductivity

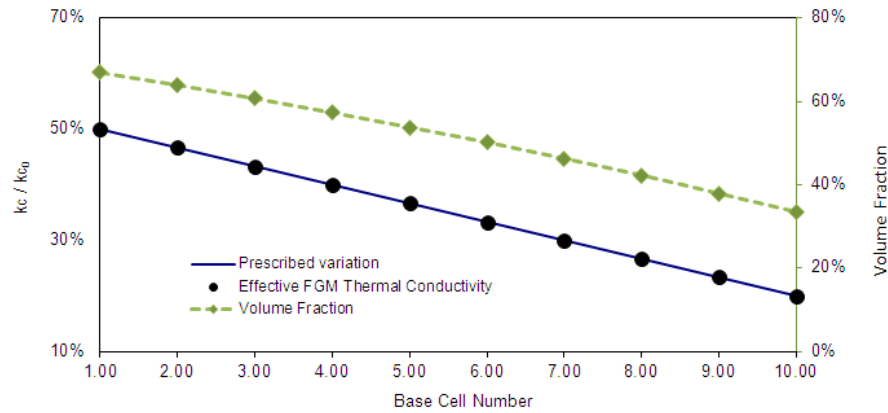


Figure 6.15: Variation of thermal conductivity and volume fractions for the 2D FGM where  $k_{c0}$  is the thermal conductivity of the solid phase

The generated topology with appropriate connection between base cells is shown in Figure 6.14. The total number of iterations is 166. The resulting average thermal conductivity and volume fractions are also presented in Figure 6.15, which demonstrates a very good conformity with the prescribed values; the deviation from prescribed values is less than 0.1%.

### **6.2.6 3D FGM with variation in thermal conductivity**

This example demonstrates the effectiveness of the method for topology optimization of microstructures for a 3D FGM, with prescribed variation in thermal conductivity. It is assumed that the FGM consists of 8 base cells with dimensions  $25 \times 25 \times 25$  which are discretized into  $25 \times 25 \times 25$  cubic elements. The BESO design parameters are selected as the evolutionary rate  $ER = 0.02$ , the filter radius  $r_{\min} = 3$  and the penalty exponent  $p = 3$ . The prescribed thermal conductivity of the FGM is set to vary between 55% and 25% of the nonporous solid phase. As before, It is assumed that the eigenvalue of the thermal conductivity of the solid material is  $k^s = 1$ .

The generated base cells are shown in Figure 6.16. The total number of iterations is 146. The resulting thermal conductivity and volume fractions are also presented in the Figure 6.17, which demonstrates a very good conformity with the prescribed values. The deviation from prescribed values is less than 0.2%.

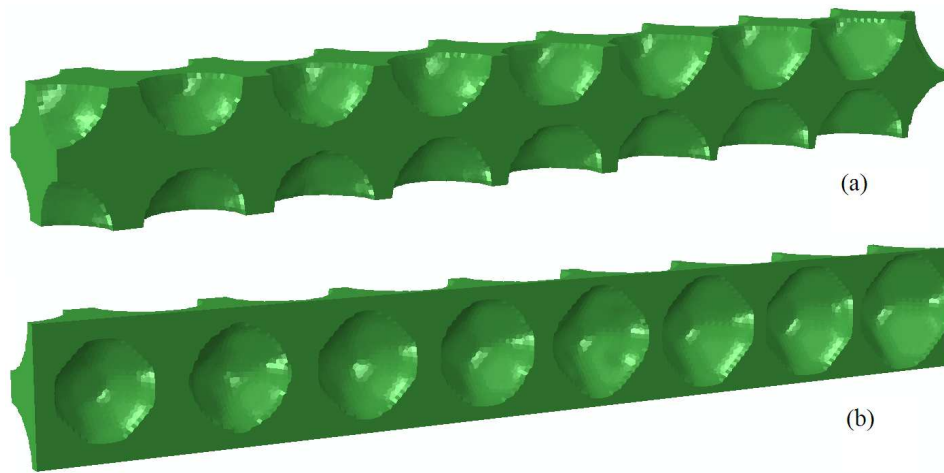


Figure 6.16: 3D FGM with variation in thermal conductivity (a) optimized microstructure (b) cross section of FGM showing internal structure.

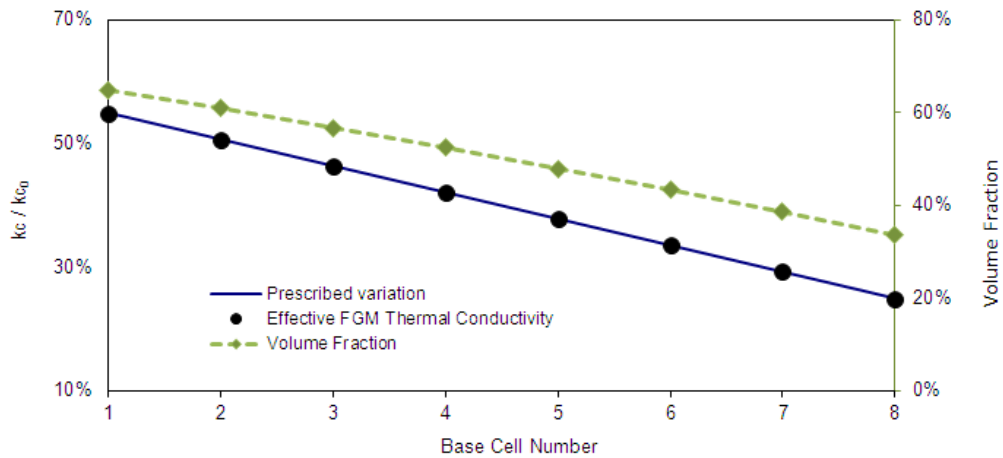


Figure 6.17: Variation of thermal conductivity and volume fractions for the 3D FGM where  $k_{c0}$  is the thermal conductivity of the solid phase

### 6.3. Concluding remarks

This study proposed a new and computationally efficient technique for the topology optimization of functionally graded cellular materials. The method addresses the connectivity issue between the adjacent base cells, by considering the topology optimization of three cells, at each stage of design and filtering their sensitivities together. The process only requires that the finite element analyses to be conducted for only two base cells in each iteration. This also considerably reduces the computational cost. Numerical examples have been presented to demonstrate the efficiency of the proposed algorithm for the topology optimization of microstructures for cellular FGMs, with gradual changes in bulk modulus, shear modulus or thermal conductivity with the minimum volume (or weight) of the solid material. Due to the existence of local optima in material design, different topologies can be achieved by selecting different design parameters. The proposed procedure can be applied to the designing of FGMs with gradation in other functional properties, such as magnetic permeability or electrical permittivity. In the next chapter the method will be used for topology optimization of multi-phase FGM with two functional properties.

## **Chapter 7**

---

### **Topology optimization of multi-objective graded composites**

#### **Background**

In the previous chapter a systematic method utilising topology optimization techniques, has been proposed for the design of FGMs. The cellular FGM was represented with a series of base cells and the structural topology optimization is applied to find the optimal material distribution within the base cells, so that the FGMs develop a gradual variation in the prescribed property. As discussed in Chapter 2, multi-functional materials are inevitably composites of two or more constituent phases (Gibson, 2010). In comparison with cellular materials, composites of two or more materials are more advantageous, for practical application. This is attributed to the fact that by combining different constituent phases, a

wider range of possible properties can be achieved, which are not attainable using individual phases.

The common approach for the topology optimization of materials for multi-functional properties is to extremize a combination of functional properties (Cadman et al., 2013). Assuming two functional properties of  $P_1$  and  $P_2$  for the composite, the optimization objective function is usually defined by applying some weighting factors to different parts of the objective functions:

$$w_1 P_1 + w_2 P_2 \tag{7.1}$$

By varying the weighting factors  $w_1, w_2$ , materials with different properties can be achieved due to varying effects of  $P_1$  and  $P_2$  on the objective function (de Kruijf et al., 2007, Torquato et al., 2003, Guest and Prévost, 2006, Cadman et al., 2013). However, a drawback of such an approach is that by applying different  $w_1 / w_2$  rates, a proportional variation in the objective functions cannot be anticipated (de Kruijf et al., 2007). One reason for such a phenomenon is the possible non-linear cross-properties of the objective functions, especially when these functional properties are selected from different physical characteristics. More importantly, it is largely attributed to the existence of local optima in material design. When pairs of fixed weighting factors are used during the whole optimization procedure, the existence of the local optima may cause the topology optimization algorithms to trap in a nearby solution and hence, by varying  $w_1 / w_2$  irregular fluctuations appears in the final material performance. As a consequence, the results of such an optimization problem statement are usually expressed with a generated Pareto front (Chen et al., 2009, 2010, de Kruijf et al., 2007). This provides a



visual representation of attainable functional properties with respect to a particular set of design parameters. However in the case of designing an FGM where a prescribed gradual variation in functional properties is desirable, this optimization method with given fixed weighting factors, is not appropriate because of the uncontrolled fluctuations in resulted properties.

In this chapter, a computational technique for topological design of microstructures for FGMs with multiple graded properties, e.g. bulk modulus and thermal conductivity, is presented. It is assumed that the FGM is composed of two non-zero constituent phases. As before, the FGM is divided into of a series of base cells and the topology optimization is utilized to design the base cells for desire functional properties. Instead of applying pairs of fixed weighting factors to different terms of the objective function, an optimization problem statement is defined to maximize one functional property, with the constraint being the gradual change of another functional property. Similar to the method proposed in the previous chapter for cellular FGM, to improve the connectivity of adjacent base cells, they are optimized progressively by considering three base cells at each stage and filtering their sensitivities together. Numerical examples will be presented to demonstrate the effectiveness of the proposed method in controlling the functional properties.

## **7.1. Methodology**

### **7.1.1. Problem statement and sensitivity numbers**

By assuming that the FGM totally consists of  $N$  base cells along the gradation direction (see Figure6.1), the topology optimization statement for designing the  $j^{th}$  base cell with maximum

bulk modulus and prescribes variation of thermal conductivity and volume fraction can be expressed as:

$$\text{Maximize} \quad K^j \quad (7.1a)$$

$$\text{Subject to:} \quad k_c^j = k_c^{j*} \quad (7.1b)$$

$$V^j = \sum_{i=1}^M x_i^j V_i^j$$

$$x_i^j = x_{\min} \quad \text{or} \quad 1 \quad (7.1c)$$

(  $i = 1, 2, \dots, M$  ) and (  $j = 1, 2, \dots, N$  )

where  $M$  denotes the number of total elements within the model of each base cell. It is assumed that the material is composed of two non-zero constituent phases with the Young's modulus and thermal conductivity of  $E^1$  and  $k^1$  for material 1 and  $E^2$  and  $k^2$  for material 2;  $V^j$  represents the volume (or weight) of material 1 in the  $j^{\text{th}}$  base cell;  $K^j$  is the bulk modulus of the  $j^{\text{th}}$  base cell which is defined in equation (3.3);  $k_c^j$  is the effective thermal conductivity of the  $j^{\text{th}}$  base cell defined with equation (3.5) and  $k_c^{j*}$  is its prescribed value of the materials thermal conductivity which is determined by the desired gradation of thermal conductivity of FGM.

The  $x_i^j$  is the design variable of the  $i^{\text{th}}$  element within the  $j^{\text{th}}$  base cell; it can be defined in such a way to take a binary value of either 1 or a small value (i.e. 0.001) for elements with

material 1 or 2 respectively. The local material of an element within the base cells is assumed to be isotropic, with the physical property that varies between the properties of the two constituent phases. For the cases in which the two materials are well-ordered (i.e.  $E^1 > E^2$  and  $k^1 > k^2$ ), the following power-law interpolation scheme is applicable (Rozvany et al., 1992, Bendsøe and Sigmund, 2003):

$$D_{ij} = x_i^p D_{ij}^1 + (1 - x_i^p) D_{ij}^2 \quad (7.2a)$$

$$k_{ij} = x_i^p k_{ij}^1 + (1 - x_i^p) k_{ij}^2 \quad (7.2b)$$

in which  $D_{ij}$  and  $k_{ij}$  are the elements of stiffness and thermal conductivity matrices respectively; the superscripts denotes the constituent phase numbers;  $p$  is the penalty exponent ( $p = 3$  is used). When the two constituent phases have ill-ordered properties, (i.e.  $E^1 > E^2$  and  $k^1 < k^2$ ) the interpolation schemes are defined as:

$$D_{ij} = x_i^p D_{ij}^1 + (1 - x_i^p) D_{ij}^2 \quad (7.3a)$$

$$\frac{1}{k_{ij}} = \frac{x_i}{k_{ij}^1} + \frac{(1 - x_i)}{k_{ij}^2} \quad (7.3b)$$

As before, for the calculation of the overall properties of composite materials the Homogenization theory is used (Bendsøe and Kikuchi, 1988, Hassani and Hinton, 1998a, 1998b). For calculation of the elements of stiffness and thermal conductivity matrices, the appropriate expressions are given by equations (3.14) and (3.16) respectively. Using

equations (7.2) or (7.3), the derivation of stiffness matrix  $\mathbf{D}^H$  with respect to the design variables  $x_i$ , is found by using the adjoint method as given by equation (3.15). Similarly, the sensitivity numbers of the conductivity matrix  $\mathbf{k}^H$  with respect to the design variable, can be calculated via equation (3.17).

### 7.1.2. Solution method and Lagrangian multipliers

For solving the optimization problem (7.1), it is necessary to modify the original objective function by adding the constraint function through introducing a Lagrangian multiplier  $\lambda$ . Similar to the method introduced in Chapter 4 for imposing isotropy, the objective function is modified as:

$$f(\mathbf{x}) = K^j + \lambda(k_c^j - k_c^{j*}) \quad (7.4a)$$

or by setting  $\lambda = \frac{\ell}{(1-|\ell|)}$  it can be rewritten as:

$$f(\mathbf{x}) = K^j + \frac{\ell}{(1-|\ell|)}(k_c^j - k_c^{j*}) \quad ; -1 \leq \ell \leq 1 \quad (7.4b)$$

where the Lagrangian multiplier  $\lambda$  can take any value, if the prescribed thermal conductivity is attained. Otherwise, it is determined in such a way that the thermal conductivity  $k_c^j$  tends towards its prescribed value  $k_c^{j*}$  in the subsequent iterations. The  $i^{\text{th}}$  element sensitivity number is defined by the sensitivity of the modified objective function in (7.4) as:

$$\alpha_i = \frac{\partial f(\mathbf{x})}{\partial x_i} = \alpha_{1i} + \frac{\ell}{(1-|\ell|)} \alpha_{2i} \quad (7.5a)$$

Since just the ranking of elements matters it can be rewritten as:

$$\alpha_i = (1-|\ell|)\alpha_{1i} + \ell\alpha_{2i} \quad (7.5b)$$

where  $\alpha_{1i}$  and  $\alpha_{2i}$  are expressed by

$$\alpha_{1i} = \frac{1}{\eta^2} \sum_{i,j=1}^{\eta} \frac{\partial D_{ij}^H}{\partial x_i} \quad (7.6.a)$$

$$\alpha_{2i} = \frac{1}{\eta} \sum_i^{\eta} \frac{\partial k_{ii}^H}{\partial x_i} \quad (7.6.b)$$

which can be readily calculated numerically by applying (3.15) and (3.17). To determine  $\ell$ , it is necessary to estimate the variation of the thermal conductivity due to the changes of the design variables. The thermal conductivity of the next iteration can be estimated based on the material's thermal conductivity at the current iteration by exploiting the following equation:

$$(k_c^j)^{t+1} = (k_c^j)^t + \sum_i \frac{d(k_c^j)_t}{dx_i} \Delta x_i \quad (7.7)$$

in which superscripts of  $t$  and  $t+1$  denote the current and next iteration numbers respectively.

Similar to the method described in Chapter 4, the Lagrangian multiplier  $\lambda$  is determined in such a way that the constraint on the thermal conductivity is satisfied in the subsequent

iterations. For instance, in the challenging case where the two constituent phases have ill ordered properties, the initial elemental sensitivity numbers are calculated by assuming  $\ell = 0$ . Then, by ranking the sensitivity of elements and imposing the volume constraint, a possible new set of design variables are evaluated. The thermal conductivity in subsequent iteration  $(k_c^j)^{t+1}$  is estimated using equation (7.7). If the thermal conductivity  $(k_c^j)^{t+1}$  is less than the prescribed value  $k_c^{j*}$ , then  $\ell$  has to be gradually increased, which means that the modified objective of optimization gradually turns to the maximization of thermal conductivity. On the other hand, in the case where the two constituent phases have ill ordered properties, gradual decreasing the Lagrangian multiplier to 0 will convert the optimization to the maximization of bulk modulus, in which the thermal conductivity gradually reduces due to the opposite effects of ill ordered constituent phases.

The precise value of  $\ell$  could be determined using the bisection algorithm in an internal loop, by exploiting two auxiliary variables  $\ell_{low}$  and  $\ell_{up}$ . When the constituent phases are ill-ordered at the beginning of each iteration they are set equal to 0 and 1 respectively. If the calculated value  $(k_c^j)^{t+1} - k_c^{j*}$  is negative, then the lower bound of auxiliary variables is updated as  $\ell_{low} = \ell$  and  $\ell = (\ell_{low} + \ell_{up})/2$ . The sensitivity numbers are updated according to equation (7.5) and new set of design variables, as well as  $(k_c^j)^{t+1}$ , are calculated. Every time that the predicted thermal conductivity is less than prescribed value (i.e.  $(k_c^j)^{t+1} < k_c^{j*}$ ), the above updating scheme ( $\ell_{low} = \ell$  and  $\ell = (\ell_{low} + \ell_{up})/2$ ) is applied; otherwise the upper bound is updated as  $\ell_{up} = \ell$  and  $\ell = (\ell_{low} + \ell_{up})/2$ . The internal loop is halted when the

difference between auxiliary variables ( $\ell_{low}$ ,  $\ell_{up}$ ) is acceptably small (e.g.  $10^{-5}$ ). To stabilize the procedure, the coefficient  $\ell$  can be averaged with previous iteration value before final adding and removing of elements.

### 7.1.3. Numerical implementation

As discussed in the previous chapter, in the design of a series of base cells for an FGM, the transition between adjacent unit cells is an important issue that should be considered. In the optimization procedure implemented in this chapter, the proposed method from Chapter 6 is utilized, to provide a smooth transition between base cells. This means, at each stage of the design, three base cells are considered and their sensitivities are filtered together. The filtering is made by averaging the sensitivity number of each element with its neighbouring elements (Huang and Xie, 2007b, 2010b). As pointed out before, the same filtering scheme can effectively circumvent the numerical instabilities of the checkerboard pattern and mesh-dependency in the BESO procedure. The filtering is performed using equation (6.5).

The whole optimization procedure can be summarized in the following steps:

Step 1: Define constituent materials properties, prescribed thermal conductivity and volume fraction ( $V^*$ ) for the different regions of the FGM. Define the BESO design parameters of evolutionary rate ( $ER$ ), filter radius ( $r_{min}$ ) and penalty exponent;

Step 2: Initiate finite element models for the base cells  $j$  and  $j-1$  (if  $j > 1$ ) for structural analysis; apply periodic boundary conditions and uniform strain fields. As described in Chapter 3, in 2D problems 3 independent load cases and in 3D cases 6 independent

load cases are required. Carry out the finite element analysis to obtain the output displacement fields;

Step 3: Initiate separate finite element models of the base cells  $j$  and  $j-1$  with appropriate periodic boundary conditions and uniform heat fluxes for thermal analysis. In 2D problems 2 independent fields of heat fluxes and in 3D cases 3 independent fields are required. Carry out the finite element analysis to obtain the induced temperature fields;

Step 4: Calculate the sensitivities  $\alpha_{1i}$  and  $\alpha_{2i}$  using equations (7.6) for base cells  $j$  and  $j-1$ .

Use the saved sensitivity numbers of the base cell  $j-2$  (if  $j > 2$ ) and filter the sensitivities of the elements within these three base cells using equation (6.5); Let  $\ell = 0$ ;

Step 5: Calculate  $\alpha_i = (1 - \ell)\alpha_{1i} + \ell\alpha_{2i}$  for the elements of the base cells  $j$  and  $j-1$ ; rank elemental sensitivity numbers ; obtain new set of design variables  $x_i$  by applying volume constraint on material 1 for base cells  $j$  and  $j-1$  separately as:

$$V^{t+1} = \max(V^t(1 - ER), V^*);$$

Step 6: Calculate the effective thermal conductivities  $(k_c^j)^t$  and  $(k_c^{j-1})^t$ ; calculate their next iteration approximations  $(k_c^j)^{t+1}$  and  $(k_c^{j-1})^{t+1}$  using equation (7.7) for base cells  $j$  and  $j-1$  respectively;

Step 7: Use the above explained method to calculate the modified  $\ell$  for base cells  $j$  and  $j-1$ ;

Step 8: Repeat steps 5 through 7 until  $\ell$  converges to a constant value;



Step 9: Average the sensitivity numbers of the base cells  $j$  and  $j-1$  with their values from the previous iteration if applicable; update the design variables  $x_i$  by changing from 1 to  $x_{\min}$  for elements with lower sensitivity numbers and from  $x_{\min}$  to 1 for elements with higher sensitivity numbers;

Step 10: Repeat steps 2 to 9 until both the volume constraints and the thermal conductivities of base cells  $j$  and  $j-1$  are converged to their corresponding prescribed values;

Step 11: Use the final topology of base cell  $j$  to construct the starting model for the base cell  $j+1$ .

Step 12: Repeat steps 2 to 11 until optimized topologies of all base cells are achieved.

## 7.2. Results and discussion

### 7.2.1. 2D Examples

The objective of the first example is to design an FGM with maximum bulk modulus, while the thermal conductivity varies linearly from the Hashin-Shtrikman (HS) lower bound corresponding to 60% volume fraction of material 1, to the upper bound corresponding to 40% of material 1 (Hashin and Shtrikman, 1962). The design domain of the FGM has been divided into 16 base cells and it is assumed that the base cells are composed of two ill-ordered constituent phases. The non-dimensional Young's modulus and thermal conductivity of material 1 are selected as  $E^1 = 3$  and  $k^1 = 1$  respectively; the Young's modulus and thermal conductivity of material 2 are assumed  $E^2 = 1$  and  $k^2 = 3$ . Each base cell with dimensions of  $60 \times 60$  is discretized into  $60 \times 60$ , 4-node square elements. The initial topology of the first base cell consists of four elements with material 2 properties, while other elements are

assigned with material 1 properties. The BESO design parameters are the evolution rate of  $ER = 0.04$ , filter radius  $r_{\min} = 3$  and the penalty exponent  $p = 3.0$ .

The generated microstructures for the FGM are demonstrated in Figure 7.1. The total iteration numbers for the procedure is 178. Figure 7.2 shows the variations of the bulk modulus and thermal conductivity along the FGM gradation direction. It can be seen that the bulk modulus gradually decreases from the left to the right while the thermal conductivity gradually increases. It is noted that the resulting thermal conductivity conforms well to the prescribed values, with a deviation of less than 1.5%.

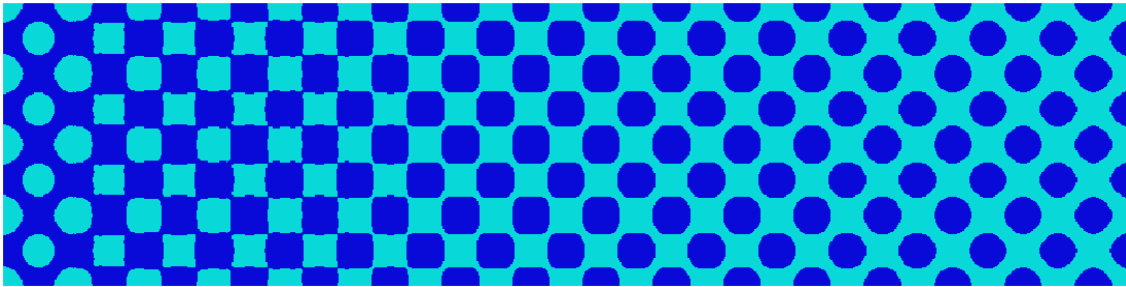


*Figure 7.1: Four rows of 2D base cells designed for the FGM with prescribed thermal conductivity and volume fraction; the volume fraction of material 1 (shown in dark blue) varies between 60% and 40% of the total volume of the cell*

When the prescribed volume fraction of material 1 is 50% for all base cells, the microstructures that are shown in Figure 7.3 are generated. The variation of thermal conductivity and bulk modulus of this case are shown in Figure 7.3. The figure demonstrates a good conformity between the attained thermal conductivity and prescribed values. The bulk

modulus also demonstrates a smooth variation, although the constraint is only imposed on the thermal conductivity of material.

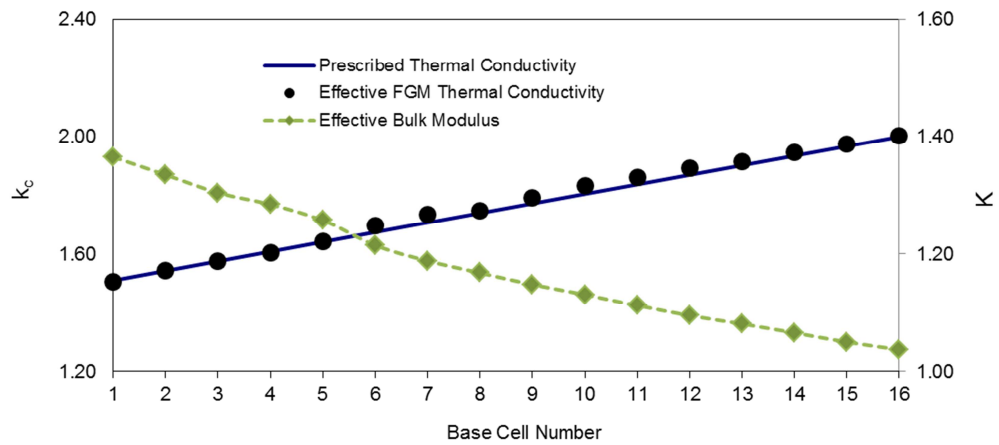


Figure 7.2: Variation of thermal conductivity and bulk modulus along the gradation direction, ( $k_c$ : thermal conductivity;  $K$ : bulk modulus)

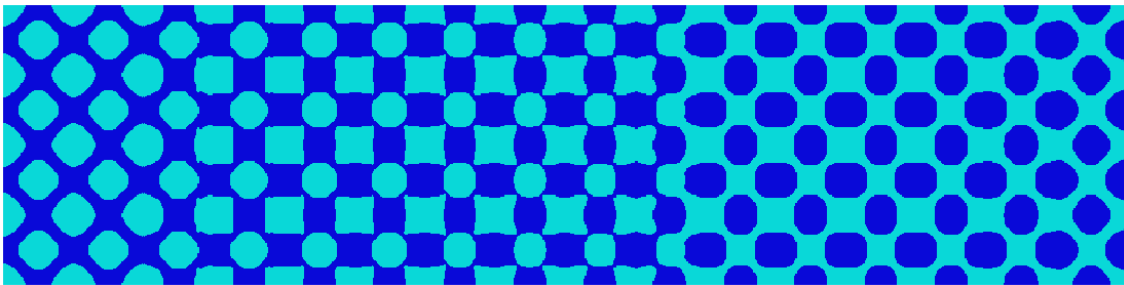


Figure 7.3: Four rows of 2D base cells designed for the FGM with variation in thermal conductivity; the prescribed volume fraction of material 1 (shown in dark blue) is 50% in all base cells

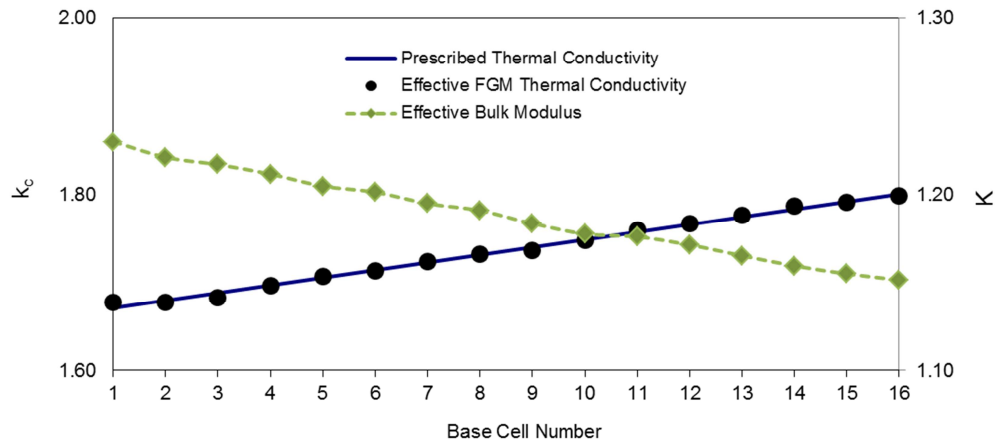


Figure 7.4: Variation of thermal conductivity and bulk modulus along the gradation direction, ( $k_c$ : thermal conductivity;  $K$ : bulk modulus)

When the prescribed volume fraction of material 1 is 50% for all base cells, the microstructures that are shown in Figure 7.3 are generated. The variation of thermal conductivity and bulk modulus of this case are shown in Figure 7.3. The figure demonstrates a good conformity between the attained thermal conductivity and prescribed values. The bulk modulus also demonstrates a smooth variation, although the constraint is only imposed on the thermal conductivity of material.

### 7.2.2. 3D Examples

To verify the proposed procedure in 3D cases, an FGM is modelled with variation of thermal conductivity from the HS lower bound to the upper bound, while the prescribed volume fraction of material 1 varies between 80% and 50% of the total volume of FGM. The domain of FGM is divided into 12 base cells and each cell is discretized into  $23 \times 23 \times 23$ , 8-node cubic elements. As before, the non-dimensional Young's modulus and thermal conductivity of

material 1 are selected as  $E^1 = 3$  and  $k^1 = 1$ . For material 2 the corresponding values are  $E^2 = 1$  and  $k^2 = 3$ . The initial design of the first base cell is constructed by assigning material 1 to all elements, except for eight elements at the corners of the base cell which are assigned with material 2 properties.

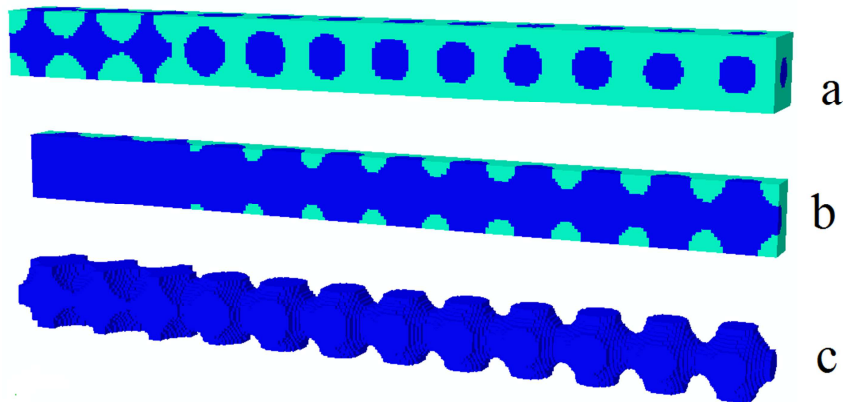


Figure 7.5: (a) 3D cells for the FGM with variation in thermal conductivity and volume fraction of materials; (b) longitudinal sections of (a); (c) topology of material 1 (dark blue)

The final topology of the optimized FGM is shown in Figure 7.5. This shows a smooth transition between the generated base cells. Figure 7.6 presents the variation of the bulk modulus and thermal conductivity along the gradation direction of the FGM. The thermal conductivity agrees to the prescribed values, with less than 1.3% deviation. The bulk modulus also varies smoothly.

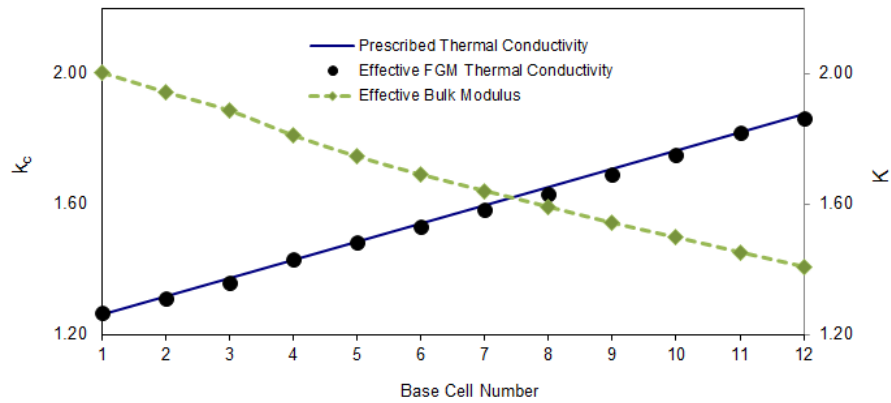


Figure 7.6: Variation of thermal conductivity and bulk modulus along the gradation direction of 3D FGM, ( $k_c$ : thermal conductivity;  $K$ : bulk modulus)

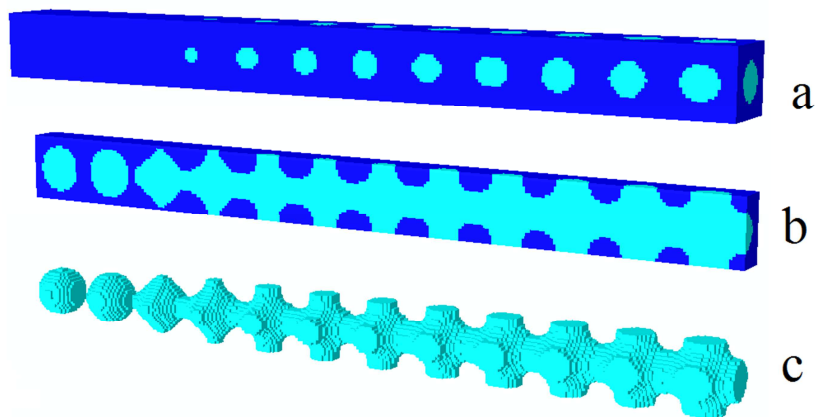


Figure 7.7: (a) 3D cells for the FGM with variation in thermal conductivity and volume fraction of materials; (b) longitudinal sections of (a); (c) topology of material 2 (light blue)

Figure 7.7 demonstrate another optimization example with the above parameters, but with different initial design. A series of microstructures have been generated, in which the initial topology of the first base cells contains one element of material 2 at the centre of the first base cell, while other elements are assigned with material 1. By repeating the base cells

perpendicular to the direction of gradation, it can be shown that Figures 7.5 and 7.7 are essentially referring to identical microstructures for FGM. The corresponding variation of the thermal conductivity and bulk modulus of the microstructure of Figure 7.7 are presented in Figure 7.8.

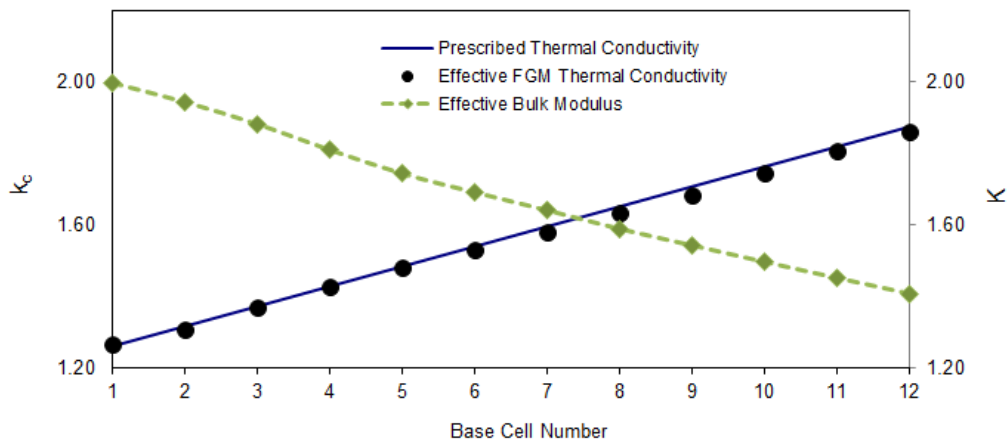


Figure 7.8: Variation of thermal conductivity and bulk modulus along the gradation direction of 3D FGM, ( $k_c$ : thermal conductivity;  $K$ : bulk modulus)

The generated microstructures are comparable with the non-functionally graded base cells found by Challis et al. (2008).

### 7.3. Conclusions

This chapter presented a computational method for the topology optimization of functionally graded composites with multi-functional properties and two non-zero constituent phases. The gradation of functional properties of the composite along one direction was attained by gradually changing the topological distribution and volume fraction of constituent phases. To

save the computational time and obtain a smooth transition between adjacent base cells, a progressive design approach based on the topology optimization of three adjacent base cells was applied at each stage. The numerical examples were presented, which demonstrate the effectiveness of the proposed approach in providing precise control over the variations of functional properties. The procedure could also be used for topology optimization of FGMs with other multi-functional properties.



## **Chapter 8**

---

### **Conclusion**

Previous studies on topology optimization at the macrostructural level have clearly indicated the advantages of Bi-directional Evolutionary Structural Optimization (BESO) in terms of lower computational costs, quality of generated microstructures, and the simplicity of the methodology in implementation with commercial software packages. Moreover, in the design of materials through topology optimization, it has been shown that the selection of the structural optimization methodology highly affects the results. The primary objective of this study was to open a pathway toward applying the BESO for the topological design of materials microstructures. Upon the successful accomplishment of the primary objective, the methodology was extended into various material design scenarios.

The literatures on several structural topology optimization algorithms that have already been used for the design of materials microstructures have been critically reviewed here. Moreover, as the process of material design usually involves the application of material modelling techniques, some of these techniques are briefly surveyed. Applications of topology optimization techniques in the design of microstructures for materials have been addressed.

In the first stage, the topology optimization of periodic microstructures using BESO has been sought for cellular materials with, maximum bulk modulus, shear modulus and thermal conductivity. By assuming the base cell as a continuum structure, the optimal spatial distribution of the solid phase within the microstructure has been determined. The effective elasticity matrix evaluation and the sensitivity analysis have been performed by applying the Homogenization theory. By ranking elements based on their sensitivity numbers and by imposing a volume constraint, the density of elements iteratively changes until the solution converges. The numerical examples clearly demonstrate the high computational efficiency of BESO in topology optimization of materials microstructures. Some interesting topological patterns for the cellular materials have been presented.

Next, an algorithm has been developed for the design of isotropic cellular materials by introducing an additional constraint to the optimization problem. The modified objective function has been constructed by introducing a Lagrange multiplier to implement the isotropy constraint. The numerical examples indicate that the extra constraint is very well incorporated in the optimization algorithm. With the established elemental sensitivity numbers, isotropic materials with maximum bulk or shear modulus have been designed. It has been shown that the developed methodology is applicable to other design scenarios.

Thereafter, the design of a multi-phase microstructure for materials with maximum bulk modulus, shear modulus or thermal conductivity has been investigated. Following the ranking of constituent phases based on their contribution to the objective function, they have been divided into some groups and the sensitivity analysis has been performed between groups. The addition and removal of elements has been performed based on the ranking of these sensitivity numbers, and by imposing volume constraint between different groups. The generated microstructures demonstrate very good agreement with known analytical bounds on material properties. The procedure has demonstrated a very stable convergence without any numerical difficulty, as opposed to other proposed procedures in the literature. The other major advantage of the BESO in the design of composites is that there are distinctive interfaces between constituent phases in the generated microstructures.

Furthermore, the methodology has been extended into the designing of a series of base cells for cellular FGMs. In particular, the approach addresses the connectivity issue between adjacent base cells by considering the topology optimization of three adjacent base cells at each stage of the design. The proposed approach performs finite element analyses for only two base cells at each stage of the design and maintains the connectivity of cells by devising a filtering scheme, thereby greatly reducing the computational cost. Numerical examples for designing FGMs with, bulk modulus, shear modulus or thermal conductivity demonstrate the effectiveness of the approach.

Finally, a computational procedure for the topology optimization of functionally graded composites with multi-functional properties has been proposed. It is assumed that the FGM consists of two non-zero material phases and the design objective is defined as the

maximization of one functional property, while a performance constraint is imposed on the variation of another functional property. To save the computational cost and obtain a smooth transition between adjacent base cells, a progressive design approach is used by performing topology optimization on three adjacent base cells at each stage. The numerical examples demonstrate the effectiveness of the approach in designing FGMs with smooth variation in maximum stiffness and prescribed variation in thermal conductivity.

The topology optimization problems solved in this thesis are rather simplified cases. However the design scenarios considered in this thesis demonstrate that the BESO method can be successfully applied in the design of microstructures for materials. For engineering applications, a variety of demands in terms of functionality or performance constraints may be placed on material systems; these issues could not be addressed in this thesis.

In Terms of the functional properties only stiffness and thermal conductivity optimization problems were considered in this thesis. Various other design objectives functions for materials can be considered in future studies. For example, materials with prescribed or tailored plasticity, viscosity or frequency characteristics can be the objective of optimization. Such materials have wider demands in advanced materials systems.

In this thesis, the topology optimization of materials with volume constraint and one performance constraint has been investigated. The methodologies in the presented form cannot be used for material optimization, when there are two or more performance constraints. When there are such kinds of demands, more advanced mathematical methodologies are needed to be developed.

Through the optimization process for the design of FGM's in the current study, periodic boundary conditions were applied on microstructures and the Homogenization theory is used for calculation of effective properties of materials. This assumption yields accurate effective properties for material only if the number of base cells in the design domain is large enough. The accuracy in the prediction of FGM characteristics can be increased by analysing FGMs in the two micro and macro scales. Inspired by the method introduced in this thesis, in which the FGM has been designed by dividing it into different stages, methodologies can be developed for topology optimization of the connected microstructures for FGMs via multi-scale analyses.

## References

---

- Adams, D. F. and D. A. Crane (1984). "Finite element micromechanical analysis of a unidirectional composite including longitudinal shear loading." Computers & Structures **18**(6): 1153-1165.
- Allaire, G., F. Jouve and A.-M. Toader (2004). "Structural optimization using sensitivity analysis and a Level-set method." Journal of Computational Physics **194**(1): 363-393.
- Allaire, G. and R. V. Kohn (1993). Topology Optimization and Optimal Shape Design Using Homogenization. Topology Design of Structures. M. Bendsøe and C. M. Soares, Springer Netherlands. **227**: 207-218.
- Ambrosio, L. and G. Buttazzo (1993). "An optimal design problem with perimeter penalization." Calculus of Variations and Partial Differential Equations **1**(1): 55-69.
- Asaadi, J. (1973). "A computational comparison of some non-linear programs." Mathematical Programming **4**(1): 144-154.
- Aubert, G. and P. Kornprobst (2006). Mathematical problems in image processing: partial differential equations and the calculus of variations New York, Springer.
- Bakhvalov, N. and G. Panasenko (1989). The Concept of Asymptotic Expansion. A Model Example to Illustrate the Averaging Method. Homogenization: Averaging Processes in Periodic Media, Springer Netherlands. **36**: 12-31.
- Barbero, E. J. (1999). Introduction to composite materials design, Taylor & Francis.
- Beaupre, G. S. and W. C. Hayes (1985). "Finite Element Analysis of a Three-Dimensional Open-Celled Model for Trabecular Bone." Journal of Biomechanical Engineering **107**(3): 249-256.
- Bendsøe, M. P. (1989). "Optimal shape design as a material distribution problem." Structural and Multidisciplinary Optimization **1**(4): 193-202.
- Bendsøe, M. P., J. M. Guedes, R. B. Haber, P. Pedersen and J. E. Taylor (1993). "An Analytical Model to Predict Optimal Material Properties in the Context of Optimal Structural Design." Journal of Applied Mechanics **61**(4): 930-937.
- Bendsøe, M. P. and N. Kikuchi (1988). "Generating optimal topologies in structural design using a homogenization method." Computer Methods in Applied Mechanics and Engineering **71**(2): 197-224.
- Bendsøe, M. P. and O. Sigmund (1999). "Material interpolation schemes in topology optimization." Archive of Applied Mechanics **69**(9): 635-654.
- Bendsøe, M. P. and O. Sigmund (2003). Topology Optimization: Theory, Methods and Application. Berlin, Springer.
- Benssousan, A., J. L. Lions and G. Papanicoulau (1978). Asymptotic Analysis for Periodic Structures. North-Holland, Amsterdam.
- Benveniste, Y. (1987). "A new approach to the application of Mori-Tanaka's theory in composite materials." Mechanics of Materials **6**(2): 147-157.

- Beran, M. (1965). "Statistical Continuum Theories." Transactions of the Society of Rheology **9**(1): 339-355.
- Berryam, J. G. and G. W. Milton (1988). "Microgeometry of random composites and porous media." J. Phys. D: Appl. Phys. **21**: 87-94.
- Bever, M. B. and P. E. Duwez (1972). "Gradients in composite materials." Materials Science and Engineering **10**(0): 1-8.
- Birman, V. and L. W. Byrd (2007). "Modeling and Analysis of Functionally Graded Materials and Structures." Applied Mechanics Reviews **60**(5): 195-216.
- Bourdin, B. (2001). "Filters in topology optimization." International Journal for Numerical Methods in Engineering **50**(9): 2143-2158.
- Budiansky, B. (1965). "On the elastic moduli of some heterogeneous materials." J. Mech. Phys. Solids **13**: 223-227.
- Burger, M., B. Hackl and W. Ring (2004). "Incorporating topological derivatives into level set methods." Journal of Computational Physics **194**(1): 344-362.
- Burger, M. and S. J. Osher (2005). "A survey on level set methods for inverse problems and optimal design." European Journal of Applied Mathematics **16**(02): 263-301.
- Burns, S. A., Ed. (2002). Recent advances in optimal structural design. USA, ASCE.
- Cadman, J., S. Zhou, Y. Chen and Q. Li (2013). "On design of multi-functional microstructural materials." Journal of Materials Science **48**(1): 51-66.
- Cahn, J. W. and J. E. Hillard (1958). "Free Energy of nonuniform system. I. Interfacial free energy." J Chem Phys **28**(1): 258-267.
- Challis, V. (2010). "A discrete Level-set topology optimization code written in Matlab." Structural and Multidisciplinary Optimization **41**(3): 453-464.
- Challis, V. J., A. P. Roberts and A. H. Wilkins (2008). "Design of three dimensional isotropic microstructures for maximized stiffness and conductivity." Inter. J. Solids Struct. **45**: 4130-4146.
- Chen, B. C., E. Silva and N. Kikuchi (2001). "Advances in computational design and optimization with application to MEMS." Int J Numer Methods Eng **52**(1-2): 23-62.
- Chen, K.-Z. and X.-A. Feng (2004). "CAD modeling for the components made of multi heterogeneous materials and smart materials." Computer-Aided Design **36**(1): 51-63.
- Chen, Y., S. Zhou and Q. Li (2009). "Computational design for multifunctional microstructural composites." International Journal of Modern Physics B **23**(06n07): 1345-1351.
- Chen, Y., S. Zhou and Q. Li (2010). "Multiobjective topology optimization for finite periodic structures." Computers & Structures **88**(11-12): 806-811.
- Cheng, K. T. and N. Olhoff (1981). "An investigation concerning optimal design of solid elastic plates." Int. J. Solids struct. **17**: 305-323.
- Cherkaev, A. (2000). Variational methods for structural optimization, Springer-Verlag.

- Cherkaev, A. V. and L. V. Gibiansky (1993). "Coupled estimates for the bulk and shear moduli of a two-dimensional isotropic elastic composite." Journal of the Mechanics and Physics of Solids **41**(5): 937-980.
- Christensen, R. M. (1979). Mechanics of composite materials. New York, Wiley.
- Christensen, R. M. (1986). "Mechanics of low density materials." Journal of the Mechanics and Physics of Solids **34**(6): 563-578.
- Christensen, R. M. and K. H. Lo (1979). "Solutions for effective shear properties in three phase sphere and cylinder models." Journal of the Mechanics and Physics of Solids **27**(4): 315-330.
- Chu, D. N., Y. M. Xie, Y. M. Hira and G. P. Steven (1996). "Evolutionary structural optimization for problems with stiffness constraints." Finite Elements in Analysis and Design **21**: 239-251.
- Coello, C. A., M. Rudnick and A. D. Christiansen (1994). Using genetic algorithms for optimal design of trusses. Tools with Artificial Intelligence, 1994. Proceedings., Sixth International Conference on.
- Coville, A. R. (1968). A comparative study on nonlinear programming codes. IBM N.Y., Scientific Center Report. **320-2949**.
- Cree, D. and M. Pugh (2010). "Production and characterization of a three-dimensional cellular metal-filled ceramic composite." Journal of Materials Processing Technology **210**(14): 1905-1917.
- Dantzig, G. (1963). Linear programming and extensions. Princeton, NJ, Princeton University Press.
- de Gournay, F., G. Allaire and F. Jouve (2008). "Shape and topology optimization of the robust compliance via the Level-set method." ESAIM: Control, Optimization and Calculus of Variations **14**(01): 43-70.
- de Kruijf, N., S. Zhou, Q. Li and Y.-W. Mai (2007). "Topological design of structures and composite materials with multiobjectives." International Journal of Solids and Structures **44**(22-23): 7092-7109.
- Díaz, A. and O. Sigmund (1995). "Checkerboard patterns in layout optimization." Structural Optimization **10**(1): 40-45.
- Dominguez, D. and I. Sevostianov (2011). "Cross-Property Connection between Work-Hardening Coefficient and Electrical Resistivity of Stainless Steel During Plastic Deformation." International Journal of Fracture **167**(2): 281-287.
- Dorn, W. S., R. E. Gomory and H. J. Greenberg (1964). "Automatic design of optimal structures." Journal de Mecanique **3**: 25-52.
- Drago, A. and M.-J. Pindera (2007). "Micro-macromechanical analysis of heterogeneous materials: Macroscopically homogeneous vs periodic microstructures." Composites Science and Technology **67**(6): 1243-1263.



- Duan, H. L., J. Wang, B. L. Karihaloo and Z. P. Huang (2006). "Nanoporous materials can be made stiffer than non-porous counterparts by surface modification." Acta Materialia **54**(11): 2983-2990.
- Einstein, A. (1906). "Eine neue bestimmung der molekuldimensionen." Ann. Phys. **19**: 289-306.
- Erdogan, F. (1995). "Fracture mechanics of functionally graded materials." Composites Engineering **5**(7): 753-770.
- Eschenauer, H. A. and N. Olhoff (2001). "Topology optimization of continuum structures: A review." Applied Mechanics Reviews **54**(4): 331-390.
- Eshelby, J. D. (1957). "The Determination of the Elastic Field of an Ellipsoidal Inclusion, and Related Problems." Proceedings of the Royal Society of London. Series A. Mathematical and Physical Sciences **241**(1226): 376-396.
- Evans, A. G., J. W. Hutchinson, N. A. Fleck, M. F. Ashby and H. N. G. Wadley (2001). "The topological design of multifunctional cellular metals." Progress in Materials Science **46**(3-4): 309-327.
- Fan, Z., P. Tsakirooulos and A. P. Miodownik (1994). "A generalized law of mixtures." Journal of Materials Science **29**(1): 141-150.
- Fanjoy, D. W. and W. A. Crossley (2002a). "Topology Design of Planar Cross-Sections with a Genetic Algorithm: Part 1--Overcoming the Obstacles." Engineering Optimization **34**(1): 1-22.
- Fanjoy, D. W. and W. A. Crossley (2002b). "Topology Design of Planar Cross-Sections with a Genetic Algorithm: Part 2--Bending, Torsion and Combined Loading Applications." Engineering Optimization **34**(1): 49-64.
- Fleury, C. (1979). "Structural weight optimization by dual methods of convex programming." International Journal for Numerical Methods in Engineering **14**(12): 1761-1783.
- Fleury, C. and V. Braibant (1986). "Structural optimization: A new dual method using mixed variables." International Journal for Numerical Methods in Engineering **23**(3): 409-428.
- Fujii, D., B. C. Chen and N. Kikuchi (2001). "Composite material design of two-dimensional structures using the homogenization design method." INTERNATIONAL JOURNAL FOR NUMERICAL METHODS IN ENGINEERING **50**: 2031-2051.
- Fung, Y. C. (1965). Foundations of Solid Mechanics. Englewood Cliffs, New Jersey, Prentice-Hall, INC.
- Gibiansky, L. V. (1993). Bounds on the Effective Moduli of Composite Materials. S. o. Homogenization, Princeton University.
- Gibiansky, L. V. and S. Torquato (1995). "Geometrical-parameter bounds on the effective moduli of composites." Journal of the Mechanics and Physics of Solids **43**(10): 1587-1613.
- Gibiansky, L. V. and S. Torquato (1996a). "Connection between the Conductivity and Bulk Modulus of Isotropic Composite Materials." Proceedings of the Royal Society of

- London. Series A: Mathematical, Physical and Engineering Sciences **452**(1945): 253-283.
- Gibiansky, L. V. and S. Torquato (1996b). "Bounds on the effective moduli of cracked materials." Journal of the Mechanics and Physics of Solids **44**(2): 233-242.
- Gibiansky, V. L. and O. Sigmund (2000). "Multiphase composites with extremal bulk modulus." Journal of the Mechanics and Physics of Solids **48**(3): 461-498.
- Gibson, L. J. and M. F. Ashby (1982). "The Mechanics of Three-Dimensional Cellular Materials." Proceedings of the Royal Society of London. A. Mathematical and Physical Sciences **382**(1782): 43-59.
- Gibson, L. J. and M. F. Ashby (1997). Cellular solids, structure and properties, Cambridge University press.
- Gibson, R. F. (2010). "A review of recent research on mechanics of multifunctional composite materials and structures." Composite Structures **92**(12): 2793-2810.
- Goldberg, D. E. and M. P. Samtani (1986). Engineering Optimization Via Genetic Algorithm. 9th Conference on Electronic Computation, ASCE, New York.
- Goldberg, D. E. (1989). Genetic Algorithms in Search, Optimization, and Machine Learning, Addison-Wesley Professional.
- Grierson, D. E. and W. H. Pak (1993). "Optimal sizing, geometrical and topological design using a genetic algorithm." Structural Optimization **6**(3): 151-159.
- Guest, J. K. and J. H. Prévost (2006). "Optimizing multifunctional materials: Design of microstructures for maximized stiffness and fluid permeability." International Journal of Solids and Structures **43**(22-23): 7028-7047.
- Guest, J. K., J. H. Prévost and T. Belytschko (2004). "Achieving minimum length scale in topology optimization using nodal design variables and projection functions." International Journal for Numerical Methods in Engineering **61**(2): 238-254.
- Haber, R. B., M. P. Bendsøe and C. S. Jog (1996). "A new approach to variable topology shape design using a constraint on the perimeter." Struct Optim **11**: 1-12.
- Hajela, P. and E. Lee (1995). "Genetic algorithms in truss topological optimization." International Journal of Solids and Structures **32**(22): 3341-3357.
- Hale, D. K. (1976). "The physical properties of composite materials." Journal of Materials Science **11**(11): 2105-2141.
- Hashin, Z. (1983). "Analysis of composite materials-A survey." J.App.Mech **50**: 481-505.
- Hashin, Z. and S. Shtrikman (1962). "A Variational approach to the theory of the effective magnetic permeability of multiphase materials." Journal of Applied Physics **33**(10): 3125-3131.
- Hashin, Z. and S. Shtrikman (1963). "A variational approach to the theory of the elastic behaviour of multiphase materials." Journal of the Mechanics and Physics of Solids **11**(2): 127-140.

- Hassani, B. and E. Hinton (1998a). "A review of homogenization and topology optimization II—analytical and numerical solution of homogenization equations." Computers and Structures **69**(6): 719-738.
- Hassani, B. and E. Hinton (1998b). "A review of homogenization and topology optimization I—homogenization theory for media with periodic structure." Computers and Structures **69**(6): 707-717.
- Hassani, B. and E. Hinton (1998c). "A review of homogenization and topology optimization III—topology optimization using optimality criteria." Computers and Structures **69**(6): 739-756.
- Hassani, B. and E. Hinton (1998d). Homogenization and Structural Topology Optimization: Theory, Practice and Software, Springer.
- Haug, E. J., K. K. Choi and V. Komkov (1986). Design Sensitivity Analysis of Structural Systems. Orlando, Academic Press.
- Haug, J. and J. Céa (1981). Optimization of distributed parameter structures, Sijthoff & Noordhoff.
- Hill, R. (1963). "Elastic properties of reinforced solids: Some theoretical principles." Journal of the Mechanics and Physics of Solids **11**(5): 357-372.
- Hill, R. (1965). "A self-consistent mechanics of composite materials." Journal of the Mechanics and Physics of Solids **13**(4): 213-222.
- Hinton, E. and J. Sienz (1995). "Fully stressed topological design of structures using an evolutionary procedure." Eng. Comput. **12**: 229-244.
- Hirai, T. and L. Chen (1999). "Recent and Prospective Development of Functionally Graded Materials in Japan." Materials Science Forum **308-311**: 509-514.
- Holland, J. H. (1975). Adaptation in natural and artificial systems, Ann Arbor: The University of Michigan Press.
- Hollister, S. J. and N. Kikuchi (1992). "A comparison of homogenization and standard mechanics analyses for periodic porous composites." Computational Mechanics **10**(2): 73-95.
- Huang, X., Y. Xie, B. Jia, Q. Li and S. Zhou (2012). "Evolutionary topology optimization of periodic composites for extremal magnetic permeability and electrical permittivity." Structural and Multidisciplinary Optimization: 1-14.
- Huang, X. and Y. M. Xie (2007a). "Bi-directional evolutionary structural optimization for structures with geometrical and material nonlinearities." AIAA J. **45**(1): 308-313.
- Huang, X. and Y. M. Xie (2007b). "Convergent and mesh-independent solutions for the bi-directional evolutionary structural optimization method." Finite Elements in Analysis & Design **43**(14): 1039-1049.
- Huang, X. and Y. M. Xie (2008a). "Optimal design of periodic structures using evolutionary topology optimization." Structural and Multidisciplinary Optimization **36**(6): 597-606.

- Huang, X. and Y. M. Xie (2008b). "Topology optimization of nonlinear structures under displacement loading." Eng. Struct **30**(30): 2057-2068.
- Huang, X. and Y. M. Xie (2009a). "Bi-directional evolutionary topology optimization of continuum structures with one or multiple materials." Comp. Mech. **43**(3): 393-401.
- Huang, X. and Y. M. Xie (2009b). "Evolutionary topology optimization of continuum structures with a local displacement constraint." Struct Multidisc Optim **33**: 375-386.
- Huang, X. and Y. M. Xie (2010a). "Evolutionary topology optimization of continuum structures with an additional displacement constraint." Structural and Multidisciplinary Optimization **40**(1-6): 409-416.
- Huang, X. and Y. M. Xie (2010b). Evolutionary Topology Optimization of Continuum Structures: Methods and Applications, John Wiley & Sons Ltd.
- Huang, X. and Y. M. Xie (2010c). "A further review of ESO type methods for topology optimization." Structural and Multidisciplinary Optimization **41**(5): 671-683.
- Huang, X., Y. M. Xie and G. Lu (2007). "Topology optimization of energy-absorbing structures." International Journal of Crashworthiness **12**(6): 663-675.
- Huang, X., Z. H. Zuo and Y. M. Xie (2010). "Evolutionary topological optimization of vibrating continuum structures for natural frequencies." Computers & Structures **88**(5-6): 357-364.
- Huber, A. T. and L. J. Gibson (1988). "Anisotropy of foams." Journal of Materials Science **23**(8): 3031-3040.
- Jakiela, M. J., C. Chapman, J. Duda, A. Adewuya and K. Saitou (2000). "Continuum structural topology design with genetic algorithms." Computer Methods in Applied Mechanics and Engineering **186**(2-4): 339-356.
- Jenkins, W. M. (1991). "Towards structural optimization via the genetic algorithm." Computers & Structures **40**(5): 1321-1327.
- Jog, C. S. and R. B. Haber (1996). "Stability of finite element models for distributed-parameter optimization and topology design." Computer Methods in Applied Mechanics and Engineering **130**(3-4): 203-226.
- Kamat, M. P. (1993). Structural optimization: status and promise, American Institute of Aeronautics and Astronautics, Inc.
- Kane, C. and M. Schoenauer (1996). "Topological optimum design using genetic algorithms." Control and Cybernetics **25**(5): 1059-1088.
- Karush, W. (1939). Minima of functions of several variables with inequalities as side constraints. Master's thesis, University of Chicago.
- Kohn, R. V. and G. Strang (1986). "Optimal design and relaxation of variational problems, I." Communications on Pure and Applied Mathematics **39**(1): 113-137.
- Koizumi, M. (1997). "FGM activities in Japan." Composites Part B: Engineering **28**(1-2): 1-4.

- Kuhn, H. W. and A. W. Tucker (1951). Nonlinear programming. Proceedings of 2nd Berkeley symposium, Berkeley, University of California press.
- Lakes, R. (1993). "Materials with structural hierarchy, review article." Nature **361**: 511-515.
- Lannutti, J. J. (1994). "Functionally graded materials: Properties, potential and design guidelines." Composites Engineering **4**(1): 81-94.
- Ledbetter, H. and A. Migliori (2006). "A general elastic-anisotropy measure." Journal of Applied Physics **100**(6): 063516.
- Li, Q., G. P. Steven and Y. M. Xie (1999). "On equivalence between stress criterion and stiffness criterion in evolutionary structural optimization." Structural Optimization **18**(1): 67-73.
- Li, Q., G. P. Steven and Y. M. Xie (2001). "A simple checkerboard suppression algorithm for evolutionary structural optimization." Structural and Multidisciplinary Optimization **22**(3): 230-239.
- Lin, C. Y., C. C. Hsiao, P. Q. Chen and S. J. Hollister (2004). "Interbody fusion cage design using integrated global layout and local microstructure topology optimization." Spine **29**(16): 1747-1754.
- Lin, C. Y., R.M.Schek, A. S. Mistry, X. F. Shi, A. G. Mikos, P. H. Krebsbach and S. J. Hollister (2005). "Functional bone engineering using ex vivo gene therapy and topology-optimized, biodegradable polymer composite scaffolds." Tissue Eng. **11**(9-10): 1589-1598.
- Lions, J. L. (1981). "Some Methods in the Mathematical Analyses of Systems and their Control " (Science press, Beijing,China, 1981) and (Gordon and Breach, New York).
- Love, A. (1934). A treatise of the mathematical theory of elasticity. London, Cambridge University Press.
- Manickarajah, D., Y. M. Xie and G. P. Steven (1998). "An evolutionary method for optimization of plate buckling resistance." Finite Elements in Analysis and Design **29**(3-4): 205-230.
- Markworth, A. J., K. S. Ramesh and W. P. Parks (1995). "Modelling studies applied to functionally graded materials." Journal of Materials Science **30**(9): 2183-2193.
- Maxwell, J. C. (1873). Treatise on Electricity and Magnetism. Clarendon Press, Oxford.
- Mei, Y. L. and X. M. Wang (2004). "A level set method for microstructure design of composite materials." Acta. Mech.Solida Sinica **17**(3): 239-250.
- Mercier, J. P., G. Zambelli and W. Kurz (2002). Introduction to Material Science. France, Elsevier.
- Metzger, K. (1893). "Mundener Forstliche Hefte." Springer, Berlin Heidelberg New York.
- Michell, A. (1904). "The limits of economy of material in frame structures." Phil Mag **8**: 589-597.

- Milton, G. W. (1984). "Correlation of the electromagnetic and elastic properties of composites and microgeometries corresponding with effective medium approximations." AIP Conference Proceedings **107**(1): 66-77.
- Milton, G. W. (1997). Composites: a myriad of microstructure independent relations. Theoretical and Applied Mechanics. T. Tatsumi and e. al., Elsevier: 443-459.
- Milton, G. W. and R. V. Kohn (1988). "Variational bounds on the effective moduli of anisotropic composites." Journal of the Mechanics and Physics of Solids **36**(6): 597-629.
- Mori, T. and K. Tanaka (1973). "Average stress in matrix and average elastic energy of materials with misfitting inclusions." Acta Metallurgica **21**(5): 571-574.
- Mutmta, K. A. and N. Hopkinson (2007). "Laser melting functionally graded composition of Waspaloy and Zirconia powders." J. Mater. Sci. **42**(18): 7647-7656.
- Nemat-Nasser, S., T. Iwakuma and M. Hejazi (1982). "On composites with periodic structure." Mechanics of Materials **1**(3): 239-267.
- Neves, M. M., H. Rodrigues and J. M. Guedes (2000). "Optimal design of periodic linear elastic microstructures." Computers and Structures **76**: 421-429.
- Ohsaki, M. (1995). "Genetic algorithm for topology optimization of trusses." Computers & Structures **57**(2): 219-225.
- Olhoff, N. and J. E. Taylor (1979). "On optimal structural remodeling." J. Optimization Th. App. **27**: 571-582.
- Osher, S. and J. A. Sethian (1988). "Fronts propagating with curvature-dependent speed: Algorithms based on Hamilton-Jacobi formulations." Journal of Computational Physics **79**(1): 12-49.
- Osher, S. J. and F. Santosa (2001). "Level-set Methods for Optimization Problems Involving Geometry and Constraints: I. Frequencies of a Two-Density Inhomogeneous Drum." Journal of Computational Physics **171**(1): 272-288.
- Patil, S., S. Zhou and Q. Li (2008). "Design of Periodic Microstructural Materials by Using Evolutionary Structural Optimization Method." Advanced Materials Research **32**: 279-283.
- Peiponen, K.-E. and E. Gornov (2006). "Description of Wiener bounds of multicomponent composites by barycentric coordinates." Opt. Lett **31**: 2202-2204.
- Petersson, J. and O. Sigmund (1998). "Slope constrained topology optimization." International Journal for Numerical Methods in Engineering **41**(8): 1417-1434.
- Pezeshk, S. (2000). "Design of Nonlinear Framed Structures Using Genetic Optimization." Journal of Structural Engineering **126**(3): 382-388.
- Phan-Thien, N. and B. L. Karihaloo (1994). "Materials with negative Poisson's ratio: A qualitative microstructural model." Journal of Applied Mechanics **61**(4): 1001-1004.

- Prager, W. (1969). "Optimality criteria derived from classical extremum principles." Technical report, SM Studies Series, Solid Mechanics Division University of Waterloo, Ontario, Canada.
- Prager, W. (1974). "A note on discretized michell structures." Computer Methods in Applied Mechanics and Engineering **3**(3): 349-355.
- Prager, W. and G. Rozvany (1977). Optimization of the structural geometry. Bednarek AR, Cesari L (eds) Dynamical systems (Proceedings of the International Conference, Gainesville, Florida), NewYork.
- Proos, K. A., G. P. Steven, O. M. Querin and Y. M. Xie (2001). "Stiffness and inertia multicriteria evolutionary structural optimization." Computer Methods in Applied Mechanics and Engineering **18**: 1031-1054.
- Querin, O. M., G.P.Steven and Y. M. Xie (1998). "Evolutionary structural optimization (ESO) using a bi-directional algorithm." Eng. Comp. **15**: 1031-1048.
- Querin, O. M., G. P. Steven and Y. M. Xie (2000a). "Evolutionary structural optimization using an additive algorithm." Finite Elements in Analysis and Design **34**(3-4): 291-308.
- Querin, O. M., V. Young, G. P. Steven and Y. M. Xie (2000b). "Computational efficiency and validation of bi-directional evolutionary structural optimization." Computer Methods in Applied Mechanics and Engineering **189**(2): 559-573.
- Rajeev, S. and C. Krishnamoorthy (1992). "Discrete Optimization of Structures Using Genetic Algorithms." Journal of Structural Engineering **118**(5): 1233-1250.
- Rao, S. S. (1995). Engineering Optimization : Theory and practice, Wiley-Interscience.
- Reiter, T., G. J. Dvorak and V. Tvergaard (1997). "Micromechanical models for graded composite materials." Journal of the Mechanics and Physics of Solids **45**(8): 1281-1302.
- Reuss, A. (1929). " Berechnung der Fließgrenze von Mischkristallen auf Grund der Plastizitätsbedingung Einkristalle." Z. Angew. Math. Mech. **9**: 49-58.
- Rossow, M. and J. Taylor (1973). "A finite element method for optimal design of variable thickness sheets." AIAA J. **11**: 1566-1569.
- Rozvany, G. (2009). "A critical review of established methods of structural topology optimization." Structural and Multidisciplinary Optimization **37**(3): 217-237.
- Rozvany, G., V. Pomezanski, O. Querin, Z. Gaspar and J. Logo (2006). Some Basic Issues of Topology Optimization. IUTAM Symposium on Topological Design Optimization of Structures, Machines and Materials. M. P. Bendsøe, N. Olhoff and O. Sigmund, Springer Netherlands. **137**: 77-86.
- Rozvany, G. I. N. (1989). Structural Design via Optimality Criteria. The Netherlands, Kluwer Academic Publishers.
- Rozvany, G. I. N. (2001a). "Aims, scope, methods, history and unified terminology of computer-aided topology optimization in structural mechanics." Structural and Multidisciplinary Optimization **21**(2): 90-108.

- Rozvany, G. I. N. (2001b). "Stress ratio and compliance based methods in topology optimization – a critical review." Structural and Multidisciplinary Optimization **21**(2): 109-119.
- Rozvany, G. I. N., M. Zhou and T. Birker (1992). "Generalized shape optimization without homogenization." Structural and Multidisciplinary Optimization **4**(3): 250-252.
- Sabina, F. J., R. Rodríguez-Ramos, J. Bravo-Castillero and R. Guinovart-Díaz (2001). "Closed-form expressions for the effective coefficients of a fibre-reinforced composite with transversely isotropic constituents. II: Piezoelectric and hexagonal symmetry." Journal of the Mechanics and Physics of Solids **49**(7): 1463-1479.
- Sadd, M. H. (2005). Elasticity theory, application and numerics, Elsevier Inc.
- Sandgren, E., E. Jensen and J. Welton (1990). Topological design of structural components using genetic optimization methods. Proceedings of the Winter Annual Meeting of the American Society of Mechanical Engineers. S. Saigal and S. Mukherjee. **115**: 31-43.
- Save, M. A. (1975). "A general criterion for optimal structural design." Journal of Optimization Theory and Applications **15**(1): 119-129.
- Schittkowski, K., C. Zillober and R. Zotemantel (1994). "Numerical comparison of nonlinear programming algorithms for structural optimization." Structural and Multidisciplinary Optimization **7**(1): 1-19.
- Schmit, L. A. and B. Farshi (1974). "Some Approximation Concepts for Structural Synthesis." AIAA Journal **12**(5): 692-699.
- Schramm, C. and M. Zhou (2006). Recent developments in the commercial implementation of topology optimization. Netherland, Springer.
- Seepersad, C., R. Kumar, J. Allen, F. Mistree and D. McDowell (2004). "Multifunctional design of prismatic cellular materials." Journal of Computer-Aided Materials Design **11**(2-3): 163-181.
- Sethian, J. A. and A. Wiegmann (2000). "Structural boundary design via Level-set and immersed interface method." J. Comp. Phys. **163**(2): 489-528.
- Shen, M. and M. B. Bever (1972). "Gradients in polymeric materials." Journal of Materials Science **7**(7): 741-746.
- Sigmund, O. (1994a). Design of material structures using topology optimization. PhD Thesis, Technical University of Denmark.
- Sigmund, O. (1994b). "Materials with prescribed constitutive parameters: An inverse homogenization problem." International Journal of Solids and Structures **31**(17): 2313-2329.
- Sigmund, O. (1995). "Tailoring materials with prescribed elastic properties." Mechanics of Materials **20**(4): 351-368.
- Sigmund, O. (1997). "On the Design of Compliant Mechanisms Using Topology Optimization\*." Mechanics of Structures and Machines **25**(4): 493-524.



- Sigmund, O. (2000). "A new class of extremal composites." Journal of the Mechanics and Physics of Solids **48**(2): 397-428.
- Sigmund, O. (2001). "A 99 line topology optimization code written in Matlab." Structural and Multidisciplinary Optimization **21**(2): 120-127.
- Sigmund, O. (2007). "Morphology-based black and white filters for topology optimization." Structural and Multidisciplinary Optimization **33**(4): 401-424.
- Sigmund, O. and J. Petersson (1998). "Numerical instabilities in topology optimization: A survey on procedures dealing with checkerboards, mesh-dependencies and local minima." Structural and Multidisciplinary Optimization **16**(1): 68-75.
- Sigmund, O. and S. Torquato (1997). "Design of materials with extreme thermal expansion using a three-phase topology optimization method." J Mech Phys Solids **45**(6): 1037-1067.
- Staab, G. H. (1999). Laminar composites, Elsevier.
- Steven, G. (2006). "Homogenization and inverse homogenization for 3D composites of complex architecture." Engineering Computations **23**(4): 432-450.
- Strang, G. and R. V. Kohn (1986). "Optimal design in elasticity and plasticity." International Journal for Numerical Methods in Engineering **22**(1): 183-188.
- Sun, C. T. and R. S. Vaidya (1996). "Prediction of composite properties from a representative volume element." Composites Science and Technology **56**(2): 171-179.
- Suquet, P. (1987). Elements of homogenization theory for inelastic solid mechanics. Homogenization techniques for composite media. E. Sanchez-Palencia and A. Zaoui. Berlin, Heidelberg, New York, Springer: 94-278.
- Suzuki, K., N. Kikuchi (1991). "A homogenization method for shape and topology optimization". Computer Methods in Applied Mechanics and Engineering. **93**: 291-318.
- Svanberg, K. (1987). "The method of moving asymptotes—a new method for structural optimization." International Journal for Numerical Methods in Engineering **24**(2): 359-373.
- Swan, C. C. and I. Kosaka (1997). "VOIGT-REUSS topology optimization for structures with linear elastic material behaviours." International Journal for Numerical Methods in Engineering **40**: 3033-3058.
- Tamura, I., Y. Tomota and H. Ozawa (1973). The 3rd international conference on strength of metals and alloys, London, Institute of metals and iron and steel institute.
- Tanskanen, P. (2002). "The evolutionary structural optimization method: theoretical aspects." Computer Methods in Applied Mechanics and Engineering **191**(47-48): 5485-5498.
- Terada, K., N. Kikuchi (1996). "Microstructural design of composites using the homogenization method and digital images." Materials science research international. **2**: 65-72.

- Teraki, J., T. Hirano and K. Wakashima (1993). "An Elastic-Plastic Analysis of Thermal Stresses in a FGM Plate Under Cyclic Thermal Load." Ceramic transactions 34: 67-74
- Torquato, S. (1991). "Random Heterogeneous Media: Microstructure and Improved Bounds on Effective Properties." Applied Mechanics Reviews 44(2): 37-76.
- Torquato, S. (1998). "Morphology and effective properties of disordered heterogeneous media." Int. J. Solids 35(19): 2385–2406
- Torquato, S. (2000). "Modeling of physical properties of composite materials." International Journal of Solids and Structures 37(1–2): 411-422.
- Torquato, S. (2002). Random Heterogeneous Materials: Microstructure and Macroscopic Properties. New York, Springer-Verlag.
- Torquato, S. (2010). "Optimal Design of Heterogeneous Materials." Annual Review of Materials Research 40(1): 101-129.
- Torquato, S. and A. Donev (2004). "Minimal surfaces and multifunctionality." Proceedings of the Royal Society of London. Series A: Mathematical, Physical and Engineering Sciences 460(2047): 1849-1856.
- Torquato, S., S. Hyun and A. Donev (2003). "Optimal design of manufacturable three-dimensional composites with multifunctional characteristics." Journal of Applied Physics 94(9): 5748-5755.
- Tyrus, J. M., M. Gosz and E. DeSantiago (2007). "A local finite element implementation for imposing periodic boundary conditions on composite micromechanical models." International Journal of Solids and Structures 44(9): 2972-2989.
- Voigt, W. (1889). "Über die Beziehung zwischen den beiden Elastizitätskonstanten isotroper Körper." wied. Ann. 38: 573-587.
- Wakashima, K., T. Hirano and M. Nino (1990). Space application of advanced structural materials, European space agency.
- Walpole, L. J. (1966). "On bounds for the overall elastic moduli of inhomogeneous systems—I." Journal of the Mechanics and Physics of Solids 14(3): 151-162.
- Walpole, L. J. (1969). "On the overall elastic moduli of composite materials." Journal of the Mechanics and Physics of Solids 17(4): 235-251.
- Wang, L., J. Lau, E. L. Thomas and M. C. Boyce (2011). "Co-Continuous Composite Materials for Stiffness, Strength, and Energy Dissipation." Advanced Materials 23(13): 1524-1529.
- Wang, M. Y. and S. Wang (2005a). "Bilateral filtering for structural topology optimization." International Journal for Numerical Methods in Engineering 63(13): 1911-1938.
- Wang, M. Y. and X. Wang (2005b). "A Level-set based variational method for design and optimization of heterogeneous objects." Computer-Aided Design 37: 321-337.
- Wang, M. Y., X. M. Wang and D. M. Guo (2003). "A Level-set method for structural topology optimization." Comp. Meth. Appl. Mech. Eng. 192: 227-246.

- Wang, M. Y., S. Zhou and H. Ding (2004a). "Nonlinear diffusions in topology optimization." Structural and Multidisciplinary Optimization **28**(4): 262-276.
- Wang, S. Y., K. Tai and M. Y. Wang (2006). "An enhanced genetic algorithm for structural topology optimization." Int. J. Num. Meth. Eng **65**: 18-44.
- Wang, X., Y. Mei and M. Y. Wang (2004b). "Level-set method for design of multi-phase elastic and thermoelastic materials." International Journal of Mechanics and Materials in Design **1**(3): 213-239.
- Wang, Y., Z. Kang and Q. He (2013). "An adaptive refinement approach for topology optimization based." Computers and Structures **117**: 10-22.
- Watanabe, R. and A. Kawasaki (1990). Proceeding of the 1st international symposium of FGM. Sendai, Japan.
- Wilkins, A. H., C. J. Challis and A. P. Roberts (2007). Isotropic, stiff, conducting structures via topology optimization. 7th world congress on structural and multidisciplinary optimization. Seol, Korea.
- Willis, J. R. (1981). Variational and Related Methods for the Overall Properties of Composites. Advances in Applied Mechanics. Y. Chia-Shun, Elsevier. **21**: 1-78.
- Willis, J. R. (1992). "On methods for bounding the overall properties of nonlinear composites: Correction and addition." Journal of the Mechanics and Physics of Solids **40**(2): 441-445.
- Xie, Y. M. and G.P.Steven (1996). "Evolutionary structural optimization for dynamic problems." Comput. & Struct. **58**: 1067-1073.
- Xie, Y. M. and G. P. Steven (1993). "A simple evolutionary procedure for structural optimization." Comp. & Struct. **49**: 885-896.
- Xie, Y. M. and G. P. Steven (1997). Evolutionary Structural Optimization. London, Springer.
- Yamanoushi, M., M. Koizumi, T. Hirai and I. Shiota (1990). Proceedings of the First International Symposium on Functionally Gradient Materials, Japan.
- Yang, J., H. Ouyang and Y. Wang (2010). "Direct metal laser fabrication: machine development and experimental work." The International Journal of Advanced Manufacturing Technology **46**(9-12): 1133-1143.
- Yang, X. Y., Y. M. Xie, G. P. Steven and O. M. Querin (1999). "Bidirectional evolutionary method for stiffness optimization." AIAA Journal **37**: 1483-1488.
- Yin, L. and W. Yang (2001). "Optimality criteria method for topology optimization under multiple constraints." Comput. Struct. **79**: 1839-1850.
- Zener, C. (1948). Elasticity and anelasticity of metals, University of Chicago Press.
- Zhao, C., G. P. Steven and Y. M. Xie (1997). "Evolutionary natural frequency optimization of two-dimensional structures with additional non-structural lumped masses." Engineering Computations **14**(2): 233-251.
- Zhao, Z. and Z. Luc (2000). "Adaptive direct slicing of the solid model for rapid prototyping." International Journal of Production Research **38**(1): 69-83.

- Zhikov, V. V., S. M. Kozlov, O. A. Oleinik and K. T. e. Ngoan (1979). "averaging and g-convergence of differential operators " Russ Math Surv **34**(5): 69-147.
- Zhou, M. and G. I. N. Rozvany (1991). "The COC algorithm, Part II: Topological, geometrical and generalized shape optimization." Computer Methods in Applied Mechanics and Engineering **89**(1-3): 309-336.
- Zhou, M. and G. I. N. Rozvany (2001). "On the validity of ESO type methods in topology optimization." Structural and Multidisciplinary Optimization **21**(1): 80-83.
- Zhou, S. and Q. Li (2007). "The relation of constant mean curvature surfaces to multiphase composites with extremal thermal conductivity." J. Phys. D. Appl. Phys. **40**: 6083-6093.
- Zhou, S. and Q. Li (2008a). "Computational design of multi-phase microstructural materials for extremal conductivity." Computational Materials Science **43**(3): 549-564.
- Zhou, S. and Q. Li (2008b). "Design of graded two-phase microstructures for tailored elasticity gradients." Journal of Materials Science **43**(15): 5157-5167.
- Zhou, S. and Q. Li (2008c). "Microstructural design of connective base cells for functionally graded materials." Material Letters **62**: 4022-4024.
- Zhou, S. and Q. Li (2008d). "A microstructure diagram for known bounds in conductivity." Journal of Materials Research **23**(03): 798-811.
- Zhou, S., W. Li, Y. Chen, G. Sun and Q. Li (2011). "Topology optimization for negative permeability metamaterials using Level-set algorithm." Acta Materialia **59**(7): 2624-2636.
- Zhou, S., W. Li, G. Sun and Q. Li (2010). "A Level-set procedure for the design of electromagnetic metamaterials." Opt. Express **18**(7): 6693-6702.
- Zhou, S. and M. Y. Wang (2007). "Multimaterial structural topology optimization with a generalized Cahn–Hilliard model of multiphase transition." Structural and Multidisciplinary Optimization **33**(2): 89-111.
- Zhu, F., K.-Z. Chen and X.-A. Feng (2006). "Visualized CAD models of objects made of a multiphase perfect material." Advances in Engineering Software **37**(1): 20-31.
- Zhu, J. H., W. H. Zhang and K. P. Qiu (2007). "Bi-Directional Evolutionary Topology Optimization Using Element Replaceable Method." Computational Mechanics **40**(1): 97-109.
- Zohdi, T. I. (2002). "On tailoring of microstructures with prescribed elastic properties." Int.J.Fracture **118**(4): 89-94.
- Zuiker, J. R. (1995). "Functionally graded materials: Choice of micromechanics model and limitations in property variation." Composites Engineering **5**(7): 807-819.
- Zuo, Z. H., Y. M. Xie and X. Huang (2009). "Combining genetic algorithms with BESO for topology optimization." Structural and Multidisciplinary Optimization **38**(5): 511-523.